STUTZMAN

NATIONAL ACADEMIES OF SCIENCES AND ENGINEERING

NATIONAL RESEARCH COUNCIL

of the

UNITED STATES OF AMERICA

UNITED STATES NATIONAL COMMITTEE

International Union of Radio Science

National Radio Science Meeting

9–13 January 1996

Sponsored by USNC/URSI

University of Colorado
Boulder, Colorado
U.S.A.

Condensed Technical Program

Tuesday, 9 January

0855-1200

B/A/D-1	ADVANCED MATERIALS AND ELECTROMAGNETIC APPLICATIONS	CR2-28
D/J-1	SUPERCONDUCTING DEVICES AND DEVICES FOR RADIOASTRONOMY	CR0-30
F-1	EARTH-SATELLITE PROPAGATION EFFECTS	CR1-42
G-1	IMPACT OF NEAR-EARTH ENVIRONMENT ON COMMUNICATION AND NAVIGATION SYSTEMS	CR2-26
H-1	LABORATORY SIMULATIONS OF SPACE PLASMAS	CR2-6
K-1	BIOELECTROMAGNETIC INTERACTIONS	CR1-40

1335-1700

B-1	RANDOM AND ROUGH SURFACES	CR1-9
D-1	NOVEL DEVICES	CR2-28
F-2	PROPAGATION MODELING AND MEASUREMENTS RELATED TO PROPAGATION	CR1-42
G-2	ELECTRON DENSITY PROFILES: MODELS AND DATA (ADOLF PAUL MEMORIAL SESSION)	CR2-26
J-1	TECHNIQUES FOR REDUCING ANTENNA NOISE IN RADIO TELESCOPES	CR0-30

1355-1700

H-2	LABORATORY SIMULATIONS OF SPACE PLASMAS	CR2-6

2000-2400

USNC-URSI Meeting	Broker Inn

Wednesday, 10 January

0815-1200

PLENARY SESSION	MATH 100

1335-1700

A-1	ELECTROMAGNETIC FIELD METROLOGY	CR1-40
B-2	ANTENNAS	CR2-6
D/B-1	MODELING OF HIGH FREQUENCY DEVICES	CR2-28
E/J-1	TECHNIQUES FOR RFI MONITORING, EXCLUSION, AND REMOVAL	CR0-30
F/B-1	SCATTERING FROM ROUGH SURFACES	CR1-42

1355-1700

G-3	TOMOGRAPHIC STUDIES OF IONOSPHERIC PLASMAS-I	CR2-26

1700-1800

Commission A Business Meeting	CR1-40
Commission D Business Meeting	CR2-28
Commission E Business Meeting	CR0-30
Commission F Business Meeting	CR1-42
Commission H Business Meeting	CR2-26

Thursday, 11 January

0835-1200

A-2	TIME DOMAIN, ANTENNA, AND MATERIAL METROLOGY	CR1-40
D-2	DEVICE/CIRCUIT INTERACTIONS, AND ACTIVE ANTENNAS	CR2-28
F-3	MOBILE AND PERSONAL ACCESS RADIO PROPAGATION	CR1-42
J/F-1	RADIO FREQUENCY PHASE SHIFTS CAUSED BY THE TROPOSPHERE	CR0-30

0855-1200

B-3	HYBRID TECHNIQUES	CR1-9
G/H-1	INTERMEDIATE IONOSPHERIC LAYERS	CR2-6

United States National Committee

INTERNATIONAL UNION OF RADIO SCIENCE

PROGRAM AND ABSTRACTS

National Radio Science Meeting
9-13 January 1996

Sponsored by USNC/URSI

39
40
41
42

100
101

105
106

158
160
161
162
163
164
165
166

245
246

NOTE:

Programs and Abstracts of the USNC/URSI Meetings are available from:

USNC/URSI
National Academy of Sciences
2101 Constitution Avenue, N.W.
Washington, DC 20418

at $5 for 1983-1996 meetings.

The full papers are not published in any collected format; requests for them should be addressed to the authors who may have them published on their own initiative. Please note that these meetings are national. They are not organized by the International Union, nor are the programs available from the International Secretariat.

MEMBERSHIP
United States National Committee
INTERNATIONAL UNION OF RADIO SCIENCE

Chair:	Dr. David C. Chang*
Vice Chair:	Dr. Charles M. Rush*
Secretary:	Dr. Susan K. Avery*
Immediate Past Chair:	Dr. Chalmers M. Butler*

Members Representing Societies, Groups, and Institutes:

American Geophysical Union	Dr. George C. Reid
IEEE Antennas & Propagation Society	Dr. Gary S. Brown
IEEE Microwave Theory and Techniques Society	Dr. A. A. Oliner
IEEE Geosciences and Remote Sensing Society	Dr. Roger Lang
American Meterological Society	vacant

Members-at-Large:	Dr. Albin Gasiewski
	Dr. R. Pogorzelski
	Dr. W. Russ Stone
	Dr. J. Tartar
	Dr. Roland T. Tsunoda
	Dr. Edgeworth R. Westwater

Liaison Representatives from Government Agencies:

National Telecommunications & Information Administration	Dr. Hans Liebe
National Science Foundation	Dr. Hugh Van Horn
Federal Communications Commission	Mr. John C.H. Wang
Department of the Navy	Mr. William J. Cook
Department of the Army	Mr. Earl J. Holliman
NASA	Dr. Erwin R. Schmerling

Chairs of the USNC/URSI Commissions:

Commission A	Dr. Sedki Riad
Commission B	Dr. Donald G. Dudley
Commission C	Dr. David J. Thomson
Commission D	Dr. Michael Shur
Commission E	Dr. Robert L. Gardner
Commission F	Dr. Julius Goldhirsh
Commission G	Dr. Sunanda Basu
Commission H	Dr. Paul A. Bernhardt
Commission J	Dr. Michael M. Davis
Commission K	Dr. James C. Lin

* Member of USNC/URSI Executive Committee

Officers, Chairs and Vice Chairs of Commissions of URSI resident in the United States:

Honorary President	Dr. William E. Gordon
Vice President	Dr. Thomas B.A. Senior
Vice Chair, Commission A	Dr. Motohisa Kanda
Vice Chair, Commission B	Dr. Chalmers M. Butler
Chair, Commission D	Dr. Tatsuo Itoh
Chair, Commission F	Dr. Richard K. Moore
Vice Chair, Commission G	Dr. Bodo W. Reinisch
Vice Chair, Commission K	Dr. James C. Lin
Foreign Secretary of the U.S. National Academy of Sciences	Sherwood Rowland
Honorary Members	Dr. Ernst Weber
Director, Board on Physics and Astronomy, National Research Council	Dr. Donald C. Shapero
Associate Director, U.S. Board on Physics and Astronomy, National Research Council	Dr. Robert L. Riemer

DESCRIPTION OF THE INTERNATIONAL UNION OF RADIO SCIENCE

The International Union of Radio Science is one of the world scientific unions organized under the International Council of Scientific Unions (ICSU). It is commonly designated as URSI (from its French name, Union Radio Scientifique Internationale). Its aims are (1) to promote the scientific study of radio communications, (2) to aid and organize radio research requiring cooperation on an international scale and to encourage the discussion and publication of the results, (3) to facilitate agreement upon common methods of measurement and the standardization of measuring instruments, and (4) to stimulate and to coordinate studies of the scientific aspects of telecommunications using electromagnetic waves, guided and unguided. The International Union itself is an organizational framework to aid in promoting these objectives. The actual technical work is largely done by the National Committee in the various countries.

The new officers of the International Union are:

President:	Dr. P. Bauer (France)
Past President:	Prof. E.V. Jull (Canada)
Vice Presidents:	Prof. J. Bach Andersen (Denmark) Prof. P.J.B. Clarricoats (U.K.) Prof T. Okoshi (Japan) Prof. T.B.A. Senior (U.S.A.)
Secretary-General:	Prof. P. Lagasse (Belgium)
Adjoint Secretary-General:	Prof. P. Van Daele (Belgium)
Administrative Secretary:	Mme. Iren Heleu (Belgium)
Honorary Presidents:	Sir G. Beynon (U.K.) Dr. W. Dieminger (West Germany) Prof. W. Christiansen (Australia) Prof. W.E. Gordon (U.S.A.) Dr. F.L.H.M. Stumpers (Netherlands)

The Secretary-General's office and the headquarters of the organization are located at Avenue Albert Lancaster, 32, B-1180 Brussels, Belgium. The Union is supported by contributions (dues) from 38 member countries. Additional funds for symposia and other scientific activities of the Union are provided by ICSU from contributions received for this purpose from UNESCO.

The International Union, as of the XXIVth General Assembly held in Kyoto, Japan, August 25-September 3, 1993, has ten bodies called Commissions for centralizing studies in the principal technical fields.

Every three years the International Union holds a meeting called the General Assembly. The next is the XXVth, to be held in 1996, in Lille, France. The Secretariat prepares and distributes the Proceedings of the General Assemblies. The International Union arranges international symposia on specific subjects pertaining to the work of one or several Commissions and also cooperates with other Unions in international symposia on subjects of joint interest.

Radio is unique among the fields of scientific work in having a specific adaptability to large-scale international research programs, since many of the phenomena that must be studied are worldwide in extent and yet are in a measure subject to control by experimenters. Exploration of space and the extension of scientific observations to the space environment are dependent on radio for their research. One branch, radio astronomy, involves cosmic phenomena. URSI thus has a distinct field of usefulness in furnishing a meeting ground for the numerous workers in the manifold aspects of radio research; its meetings and committee activities furnish valuable means of promoting research through exchange of ideas.

Session B/A/D-1, 0855-Tues., CR2-28
ADVANCED MATERIALS AND ELECTROMAGNETIC APPLICATIONS
Chairperson and Organizer: P.L.E. Uslenghi, Dept. of Electrical Engineering and Computer Science, Univ. of Illinois at Chicago, Chicago, IL 60607

B/A/D1-1 0900 AN OVERVIEW OF PROPERTIES OF MAGNETOELECTRIC MEDIA

Piergiorgio L. E. Uslenghi
Department of Electrical Engineering and Computer Science
University of Illinois at Chicago
851 South Morgan Street, Chicago, IL 60607-7053

The electromagnetic behavior of magnetoelectric, or bianisotropic, materials is reviewed in the light of recent analytical developments with the goal of outlining potential practical applications to microwave devices and components. First, a brief historical review of magnetoelectrics is presented. This is followed by a classification of the various types of bianisotropic materials and their particular cases, which include anisotropic, chiral, biisotropic, etc. materials. A discussion of the constitutive relations of these materials is outlined, and some of the values of the constitutive parameters of realized materials are given.

The results obtained in the last few years in analyzing the guiding properties of magnetoelectric media are summarized. These include: published results on nonreciprocity of propagation in parallel-plate, slab, rectangular and circular waveguides filled with different magnetoelectric media, including coupling phenomena between such guiding structures, and possible microwave devices and components (e.g., isolators); recently announced results on TE-TM field decoupling in rectangular and cylindrical coordinates for the most general linear media; and some as yet unpublished results on widening of the operating bandwidth of the fundamental mode for waveguides filled with such materials.

Finally, the use of such materials in open structures such as patch antennas and arrays makes it necessary to study the scattering behavior of complicated structures involving conductors and penetrable bianisotropic materials. A general formulation in terms of integral equations is presented, that is especially suitable for MoM applications, and several particular cases are discussed. The formulation is based on an equivalent macroscopic vs. microscopic view of matter, and on a generalization of the concept of electric and magnetic polarizations. As a byproduct, a novel and general formulation of the boundary conditions at the interface between two different bianisotropic media is given.

B/A/D1-2
0920

A CERTAIN CLASS OF ARTIFICIAL MATERIALS; REALIZATION AND MODELING.

Nicolaos Alexopoulos†, Rodolfo Diaz‡, Hung-Yu Yang*
†Department of Electrical Engineering
University of California, Los Angeles
Los Angeles, CA 90024
‡Northrop Grumman, Chandler, AZ 85224
*Department of Electrical Engineering and
Computer Science, University of Illinois,
Chicago, IL 60607-7053

A class of artificial materials will be discussed, where the electromagnetic properties are defined by certain effective parameter characteristics such as dielectric and magnetic constants. As an example, the feasibilty of artificial materials with complex effective dielectric constant $\epsilon_{\text{eff}} = \epsilon_{\text{er}} + j\epsilon_{\text{ei}}$ with $-\infty < \epsilon_{\text{er}}, \epsilon_{\text{ei}} < \infty$ will be demonstrated. The basic properties of such materials i.e. causality, analyticity (R.E. Diaz, The Analytic Continuation Method for the Analysis and Design of Dispersive materials, PhD Dissertation, UCLA 1991) and realizability, as well as modeling methods of real physical artificial material structures will be introduced. There are many potential applications of such materials in various technologies. For example, articifial materials are included in layered composite structures in microwave and millimeter-wave integrated circuits and antennas to obtain desirable performance which is otherwise not possible. Composite absorbing layers including artificial materials are also useful for broadband applications. In particular, certain surface wave structures with material properties of $0 < \epsilon_{\text{er}} < 1$ and $\epsilon_{\text{er}} < 0$ (Evanescent Materials, Phraxos Research and Development Inc., Technical Report 94012, 1994) will be introduced and analyzed to further demonstrate important applications of such artificial materials in electromagnetic technologies.

B/A/D1-3 0940

A RECASTING OF PERCOLATION THEORY INTO THE LANGUAGE OF ARTIFICIAL DIELECTRICS

Nicolaos G. Alexopoulos and William Merritt
Electrical Engineering Department
University of California at Los Angeles

Percolation Theory presents the electromagnetics engineer with a novel approach for the modeling of random particle dispersions. Its ability to model realistic manufacturing processes in terms of their stochastic behavior and to yield the effective media parameters for the permittivity and the permeability of the aggregate structure make it a powerful tool in the design of synthetic electromagnetic materials. However, the results are cast in such a form that it is difficult to separate the probabilistic contributions from the purely electromagnetic effects. If properly recast into the language of artificial dielectrics, the Percolation Theory model should separate into two effects: a probabilistic model of the dispersion, which yields the mean geometry of an array of particles (or clusters), and an electromagnetic model of the properties of that assemblage of particles (or clusters) resulting from the interaction of their intrinsic properties with the geometry of the array. In other words, the stochastic model of Percolation Theory should be reducible to a deterministic model of a classical artificial dielectric. That reduction is presented in this paper for the specific case of a thin layer of a dispersion of conducting particles in a dielectric binder. Its similarities to the behavior of a classic Frequency Selective Surface layer are demonstrated.

B/A/D1-4 1000

FERROELECTRIC MATERIALS FOR MICROWAVE APPLICATIONS

Franco De Flaviis, Nicolaos G. Alexopoulos,
Oscar M. Stafsudd, David Chang
Electrical Engineering Department
University of California at Los Angeles

Ferroelectric materials are nonlinear dielectrics having a dielectric constant which is a function of electric field. The nonlinear behavior of these materials makes them candidates for the realization of advanced microwave and millimeter wave devices. Ferroelectrics have been successfully employed in many optical devices, but their application in microwave and millimeter wave systems has been limited, mostly due to the high losses and to the large bias voltage required to significantly change the electrical properties of the bulk material. However, today there are several new techniques available to produce high quality ferroelectric thin ceramics and thin films which require only a medium or low bias voltage to change significantly the dielectric constant. These processes open the way for development of a new family of devices which are fully compatible with conventional analog and digital electronic circuits. Also use of thin ceramics in combination with conventional microwave circuit, result an attractive configuration which allow to minimize the losses and to have many new design. Very accurate investigation based on X-rays analysis, thermal analysis and electrical measurement on $PbTiO_3$, $Pb_xCa_{1-x}TiO_3$, $BaTiO_3$, $Ba_xSr_{1-x}TiO_3$ has been conduced. The results shows that new devices as tunable phase shifter, tunable filters, and tunable beam antennas can be realized. Because the low cost of high purity ferroelectric material obtained by the Sol-gel process, and the reduce size, those materials are particularly suitable for portable communication systems, or any system where reduced size and low cost are major issues.

B/A/D1-5 Paper Withdrawn
1040

B/A/D1-6 Paper Withdrawn
1100

B/A/D1-7 Paper Withdrawn
1120

B/A/D1-8 Paper Withdrawn
1140

B/A/D1-9 Roundtable Discussion
1200

Session D/J-1, 0855-Tues., CR0-30
SUPERCONDUCTING DEVICES AND DEVICES FOR RADIOASTRONOMY
Chairperson and Organizer: Z.B. Popović, Dept. of Electrical and Computer Engineering, Univ. of Colorado at Boulder, Boulder, CO 80309

D/J1-1 0900

LOW-NOISE, CRYOGENICALLY-COOLABLE AMPLIFIERS AND RECEIVERS USING AlInAs/GaInAs/InP HEMT'S - A REVIEW

Marian W. Pospieszalski
National Radio Astronomy Observatory*
2015 Ivy Road
Charlottesville, VA 22903

Design, construction and performance of several cryogenically-coolable millimeter-wave amplifiers for radio astronomy applications using AlInAs/GaInAs/InP HEMT's are presented. Signal and noise models of InP HFET's, both at room and cryogenic temperatures, which form a basis for amplifier designs are discussed. The examples include amplifiers for the following frequency ranges: 26-36 GHz, 38-45 GHz, 40-50 GHz and 60-80 GHz. Also, the performance of radio astronomy receivers using these amplifiers is discussed. A summary of noise performance of HEMT receivers and a comparison with NRAO SIS mixer receivers is shown in Fig. 1. In conclusion, HEMT receivers should be competitive with SIS receivers for frequencies up to 120 GHz.

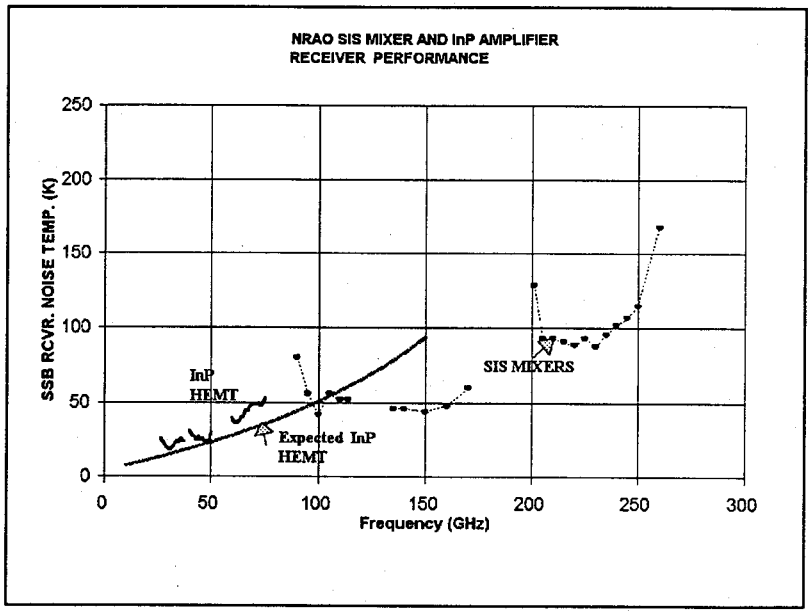

Fig. 1. A comparison of noise performance of InP HEMT receivers and SIS mixer receivers. (SIS mixer data courtesy of A. R. Kerr and S.-K. Pan.)

*The National Radio Astronomy Observatory is a facility of the National Science Foundation operated under cooperative agreement by Associated Universities, Inc.

D/J1-2
0940

BOLOMETERS IN RADIO ASTRONOMY RECEIVERS

Peter Timbie, Khurram Farooqui, Grant Wilson, and Jun-Wei Zhou
Department of Physics
Brown University
Providence, RI 02912

Bolometers are used extensively as detectors for observations in radio astronomy at wavelengths throughout the microwave, millimeter, and submillimeter portions of the electromagnetic spectrum. They are particularly useful for applications in low-background conditions requiring wide bandwidth and high sensitivity, such as observations of the Cosmic Microwave Background Radiation (CMBR). Traditionally bolometers have been used in optical systems which couple to multiple electromagnetic modes using geometrical optics. However, an extremely powerful technique is to couple bolometers directly to single-mode waveguide to exploit such advantages of waveguide technology as high quality filters and low-sidelobe antennas. Another advantage of this technique is that the bolometer dimensions can be made much smaller than a wavelength, yielding a short time constant. We address such general issues as coupling to bolometers, filtering, sensitivity, cooling, low-noise readout amplifiers, and astronomical applications.

We have recently measured the performance of a monolithic silicon bolometer mounted in waveguide and operated at ~100 mK and obtained an electrical Noise Equivalent Power (NEP) of $\approx 10^{-17}\ \mathrm{W}/\sqrt{\mathrm{Hz}}$. This sensitivity is comparable to the background noise in many low-background astrophysical observations. The detectors are used in a receiver that covers the spectral range from 65 GHz to 170 GHz in 5 filter bands. The receiver is integrated with a balloon-borne telescope for measurements of the 2.7 K CMBR at the level of $30\ \mu\mathrm{K}$.

In a new device, the hot-electron microbolometer, radiation is coupled from a waveguide probe or a planar antenna into a normal metal strip of sub-micron dimensions deposited on a substrate. The power is absorbed by the electrons in the metal. At low temperature (less than ~ 500 mK) the electrons are thermally decoupled from the metal lattice and the substrate, so the electron temperature increases. This temperature rise is a measure of the incident power, and can be determined using a normal-insulating-superconducting (NIS) junction. The hot-electron microbolometer promises much simpler fabrication and improved sensitivity compared to conventional bolometers.

D/J1-3
1000

LOW-NOISE, WIDE BANDWIDTH, HOT ELECTRON BOLOMETER MIXERS FOR SUBMILLIMETER WAVELENGTHS

W.R. McGrath[1], A. Skalare[1], B. Karasik[1], B. Bumble[1], H.G. LeDuc[1], P.J. Burke[2], R. Schoelkopf[2], D.E. Prober[2]
[1]Center for Space Microelectronics Technology, Jet Propulsion Laboratory, California Institute of Technology, Pasadena, CA 91109
[2]Dept. of Applied Physics, Yale University, New Haven, CT 06520-8284

Recently a novel superconductive hot-electron micro-bolometer has been proposed which is both fast and sensitive (D.E. Prober, Appl. Phys. Lett. 62, 2119, 1993). This device has several important properties which make it useful as a heterodyne sensor for radioastronomy applications at frequencies above 1 THz. The thermal response time of the device is fast enough, several 10's of picoseconds, to allow for IF's of several GHz. This bolometer mixer should operate well up to at least 10 THz. There is no energy gap limitation as in an SIS mixer, since the mixing process relies on heating of the electron gas. In fact, *rf* power is absorbed more uniformly above the gap frequency. The mixer noise should be near quantum-limited, and the local oscillator (LO) power requirement is very low: ≈ 10 nW for a Nb device. One of the unique features of this device is that it employs rapid electron diffusion into a normal metal, rather than phonon emission, as the thermal conductance that cools the heated electrons. In order for diffuion to dominate over phonon emission, the device must be short, less than 0.5 μm.

We have measured the heterodyne performance of a submicron Nb bolometer mixer at 530 GHz in a waveguide receiver, originally designed for observation of H_2O in the interstellar medium (A. Skalare, W. McGrath, B. Bumble, H. LeDuc, P. Burke, A. Verheijen, D. Prober, IEEE Trans. Appl. Superconductvity 5, 2236, 1995). The double sideband (DSB) receiver noise temperaure is 650 K with an *IF* of 1.4 GHz. The 3 dB *IF* rolloff frequency is measured at 1.7 GHz, and the estimated LO power is 10-20 nW. This represents the widest bandwidth achieved in a low noise bolometer mixer for submillimeter wavelengths. The LO frequency of 530 GHz is above the gap frequency of ≈400 GHz for the Nb film used in this device (the film thickness is ≈10 nm, which leads to a "dirty" film with reduced $T_c \approx 5.5$ K. The "dirty limit" is required for enhanced electron-electron interactions which leads to a hot electron gas when *rf* power is absorbed). An important property of these devices is the predicted frequency independence of the heterodyne performance. To test this prediction, we are reconfiguring our receivers to measure the noise temperature, bandwidth, and LO power at 1200 GHz and 2500 GHz. Results will be discussed.

The research described in this abstract was performed by the Center for Space Microelectronics Technology, Jet Propulsion Laboratory, and by Yale University and was jointly sponsored by the National Science Foundation and the National Aeronautics and Space Administration, Office of Space Access and Technology.

D/J1-4
1100

CHARACTERIZATION OF THIN FILM $SrTiO_3$ FOR MICROWAVE DEVICES

David Galt and John C. Price
Department of Physics
University of Colorado
Boulder, CO 80309-0390

The voltage tunable dielectric function of thin film ferroelectrics has applications to integrated microwave filters, phase shifters, and matching networks. To properly engineer these devices, the dielectric constant and loss tangent of thin film ferroelectrics must be fully characterized at the frequencies of interest. We describe a novel technique to carry out the necessary characterization. The method involves an approximately open-circuit-terminated microstrip resonator which incorporates a ferroelectric capacitor at its center (See Fig. 1). Due to the capacitor's central location, antisymmetric resonant modes are sensitive to the loading and losses of the capacitor while symmetric resonant modes are not. Studying all available resonances allows us to 1) unambiguously calculate the ferroelectric capacitance and 2) subtract-out background losses (originating in the resonator's conductors, substrate, and coupling) to arrive at a loss tangent for the ferroelectric capacitor. A dc voltage bias is applied to the capacitor through adjustable needle probes (not shown). These probes contact the microstrip at the voltage nodes of the resonance under investigation thus minimizing their influence on the resonant Q and frequency. To demonstrate this method we have fabricated a superconducting microstrip resonator from a laser ablated $YBa_2Cu_3O_{7-x}$ (YBCO) film on a $LaAlO_3$ (LAO) substrate with a $SrTiO_3$ (STO) capacitor at its center. We report the observed dielectric behavior of the STO laser ablated film as a function of bias at liquid He and N_2 temperatures and at high and low frequencies. It is observed that the electrically tunable dielectric constant of the STO film is roughly independent of frequency up to 20 GHz (especially at high bias). The loss tangent of the STO/LAO capacitor decreases with increasing bias and is independent of frequency between 6 and 20 GHz. Applications of STO/YBCO tunable capacitors to superconducting microwave devices will be discussed.

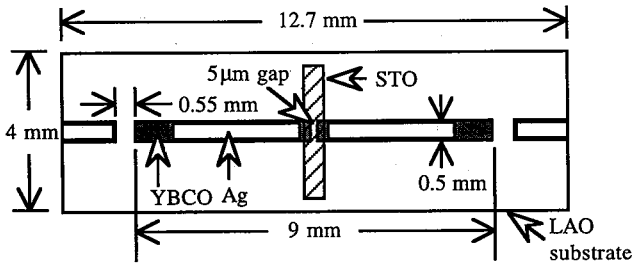

Fig.1 Microstrip Resonator Layout

Work supported by ONR, SCT Inc., ARPA, and Wright-Patterson AFB.

D/J1-5
1120

SUPERCONDUCTING BOLOMETERS ON FREE-STANDING YSZ MEMBRANES

S. J. Berkowitz* A. Hirahara K. Char
Conductus,Inc.
969 W. Maude Ave.
Sunnyvale, CA 94086 E. Grossman
NIST
325 Broadway
Boulder, CO 80303

High-temperature superconducting bolometers offer the promise of combining the sensitivity of HgCdTe detectors with the ability to extend the wavelength detection range out to 30 microns. We have made array-compatible superconducting pixels with noise equivalent powers (NEP) as low as $1.5 \times 10^{-12} W/\sqrt{Hz}$. This value is equal to the lowest reported NEP for a superconducting bolometer (B. R. Johnson, et al, submitted SPIE Advanced Microdevices and Space Sensors, July 1994), but the time constant of our device is about 50 times faster.

The pixels consisted of a 100 nm thick yttria stabilized zirconia (YSZ) free-standing membrane supported by four thin legs and a YBCO thermometer. The membranes are fabricated using a micromaching technology (L. P. Lee, et al , *Appl. Phys. Lett.*, **61**, 2706, 1992) and offer an advance in manufacturability over previous high-sensitivity YBCO bolometers on thinned sapphire (S. Verghese, et al, *SPIE Proceedings*, **1292**, 137, 1990). The area of the membrane is 50 μm by 50 μm. We are investigating larger membranes at this time. The aspect ratio of the legs was varied from 5 to 20 squares. Due to the low thermal conductivity of YSZ, a value of the thermal conductance (G) as low as $6 \times 10^{-7} W/K$ was obtained. A single strip of superconductor was used as a thermometer, with a typical resistance of 70 Ω at the midpoint of the transition. The resistance was measured using four leads (one on each leg). The transitions of these devices were broad (dR/dT = 22 Ω/K).

The electrical responsivity (S) was 4300 V/W for the bolometer with the lowest thermal conductance. The optical responsivity for the same device was 2400 V/W indicating an optical efficiency of 45incorporate an absorber into the structure had been made. The measured noise in this device was 3.5 $nV/\sqrt{Hz}$ at 35 Hz, which implies approximately 2.5 $nV/\sqrt{Hz}$ of film noise. The time constant, which ranged from 0.5-1.5 msec, was determined from a Lorentzian fit to the roll-off in optical response.

D/J1-6 PHASE-LOCKED JOSEPHSON JUNCTION OSCILLATORS
1140

S. P. Benz
National Institute of Standards and Technology
325 Broadway
Boulder, CO 80303, USA

The supercurrent of a Josephson junction in the voltage state oscillates at well-defined fundamental frequency f =3D V/ phi-zero , where phi-zero =3D h/2e 2.07 mV/THz is the flux quantum unit and V is the time-averaged (dc) voltage across the junction. Since frequency and voltage are proportional through fundamental constants, the Josephson junction is a perfect voltage-to-frequency transducer, and can be used to make a high-frequency oscillator. The voltage standard, an important application now based on this relationship, is in use in about forty laboratories worldwide. Oscillators using conventional superconductors, such as niobium, can be expected to reach frequencies as high as 2 THz and up to at least 10 THz using high temperature superconductors, such as YBCO. High frequencies, tunability and large bandwidth are some of the important features offered by Josephson oscillators.

Applications of single junction oscillators have been difficult to implement because they have low output power (10 nW) and their low (1-20ohm) impedances do not match to typical high-impedance loads. In order to achieve useful power (less than 0.1 mW) and impedance matching, arrays of phase-locked junctions are needed for most practical applications. One-dimensional (1D) and two-dimensional (2 D) arrays of phase-locked junctions offer potential solutions to these problems. When the junctions in an array are phase-locked, arrays can provide higher output power with narrower linewidths to a matched load impedance. However, phase-locking is difficult because of the complex dynamics associated with these multi-dimensional systems.

Research at NIST has focused on understanding the phase-locking mechanisms in 2D arrays. 2 arrays are less sensitive to nonidentical junctions than 1D arrays. Complete phase locking has been demonstrated in 2D arrays through agreement between theory and experimentally measured power and linewidths . Recent experiments of 10 x 10 arrays coupled to antipodal finline antennas detected a single voltage-tunable peak from 53 - 230 Ghz and measured linewidths as narrow as 10 kHz.

This talk will begin with the simplest oscillator design based on the resistively shunted junction (RSJ) model, followed by a presentation of the recent efforts at NIST toward understanding intrinsic phase locking in 2D arrays. The physical limitations, like junction capacitance, internal and external resonances, and finite array size, that constrain the application of phase-locked oscillators at high power and high frequency will be discussed. Finally, the latest high power results, 0.85 mW at 240 GHz, using a novel shunted tunnel junction fabrication technology will be presented.

F1-1
0900

SPACE DIVERSITY RESULTS USING THE ACTS 20 GHZ BEACON SIGNAL AT THREE SITE LOCATIONS

Julius Goldhirsh[1], Bert H. Musiani[1]
Asoka Dissanayake[2], K. T. Lin[2]
[1]The Johns Hopkins University, Applied Physics Laboratory
Johns Hopkins Road, Laurel, Maryland, 20723-6099
[2]COMSAT Laboratories, 22300 COMSAT Drive
Clarksburg, Maryland, 20871

Space diversity results are described for a three receiver terminal diversity configuration in the mid-eastern part of the United States in which 20 GHz beacon signals are simultaneously received. The sites form a triangle with baselines of approximately 33 km, 30 km, and 45 km. Diversity operation for each of the baselines are respectively referred to as the APL-COMSAT, COMSAT-Mitre (later changed to COMSAT-Stanford Telecom) and APL-Mitre segments. The elevation angle to the satellite is approximately 39°, the satellite azimuth relative to the APL-COMSAT baseline is approximately 66°, and the azimuth relative to the COMSAT-Mitre baseline is 25°.

As of this writing, an analysis of the first three months of measurements (September 1 – November 30, 1994) associated with the APL-COMSAT configuration revealed the following: (1) Assuming a 0.01% probability for diversity operation, 6 dB of rain fade margin is required compared to a required single terminal fade at APL and COMSAT of 21 dB and 16 dB, respectively. Hence, the APL and COMSAT sites experience diversity gains of 15 dB and 10 dB, respectively, at the 0.01% probability. (2) The required monthly fade margins at the 0.01% probability assuming diversity operation was 8 dB for September, 4 dB for October, 6 dB for November, resulting in a 4 dB variability over the three month period. (3) Diversity gains associated with the COMSAT and APL terminals were found to be within 2 dB of one another over the approximate probability range of 1% to 0.01%. (4) Assuming a 10 dB single terminal fade, the month-month variability in diversity gain was 2 dB for APL and 1 dB for COMSAT.

In this paper, corresponding results will be described for a full year period and for the three site configuration.

F1-2
0920

FADE-DYNAMICS STATISTICS ON THE ACTS-VANCOUVER PATH

M. Kharadly, R. Ross and B. Dow
Department of Electrical Engineering
University of British Columbia
2356 Main Mall
Vancouver, B.C., Canada V6T 1Z4

The objective of this paper is to provide some fade-dynamics information on the ACTS-Vancouver path at both of the ACTS frequencies (nominally, 20 and 30 GHz). Specifically, "worst" month and a full year statistics of fade duration and fade slopes, with fade depth as a parameter, are presented. Worst month is defined as in ITU-R recommendation 581. Fade depth is the attenuation in dB, fade duration is the time interval in seconds, during which attenuation is above a specified threshold, and fade slope is the first derivative of attenuation with respect to time at that threshold.

The Vancouver receiver site (at the University of British Columbia) has the coordinates 49° 15′ N latitude and 123° 15′ W longitude, and is 164.6 metres above mean sea level. The elevation angle for the terminal is 29.4° with azimuth 150° clockwise from true north. Vancouver is located in ITU-R rain climatic zone D and on the boundary between rain zones B1 and C in Crane's classification. Few propagation data, and no known Ka-band data, are available for this climate.

The collected raw data, sampled once per second, is in the form of a time series of received beacons signal levels of "arbitrary" reference. These are initially preprocessed using already available software to obtain attenuation relative to clear air, with "bad" data and the effect of ranging tones and calibration periods removed. The data are further processed by using block averages of attenuation to reduce the effect of scintillations on the generated statistics. In this investigation, various block durations are used to ascertain the impact of block averaging on the generated statistics.

F1-3
0940

RESULTS FROM COLORADO STATE UNIVERSITY'S ACTS PROPAGATION EXPERIMENT, DURING JUNE 1995

J. Beaver* V. N. Bringi
Department of Electrical Engineering
Colorado State University
Ft Collins, CO 80523

NASA's Advanced Communications Technology Satellite (ACTS) propagation experiment has been on–going since December 1, 1993. Colorado State University (located in the B2 climatic zone) is one of eight sites located across North America participating in the experiment. The ACTS satellite is in geostationary orbit , near 100°W longitude, and employs two Ka–band beacons, one at 20.185 GHz and the other at 27.505 GHz. The slant path for the CSU ACTS propagation terminal (CSU–APT) is located at 172° in azimuth (from the north) and at an elevation angle of 43°. At Ka-band frequencies attenuation due to rain and tropospheric scintillation can adversely effect satellite communications. With each site located in a different climatic zone the main objective of the propagation experiment is to obtain a statistical data base to quantify the attenuation effects at Ka–band. Data for the period of December 1, 1993 to January 1, 1995 is being processed at CSU and preliminary attenuation statistics for the year will be presented.

In addition to conducting a statistical analysis, CSU is using an S–band radar to obtain Ka–band attenuation estimates. The CSU–CHILL fully polarimetric radar is used to take measurements along the ACTS propagation path. The radar data is used to initialize a radar driven propagation model that incorporates the Mueller and extinction matrices. The CSU–APT is located at the CHILL radar site, just north of Greeley, Colorado. In 1994, two significant weather events were studied. Ka-band attenuation estimates were obtained from S-band radar data for both a "bright band" and a convective case that were measured along the ACTS slant path. These estimates were compared to CSU–APT attenuation measurements with favorable results (J. Beaver, J Turk and V.N. Bringi, Proceedings of 27th Conference on Radar Meteorology, to be published). Currently, a second bright band case is being studied, as well as a second convective case, both of which were observed in June 1995. The results of these two cases will be presented here.

F1-4
1000

ATTENUATION PREDICTION FOR LOW AVAILABILITY SYSTEMS

Glenn Feldhake and Dr. Louis Ippolito
Stanford Telecom
1761 Business Center Dr.
Reston, VA 22909

Demand by small user for VSAT technology has recently experienced a surge. Fixed service systems such as direct digital broadcast as well as mobile applications have all found their way into the hands of small users. This demand has required system designers to develop equipment which fits in the budgets of their new customers. However, the benefit of affordability often comes with the cost of a low fade margin. Low margin or low availability systems (LAS) have many benefits including small hardware size, portability, and affordability. Unfortunately, standard methods for determining propagation losses may not take all the proper considerations into account in the case of LAS.

Traditional methods for determining propagation losses have been developed for larger systems. For systems with an intended availability of 99.99%, the predominant propagation concern is rain. Models such as the Crane global model will provide strong predictions of potential annual losses due to rain for the worst 0.01% of the year. Rain attenuation is then typically added to a gaseous absorption constant based on a mean value for the year.

When considering atmospheric losses experienced by a LAS, attenuations due to low rain rates are more important than losses due to high rain rates. Research at Stanford Telecom (STel) has also found a system may experience losses due to atmospheric absorption in excess of those caused by low rain rates. Because of the sensitivity of LAS to smaller atmospheric effects, it is essential that distributions of atmospheric characteristics be made monthly or seasonally. Data from the Washington, DC area shows how atmospheric characteristics change on a monthly and seasonal basis. Additional research has been performed to determine the differences in typical atmospheric conditions during rainy and nonrainy periods of time. Methods for combining the attenuations due to each effect have been developed. These combinational methods may be implemented to produce best and worst case estimates.

F1-5
1040

FLORIDA ACTS Ka-BAND PROPAGATION MEASUREMENTS

Prof.Henry Helmken*, Rudolf Henning**
*Florida Atlantic University
777 West Glades Road
Boca Raton, Florida 33431
**University of South Florida
4202 Fowler Avenue
Tampa, Florida 33620

The 20.185 GHz and 27.505 GHz beacons aboard NASA's Advanced Communications Technology Satellite (ACTS) have been operational since September 1993. The series of seven strategically placed NASA propagation terminals, distributed in several climactic rain zones, have been collecting calibrated propagation and radiometer data since December, 1993. One of these terminal is located on the Campus of the University of South Florida, Tampa Florida (Lat 28.06, Long 82.42, CCIR rain zone N). At Tampa, the elevation angle to ACTS is 52 degrees.

This paper will focus on the analysis and results of the Florida measurements to date. After several iterations, a consistent set of analysis software has been developed. Data have been processed to remove all known artifacts. Discussion will include an explanation of the methodology used to extrapolate over calibration periods and the selection of an appropriate averaging interval to remove high frequency scintillation effects. The latter item is particularly relevant since part of the primary analysis has been on fade statistics. Results will be presented in terms of Cumulative Distribution Functions (CDF), and the statistics of fade duration and fade slopes vs. fade depths.

Results will be compared with the predictions of the CCIR and Global rain models. Initial results indicate that new rain models may be needed for the Florida subtropical region. The occurrence of long (tens of minutes), deep fades precludes any attempt of fade mitigation via error correcting codes and supports the value of incorporating site diversity in any commercial operation in this region.

A second area of major interest is the analysis radiometer measurements. Results to date indicate that a radiometer tracks the approach and onset of a significant fade better than any individual or combination of weather instruments. Results suggest that a simple broad band radiometer will be very useful in the operation of a site diversity terminal system.

F1-6
1100

ESTIMATION OF TOTAL SLANT PATH ATTENUATION AT 40 AND 50 GHZ FROM ITALSAT BEACON AND RADIOMETER DATA – DAILY EDITING AND MONTHLY STATISTICS

Apolonia Pawlina Bonati *
CNR Centro di Studio per le Telecomunicazioni Spaziali (CSTS)
Politecnico di Milano, DEI, P.za L. da Vinci 32
20133 Milano, Italy

The ITALSAT spacecraft of Italian Space Agency (ASI), in geo orbit at 13° East since January 1991, carries three beacons (18.68, 39.59 and 49.49 GHz) which are received since 1993 at the Spino d'Adda station in northern Italy (45.4° lat., 9.5° long.) run by CSTS (A. Paraboni et al., "First prop. meas. of Italsat Experiment" URSI Comm.F Open Symp. 1992, UK, pp.7.4.1-8) by the ground terminal manufactured by Alenia Spazio (3.5 m Cassegrain off-set, monopulse tracking, 40.9 dB dynamic range for 50 GHz). For the calibration of beacon signals the double-frequency (vapour sensitive 23.8 GHz and water sensitive 31.7 GHz) radiometer set of Elektronik Centralen is used, while three-frequency radiometer set (22.22, 31.65 and 50.2 GHz) of Farran Technology supplies independent data since 1994. The S-band meteorological radar scans along the satellite link and slant plane.

Considering that 1% of outage time is now accepted in some incoming services (e.g. business VSAT's) and that in 40-50 GHz frequency range (temperate climate) such levels correspond to the total tropospheric attenuation of several dB's, the accurate attenuation estimation implies knowing the contributions of light rain, clouds containing liquid water, water vapour and oxygen. The problem was given much attention by OPEX (Olympus Propagation Experimenters) leading to the assessement of algorithms for determining low attenuations from sky noise temperatures measured by a pair of radiometers, and for using these estimates in the removal of non atmospheric effects from beacon data (OPEX 2-nd Workshop, Vol. 1 and Vol.3 Ref. Books, 1994,ESA/WPP 083).

The present work is reporting on the experience with Spino d'Adda Italsat data, dealing with statistics of copolar attenuation in excess of free space, with particular attention to the "clear sky" and low attenuation levels. In this context the removal of unwanted effects may become quite problematic in case of superposition of: (a) long rain events (b) minor receiver malfunctions (e.g. abrupt level changes), (c) no automatic antenna tracking. The paper addresses some practical solutions, illustrating typical situations. Selected events analysis and monthly statistics are presented for climatically representative periods of 1994 and 1995. The relation between directly measured and radiometrically determined attenuations and the frequency scaling for clear sky and light rain conditions are some of enhanced aspects.

The contribution is supported by Italsat Program of ASI.

F1-7 1120 Scintillation Occurrence Statistics at 20 and 27 GHz Observed using the ACTS Beacons in Norman, Oklahoma

Robert K. Crane
School of Meteorology
University of Oklahoma
Norman, OK 73019

Abstract

The ACTS Propagation Terminal equipment continuously collects beacon signal level data and simultaneous radiometer observations at the same frequencies as the beacon measurements. The standard deviation of the beacon signal level within a minute provides an estimate of the intensity of scintillation due to turbulence in the clear atmosphere or of the variations caused by clouds and rain in addition to turbulence during the rest of an observation period. Data recorded over the past two years were separated by meteorological conditions: clear sky, cloudy, or raining, and used to compile empirical distribution functions of the standard deviation estimates.

Under clear sky conditions, power spectra calculated from the time series for each beacon frequency display the shape expected for scintillation produced by turbulence. The intensity of the scintillations show the expected frequency dependence after correction for the additional variations caused by receiver noise. The intensity occurrence statistics are in reasonable agreement with the predictions of the ITU-R (formerly the CCIR) model for scintillation on earth-space paths.

Session G-1, 0855-Tues., CR2-26
IMPACT OF NEAR-EARTH ENVIRONMENT ON COMMUNICATION AND NAVIGATION SYSTEMS
Chairperson and Organizer: Santimay Basu, Phillips Laboratory, GPIA, Hanscom AFB, MA 01731

G1-1 0900 IONOSPHERIC STUDIES USING THE GLOBAL POSITIONING SYSTEM

K. Davies*
NOAA/SEL
325 Broadway
Boulder, CO 80303
G. K. Hartmann
Max-Planck-Institut für Aeronomie
Max-Planck-Str. 2
D-37191 Katlenburg-Lindau, Germany

The Global Positioning System (GPS) is a valuable tool for mapping certain ionospheric characteristics (e.g. total electron content (tec), plasma irregularities, traveling ionospheric disturbances) on global and/or regional scales. These satellites are one of several classes of satellites used in ionospheric research, other classes are: geostationary satellites and low-altitude polar orbit satellites. Studies are underway to compare and combine ionospheric electron contents obtained from these three satellite systems. In order to see whether hourly GPS-tecs can be used to replace the somewhat different hourly Faraday contents we have intercompared geostationary NOAA/GOES2 Faraday tecs with GPS tecs over the interval January 1994 through January 1995 measured at Boulder. These show agreement provided that the receivers are carefully maintained. Because of the several assumptions made in the reduction of measured GPS time delays to vertical tecs, the estimated accuracy of a GPS tec measurement, over an interval of 15 min. is about 2×10^{16} el·m^{-2}. This is about half of the total content in a winter night at low sunspot numbers. Regional contour maps (latitude and longitude) over Central Europe have been constructed using radio time delays from the International GPS Geodynamics Service (IGS). These contour maps will be compared with corresponding maps derived from the low polar orbit NNSS.

The GPS time delays may be used also in the determination of the wet part of the troposphere provided that the ionospheric delays can be removed to at least 99.9 percent, and the motion of the Earth's crust is taken into consideration. Thus users of this method need carefully monitored and validated time series to ensure that their data are free of ionospheric contamination.

G1-2
0920

IONOSPHERIC PROFILING AND TOMOGRAPHY WITH GPS/MET

George A. Hajj and Larry J. Romans
Jet Propulsion Laboratory, California Institute of Technology
4800 Oak Grove Drive
Pasadena, CA. 91109

The effects of the Earth's neutral atmosphere and ionosphere on signals of the Global Positioning System (GPS) present themselves as a source of error for navigation on the one hand and a very effective means for studying the Earth's neutral atmosphere and ionosphere on the other hand. After reviewing the effects of the ionosphere on the GPS signal including group delay, bending and scintillation, we will present how these effects are used to map electron densities and irregularities in the ionosphere. Particularly we will talk about the GPS radio occultation technique and how it provides a powerful method for monitoring the ionosphere.

The idea of using radio occultations to sense the neutral atmosphere and the ionosphere was first used in planetary exploration, and has a heritage of about 30 years. As part of NASA's Mission To Planet Earth program, scientist at JPL (Yunck T. P. et al., Proc. of IEEE position location and navigation symposium, Orlando, 1988) proposed putting a receiver on a Low-Earth Orbiter to track GPS as it occults behind the ionosphere and neutral atmosphere. The bending induced by the atmosphere on the signal is detectable through the extra Doppler shift induced on the signal. Using a spherically symmetric model of the ionosphere in the locality of the occultation, a refractivity profile of the atmosphere can then be obtained from the bending information via an Abel integral transform. This concept was first realized with the launch of Microlab-I in March 1995 by the Orbital Sciences Corporation. This 730 km altitude, 70 deg. inclination satellite carries a flight qualified TurboRogue receiver developed at JPL and collects nearly 100 setting occultations per day. The experiment, known as GPS/MET and managed by the University Corporation for Atmospheric Research, has successfully demonstrated the usability of the GPS radio occultation signals to obtain accurate profiles of temperature in the upper troposphere and lower stratosphere. Profiles of electron densities are also obtained in the ionosphere and are currently being examined to estimate their accuracy by comparing them to models such as the Parametrized Ionospheric Model (PIM) and ionospheric images obtained from ionosondes and incoherent scatter radars.

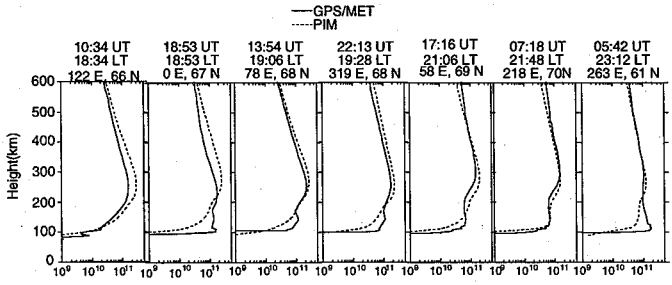

Examples of electron density profiles (e/m^3) obtained with the GPS/MET and PIM for May 4, 1995. Indicated on the figure are geodetic latitude and longitude, universal time (UT) and local time (LT) for each occultation. The profiles are ordered in increasing local time and they correspond to about the same latitude.

Our presentation will explain the radio occultation technique and show results from the GPS/MET experiment in the ionosphere. We will also present results on applying tomographic imaging techniques to the same data type and show 3-D images of electron densities and irregularities in the ionosphere.

G1-3
0940

THE EFFECT OF THE ATMOSPHERE ON SATELLITE SYSTEMS

Allen L. Johnson
Wright Laboratory
WPAFB Ohio 45433-7301

Satellite Communications (SATCOM) is becoming less expensive and more convenient with the introduction of high-power direct broadcast satellites and personal communications systems. Users are attracted by the distance independence aspect and the wireless interface which SATCOM provides. Current and near-term satellite communications and navigation systems operate in a variety of frequency bands, including UHF, L-Band, C-Band, Ku-Band, and EHF.

Many users are unaware of the effect of the atmosphere and troposphere on SATCOM reception and transmission. Atmospheric gasses can cause severe attenuation to the SATCOM signals. Surface inversion layers and elevated inversion layers can cause multipath fading or loss of signal through ducting or trapping. These effects are frequency and elevation angle dependent.

This paper discusses the characteristics of near-earth attenuation, ducting, multipath and the effect such phenomena will have on communications and navigation systems. Mitigation techniques to overcome the detrimental effects will be discuss for several communications and navigation systems.

G1-4
1000

IONOSPHERIC EFFECTS AND MITIGATION IN RF TRANS-IONOSPHERIC SYSTEMS

Gregory. J. Bishop
Phillips Laboratory, U. S. Air Force Materiel Command
Geophysics Directorate, Ionospheric Effects Division
29 Randolph Road
Hanscom AFB, MA 01731-3010

Andrew J. Mazzella and Susan Rao
NorthWest Research Associates
300 120th Avenue NE
Bellevue, WA 98005

All RF systems that link ground/air and space at or above 100 km altitude, and operate at frequencies up to 4 Ghz are affected by the ionosphere. Ionospheric scintillation can cause message errors in satellite communication links and reduced availability of satellites for GPS navigation. Ionospheric range errors can result in position errors for GPS single-frequency users, and loss of accuracy or resolution in surveillance. The determination of whether the ionosphere will generate significant system degradation involves both environmental and system parameters. Mitigation, if possible, must be adapted to the characteristics and mission of each operational system. Two-frequency GPS navigation performs ionospheric measurement for range error mitigation, subject to several error sources. Procedures are now becoming available to mitigate most of these errors. Single-frequency GPS, on the other hand, must depend on statistical models or adjunct differential techniques for ionospheric range error correction. Now a new technique promises significant capability in single-frequency GPS measurement of ionospheric range error without the necessity to assume an ionospheric model or profile. Ionospheric scintillation can reduce availability of satellites for maintaining GPS navigation integrity, but GPS navigation systems can be designed to monitor signal quality and employ adjunct inertial systems as needed. For some communication systems special equipment and signal formats can reduce message errors. Local measurement-warning systems can also be used to monitor ionospheric disturbances, and identify satellite links that remain clear. When linked to a scintillation model, such warning systems can provide regional capability to identify "windows" for good operation of both surveillance and communication. Similarly, measuring systems that monitor ionospheric range error may be linked to region-adapted ionospheric models for generating system corrections. For systems with a wider mission, corrections may be obtained from global networks of ionospheric sensors providing real-time input to global ionosphere and space weather models.

G1-5
1040

CHANNEL PROBE MEASUREMENTS OF SPREAD F EFFECTS ON A TRANSEQUATORIAL HF PATH

T. Joseph Fitzgerald
Space and Atmospheric Sciences Group
MS D466
Los Alamos National Laboratory
Los Alamos, NM 87545

The ionospheric phenomenon called Equatorial Spread F encompasses a variety of effects associated with plasma irregularities occurring in the post-sunset and nighttime ionosphere near the magnetic equator. These irregularities can seriously degrade the performance of systems which involve either of necessity or inadvertently radio propagation through the equatorial ionosphere. An example of such a system is Over-the-Horizon (OTH) radar which operate in the high-frequency (hf) band and use ionospheric reflection for forward and backscatter propagation to ranges of thousands of kilometers.

In January, 1994 Los Alamos participated in a campaign to measure Spread F effects on OTH propagation from the United States looking towards South America in conjunction with local diagnostics in Peru. During the campaign Los Alamos fielded a 1600 km bistatic path between Piura, Peru, and Arequipa, Peru; the one-hop reflection region for this path was near the magnetic equator. We obtained four types of measurements: an oblique ionogram between Piura and Arequipa every three minutes; Doppler spread and spatial correlation for a single frequency cw path between Piura and Arequipa; Doppler spread, time-delay spread, and spatial coherence for a 10 kHz bandwidth path between Piura and Arequipa; and Doppler spread and time-delay spread for the one-way path between the AVA radar in New York and Arequipa, Peru. We describe the diagnostic experiments that we carried out and summarize the statistics of Doppler spread, time-delay spread, and spatial coherence that we observed.

G1-6
1100

CORRELATION OF SPORADIC E WITH GPS PHASE MEASUREMENTS

T. L. Gaussiran II, D. S. Coco D. S. Coco*
Applied Research Laboratories
The University of Texas at Austin
P.O. Box 8029
Austin, TX 78713

Sporadic E events in a mid-latitude, summer ionosphere are correlated with small scale variations in total electron content (TEC) derived from GPS phase measurements. It is believed that the 'patchy' nature of the sporadic E structures causes the variations in the TEC as the satellite-to-receiver line-of-sight crosses the patches. Even though the bulk of the electron density is in the F region, this region is relatively smooth compared to the E region when sporadic E is present.

In this study, the sporadic E events are identified from ionograms collected from an ionosonde that was operated on a continual basis throughout the summer. The TEC variations are derived from dual-frequency GPS phase measurements, which provide very precise, biased measurements of the TEC. A sporadic E detection algorithm was developed for the TEC measurements by investigating the TEC signatures that occurred during sporadic E events. This algorithm uses a high pass Butterworth filter with a cutoff frequency corresponding to 10 min to isolate the small scale TEC variations. The standard deviation of the filtered TEC is then calculated using a sliding 20 min window. This standard deviation, σ_{E_s}, is used as a measure of the small scale variations (less than 1 km) in TEC in the E region. The value of σ_{E_s} is found to be correlated with the presence of sporadic E .

This study indicates that GPS phase measurements may be able to be used to predict sporadic E in situations where an ionosonde is not available. Limitations and potential improvements to this technique are also discussed.

G1-7
1120

f_oF_2 CORRELATIONS WITH GPS DERIVED TEC

T. L. Gaussiran II, C. Coker T. L. Gaussiran II*
Applied Research Laboritories
The University of Texas at Austin
P.O. Box 8029
Austin, TX 78713

f_oF_2 values are correlated with total electron content (TEC) measurements for various locations. Using f_oF_2 values extracted from ionosonde data correlations are sought with GPS measured TEC to estimate f_oF_2. To correlate TEC with f_oF_2 an accurate absolute TEC value must be obtained. To obtain the accurate measurement needed for this correlation both range and phase data are utilized.

Data are presented from various sites and events of interest. Correlations are shown between TEC and f_oF_2. The data sets offer an interesting look at the potential for a large scale data collection project.

Mid-latitude data predications of f_oF_2 utilizing a simple time dependent slab thickness model indicate that the error in the prediction of $foF2$ from TEC is $\sigma(f_oF_2) = 1.2$ MHz. If the error is attributed to a mismeasurement of TEC it would imply an error of 5 TECU (1 TECU = 10^{16} electrons / meter^2). However, estimates for the error of phase averaged GPS TEC are 1–3 TECU. Even considering that not all of the electron density resides in the F2 region and that in fact about 5% is accounted for in the E region still leaves more error than is expected. In fact, the obvious problem is that f_oF_2 is sensitive to the maximum electron density where TEC is an integrated quantity. So any distribution of this sort must be smeared due to the fact that the ionosphere has a more complicated profile. Thus it is expected that any correlation of these two data sets would have an error larger than what is expected from considering only measurement errors of TEC.

G1-8
1140

SPECTRAL EFFECT OF IONOSPHERIC IRREGULARITIES ON THE SCINTILLATION OF TRANSIONOSPHERIC SIGNALS*

Ruthie Lyle, S. P. Kuo, and Joe Huang
Weber Research Institute, Polytechnic University
Route 110 Farmingdale, NY 11735

A quasi-particle theory has been developed to study wave propagation and scattering in plasma having a two dimensional density modulation on a uniform background.[1] The method treats wave as a group of quasi-particles having a Wigner distribution and colliding with the periodic density modulation. In this work we apply this theory to analyze the spectral effect of equatorial ionospheric irregularities on the scintillation of transionospheric signals. The bottomside sinusoidal (BSS) irregularities found in the equatorial F region are the scatters, modeled by a two dimensional periodic density modulation. The dependences of the scintillation index S_4 of the transionospheric electromagnetic signal on Δk for three different wave frequencies: 250MHz, 1541MHz, and 3954MHz are evaluated. In each frequency case S_4 is optimized by choosing the density modulation's longitudinal and transverse scale lengths corresponding to the frequency dependent Fresnel size. The parametric dependences of S_4 on the longitudinal and transverse scale lengths of the density irregularities are also presented. The results show that S_4 depends strongly on $\Delta k/k$ and signal frequency. As expected, S_4 decreases with the signal frequency. Moreover, S_4 also decreases, in each frequency case, with $\Delta k/k$ to a minimum, therewith exhibiting a damped oscillation. At the minimum, S_4 reduces to a negligibly small value almost independent of the longitudinal scale length of the modulation. Since the minimum location of S_4 is also frequency dependent, measurements of S_4 with different signal frequencies can be used to clarify if a small S_4 value is the result of a low level of irregularities, or irregularities with a large spectral width.

* *Work Supported by the AFOSR*

1. A. Y. Ho et al., Radio Science, 29(5), 1179-1186, 1994

Session H-1, 0855-Tues., CR2-6
LABORATORY SIMULATIONS OF SPACE PLASMAS
Chairperson: M.E. Koepke, Dept. of Physics, West Virginia Univ., Morgantown, WV 26506
Organizers: M.E. Koepke; and M.C. Lee, MIT Plasma Fusion Center, Cambridge, MA 02139

H1-1
0900

THE PARALLEL VELOCITY SHEAR INSTABILITY IN A MAGNETIZED PLASMA

N. D'Angelo
Department of Physics and Astronomy
University of Iowa
Iowa City, IA 52242

A review is given of the work done over many years by the author and several co-workers on the instability produced in a low-β plasma by shear in the ion flow velocity parallel to the magnetic field lines.

After a brief discussion of the early theoretical (N. D'Angelo, *Phys. Fluids*, **8**, 1748–1750, 1965) and experimental (N. D'Angelo and S. von Goeler, *Phys. Fluids*, **9**, 309–313, 1966) work, the relevance of the instability to certain space physics situations is examined. These include: a) wave activity at the equatorward border of the earth's polar cusp, and b) wave motion in ionized (type I) comet tails, with formation of helical structures.

Next, more recent theoretical work is summarized dealing with the instability in plasmas containing an appreciable fraction of negative ions and in dusty plasmas.

It is found that for ratios m_-/m_+ between the mass of the negative ions and that of the positive ions less than approximately 100, the presence of the negative ions has a destabilizing effect, thus lowering the value of the critical shear.

For dusty plasmas with negatively charged dust grains (for which $m_-/m_+ \rightarrow \infty$) the dust has, instead, a stabilizing effect, thus raising the value of the critical shear.

Results are presented from a recent experiment performed in a double-ended Q-machine, in which the presence of SF_6^- negative ions in a K^+ plasma makes the plasma more unstable to the velocity shear instability, as expected from the earlier theoretical work.

Finally, plans are briefly discussed for a similar experiment to be performed in a Q-machine K^+ plasma with negatively charged dust grains.

H1-2
0940

POTENTIAL-DRIVEN ION-CYCLOTRON OSCILLATIONS IN A PLASMA

Noriyoshi Sato and Rikizo Hatakeyama
Department of Electronic Engineering
Tohoku University
Sendai 980-77, Japan

Phenomena regarding electrostatic ion cyclotron oscillations have been considered to play an important role in ionoshperic and magnetosheric processes. Their first clear-cut observation was performed in a laboratory plasma, where they were driven by applying a positive potential to a small electrode immersed in a single-ended Q machine with uniform magnetic field. Since an electron current is generated in the plasma column along the magnetic field under this configuration, the oscillations observed were ascribed to current-driven electrostatic ion cyclotron instability predicted by a plasma kinetic theory.

However, experimental results in nonuniform magnetic fields called this explanation into question, pointing out an importance of two-dimensional potential structure near the disc plate. Recently, measurements have been performed on ion cyclotron oscillations induced by small emissive disc plate floating in a magnetized collisionless plasma column. The oscillations are oberved when the emission is so large that the disc potential is higher than the plasma potential. This means that the oscillations are generated even in the absence of dc electric current passing through the plasma column if the disc potential is positive with respect to the plasma potential. The situation is in contrast with the case of applying positive potentials to a small cold disc plate mentioned firstly.

Concerning this historically-controversial problem a new mechanism for the generation of the electrostatic ion cyclotron oscillations has been proposed. The mechanism is based on a direct plasma response to the applied potential, which gives rise to a two-dimensional relaxation oscillation in a magnetized plasma. The model of this two-dimensional potential-driven oscillation is well consistent with main features of the oscillations induced by both the disc plates described above under uinform and nonuniform configurations of magnetic field.

H1-3
1020

IEDD ION-CYCLOTRON INSTABILITY EXPERIMENTS IN THE WVU Q-MACHINE*

James J. Carroll III, M.E. Koepke, W.E. Amatucci, C.A. Selcher, and M.W. Zintl
Department of Physics, West Virginia University
Morgantown, WV 26506-6315.

The inhomogeneous energy-density driven (IEDD) instability (Ganguli *et al.*, Phys. Fluids, 31, 823, 1988) is driven by transverse velocity shear commonly caused by a transverse, localized, electric field. The combination of shear and magnetic field-aligned current (FAC) destabilize IEDD waves in the ion-cyclotron frequency range that propagate in the transverse-flow direction, and can be broadband in frequency. Laboratory experiments in the WVU Q-machine on the influence of transverse velocity shear on the current-driven electrostatic ion-cyclotron (CDEIC) instability (Motley and D'Angelo, Phys. Fluids, 6, 296, 1963) have observed a transition to the IEDD ion-cyclotron instability at values of FAC significantly (~50%) below the critical value for CDEIC waves, with experimentally determined values of $k_\theta\rho_i = 0.4$, $k_z/k_\theta = 0.1$, and a peak in the oscillation amplitude in the region of large shear (Koepke *et al.*, Phys. Plasmas, 2, 2523, 1995). The transition between the two instabilities is related to the ratio of the azimuthal and axial Doppler shifts $R=k_\theta v_E/k_z v_d$ where k_θ, k_z, v_E, and v_d are the wave vectors and particle flows across and along the ambient magnetic field, respectively. Experimentally measured values of the shear-layer thickness, normalized to the ion-gyroradius, vary from 0.3 to 1.5 as the ambient magnetic field is increased. A transition from CDEIC waves to IEDD waves at large values of magnetic field suggests the possibility of a "filamental enhancement" process that increases the IEDD growth rate. This is in contrast to the previously established "filamental quenching" process (Cartier *et al.*, Phys. Fluids, 28, 432, 1985) that decreases the CDEIC growth rate when the FAC channel radius normalized to the ion gyroradius decreases to order unity. In preparation for the next series of experiments on transverse-velocity-shear-driven waves, the WVU Q-machine has been upgraded. The device is expected to expand the observed frequency range of shear-driven fluctuations considerably. Optical techniques will be employed to investigate the heating of plasma ions interacting with velocity-shear-driven waves.

* Research supported by the Office of Naval Research and the National Science Foundation.

H1-4
1040

VELOCITY-SHEAR-DRIVEN ION-CYCLOTRON WAVE EXCITATION**

W. E. Amatucci[a]* D. N. Walker D. Duncan[b] J. A. Antoniades
G. Ganguli V. Gavrishchaka[c] M. E. Koepke[c] J. H. Bowles[b]
C. J. Pollock[d]
Plasma Physics Division, Code 6756
Naval Research Laboratory
Washington, DC 20375

In situ ionospheric observations indicate a correlation between transverse ion energization and velocity-shear layers believed to arise from naturally occurring transverse, localized, dc electric fields. The plasma response to the presence of narrow velocity-shear layers is the subject of an experimental investigation underway in the Naval Research Laboratory's Space Physics Simulation Chamber (SPSC). Sheared $\mathbf{E} \times \mathbf{B}$ flow is induced within the SPSC plasma column by application of unequal potentials to sections of a highly transparent grid structure made from eleven concentric, coplanar, conducting ring electrodes. This structure produces a controllable transverse, localized, dc electric field with scale length on the order of an ion gyroradius which extends axially into the plasma column, while inducing minimal magnetic-field-aligned current. Ion-cyclotron waves which propagate in the direction of $\mathbf{E} \times \mathbf{B}$ rotation have been observed within the narrow velocity-shear layer created by this electric field. The oscillation frequency varies with the strength of the applied electric field, ranging from $1.5\Omega_i$ to $4\Omega_i$. The measured azimuthal and axial wavenumbers are $k_\theta = 0.11$ cm^{-1} and $k_z = 0.0045$ cm^{-1}, respectively. These ion-cyclotron waves have been destabilized at values of magnetic field-aligned electron drift velocities as low as two times the ion thermal speed, well below the critical drift velocity necessary for onset of the current-driven electrostatic ion-cyclotron instability. Comparison with theoretical predictions indicate that the observed waves result from the reactive Inhomogeneous Energy-Density Driven Instability. Ion heating associated with these waves will be measured with the Thermal Electron Capped Hemisphere Spectrometer (TECHS), a space qualified 2D (pitch angle/energy) spectrometer developed at NASA's Marshall Space Flight Center and suitably modified for ion diagnostics.

** Work supported by ONR.

[a]NRCPostdoc, [b]Sachs Freeman Assoc., Landover MD, [c]Department of Physics, West Virginia University, Morgantown, WV, [d]Marshall Space Flight Center, Huntsville, AL.

H1-5
1100

RADIAL ELECTRIC FIELD EFFECTS ON LOW-FREQUENCY INSTABILITIES IN A MAGNETIZED PLASMA COLUMN

Roman W. Schrittwieser
Institute for Ion Physics, University of Innsbruck,
Technikerstr. 25, A-6020 Innsbruck, Austria

A brief review is given on the influence of either an extended or localized radial electric field on the magnetized collisionless plasma column of a Q-machine. The behaviour of two typical low-frequency instabilities and the global properties of the plasma column are discussed. These instabilities are the **p**otential **r**elaxation **i**nstability (PRI) (S. Iizuka et al., *J. Phys. Soc. Japan* **54**, 2516, 1985) and the **c**ollisionless **d**rift **i**nstability (CLDI) (P.A. Politzer, *Phys. Fluids* **14**, 2410, 1971).

When a radial electric field, E_r, is applied by biasing an isolated metallic cylinder around the plasma column, the PRI can either be quenched or amplified, depending on the direction of E_r. This effect can be explained by the radial transport of ions from the plasma column towards the cylinder, which is either prevented or enhanced respectively. This investigation has shown that the high positive plasma potential, which prevails during the maximum of the oscillation, can lead to a considerable radial loss of ions whereas in the one-dimensional case these ions move partly back to the plasma source (S. Iizuka, R. Schrittwieser, *Plasma Phys. Contr. Fus.* **35**, 77, 1993).

If the radial cylinder is replaced by just a limiter, inserted about 30 mm in front of the plasma source (M. Zimmerling, R. Schrittwieser, *Phys. Lett. A* **205**, 189, 1995), a positive or negative bias of this limiter leads also to a damping or an amplification of the PRI, respectively. Thus a local radial electric field suffices to obtain a similar effect as an extended E_r. The most plausible explanation is that the thermal barrier (a potential dip at the low-potential side of a travelling double layer), which causes the current limitation during the minimum of the PRI cycle, is either filled up with ions or emptied, respectively, due to E_r. These findings may also be relevant for the so-called magnetoelectric confinement of plasma that is increasingly discussed and investigated in fusion experiments.

For higher negative biases of the limiter the diameter of the plasma column can be decreased until the plasma is completely quenched. For smaller positive biases only the radial density gradient and the radial electric field are affected and the CLDI at the plasma column's edge changes its frequency and band-width.

H1-6
1120

NONAXISYMMETRIC INSTABILITY INDUCED BY LARGE RADIAL ELECTRIC FIELD IN A COLLISIONLESS PLASMA

Rikizo Hatakeyama and Noriyoshi Sato
Department of Electronic Engineering
Tohoku University
Sendai 980-77, Japan

According to the observations above the Earth's auroral oval, the electrostatic potential appears to have a three-dimensional (3D) profile with U- (or V-) shaped double-layer (DL) structure, where the electric field perpendicular to the magnetic field is accompanied with electrostatic fluctuations near the ion cyclotron frequency $\omega_{ci}/2\pi$. For the purpose of contribution to a better understanding of such geospace processes we have performed a laboratory experiment on electrostatic instability induced by large radial electric field, which is also related to transverse-velocity shear driven instabililty discussed recently.

The 3 D DL is generated under a strong magnetic field B by applying a potential difference between two plasma sources with different diameters. The 3D structure is characterized by a strong radial electric field E_r on the low-potential side. The position and shape of the U-shaped DL are controlled by the formation of mirror configurations of magnetic field. The DL is found to induce electrostatic oscillations with frequencies above $\omega_{ci}/2\pi$ and its harmonics, in contrast to a 1D DL.

A peak of the fluctuations is found at the position of the maximum radial potential slope on the low-potential side. On the other hand, the fluctuations are negligible small on the high-potential side. No phase change is observed along the amgnetic field. The fluctuations, however, propagate azimuthally with mode number m =1, 2, 3, ... in the direction of $\mathbf{E}_r \times \mathbf{B}$. The phase difference between density and potential fluctuations is about 180° , indicating a flute-type instability. By varing B on the high-potential side and/or on the low-potential side of the DL, the frequency is found to depend only on B on the low-potential side where the strong E_r is formed in the plasma. In our experiment the instabillilty is observed in the wide range of $(E_r/B)/v_i = 2.9-81.0$ (v_i: ion thermal speed), where the radial ion motion is quite important. These values of E_r are different from those for a theoretical-predicted branch of plasma oscillation driven by velocity shear, $(E_r/B)/v_i = 2.8 - 3.2$.

H1-7
1140

GENERATION OF ARTIFICIAL PLASMA LAYERS IN THE UPPER ATMOSPHERE BY GROUND-BASED HIGH POWER MICROWAVES: SIMULATION AND CHAMBER EXPERIMENTS

S.P. Kuo* J. Kim
Weber Research Institute
Polytechnic University
Framingdale, New York 11735
M.C. Lee
MIT Plasma Fusion Center
Cambridge, MA 02139
P.A. Kossey
Ionospheric Physics Division
Phillips Laboratory
Hanscom AFB, Massachusetts 01731

Numerical simulations have been performed to investigate the propagation characteristics of an intense microwave pulse such as intensity, frequency, pulse width and shape in the air. An empirical relation: $P^3W = C_0 =$ constant is found, where P and W are the incident power and width of the pulse, respectively. C_0 depends on the percentage of the pulse energy transferred from the ground-based source to a destined position in space. Our results show that when a single unfocused microwave pulse is transmitted upwrad from the ground, the maximum electron density produced at the altitu of, for example, 50 kilometers is below 10^6 cm due to the tail erosion effect. Different approaches using repetitive pulses and a focused beam are also examined. These two approaches can increase the maximum electron density by no more than one order of magnitutde. Further, a scheme using two obliquely propagating pulses that intersect at a selected height, for instance, 50 kilometers is considered. It is found that the generated electron density at the lowest intersecting position can be enhanced by more than two orders of magnitude. Plasma chamber experiments have been conducted to demonstrate this scheme. Our experiments show that a set of parallel plasma layers generated by two intersecting microwave pulses have high plasma density to serve effectively as a Bragg reflector for a potential application to the over-the-horizon (OTH) communications.

K1-1
0900

INTRODUCTION TO BIOELECTROMAGNETIC INTERACTIONS

James C. Lin
University of Illinois at Chicago
M/C 154, Room 1030 SEO
851 S. Morgan Street
Chicago, IL 60607-7053

The number of devices and systems that rely on electromagnetic fields and waves continues to expand and multiply for communication, security, industry, medicine and entertainment. Consequently, there has been considerable concern about the possible adverse health effect from exposure to the electromagnetics fields and waves that originate from these devices and systems. This situation is especially acute in the United States and some western European countries. Many national and international standards organizations, governmental bodies, and health authorities have promulgated or are considering recommendations of standards or guidelines to protect the public from excessive exposure. In the meantime, scientists are continuing their investigations on the responses of the biological system to these forms of radiant energy and the manufacturers are contemplating new designs and techniques that may mitigate the exposure. This paper will present some of the current uses of electomagnetic energy in biology and medicine and summarize recent progress in the effort to define more closely the biological effects of electromagnetic fields and waves using in vitro and in vivo methodologies. It will review mechanisms currently under consideration and highlight dosimetric measures to quantitate the absorbed energy. The discussion will include results from human studies and laboratory tests. The frequency will range from low frequencies to radio and microwave frequencies including the mobile telephone region of the spectrum.

National Radio Science Meeting (Boulder, CO), Jan 1996

K1-2
0920

DOSIMETRY STUDIES OF HUMAN EXPOSURE TO PORTABLE TELEPHONE FREQUENCY FIELDS

Q. Balzano, Ph.D., Oscar M. Garay
Florida Corporate Electromagnetic Research Laboratory
Motorola, Plantation, Florida 33322

The paper presents the methodologies used in the measurements of E and H fields in the immediate vicinity of mobile telephones in free space and in human simulating phantoms. The Methodologies require accurate calibration of E and H-field probes using TEM cells, radiating horns and planar phantoms of specific dielectric characteristics. Simultaneous temperature increase and field intensity measurements are required for the calibration of E-probes in simulated tissue.

Finally the results of Specific Absorption Rate (SAR) measurements collected for different size human phantoms will be presented using a variety of mobile phone devices. The dosimetry, the position and distance of the RF currents on the antenna and the radio case with respect to the body of the simulated user are the parameters that determine the values of SAR of the exposure. The dimension of the exposed organ (e.g. the size of the head of the user) is also a factor in the distribution of SAR within that organ. A typical presentation of the dosimetric results is shown in the following figure, plotting the SAR values at the depth of 0.4 cm in the simulated brain of an adult head.

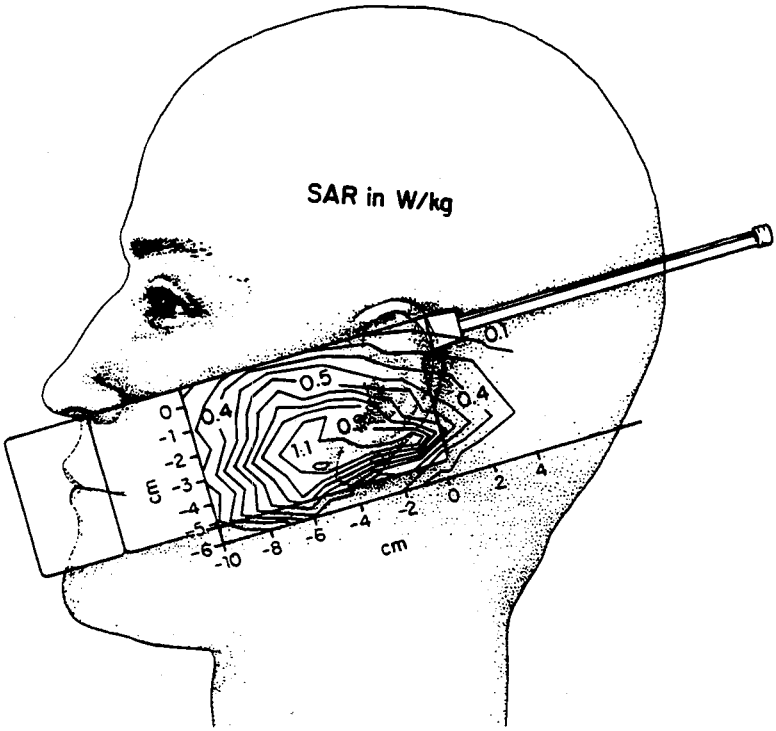

National Radio Science Meeting (Boulder, Co), Jan. 1996

K1-3
0940

BIOLOGICAL EFFECTS OF RADIO FREQUENCY FIELDS

Michael R. Murphy and James H. Merritt
Radiofrequency Radiation Division
Occupational and Environmental Health Directorate
U. S. Air Force. Armstrong Laboratory
Brooks AFB, TX 78235-5324

Radio frequency (RF) fields are increasingly omnipresent in our home, workplace, recreational, and medical environments. Many of the pleasures, conveniences, and necessities of modern society depend on the emission of RF fields. Yet, the fields that carry communications, cook food, and help predict the weather can also affect you. What are these effects? Are they hazardous?

When radio frequency (RF) fields impact biological substance, energy is deposited. The location and amount of energy deposition depend on the characteristics of the field (e.g., frequency, duration, and power density) as well as the characteristics of the biological entity (e.g., size, shape, orientation to the field, dielectric properties of the tissue components, and passive and active thermoregulatory processes). A special field of scientific study, bioelectromagnetics, has evolved in pursuit of knowledge on the biological effects of RF and other electromagnetic fields and, thousands of scientific papers have been published on the subject. Biological effects of RF fields can be roughly divided into two categories, viz., thermal, in which a measurable and somewhat general temperature rise occurs, and non-thermal (also called athermal or specific), in which interaction with biological molecules or microstructure might cause biological effects without measurable heating. Controversy continues to exist over the importance or even existence of many purported non-thermal RFR field effects. Current safety standards for human exposure to RF fields recognize a threshold for effects based upon thermal considerations.

Most of the experimental studies on the biological effects of RF fields utilize animal models or cellular preparations and involve acute exposures. Exposures over a large fraction of an animal's lifetime are much rarer, mainly due to the large expense of such long-term studies. Nevertheless, several landmark investigations have been carried out, with essentially negative results. These, and other studies, will continue to be conducted in laboratories around the world in order to fully understand the effects of exposure to RF fields. At present, however, there is no persuasive evidence that exposure at or below the established standards is harmful to human health.

National Radio Science Meeting (Boulder, CO), Jan 1996.

K1-4
1020

DOSIMETRY AND MECHANISMS OF HUMAN EXPOSURE TO POWER LINE FREQUENCY FIELDS

Charles Polk, Professor Emeritus
Department of Electrical and Computer Engineering
University of Rhode Island
Kingston, RI 02881-0805

For the dosimetry of drugs it is generally sufficient to clearly characterize the agent by giving its chemical composition and then to specify the quantity administered and the manner of administration (e.g., in solid form as a pill, dissolved in liquid, or intravenously). Dosimetry of electric and magnetic fields is in many ways more complex because it requires specification of many more parameters. First, at low frequencies (as opposed to microwave frequencies), electric and magnetic fields can to a high degree of approximation be applied separately, and therefore specifying whether the applied field is electric or magnetic is essential. Second, because electric and magnetic fields are vectors, it is essential to specify not only magnitudes but also field directions with respect to directions characteristic for the culture vessel (e.g., axial or transverse) or the exposed animal (e.g., dorsal-ventral, head-tail, etc.). For electric fields the shape of the exposed object greatly affects induced currents, and for magnetic fields, cross-sectional dimensions of the culture vessel or animal also must be specified. In addition, for both electric and magnetic fields one must know whether the exposed object was electrically insulated or electrically grounded.

Consideration is given to whether biological effects of weak ELF fields are due to the magnetically induced electric field or are a direct consequence of the magnetic field. The energies corresponding to magnitudes of electric and magnetic fields that are reported to produce a biological response are compared. Specific mechanisms for "direct" magnetic field-to-biochemical process transduction are discussed briefly, particularly motion of "magnetosomes", "parametric resonance" and magnetic field regulation of reaction rates in free radical processes. Such regulation is a consequence of Pauli's exclusion principle. It is shown that a static magnetic field should enhance rather than submerge the effect of a weak alternating magnetic field in a magneto-kinetic reaction that influences a frequency dependent (oscillatory) biological process.

National Radio Science Meeting (Boulder, CO), Jan. 1996

K1-5
1040

EMF & CANCER: EPIDEMIOLOGIC EVIDENCE TO DATE

Leeka I. Kheifets, Ph.D
Electric Power Research Institute
National Radio Science Meeting, Boulder, Colorado
January 9-13, 1996

The results of fifteen years of epidemiologic studies concentrating on the possible health risks (particularly cancer risks) associated with exposure to power frequency electric and magnetic fields (EMF) have been equivocal. While many studies suggest that EMF could pose a health risk, the risk estimates are low, and their confidence intervals often include no effect. However, if real, even a small risk of a prevalent exposure could have major public health implications. In this presentation I will review the epidemiologic studies that have examined residential exposure and cancer in children as well as those of occupational exposures and adult cancer.

Although there have been more than 100 epidemiologic studies in this area, many early studies of EMF were too limited in design and scope to do more than generate hypotheses. The number of epidemiologic studies with the methodologic wherewithal to test hypotheses is growing. Among the improvements in this new generation of studies are: a priori specification of hypotheses-- to better distinguish between chance occurrence and real association; examination of specific cancers, which should allow for the identification of agents specific to the etiology of a particular cancer; larger numbers of subjects to improve the precision of risk estimates; improved exposure assessment to reduce misclassification of exposure; and evaluation of a variety of potential confounders to minimize the possibility of a spurious association.

Unfortunately, the improvements in study quality have not led to a concomitant improvement in the clarity of our picture of the relationship between EMF and cancer risk. The discussion will include comments on what we have learned and why studying EMF exposure poses unique and substantial difficulties.

Session B-1, 1335-Tues., CR1-9
RANDOM AND ROUGH SURFACES
Chairperson: A.A. Maradudin, Dept. of Physics and Astronomy, Univ. of California, Irvine, CA 92717

B1-1
1340

X-RAY SCATTERING FROM A RANDOMLY ROUGH SURFACE

T. A. Leskova
Institute of Spectroscopy
Troitsk
Russia
A. A. Maradudin*
Department of Physics and Astronomy
Irvine, CA 92717
USA

When x-rays are scattered at near grazing incidence from a multilayer structure whose lamina are parallel to its surface, and whose surface and interfaces are randomly rough, the dependence of the mean differential reflection coefficient on the scattering angle displays wings on either side of the specular peak. These wings, sometimes called Yoneda bands, do not appear to have a theoretical explanation, until now. In this paper, on the basis of two simplifying, but not essential, assumptions, we present a simple theoretical explanation of these bands. The assumptions are that the multilayer nature of the scattering medium is not crucial to the existence of these bands, and that the surface of the scattering medium can be regarded as one-dimensional, with the plane of incidence normal to the generators of the surface. We thus consider the scattering of a p-polarized plane wave from a one-dimensional, randomly rough metallic surface in contact with vacuum. The reduced Rayleigh equation for the scattering amplitude is obtained, and is then solved to first nonzero order in the small parameter of the theory, viz. $\epsilon(\omega) - 1$ where $\epsilon(\omega)$ is the dielectric function of the metal. This difference for x-rays has values in the range from 10^{-6} to 10^{-4}. The resulting solution is valid to all orders in the surface profile function. The mean differential reflection coefficient can be calculated analytically when the surface profile function is a zero-mean, stationary, Gaussian random process, with a Gaussian power spectrum. If the transverse correlation length of the surface roughness is large enough, say several hundred angstroms, the resulting angular dependence of the scattered intensity displays wings on both sides of the specular peak that closely resemble the Yoneda bands.

B1-2
1400

RESONANT SCATTERING OF ELECTROMAGNETIC WAVES FROM GROOVES AND RIDGES ON METALLIC SURFACES

T. A. Leskova
Institute of Spectroscopy
Troitsk
Russia
A. A. Maradudin*
Department of Physics and Astronomy
Irvine, CA 92717
USA E. R. Méndez
CICESE
Ensenada, Baja California
Mexico

It is well known that an isolated protuberance or indentation on an otherwise planar surface of a metal in contact with vacuum supports electromagnetic surface shape resonances. These are electromagnetic excitations that are localized in the vicinity of the surface perturbation. They are characterized by discrete frequencies that depend on the shape of the protuberance or indentation, and are complex due to the radiative damping of these excitations. Until now no direct experimental evidence for the existence of electromagnetic surface shape resonances has been provided, although they are believed to play an important role in surface enhanced Raman scattering and in the enhancement of second harmonic generation in reflection from a rough metal surface. In this paper we present the theory underlying a method for observing these resonances experimentally. We consider a vacuum-metal interface on which an isolated ridge or groove has been ruled. The equation of the surface is $x_3 = \zeta(x_1) = A\exp(-x_1^2/R^2)$; the region $x_3 > \zeta(x_1)$ is vacuum; the region $x_3 < \zeta(x_1)$ is a metal characterized by the dielectric function $\epsilon(\omega) = 1 - (\omega_p^2/\omega^2)$, where ω_p is the plasma frequency of the conduction electrons. On the assumption that the x_1x_3-plane is the plane of incidence, the frequencies of p-polarized electromagnetic surface shape resonances are calculated as functions of the ratio A/R by both the Rayleigh method, and by an exact method based on Green's second integral identity. With the frequencies of these resonances determined we next examine the scattering of a beam of p-polarized light incident normally on this surface. As the frequency of the incident light is tuned through the value that corresponds to the real part of the frequency of one of these resonances, the angular dependence of the intensity of the scattered light undergoes a significant rearrangement due to the excitation of that surface shape resonance. This rearrangement should be clearly visible in the results of an actual experiment.

B1-3
1420

PROPAGATION MODELING OVER TERRAIN BY COORDINATE TRANSFORMATION OF THE PARABOLIC WAVE EQUATION

D. J. Donohue
Applied Physics Laboratory
Johns Hopkins University
Johns Hopkins Road
Laurel, MD 20723

We are investigating various techniques for incorporating a rough boundary within a parabolic equation based propagation model. As a first approach, we examine a coordinate transformation (A. Beilis and F. D. Tappert, J. Acoust. Soc. Am. 66, 811, 1979) that maps the rough boundary to a flat surface. The fluctuations due to surface roughness are then incorporated into a modified refractivity term containing the second derivative of the surface height. In addition, a new phase term is introduced into the envelope of the field. The purpose of the coordinate transformation is to remove the range-dependent boundary condition, thereby retaining the parabolic form of the wave equation, which may be solved by numerically efficient marching techniques. We use the split-step Fourier algorithm (A. E. Barrios, IEEE Trans. Antennas Propagat. 42, 90-98, 1994, J. R. Kuttler and G. D. Dockery, Radio Science 26, 381-393, 1991), which has been generalized to vertical and horizontal polarization over imperfectly conducting surfaces. We will report our progress on the numerical implementation of the coordinate transform method, which will first be applied to an example problem of propagation over irregular terrain.

B1-4
1440

DERIVATION OF BOUNDARY INTEGRAL EQUATIONS FOR SCATTERING BY AN INFINITE ROUGH SURFACE

J. A. DeSanto P. A. Martin*
Department of Mathematical and Computer Sciences
Colorado School of Mines
Golden, CO 80401-1887

A crucial ingredient in the formulation of boundary-value problems for acoustic scattering of time-harmonic waves is the *radiation condition*. This is well understood when the scatterer is a *bounded* three-dimensional obstacle, with surface S. In the far field, one requires that the scattered wave u behaves like an outgoing spherical wave, $u(\mathbf{x}) \sim \mathrm{e}^{\mathrm{i}kR}\, R^{-1}\, f$ as $R = |\mathbf{x}| \to \infty$, where f is the far-field pattern (the time-dependence is $\mathrm{e}^{-\mathrm{i}\omega t}$). This behavior will be imposed if u satisfies the Sommerfeld radiation condition,

$$R(\partial u/\partial R - \mathrm{i}ku) \to 0 \qquad \text{as } R \to \infty. \tag{1}$$

Furthermore, we can derive a boundary integral equation (BIE) over S by applying Green's theorem to u and the free-space Green's function $G(\mathbf{x}, \mathbf{y}) = \mathrm{e}^{\mathrm{i}k|\mathbf{x}-\mathbf{y}|}/|\mathbf{x} - \mathbf{y}|$; the radiation condition ensures that the contribution from integrating over a large sphere of radius R, S_R, vanishes as its radius increases:

$$I(S_R) \equiv \int_{S_R} \left(u \frac{\partial G}{\partial R} - G \frac{\partial u}{\partial R} \right) ds \to 0 \qquad \text{as } R \to \infty. \tag{2}$$

Now, suppose that we want to scatter a plane wave by an infinite rough surface, $z = s(x, y)$, say. (For simplicity, we suppose that the acoustic medium occupies $z > s$, with an impenetrable boundary at $z = s$.) It is difficult to formulate a precise radiation condition, comparable to (1). Physically, we expect that there will be a spectrum of reflected plane waves (these do not decay!) and some evanescent waves (which decay exponentially). Given this expectation, we can attempt to derive a BIE for the scattered field. To do this, we apply Green's theorem to u and G, as for a bounded scatterer. However, instead of (2), we now have to integrate over a large *hemisphere*, H_R. Can we discard the contribution from this integral, i.e. do we have $I(H_R) \to 0$ as $R \to \infty$? This question cannot be answered by appealing to what we know from the case of bounded scatterers, because u does not decay with R.

We show that $I(H_R)$ does decay with R, provided that u corresponds to a superposition of plane waves that exits to infinity *through* the hemisphere. It is false if any plane-wave component of u propagates inwards through H_R (so that it is false if u is replaced by the incident plane wave). requires proof). This result can be proved in two ways: find an asymptotic approximation to the integral, using the method of stationary phase; or direct evaluation of the integral, using expansions of u and G in terms of Bessel functions and spherical harmonics. It can also be proved (more easily) in two dimensions. Implications of the result will be discussed, as will previous work on this topic.

B1-5
1520

NUMERICAL SOLUTION OF THE REDUCED RAYLEIGH EQUATION FOR THE SCATTERING OF ELECTROMAGNETIC WAVES FROM ROUGH DIELECTRIC FILMS ON CONDUCTING SUBSTRATES

A. Madrazo
Universidad Autonoma
Madrid
SPAIN
A. A. Maradudin*
Department of Physics and Astronomy
University of California
Irvine, CA 92717-4575

In the scattering of electromagnetic waves from a one-dimensional surface the reduced Rayleigh equation is the single integral equation satisfied by the scattering amplitude that is obtained from the pair of coupled Rayleigh equations for the amplitudes of the scattered and transmitted fields when the electromagnetic field inside the scattering medium has been eliminated from the problem by the use of Green's second integral identity. The purely numerical, non-perturbative solution of this equation has been little studied until now, except in the recent work of Michel (JOSA **A11**, 1874 (1994)) and of Michel, Knotts, and O'Donnell (JOSA **A12**, 548 (1995)). In that work, devoted to the scattering of electromagnetic waves from one-dimensional, randomly rough metal surfaces, a segment of rough surface of length L along the x_1-axis is generated numerically, and then replicated periodically to form a classical grating with period L. The integral equation for the scattering amplitude is converted into a matrix equation for the amplitudes of the propagating and evanescent Bragg beams diffracted by this grating. If the period L is sufficiently large compared to the wavelength λ of the incident electromagnetic field, the scattering angles corresponding to the propagating beams are nearly continuously distributed. By solving this matrix equation for an ensemble of random surfaces, and averaging the results over this ensemble, the cross sections for specular and diffuse scattering can be obtained. This approach should be very useful in the study of scattering from surfaces that are rougher than those for which low-order perturbation theory is valid, but are less strongly rough than those for which the computer simulation approach is effective, due to the long mean free paths of the surface or guided waves supported by the scattering structure. We have solved the reduced Rayleigh equation numerically for the scattering of p- and s-polarized light from a one-dimensional, randomly rough dielectric film on a planar, perfectly conducting substrate when the thickness of the film is large enough that it supports two or more guided waves of each polarization. The power spectrum of the surface roughness is nonzero only in the range of the wave numbers of these guided waves. Sharply defined satellite peaks are present in the diffuse scattering cross section, in addition to the enhanced backscattering peak.

B1-6
1540

Enhanced Backscatter From Two Dimensional Random Rough Surfaces

M. El-Shenawee and E. Bahar
Department of Electrical Engineering/Center for Electro-Optics
University of Nebraska, Lincoln
Lincoln, NE 68588-0511

Full wave solutions for the single and double scatter radar cross sections from two dimensional random rough surfaces are obtained. The solutions are expressed as multi-dimensional integrals. High frequency approximations are used to reduce the dimension of the double scatter integrals to four. Thus, the large radius of curvature approximation is assumed. The single scatter cross section is given in closed form. This work is an extension of the analysis of scatter from one dimensional random rough surfaces.

The major contributions to the double and single scatter cross sections, in the high frequency limit, come from the neighborhood of the specular points on the rough surface. Thus, the surface element scattering coefficients are evaluated at the specular points (after integrating with respect to the slopes). The probability density functions of the slopes are assumed to be Gaussian.

Similar to scattering from the one dimensional random rough surfaces, the major contributions to the double scatter cross sections come from the quasi parallel and the quasi anti-parallel double scatter paths. The expressions for the total incoherent cross section is the sum of the single and the double scatter cross sections. Shadow functions are included in the expressions.

The numerical results, using the high frequency approximations, show sharp enhancement in the backscatter direction at normal and at oblique incident angles. This sharp enhancement is due to the contributions associated with the quasi anti-parallel double scatter paths. The level and width of the peak in the backscatter direction depend on the mean square height and slope of the two dimensional random rough surface.

B1-7
1600

STATISTICAL PROPERTIES OF GAUSSIAN RANDOMLY ROUGH SURFACES ENCOUNTERED IN OPTICAL SURFACE SCATTERING

A.R. McGurn and S. Simeonov
Department of Physics
Western Michigan University
Kalamazoo, Michigan 49008 U.S.A.
A.A. Maradudin
Department of Physics
University of California
Irvine, California 92717

Gaussian randomly rough surfaces which are planar on average are often used in theoretical treatments which compute the diffuse scattering of light from randomly rough planar on average surfaces. These surfaces are particularly useful in Green's functions calculations of light scattering as they allow for a Feymann diagrammatic expansion of the scattering in terms of simple two-point correlation functions involving the surface profile functions and the averages of the surface profile functions (usually taken to be zero). In addition, Gaussian random surfaces with both fully two-dimensional roughness and with one-dimensional roughness have been realized experimentally. In this talk results are presented for some of the statistical properties of commonly used one- and two-dimensionally Gaussian randomly rough surfaces. Specifically, the statistical distribution of the distance between nearest neighbor maxima (peaks on the surface), between nearest neighbor minima (valleys), and between nearest neighbor maxima-minima (peak-valley) are computed. The results are obtained using Gaussian randomly rough surfaces which are generated by computer simulation. For one-dimensional randomly rough surfaces we study the statistics of a particular Gaussian randomly rough surface recently generated by West and O'Donnell and studied experimentally for the diffuse scattering of light (C.S. West and K.A. O'Donnell, J. Opt. Soc. Am. A 12, 390-7, 1995). This surface is important as it exhibits an enhanced backscattering peak for the diffuse scattering of light and this peak is shown to arise from the resonant excitation of surface polaritons. For two-dimensional randomly rough surfaces the statistics are given for surfaces with two-point surface profile correlation functions given by Lorentzian and Gaussian forms and for a two-dimensional generalization of the one-dimensional surface studied by West and O'Donnell. These surface statistics are discussed in the context of recent theoretical and experimental studies of the scattering of light from Gaussian random surfaces.

B1-8
1620

SCATTERING OF ELECTROMAGNETIC WAVES FROM RANDOM SURFACES FORMED FROM RESONANT SCATTERERS

R. M. Fitzgerald*
University of Texas
El Paso, TX 79968
A. A. Maradudin
University of California
Irvine, CA 92717
A. R. McGurn
Western Michigan University
Kalamazoo, MI 49008

We study theoretically the scattering of p-polarized electromagnetic waves from a one-dimensional random vacuum-metal surface defined by

$$x_3 = H(x_1) = \sum_{n=-\infty}^{\infty} c_n s(x_1 - n\Delta x),$$

where the $\{c_n\}$ are independent random variables defined by the properties that $c_n = 1$ with probability p and $c_n = 0$ with probability $1 - p$, while $s(x_1)$ has the Gaussian form $s(x_1) = A\exp(-x_1^2/R^2)$. The region $x_3 > H(x_1)$ is a metal, the region $x_3 < H(x_1)$ is vacuum, and the plane of incidence is the x_1x_3- plane. A vacuum-metal surface defined by $x_3 = s(x_1)$, i.e. a surface consisting of a single Gaussian ridge on an otherwise planar surface supports electromagnetic surface shape resonances. In the small roughness approximation we determine the self-energy $M(q,\omega)$ in the ensemble-averaged surface plasmon polariton Green's function $G(q,\omega)$ exactly to first order in the concentration p. As a function of ω for fixed q it possesses poles at the frequencies of the electromagnetic surface shape resonances. In turn these poles introduce additional poles into the Green's function $G(q,\omega)$ beside the surface plasmon polariton pole it possesses. One consequence of these additional poles is that if the reflectivity of the surface is calculated as a function of the frequency of the incident light for a fixed angle of incidence, it displays dips at frequencies that coincide with the real part of the frequencies of the surface shape resonances. These dips are caused by the roughness-induced excitation of these resonances by the incident light. We also consider the enhanced backscattering of light from this kind of surface. This requires the determination of the irreducible vertex function in the Bethe-Salpeter equation, whose solution describes the diffuse scattering of light, to second order in p. The shape of the enhanced backscattering peak changes as the frequency of the incident light coincides with the real part of the frequency of a surface shape resonance.

Session D-1, 1335-Tues., CR2-28
NOVEL DEVICES
Chairperson: A. Mickelson, Dept. of Electrical and Computer Engineering,
Univ. of Colorado at Boulder, Boulder, CO 80309
Organizer: M.S. Shur, Dept. of Electrical Engineering, Univ. of Virginia, Charlottesville, VA 22903

D1-1
1340

ELECTRONIC AND OPTOELECTRONIC AlGaN/GaN HETEROSTRUCTURE FIELD EFFECT TRANSISTORS

M. Asif Khan[1] and Michael S. Shur[2]
[1]APA Optics, Inc.
2950 N. E. 84th Lane, Blaine, MN 55449
[2]Dept. of Electrical Engineering, University of Virginia
Charlottesville, VA 22903

Wide bandgap semiconductors are superior materials for field effect transistors, since the wide band energy gap should allow us to achieve a very high on-to-off ratio and high current densities and breakdown voltages. In practical devices, relatively low mobility values and technological problems, such as problems related to contacts and traps, make it difficult to realize this potential. In this paper, we show that many of these difficulties can be alleviated in Doped Channel Heterostructure Field Effect Transistors (HFETs), which combine the superior transport properties of the two-dimensional electron gas with a low series resistance and high sheet carrier concentration. We review our recent results on novel AlGaN/GaN Doped Channel HFETs and report f_T x L products in excess of 20 GHz x micron (comparable to the best GaAs FETs), transconductances over 120 mS/mm, and the maximum drain current density on the order of 1 A/mm, breakdown voltages in access of 40 V, and sheet carrier concentration close to 2 x 10^{13} cm^{-2}.

We also discuss optoelectronic AlGaN/GaN based devices. Our HFET photodetector is based on a 0.2 micron gate AlGaN/GaN HFET and utilizes a shift in the device threshold voltage caused by the light-generated carriers. Unique optical and electronic properties of GaN/AlGaN material systems open up numerous opportunities for visible-blind optoelectronic devices. These devices have a high sensitivity and a large gain-bandwidth product and can be integrated with GaN/AlGaN field effect transistors, which have already demonstrated an operation at microwave frequencies with cutoff frequencies above 36 GHz and fmax over 70 GHz.

The work at the APA Optics and University of Virginia has been partially supported by the AFOSR, ONR, and ARPA.

D1-2
1420

PERFORMANCE OF WIDE BAND GAP SEMICONDUCTOR MESFET'S FOR HIGH POWER, HIGH TEMPERATURE APPLICATIONS

R. J. Trew and M.W. Shin
Department of Electrical Engineering and Applied Physics
Case Western Reserve University, Cleveland, OH 44106-7221
Phone: (216) 368-4089
Fax: (216) 368-2668
r.trew@ieee.org

There is much interest in wide bandgap semiconductor materials for a variety of applications. In particular, GaN is of interest for optical devices throughout the entire visible spectrum and extending far into the UV. Blue LED's with excellent intensity have been demonstrated and device quality GaN will soon become available. GaN also possesses desirable material characteristics for electronic devices. Both GaN and SiC have potential for producing microwave power devices capable of high temperature operation. In this paper, we report dc and RF large-signal simulations of n-type SiC and GaN MESFET's. The calculations indicate that both these devices should produce excellent RF performance at microwave frequencies over a wide temperature range.

The dc and RF performance of SiC and GaN MESFET's were investigated using a state-of-the-art harmonic balance simulator combined with a two-dimensional device model. Experimental results are in agreement with the theoretical predictions. The electron mobility in SiC and GaN are in the range of 250-800 cm^2/V-sec at 300 K. GaN has a broad velocity peak (v_s~$2.5x10^7$ cm/sec) extending over a significant electric field range, whereas SiC has a saturation velocity of $2x10^7$ cm/sec. The peak velocity in GaN occurs at an electric field almost an order of magnitude greater than in GaAs. The mobility in GaN is more than twice that of 6H-SiC, which has a low field mobility of about 250 cm^2/V-sec at a doping level of 10^{17} cm^{-3}, but the breakdown fields are comparable. The electron mobility in GaN is predicted to have a temperature dependence proportional to $T^{-1.9}$.

The dc I-V characteristics for the GaN device demonstrate a maximum channel current of 500 mA/mm and 150 mA/mm at 300 K and 773 K, respectively. At 300 K the device produces approximately 4 W/mm RF power, 50% PAE, and 20 db linear gain. At 773 K the RF performance degrades, but the device still produces approximately 1 W/mm RF power, 33% PAE, and 13 db linear gain. SiC MESFET's produce 2-4 W/mm RF power. The small signal power gain for the GaN device yields an f_{max} of about 70 GHz at 300 K (f_T = 40 GHz), which degrades to about 35 GHz at 773 K.

These results indicate that both SiC and GaN have significant potential for microwave MESFET applications over a wide temperature range. Complete dc and microwave performance, including gate leakage and charge trapping limitations and RF operation principles will be presented.

D1-3
1440

MODELING OF GATE LEAKAGE CURRENT IN HETEROSTRUCTURE FIELD EFFECT TRANSISTORS

K. Y. Lee[1,2], B. Lund[3], T. Ytterdal[2], P. Robertson[4], E. Martinez[5], J. Robertson[2], and M. Shur[2]

[1] Dept. of Electronics Eng., Chungbuk National University, San 48 Gaeshin-Dong, Cheongju, Korea 360-763.

[2] Dept. of Electr. Eng., Univ. of Virginia, Charlottesville, VA 22903-2442.

[3] Rogaland Research, N-4004 Stavanger, Norway.

[4] Sandia National Laboratories, Albuquerque, NM 87158-5800.

[5] Solid State Tech. Directorate, Wright-Patterson AFB,OH 45433-7319.

We propose a simple and accurate circuit model for Heterostructure Field Effect Transistors (HFETs). The model is capable of simulating both the gate and the drain current characteristics accounting for hot-electron effects on gate current and the effect of the gate current on the channel current. An analytical equation that describes the effective electron temperature is developed in a simple form. This equation is suitable for implementation in circuit simulators. The model describes both the drain and gate currents at high gate bias voltages. Although previous HFET models are adequate when the gate current is small, it is shown that only the new model explains device characteristics well when the effect of the gate current on the channel current is not negligible. Furthermore, the model has been implemented in our circuit simulator AIM-Spice, and good agreement between simulated and measured results is achieved for enhancement-mode HFETs fabricated in different laboratories. Finally, the proposed equivalent circuit and model equations can be easily applied to other compound semiconductor FETs, i.e. GaAs MESFETs. Figures 1 and 2 below illustrate the quality of the model by plotting measured (symbols) and simulated (solid lines) gate and drain current characteristics, respectively, of a submicron HFET.

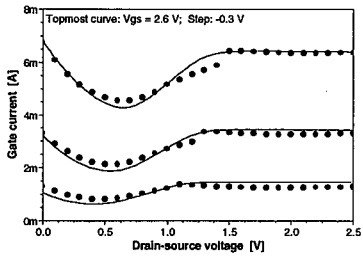

Figure 1

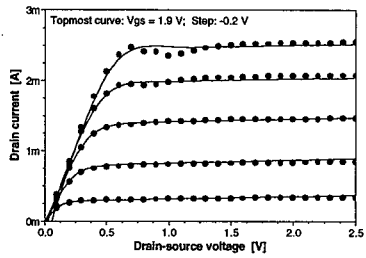

Figure 2

D1-4
1520

PLASMA WAVE ELECTRONICS: NOVEL TERAHERTZ DEVICES USING TWO-DIMENSIONAL ELECTRON FLUID

M. I. Dyakonov and M. S. Shur*
A. F. Ioffe Physico-Technical Institute
St. Petersburg 194021, Russia
*Department of Electrical Engineering, University of Virginia
Charlottesville, VA 22903-2442, USA, shur@virginia.edu
http://www.ee.virginia.edu/faculty.txt/shur.html

We discuss how the propagation of plasma waves in a High Electron Mobility Transistor (HEMT) can be used to implement a new generation of terahertz devices, including sources, resonant detectors, broad band detectors, and frequency multipliers. Our estimates show that these devices should outperform conventional terahertz devices, which use deep submicron Schottky diodes. The velocity of the plasma waves is typically on the order of 10^8 cm/s, which is much larger than the drift velocity of the two-dimensional electrons in the FET channel. This is why the propagation of plasma waves can be used for new regimes of FET operation, with a much higher frequency than for conventional, transit-time limited regimes [M. Dyakonov and M. S. Shur, Phys. Rev. Lett 71, 2465, 1993; I. Dyakonov and M. S. Shur, Appl. Phys. Lett. 67, 1137, 1995]. Under certain conditions, plasma oscillations can be excited in a FET by a dc current [M. Dyakonov and M. S. Shur, Phys. Rev. Lett 71, 2465, 1993], and the FET can be used as an oscillator operating in the terahertz range. Nonlinear properties of the plasma waves can be utilized for terahertz detectors, broad band detectors, mixers, and frequency multipliers [M. Dyakonov and M. S. Shur, Proceedings of 22nd International Symposium on GaAs and Related Compounds, 1995; M. I. Dyakonov and M. S. Shur, IEEE Transactions on Electron Devices, submitted for publication].

The plasma oscillations can be coupled to electromagnetic radiation. However, since the plasma wave velocity is much smaller than the light velocity and the device dimensions are much smaller than the electromagnetic wave length corresponding to the plasma frequency, standard antenna structures are needed for such a coupling.

D1-5
1600

HIGH-PERFORMANCE InAlAs/InGaAs MSM PHOTODETECTORS WITH Cu ELECTRODES

A. C. Davidson* F. W. Wise
Department of Applied Physics
Cornell University
Ithaca, NY 14853
D. T. Emerson J. R. Shealy R. C. Compton
School of Electrical Engineering
Cornell University
Ithaca, NY 14853

We present the results of studies performed on high-speed metal-semiconductor-metal photodetectors fabricated for detection of 1.3 micron and 1.55 micron wavelength light. The devices were designed for high-speed/low dark current. Copper was used as the Schottky contact metal, and was found to produce a high-quality junction with very low dark currents. Devices with a 20 square-micron active area fabricated on MOCVD grown material produced sub-nanoampere dark currents at 10 V bias.

The devices were fabricated on an InP substrate with an InGaAs absorbing layer and a thin InAlAs layer to enhance the otherwise small Schottky barrier of InGaAs. Both MOCVD and MBE grown material were used. The electrodes were 1 micron wide, with gaps of 2, 1, and 0.75 microns, and were formed with 20 nm Cu and 50 nm Au. The device active areas were isolated by wet-etching a mesa, and polyimide was used to prevent pad metal from contacting the sides of the mesa. Devices were positioned in long transmission lines to facilitate optical based sampling methods.

Measured dark current at 10 V bias of the devices with 2 micron gaps was found to be 600 pA for the MOCVD devices, and 1.5 nA for the devices fabricated on MBE material. Dark currents for the devices with narrower gaps were significantly larger.

Measurements of device response to 100 fs, 800 nm optical pulses using a high speed oscilloscope(20 ps rise/fall time) have shown instrument limited responses for the 1 and 0.75 micron gap devices, with a slightly longer fall time for the 2 micron gap devices.

This work is supported by the Joint Service Electronics Program.

D1-6 1620 Photoelectric Analysis Techniques for Characterization of Pseudomorphic High Electron Mobility Transistors

Fritz Schuermeyer
Wright Laboratory, Wright Patterson AFB, OH 45433-7319

Pseudomorphic high electron mobility transistors (PHEMTs) play an increasingly important role for applications where high frequency and low power dissipation are critical parameters. These heterostructure field effect transistors contain a strained InGaAs channel, embedded between GaAs and AlGaAs barriers. Optoelectric techniques, such as photoluminescence and photoreflectance are routinely used to verify the energy configuration of these material structures. Recently, optoelectronic or photoelectric techniques were extended for the evaluation of fully fabricated transistors. In these studies photoemission and conduction (PEC) was evaluated. It is feasible to utilize backside illumination for the PEC measurements since the bandgap and interband transition energies in the quantum well are smaller than the bandgap of the substrate and hence the substrate is transparent at the photon energies of interest. We perform PEC studies on-wafer, using mechanically chopped monochromatic light.

Figure 1 presents typical photo-conduction (PC) results for a PHEMT without underdoping. In such a transistor a flat quantum well is obtained for the pinched-off state. We have successfully modeled the PC spectrum by assuming that the photocurrent is proportional to the interband optical absorption coefficient of the channel. A step-like PC spectrum is predicted and the $\Delta n=0$ selection rule is strong. Our PC measurements verify the predicted step-like behavior where the steps occur at the transition energies. To better analyze these transition energies we differentiate the PC characteristics and obtain peaks, representing the indicated transitions.

The significance of this novel characterization technique is that fully fabricated PHEMTs can be evaluated. One can verify that the processing did not adversely effect the materials structure, one can evaluate uniformity over a wafer, and changes in the energy profile due to electrical and thermal stress can be studied.

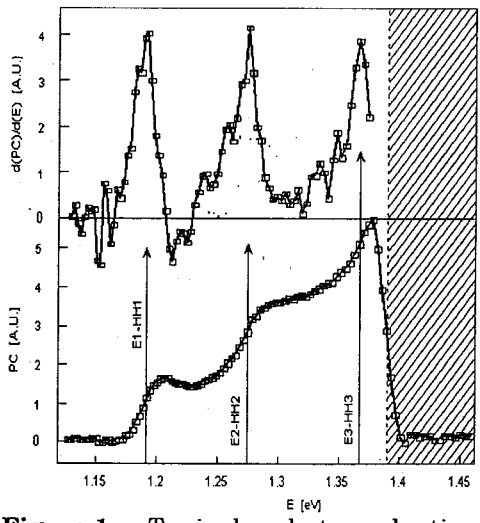

Figure 1 Typical photoconduction results of a PHEMT without underdoping

D1-7
1640

RELIABILITY OF HIGH ELECTRON MOBILITY TRANSISTORS AND STABILITY OF NEW PASSIATIONS AT ELEVATED TEMPERATURES AND HUMIDITY

A. Christou
University of Maryland
College Park, MD 20742

Recent reliability results of double-channel pseudomorphic HEMTs will be reviewed, with particular emphasis on the role of channel dislocations. It will be shown that pseudomorphic HEMTs degrade from traps in the InGaAs channel. The degradation of noise is from 0.85eV to 1.05eV.

Polyimide and Polymide/Si3N4 combinations are presently being used in a number of MMIC applications. The magnitute of leakage currents and the presence of conduction paths at the interface with GaAs is shown to be due to surface states present at the interface. Acceleration factors for accelerated testing have been determined.

F2-1
1340

A REFINED ASSESSMENT OF THE GPS/MET LIMB SOUNDER DATA

M L Exner[1], W Schreiner[1], R McCloskey[1], D Hunt[1],
S Sokolovskiy[2], B Herman[3], and D Feng[3]

1 University Corporation for Atmospheric Research
GPS/MET Program Office
3300 Mitchell Lane, Suite 245
Boulder, Colorado 80301
2 Russian Institute of Atmospheric Physics
3 University of Arizona, Dept. of Atmospheric Physics

On April 3, 1995, the first GPS receiver capable of Earth radio occultation observations was successfully placed in Low Earth Orbit (LEO) aboard the MicroLab-1 spacecraft. The primary goal of this "proof of concept mission" is to assess the potential utility and value of such active limb sounding measurements for operational weather prediction and climate change research. Secondarily, scientists hope to exploit observations through the ionosphere for "space weather" and other ionospheric propagation research.

To date, over 10,000 GPS/MET occultations have been received, many of which have been processed and analyzed at UCAR and other research centers using "quick look" data processing tools developed prior to launch. Early results, as reported in the literature (R. Ware, M. Exner, et al., GPS Sounding of the Atmosphere from Low Earth Orbit: Preliminary Results, accepted for publication, *Bull. AMS*, Jan 96), indicated that GPS/MET temperature profiles typically compare within 1-2 K with other observing systems, such as radiosondes, in the 6-35 km altitude range. Above and below these altitudes, results from the quick look inversion algorithms showed various errors and weaknesses. For example, at higher altitudes, errors due to ionospheric residuals and assumptions about the upper boundary conditions appear to limit accuracy. At lower altitudes, reduced carrier-to-noise ratio (C/N_0) exacerbates the difficulty of tracking the GPS signals as they pass through the lower troposphere, where signal dynamics reach a maximum, and closed loop carrier tracking becomes difficult.

To address the early lessons learned, improved inversion techniques are being developed. Changes include the use of a constrained linear inversion to recover refractivity and improved preprocessing data filters. The results of these advanced data processing techniques will be presented.

F2-2
1400

REMOTE SENSING OF OVER-WATER DUCTS USING NEAR-LINE-OF-SIGHT PROPAGATION DATA

L. Ted Rogers
Ocean and Atmospheric Sciences Division
Naval Command, Control and Ocean Surveillance Center
San Diego, CA 92106
(619) 553-1413
trogers@nosc.mil

An important inverse problem in radiowave propagation is the determination of the refractive medium from EM far-field measurements. Let **x** be a vector of refractivity parameters and **y** be a vector of propagation measurements. Using magnitude information, the least squares solution to the inverse problem is found by minimizing R(**x**) where

$$R(\mathbf{x})=(\mathbf{F}(\mathbf{x})-\mathbf{y})^{T}\mathbf{Q}^{-1}(\mathbf{F}(\mathbf{x})-\mathbf{y}).$$

F(**x**) is a vector of propagation estimates calculated using parameter vector **x**, **Q** is the covariance matrix, and the superscript T indicates the transpose. R(**x**) is not necessarily concave, therefore a global optimization must be performed.

Environmental models [implicit in **F**( )] are chosen to minimize the degrees of freedom of the parameter vector **x**. When ducting due to a surface based or elevated ducts is not present, a single parameter δ, the evaporation duct height corresponding to a neutral profile can be used. When surface based or elevated ducts are present, the parameter vector also includes elements describing the height of the duct and M-deficit of the duct.

The inverse problem technique is applied to propagation measurements at 3, 5.6, 10.5, 16, 35 and 94 GHz from a NATO measurement campaign (Lorient '89). First, the evaporation ducts corresponding to neutral profiles are determined. Then the ability to separate surface based ducts from evaporation ducts is examined. Finally, for the case of purely evaporative ducting, the sea-surface temperature is determined from propagation measurements and environmental priors used in the LKB evaporation duct formulation. Inverse problem results are compared to meteorology from a mid-path buoy and from radiosondes.

F2-3
1420

HUMIDITY AND TEMPERATURE MEASUREMENTS AT THE OCEAN SURFACE AS IT RELATES TO MICROWAVE EVAPORATION DUCTING MODES

John R. Rowland, Ross J. Rottier, R. T. Booling,
J. H. Meyer
The Johns Hopkins University, Applied Physics Laboratory
Johns Hopkins Road, Laurel, Maryland, 20723-6099

An extensive set of fine scale meteorological data has been collected over the last several years in an attempt to characterize the microwave evaporation duct. These measurements include water temperature at a depth of 2 cm and air temperature and humidity at heights of 2-4 cm, 1m, 2m, 6m, 10m, and 30m along with wind speed at a height of 6m. This data set includes measurements made in the vicinity of Wallops Island, Virginia, Gulfport, Mississippi, Southern California, Hawaii, Puerto Rico, and the Potomac River at the mouth of the Chesapeake Bay.

Several interesting features have been identified in this data set. The first of these results is that the humidity at the lowest level of 2-4 cm is not generally 100%. Although the vast majority of the data indicates a relative humidity at the surface between 85 and 98%, humidities below 50% are measured on occasion. Attempts have been made to parameterize the surface humidity based on measurements made at a more convenient higher level. In general the highest measured humidity approaches 98% which corresponds closely to the saturation vapor pressure over sea water. A second feature which has been noticed is a prominent notch in the probability density distribution of air sea temperature difference at +0.4°C for the 6m air temperature minus 1 cm depth sea temperature and +0.3°C difference for the 2 cm air temperature minus 1 cm depth sea temperature. The reason for this notch is unknown. Analysis of this data set has shown problems with the majority of existing microwave evaporation duct models and has suggested techniques for making improvements.

Statistics for the various measurements will be presented as well as methods for making evaporation duct predictions using bulk techniques which are superior to presently accepted methods. New instrumentation has recently been developed which provides detailed profiles of refractivity from the surface to a height of 1m as well as air temperature and humidity at a height of 5mm above the surface. Preliminary results of tests with this instrumentation will also be presented.

F2-4
1440

SIMPLIFIED MODELING OF THE SURFACE LAYER FOR EVAPORATION DUCTING

Richard A. Paulus, Kenneth D. Anderson, and L. Ted Rogers
Ocean and Atmospheric Sciences Division
NCCOSC RDTE DIV 543
49170 PROPAGATION PATH
SAN DIEGO CA 92152-7385

A recent resurgence of interest in bulk meteorological models of the marine atmospheric surface layer with application to the evaporation duct has prompted a re-examination of these models and the meteorological measurements required as inputs. The Integrated Refractive Effects Prediction System (IREPS) was introduced aboard US Navy ships in 1978 utilizing a surface layer model formulated in terms of potential refractivity (H. Jeske, *Modern Topics in Microwave Propagation and Air-Sea Interaction*, 131-148, Reidel Publishers, 1973). Jeske's algorithm has a simple determination of stability and assumes the empirical universal stability functions follow the KEYPS formula. An empirical modification to this model was subsequently applied to spuriously stable atmospheric conditions arising from thermal distortion due to the ship (R.A. Paulus, *Radio Sci., 20*, 887-896, 1985). This characterization of the evaporation duct has been used in radiowave propagation assessment for the past decade

Within the meteorological community, a widely accepted bulk formulation for the marine atmospheric surface layer is that of Liu, Katsaros, and Businger (*J. Atmos. Sci, 36*, 1722-1735, 1979). The LKB model is more physically rigorous than the Jeske model with an iterative approach to the determination of stability and temperature and moisture profiles that follow an empirical stability function proportional to the square of the KEYPS formula.

These surface layer models require bulk measurements of air temperature, relative humidity, and wind speed at known heights along with a measurement of sea surface temperature. Blanc (*J. Geophys. Res., 92*, C4, 3867-3876, 1987) has found that bulk methods yield a very crude estimate of the true stability influence and questioned how much is really gained by using a stability dependent scheme. Previous propagation studies have found that, for common departures from neutrality, the neutral surface layer profile is representative of the actual propagation conditions (K.D. Anderson, *IEEE Trans. Antennas Propagat., 38*, 746-753, 1990). In light of these findings, this paper will examine the capability of a simplified evaporation duct model, that eliminates the sea surface temperature measurement and assumes neutral stability of the surface layer, to characterize propagation. Propagation results from the simplified model will be compared to the results using more rigorous surface layer models for radio-meteorological data sets in the eastern Atlantic and the Mediterranean.

F2-5
1500

PROPAGATION FACTOR ERRORS EMPLOYING THE ASSUMPTION OF UNIFORM HOMOGENEITY OF THE REFRACTIVITY ENVIRONMENT

Julius Goldhirsh, G. Daniel Dockery
The Johns Hopkins University, Applied Physics Laboratory
Johns Hopkins Road, Laurel, Maryland, 20723-6099

In assessing propagation conditions, it is frequently assumed that the refractivity environment is laterally homogeneous. That is, a single refractivity-height profile which is assumed laterally homogeneous is often injected into an appropriate model from which the two dimensional propagation factor field is derived. Because the propagation environment, especially near coastal regions, may not be homogeneous, assumptions of uniformity may lead to serious errors in propagation factor.

The objective of this paper is to examine the extent of these errors by injecting a number of measured two dimensional refractivity profiles derived from helicopter measurements along the east and west coasts of the United States into broadly accepted propagation models at frequencies between 1 and 10 GHz. The resultant "truth" propagation factor fields are compared with "error" propagation factor fields derived when only single profiles are used employing the assumption of lateral homogeneity.

Errors are examined using propagation factor difference fields obtained by subtracting the "truth" and "error" fields in two dimensional space. Color coded representations of error levels quantized in five dB intervals are derived. Cumulative distributions in dB errors are subsequently found for defined range and height intervals relative to an at-sea reference location.

As an example, one set of results associated with a series of helicopter measurements made off the coast of Wallops Island, Virginia during a week in August 1994 showed a strong surface duct at an approximate height of 300 m at a distance of 13 km from the shore whereas a standard atmospheric profile was measured 52 km from the shore. Assuming the closest profile to the shore to be homogeneous, and a measurement box whose range extends from 10 to 55 km at a height interval of 5 to 150 m, the following error field was derived in the frequency range between 1 and 10 GHz: Five dB was exceeded over 40% to 70% of the area, and 10 dB was exceeded over 20% to 50% of the area.

A number of different cases are examined based upon the methodology described above, and general comments are made regarding error bounds associated with assuming lateral homogeneity of the environment.

F2-6
1540

Comparison and Correlation of Directly Measured Microwave and Infrared Low Altitude Propagation

J. K. Stapleton, S. Kang, W. Trahan, H. Rivera
Naval Surface Warfare Center
Dahlgren Division, Code F42
Dahlgren, VA 22448

Recent interest in the integration of shipboard microwave and infrared (IR) sensors in order to better detect and track low altitude cruise missles has raised questions about the effects of the propagation environment on the relative performance of the two sensor types. Previous analysis of microwave and IR propagation has indicated that propagation in the two frequency regimes may be negatively correlated for certain environmental conditions. The propagation environment often drives the performance of microwave and IR sensors in the low altitude region, and therefore, understanding the correlation of propagation effects between the two frequency regions will allow assessment of the relative performance of the two sensor types in a given environment and may help quantify the overall benefits of sensor integration.

During recent sensor integration experiments held at Wallops Island Virginia, measurements of microwave and IR propagation conditions were made simultaneously for collocated sensors and sources. The microwave propagation measurements were made across the 2 to 18 GHz band, and the IR propagation measurements were made in the mid-IR band (3 to 5 micrometers). The microwave and IR propagation characteristics were compared for the data set as a whole and for the data set categorized by microwave duct type. The results of these comparisons are presented in the subject presentation.

F2-7
1600

USING RADIO REFRACTIVITY INVERSION AND A PLANETARY BOUNDARY LAYER MODEL TO CHARACTERIZE REFRACTIVITY FIELDS IN A COASTAL MARINE ENVIRONMENT

Donald Boyer, Greg Gentry, and Janet Stapleton
Naval Surface Warfare Center/Dahlgren Division
17320 Dahlgren Road
Dahlgren, VA 22448-5100

With the advent of high fidelity electromagnetic wave propagation models and the portable computational power to utilize them in a tactical environment, the ability to obtain accurate meteorological representations of the refractivity fields, has become a very important issue in Naval environmental assessment systems. Direct measurement of the humidity and temperature profiles at various ranges are very difficult to obtain onboard a ship, and these profiles as well as the corresponding measurements of temperature, humidity and wind speed very near the surface are required to predict the performance of a radar system in a coastal marine environment. Also the evolution of the thermal and moisture structures over time is very difficult to predict, even if the present state of these structures is well known. In order to supplement the direct measurements of refractivity, remote sensing techniques have been proposed. This paper discusses using measurements of propagation loss over a path between two antennas, in order to estimate the structure of the refractivity fields through which the electromagnetic waves passed. The refractivity inversion algorithm determines a set of parameters which, when input to a PE model, minimizes the sum of the residuals between the modelled path losses and the corresponding measured quantities.

At the 1995 URSI Conference, Stapleton and Kang presented a paper describing an RF propagation measurement system at Wallops Island which employed 10 transmitters at the 16 frequencies, 2-18 GHz, and 4 receivers. The paths were over the ocean and all transmitters and receivers were within 30 meters of the surface. The refractivity inversion procedure will be exercised on this data set in a later paper, and this paper will present results on how to parameterize the refractivity structure over the entire marine boundary layer, so that the inversion procedure gives understandable results on meteorologically meaningful synthetic data. The surface layer is represented by the four bulk parameters in the Liu, Katsaris and Businger model, and the mixed layer is characterized in terms a piecewise linear profile. Similarity theory developed by Yamada and extended by Sorbjan can be applied above the surface layer and this is being investigated. The synthetic meteorological data is generated by a higher-order planetary boundary layer model developed by Penn State University.

F2-8
1620

A PRELIMINARY LOOK AT A HYBRID TERRAIN MODEL

Amalia E. Barrios
Ocean and Atmospheric Sciences Division
NCCOSC RDTE DIV 543
53170 WOODWARD ROAD
SAN DIEGO CA 92152-7385

Previously, a terrain parabolic equation (PE) model (TPEM) has been presented (A.E. Barrios, *URSI*, 5-8 Jan. 1993, p. 107) which is based entirely on the split-step Fourier method. While TPEM has since undergone some modifications to improve its efficiency in handling terrain effects, it has remained a pure split-step PE model and therefore, is still restricted to the transform size and memory limitations inherent with this method.

In order to provide a reasonably efficient terrain model that can be used for most practical (operational) applications, the next phase in the development of TPEM would be to incorporate existing, or develop new hybrid techniques in the same spirit as was done with the Radio Physical Optics (RPO) model (H.V. Hitney, *URSI*, 5-8 Jan. 1993, p. 105). Topics to be discussed are ray techniques to determine the field at near ranges and high angles, and a look into two different techniques to extend the PE solution at higher heights. The first technique is the extended optics method developed by Hitney (*ibid*), which extends the split-step PE solution by ray tracing techniques. The second is the Horizontal PE method (HPEM) developed by Levy (*IEEE Trans. on Ant. and Prop.*, Vol. 43, No. 2, Feb. 1995, pp. 137-144), which also extends the split-step PE solution to higher heights, but does so using a horizontal PE in which the field is now transformed in the horizontal, or range, domain.

Results using both hybrid methods with their respective capabilities and limitations will be presented, along with a discussion of problems incurred in developing a hybrid terrain PE model.

F2-9
1640

A ROUGH SURFACE SPLIT-STEP PARABOLIC EQUATION METHOD FOR RADIOWAVE PROPAGATION

R. Janaswamy*, H. V. Hitney†, A. E. Barrios†, and K. D. Anderson†
*Code EC/Js, Department of Electrical & Computer Engineering
Naval Postgraduate School
Monterey, CA 93943
†NCCOSC RDT&E Division 543
49170 Propagation Path
San Diego, CA 92152-7385

The Parabolic Equation (PE) method has emerged as an extremely valuable method for assessing radiowave propagation in the lower atmosphere in the presence of ducts. Propagation loss can be easily estimated over very long ranges of the order of a few hundred kilometers for frequencies through Super High Frequency (SHF) band, and for antenna heights extending up to several kilometers. It is also possible to directly account for finite conductivity of the earth in the PE (J. R. Kuttler and G. D. Dockery, *Radio Sci.*, 26, 2, pp. 381-393, 1991). One of the current unresolved issues is the incorporation of sea-surface roughness into the PE. Several attempts have been made in the past all of which rely on some kind of approximation or post-processing of data obtained by running the PE over smooth earth.

In this talk, we present a rigorous way of incorporating sea-surface roughness into the split-step parabolic equation method. The idea behind our approach is to cast the governing equations in terms of incident and reflected plane waves, and then use the rough surface reduction factor available for plane waves (A. R. Miller *et al., IEE Proc.*, 131, 2, pp. 114-116, 1984) directly in the spectral domain. Inclusion of surface roughness into the PE in this manner will require a re-definition of the Fourier transform pair used in the split-step algorithm. In particular, it requires an additive term in the forward transform formula. The additional term results in an integral equation for the transformed quantity in terms of the spatial function. The equation can be solved by any one of the possible techniques, including successive approximation. We name our method PEERS (Parabolic Equation Exact Rough Surface). Several examples are considered showing comparisons of PEERS with waveguide and other models.

F2-10
1700

A ROUGH SURFACE RAY OPTICS MODEL

Herbert V. Hitney
Ocean and Atmospheric Sciences Division
NCCOSC RDTE DIV 543
49170 PROPAGATION PATH
SAN DIEGO CA 92152-7385

Sea surface roughness can be an important consideration under strong surface ducting conditions, especially for frequencies above several GHz. A number of methods have been proposed to model the effects of surface roughness under these non-standard refractive conditions, but often these models give somewhat different results for the same case. A good example is sample case 3 from the Electromagnetic Propagation Workshop held at the Applied Physics Laboratory of the Johns Hopkins University in July 1995. This case is for a 20 m evaporation duct, 10 GHz, horizontal polarization, transmitter and receiver heights of 25 m, and a wind speed of 10 m/sec. At the workshop, waveguide, parabolic equation (PE), hybrid, and other models were inter-compared for this case, and all of the models gave different results to some degree. This was true even for those models that assumed the same rough surface reflection coefficient reduction factor proposed by Miller and Brown (A.R. Miller, *et al.*, *IEE Proc.*, 131, 2, pp. 114-116, 1984). Part of the variation can be explained by approximations of grazing angle made in the various PE models. However a very promising new PE model that requires no approximations of grazing angle (PEERS, presented in this session) also shows some differences to the other models.

This paper presents an overview of a ray optics model that can be used within the horizon to compute the propagation factor for rough surface and non-standard refractive conditions. This model also uses the Miller-Brown roughness model and gives full consideration to amplitude and phase variation due to refraction along both the direct and sea-reflected paths. Results from this model are compared to some of the other models for the sample case described above.

F2-11
1720

EXPERIENCE USING PREDICTION SOFTWARE AND TETHERED RADIOSONDE DATA TO VALIDATE RADAR PERFORMANCE

John L. Walters, Sukomal Talapatra, David A. Alessio,
Pamela C. Lippy[1]
Code 5330, Search Radar Branch
Naval Research Laboratory
Washington, DC 20375-5000
[1]EG&G Washington Analytical Services Center, Inc.

During the past year the detection range performance of the SPS-49A(V) radar has been verified using airborne targets of measured cross section and controlled flight paths. At the same time an aerostat borne, tethered radiosonde was operated from a boat near the flight path. The radar was instrumented to record S/N returned from the target. Radio Physical Optics (RPO) and Engineer's Refractive Effects Prediction System (EREPS) software were used to predict S/N as a function of range for the radar/target parameters and geometry. (H.V. Hitney, RPO Program, Version 1.14, August 1992 and W.L. Patterson, et alia, EREPS, Technical Document 2648, May 1994, Naval Command, Control and Ocean Surveillance Center, San Diego, CA). The recorded and predicted S/N values showed remarkable agreement.

The meteorological measurements were made 10 to 20 miles off shore from Wallops Island, VA in summer and again in winter. Radiosonde altitudes were between 1000 feet and 3 to 6 feet depending on wave height. Ascent or descent took less than ten minutes; pressure, temperature and humidity data were recorded at about one meter intervals. Modified Refractive Index (MRI) profiles were plotted in real time on a laptop computer to allow monitoring the quality of the measurement. RPO/EREPS processing was done ashore, (but can now be done on the boat).

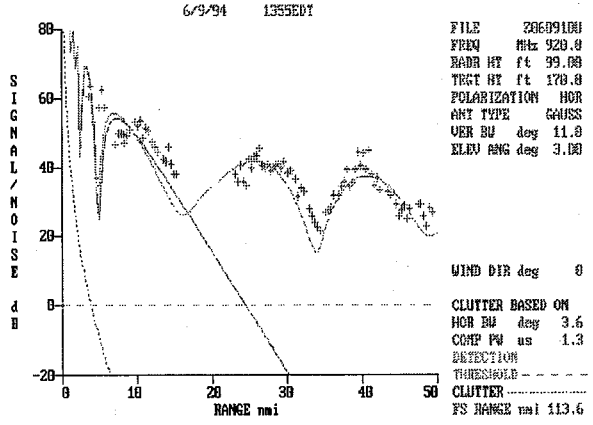

Measured & Predicted Excess S/N for 0.2 Sqm Target at 170 Feet Altitude; Wallops Island 6/9/94 1355EDT from SPS49A(V)2 and Radiosonde Data; Curve Intersecting 30 nmi Shows Normal Propagation

Session G-2, 1335-Tues., CR2-26
ELECTRON DENSITY PROFILES: MODELS AND DATA
(ADOLF PAUL MEMORIAL SESSION)
Chairperson and Organizer: B.W. Reinisch, Center for Atmospheric Research,
Univ. of Massachusetts, Lowell, MA 01854

G2-1 REMEMBERING A.K. PAUL
1340

G2-2
1400

THE SHORT-LIVED, DAYTIME EVENTS OF THE F_2 LAYER ON NOVEMBER 18, 1993 AND FEBRUARY 8, 1986 ARE COMPARED

Karen Fay O'Loughlin, Professional Research Assistant, Cooperative Institute for Research in Environmental Sciences,
University of Colorado, Boulder CO 80307

Raymond O. Conkright, Physicist,
National Geophysical Data Center, Boulder, CO 80303

Dr. Kenneth Davies, Physicist,
Space Environment Center, Boulder, CO 80303

Dr. Adolf K. Paul, Physicist (deceased)

High time resolution digital ionosonde data are now available to investigate fluctuations in ionospheric electron density over large areas. Analyses of these data indicate much larger and more rapid fluctuations than were inferred from classical ionospheric scalings.

Data recorded on November 18, 1993, from Boulder and San Diego, and February 8, 1986, from Boulder and Point Arguello, indicate that the electron density and total electron content are significantly above those on neighboring days. During both events, the true height of the maximum plasma density decreased while the critical frequency increased. During the Nov. 93 enhancement, large and rapid variations in the height of maximum of the F_2 layer were observed at San Diego, which were associated with corresponding variations in foF_2. Both events occurred over relatively brief time spans: the Feb. 86 event rose and dropped to median levels in about one hour; the Nov. 93 event took about four hours. These simultaneous, short-lived, daytime events occurred over a large horizontal scale. Such enhancements are not seen in classical scalings that are used in space-weather models.

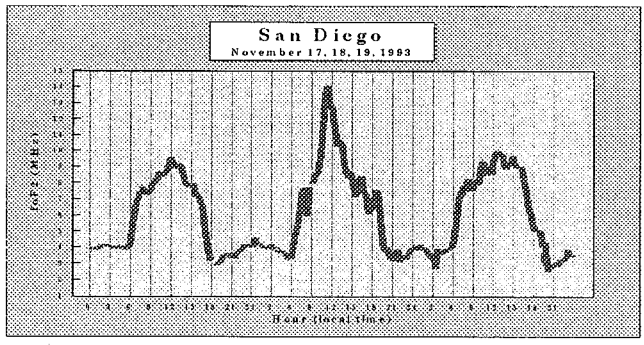

G2-3
1420

DEPENDENCE OF HIGH LATITUDE EDP ON GEOMAGNETIC CONDITIONS: IMPLICATION FOR IONOGRAM INVERSION

Jan J. Sojka and R. W. Schunk
Center for Atmospheric and Space Sciences
Utah State University
Logan, Utah 84322-4405

The bottomside high latitude ionosphere is sensitive to auroral particle precipitation and the convection electric field in different ways. In combination, these two drivers result in a myriad of possible electron density profiles (EDP). Much work, both experimentally using ionosondes and incoherent scatter radars and theoretically using physical models, has been done to elucidate the different EDP shapes. However, during geomagnetic disturbances, the local knowledge of the ionospheric drivers is poorly known. To some extent, each measurement of an EDP contains information about the drivers. This is particularly true in the bottomside where time constants are relatively short (seconds to a few minutes).

In this study, we address the question of how much information can be extracted from an EDP concerning the local convection electric field and auroral precipitation. The relevance of this question lies in improving the real-time knowledge of the ionospheric drivers needed by the National Space Weather Program (NSWP). The approach will be to present examples of the wide range of high latitude EDPs that have been modeled and observed. The EDP dependence on each driver will then be reviewed, the objective being to identify the information that can be extracted with the least ambiguity. In order to address this question from a real-time viewpoint in which ionograms are available, vertical ionograms will be generated from the modeled profiles. These will be compared so that the uniqueness of EDP features can be determined.

G2-4
1440

STUDY OF THE E-F VALLEY AND LOWER F REGION OBSERVED OVER ARECIBO DURING THE JANUARY 1993, 10 DAY WORLD DAY CAMPAIGN

C.H. Chen[1], B.W. Reinisch[1], J.L. Scali[1], Qihou Zhou[2] and P.G. Richards[3]

1 Center for Atmospheric Research, University of Massachusetts, Lowell.
2 Arecibo Observatory, POB 995, Arecibo, PR.
3. Center for Space Plasma and Aeronomic Res., University of Alabama, Huntsville

The overlapping of the E and F region ionization processes results in the formation of a valley region of reduced ionization between the E and F layer. Measurements of the valley ionization with ionosondes do not give reliable profiles and only some of the incoherent scatter radars (ISR) have adequate signal-to-noise ratios at low height to determine the E-F valley ionization profile. In the case of ionosondes, there are no echoes received from the ionization minimum (valley) making the inversion from ionograms to a true height electron density profile ambiguous.

Data from the ISR at Arecibo and Digisondes at Ramey (Puerto Rico) and Puerto Madryn (Argentina) taken during the 10 day campaign in January 1993 are used to investigate the characteristics of the E-F valley region. During this campaign the Arecibo ISR ran 600m, high-resolution power profiles. Digisonde hmF2 data from the two almost conjugate stations are used to drive the FLIP model and obtain electron density profiles. The study will compare ISR measured profiles, Digisonde derived profiles and electron density profiles reconstructed from the FLIP model. The theoretical and statistical knowledge obtained from this detailed study will contribute to better interpret the ISR profiles in and around the E-F valley , and help identify those parameters measurable with ionosondes which can be used to unambiguously identify the valley characteristics.

G2-5
1500

THE IRI ELECTRON DENSITY PROFILE

Dr. Dieter Bilitza
GSFC, Code 633.9/HSTX
Greenbelt, MD 20771

The representation of the electron density profile in the International Reference Ionosphere (IRI) will be discussed and the status of improvement efforts will be reviewed. Recent IRI workshops had focussed on global regions where the ionospheric modelling task is particularly difficult, namely the auroral/polar latitudes and the equatorial/low latitudes. Results from these workshops will be reported with particular emphasis on issues related to the electron density profile.

In 1995 an IRI Task Force activity was started at the International Center for Theoretical Physics (ICTP) in Trieste, Italy, which has the F1-region and the bottomside F2-region as its specific topic. Status and progress of this activity will be briefly reviewed summarizing the results of the most recent Task Force effort (November 1995).

New and old data sources will be discussed that could help to improve the IRI electron density profile in the topside and bottomside; this includes TEC data deduced from TOPEX altimeter measurements and as yet unexploited ISIS 1 and 2 topside sounder data.

G2-6
1540

THE BOTTOMSIDE F2 LAYER THICKNESS OF THE IRI MODEL DERIVED FROM DIGISONDE DATA

Xueqin Huang and Bodo W. Reinisch
University of Massachusetts
Center for Atmospheric Research
Lowell, MA 01854

The IRI ionospheric model is frequently used for short wave radio predictions and network design. IRI uses hmF2 and foF2 as well as foF1 values from statistical data averages. The bottomside thickness of the F2 layer is modeled in terms of exponential and hyperbolic functions (Ramakrishnan and Rawer, 1972) using two parameters, B_0 and B_1, which depend on location season and sunspot number. These parameters were empirically determined from inverted ionogram data (Gulyaeva, 1987). Comparison with Digisonde electron density profiles for several low and mid-latitude stations in the American sector show that the F2 layer thickness of the IRI profile is often incompatible with the measurements. This paper investigates whether better results can be obtained if improved B_0 and B_1 parameters are used.

The paper describes how to derive B_0 and B_1 from the coefficients of the monthly average representative profile (ARP) obtained from measured Digisonde profile data. If the ARP-derived B_0 and B_1 parameters are used in the IRI model, good representations of the actual profiles are obtained. Results are shown for a number of different stations, including Jicamarca, Ramey, Millstone Hill and Puerto Madryn.

G2-7
1600

COMPARISON BETWEEN THEORETICALLY-CALCULATED AND OBSERVED ELECTRON DENSITY PROFILES AT LOW AND MID LATITUDES

David N. Anderson
Phillips Laboratory, GPIM
Hanscom AFB, MA 01731-3010
Amanda J. Preble
HQ USAF/XOWR, 1490 AF Pentagon
Washington, D.C. 20330-1490
Dwight T. Decker
Institute for Space Research, Boston College
Chestnut Hill, MA 02167
Robert Schunk
Jan J. Sojka
CASS, Utah State University
Logan, UT 84321

In the past, comparison between ionospheric output (whether they are theoretical or climatological models) and observations have often been limited to comparisons between the ionospheric F-region peak parameters Nmax and Hmax, and less frequently to a comparison of profile shapes. This paper presents a few comparisons in the low and midlatitude region between both bottomside and topside calculated profiles and observations from coherent and incoherent scatter radar measurements. The bottomside F1 layer shape has historically been difficult to model as it represents a transition from the molecular NO+ and O2+ ions to the atomic O+ ion and comparisons with observations are difficult since the layer often cannot be measured by ground-based sounders as it is "hidden" by the daytime E layer. Using the Time Dependent Ionospheric Model (TDIM) of Utah State University for calculating NO+, O2+ and O+ densities, comparisons are presented with midlatitude observations to determine the physical processes which can account for good agreement. At low latitudes, daytime profile shapes are very broad due to the influence of the upward vertical ExB drift velocity. This is especially true during periods of high solar activity. Compared with IRI90, the theoretically-derived ionospheric parameters such as Nmax, Hmax and profile shape which are contained in the Parameterized Ionospheric Model (PIM) have been shown to be in better agreement with Jicamarca observations. We will present a PIM option to IRI90 which replaces certain ionospheric parameters within IRI90 so that the more realistic PIM profiles are reproduced. This procedure is completely transparent to the IRI90 user.

G2-8
1620

COMPARING MEASURED ELECTRON DENSITY PROFILES WITH IONOSPHERIC MODELS

Bodo W. Reinisch[1], Xueqin Huang[1], David N. Anderson[2] and Terence W. Bullett[2]
[1]University of Massachusetts
Center for Atmospheric Research
Lowell, MA 01854
[2]Geophysics Directorate, Phillips Laboratory
Hanscom AFB, MA 01731

A summary is given of the current ionogram profile inversion technique used in the Digisonde network and of available software for the post-processing of ionograms. The Digisondes are one of the major sources for N(h) profiles of the bottomside ionosphere and the accuracy of these ionogram-derived profiles was verified by comparison with N(h) profiles from incoherent scatter radar measurements. Important parameters obtained from the inversion are the peak height of the layers and their half thickness or any other assessment of the profile shape. Plotting contours of electron density (or plasma frequency) as function of time shows the diurnal variations of the profile shape and the peak heights. For the validation of ionospheric models it is not very useful to take individual profiles and compare them with the models. Instead an average representative profile (ARP) is calculated from the individual profiles measured at the same time on different days. Comparisons with the PIM and IRI models use ARP data for Jicamarca (Peru), Ramey (Puerto Rico), and Puerto Madryn (Argentina).

G2-9
1640

A QUALITY INDEX FOR SAN DIEGO VERTICAL SOUNDER DATA

Richard A. Sprague
NCCOSC, RDTE Division
San Diego, CA 92152-5235

In 1939 Booker and Seaton (Phys Rev,57,87-94,1939) showed that in an isotropic ionosphere with a single parabolic maximum of electron density the ordinary mode virtual height at a frequency equal to 0.834 times the layer peak frequency is equal to the true height of the layer for any layer semi-thickness. Model studies indicate that when the earth's magnetic field is included, with parameters typical for San Diego, the frequency ratio for which the ordinary mode virtual height is equal to the layer true height still exists but moves to a somewhat smaller value of about 0.81.

In scaling F-region parameters from San Diego ionograms a non-isotropic ionosphere with a parabolic peak is assumed. One parameter which is routinely scaled is the MUF(3000). This parameter is obtained by a numerical implementation of the 'transmission curve' technique which results in the MUF(3000) being read from the ordinary mode ionogram trace at a frequency-to-peak frequency ratio from ranging from about 0.82 to 0.98, depending on the layer semi-thickness and height. While such ratios exceed the ratio 0.815 discussed above, model studies suggest that even at these ratios the difference between the true layer height and the virtual heights at these frequencies should remain fairly constant, independent of semi-thickness. This difference can then be used as a indicator of the departure of the layer shape from parabolic and, consequently, of the expected accuracy, or quality, of scaled parameters. Results of model studies and examples of this difference parameter derived from San Diego data are presented.

Session H-2, 1355-Tues., CR2-6
LABORATORY SIMULATIONS OF SPACE PLASMAS
Chairperson and Organizer: W.E. Amatucci, Plasma Physics Div., Naval Research Lab, Washington, DC 20375

H2-1
1400

LABORATORY STUDIES OF CURRENT DRIVEN PLASMA PROCESSES WITH THE VERSATILE TOROIDAL FACILITY (VTF)

D.T. Moriarty* M.C. Lee R.J. Riddolls S.M. Murphy
MIT Plasma Fusion Center
167 Albany St.
Cambridge, MA 02139

The Versatile Toroidal Facility (VTF) has been constructed to create plasmas for wave-plasma interaction studies. This project is aimed at simulating the ionospheric plasma turbulence and cross-checking radar experiments at Arecibo, Puerto Rico. Three plasma sources may be combined to produce various conditions: RF, electron beams, and Taylor discharge. The plasma density gradients, field aligned currents, and other geometries and parameter ratios closely match the plasma conditions of the auroral and upper ionospheric regions. Microwave produced and current driven plasma waves have been observed in VTF and instability mechanisms are being studied. Spectral analysis reveals broadband emissions from below the ion cyclotron frequency, f_{ci}, to near the electron cyclotron frequency, f_{ce}. Waves with frequencies corresponding to the whistler and lower-hybrid ranges are consistent with the well known inverse Landau damping of energetic charged particles. Low frequency plasma waves driven by electric currents correspond to ion acoustic and current-convective modes. Existing theory is modified to investigate current convective modes in VTF. The modified current-convective theory predicts excited modes without the typical E x B instability present. Slight geometry differences result in perpendicular electric fields affecting the real frequencies rather that the growth rates of the instabilities. Multi-point cross-correlation measurements have been performed to determine wave numbers of the excited modes and have qualitatively confirmed the modified theory. Differences between VTF experiments and rocket/space shuttle experiments are mainly that strong density gradients do not exist in the space experiments and that VTF produces currents comprised of a drifing maxwellian rather than a beam with large drift energy vesus the local electron temperature. Comparison of VTF experiments with rocket experiments shows VTF can be used to appropriately study ionospheric plasma processes, and complement active experiments in space.

H2-2
1420

IMPLEMENTATION OF TAYLOR DISCHARGE AND MULTI-ELECTRON BEAM SYSTEM FOR SIMULATION OF IONOSPHERIC HEATING EXPERIMENTS IN THE VERSATILE TOROIDAL FACILITY (VTF)

R. J. Riddolls* M. C. Lee S. M. Murphy D. T. Moriarty
M. J. Rowlands D. A. Pooley
MIT Plasma Fusion Center
Cambridge, MA 02139

The Versatile Toroidal Facility (VTF) is a large laboratory plasma machine, approximately 1 m in major radius. The need to cross-check the results of theory and Arecibo field experiments has motivated the implementation of a Taylor discharge device in the VTF machine. The device consists of a central solenoid run resonantly in series with a large capacitor by a switching power supply. At peak performance, the 300 kW power supply is expected to produce a plasma whose ratio of ω_{pe} to ω_{ce} exceeds three. Bipolar transistors placed in a full bridge configuration in series with the LC circuit provide the AC power of 600 amps at 500 volts. Another method of plasma creation involves the use of hot cathode LaB_6 electron beam emitters. Four such emitters are mounted in the VTF machine and can produce plasma with ω_{pe}/ω_{ce} as high as two. Both plasma sources can be used simultaneously, if desired.

Overdense heating experiments performed with VTF involve the injection of a pump wave at 2.45 GHz in the O-mode from a 3 kW magnetron. According to Kuo and Lee (*GRL*, **19**, 249, 1992) PDI-generated Langmuir waves will be scattered into two obliquely-propagating Langmuir waves by background lower hybrid wave turbulence. Two types of waves are formed in the scattering process, as required by frequency and wavenumber-matching conditions. One has a frequency downshifted from the mother Langmuir wave by a local lower hybrid wave frequency (the Stokes mode) and the other has a frequency upshifted by the same local lower hybrid wave frequency (the anti-Stokes mode). The magnitude of the frequency shift can be shown to be inversely proportional to the heater pump wave frequency. Experiments which succeeded in producing the anti-Stokes mode at Arecibo in 1992 showed good agreement with the theoretical prediction of frequency shifts. In VTF, dipole antennas have been installed to observe the simulation of the anti-Stokes mode inside the vacuum vessel.

H2-3
1440

INSTABILITIES DUE TO VELOCITY SHEAR

G. Ganguli*
Beam Physics Branch
Plasma Physics Division
Naval Research Laboratory
Washington, DC 20375

The general kinetic eigenvalue condition for electrostatic waves in a magnetized plasma including inhomogeneous flows both along and across the magnetic field will be reviewed. The free energy associated with an inhomogeneous flow can excite waves in a plasma in a wide range of frequency and wavelength. This is especially pertinent to the space plasma environment where increasing stress during geomagnetically active periods can translate into a large velocity gradient. It is found observationally and by global MHD simulations that stress can build up in the magnetosphere due to solar wind compression. Evidence of this is found throughout the magnetosphere and the ionosphere. Magnetospheric boundary layers, such as the plasma sheet boundary layer and the magnetopause are often characterized by a velocity shear which intensifies during active periods. Significant velocity shear is also observed in the auroral zone. Evidence of the most intense velocity shear in the ionosphere is found to be associated with the black aurora. Strongly sheared flows are generated in chemical release experiments in space, and in laser produced plasma jets in laboratory experiments.

It is found that a stressed medium responds in a fundamentally different manner than the stress-free case. Velocity shear can severely affect the normal modes of a homogeneous plasma and give rise to a number of instabilities in a broad frequency range which can affect the dynamics and morphology of a plasma system. Depending on the magnitude of the velocity gradient, the wave frequency could be small (much smaller than the ion cyclotron frequency), large (larger than the lower hybrid frequency), or anywhere in between. The general nonlocal dispersion condition for electrostatic waves will be analyzed and the physics of the limiting cases leading to different waves will be discussed. Comparison of the theoretical model with laboratory and space experiments will be made. Importance of these waves and their dispersive properties *vis-a-vis* space plasmas will be discussed.

H2-4
1540

TRANSVERSE VELOCITY SHEAR EFFECTS ON CURRENT-DRIVEN ION-CYCLOTRON INSTABILITY: SPECTRAL FEATURES, TEMPERATURE RATIO DEPENDENCE, AND MULTI SPECIES EFFECTS

V. Gavrishchaka* M. Koepke
Physics Department
West Virginia University
Morgantown, WV 26505-6315
G. Ganguli
Beam Physics Branch
Plasma Physics Division
Naval Research Laboratory
Washington, DC 20375

We investigate ion-cyclotron fluctuations driven by the combination of a magnetic-field-aligned electron current and a localized transverse electric field with the extent of localization much larger than an ion gyro-radius. In contrast to local current-driven ion-cyclotron mode (W.E. Drummond and M.N. Rosenbluth, *Phys. Fluids*, 5, 1507-1513, 1962) with only one eigenvalue for each set of parameters, in the prersence of transverse velocity shear multiple roots of the nonlocal dispersion relation exist. We solve the nonlocal dispersion relation (G. Ganguli et al., *J. Geophys. Res.*, 99, 8873-8889, 1994) for these multiple eigenvalues and provide a simple physical explanation for the results obtained. We find that in addition to the lowering of the threshold field-aligned current the existense of multiple roots leads to the following important differences between the local current-driven ion-cyclotron mode and the ion-cyclotron modes in the presence of velocity shear: 1) Narrow spectrum of the ion-cyclotron wave in the local case transforms to a broadband frequency spectrum in the presence of velocity shear; 2) the growth rate of the local mode decreases with decreasing electron temperature T_e (J.M. Kindel and C.F. Kennel, *J. Geophys. Res.*, 76, 3055-3078, 1971), while the growth rate of the nonlocal modes does the opposite; 3) the growth rate of the local mode decreases rapidly with the increase of the ion temperature T_i (J.M. Kindel and C.F. Kennel, *J. Geophys. Res.*, 76, 3055-3078, 1971, and P.J. Palmadesso et al., *Geophys. Res. Lett.*, 1, 105-107, 1974), but in the presence of velocity shear this dependence is weak; 4) the presence of velocity shear changes significantly the behaviour of the ion-cyclotron instability in a multi-component plasma as compared to the local case discussed by J.M. Kindel and C.F. Kennel (*J. Geophys. Res.*, 76, 3055-3078, 1971). We discuss possible applications of our results to space and laboratory plasma.

H2-5
1600

CURRENT ISSUES REGARDING GEOSPACE-RELATED ELECTROSTATIC WAVES IN THE PRESENCE OF VELOCITY SHEAR

M. E. Koepke
Department of Physics, West Virginia University
Morgantown, West Virginia 26506-6315

Observations from space-borne instruments are typically interpreted using theoretical models developed to predict the properties of geospace. Laboratory experiments verify important aspects of predictions of plasma instabilities used in these theoretical models of geospace plasma processes and therefore contribute to a better understanding of space processes which cannot be subjected to controlled experimental investigation. The steady-state and dynamical properties of geospace are influenced by processes acting over a wide scale range (temporal and spatial), across which they are believed to be coupled.[1] It is likely that instabilities excited by velocity shear play an important role in this coupling.

Past laboratory experiments related to velocity-shear-driven instabilities have been performed primarily on Q machines.[2] Aspects of instabilities associated with shear in the parallel and transverse velocity have been investigated. The observed mode frequencies extend from much smaller than the ion gyrofrequency, *e.g.*, transverse[3,4] and parallel[5] Kelvin-Helmholtz modes, to comparable to the ion gyrofrequency, *e.g.*, ion-cyclotron modes,[6-8] and up to the lower-hybrid frequency, *e.g.*, a beam-related mode.[9] Recent results in devices other than Q machines have been reported of waves in the ion-cyclotron range[10] (space-physics-simulation-chamber plasma) and in the lower-hybrid range[11] (laser-produced plasma).

This session includes reviews of previous results, reports of recent results yet unpublished, and theoretical interpretations and predictions from many of the groups responsible for the work mentioned above. A roundtable discussion will be encouraged on aspects of velocity-shear excitation mechanisms that are capable of being observed in the laboratory and which are important in space plasma modeling.

[1]Ganguli *et al.*, *JGR* **99**, 8873, 1994.
[2]Rynn/D'Angelo, *RSI* **31**, 1326, 1960.
[3]Jassby, *PF* **15**, 1590, 1972.
[4]Huld *et al.*, *Phys Fluids B* **3**, 1609, 1991.
[5]D'Angelo/von Goeler, *PF* **9**, 309, 1966.
[6]Sato *et al.*, *PRL* **57**, 1227, 1986.
[7]van Niekerk *et al.*, *PP Contr. Fusion* **33**, 375, 1991
[8]Koepke *et al.*, *Phys. Plasmas* **2**, 2523, 1995.
[9]Yamada/Owens, *PRL* **38**, 1529, 1977.
[10]Amatucci *et al.*, 1995 PELS Workshop, Scotland.
[11]Peyser *et al.*, *Phys. Fluids B* **4**, 2448, 1992.

Session J-1, 1335-Tues., CR0-30
TECHNIQUES FOR REDUCING ANTENNA NOISE IN RADIO TELESCOPES
Chairperson and Organizer: P.J. Napier, National Radio Astronomy Observatory, Socorro, NM 87801

J1-1
1340

SHIELDING TELESCOPES FROM GROUND NOISE

Michael M. Davis*
Arecibo Observatory
P.O. Box 995
Arecibo, PR 00613

Ray paths linking a feed horn and the ground introduce unwanted noise. Metal screens are used frequently on radio telescopes and communications antennas to redirect these unwanted ray paths to cold sky. Practical experience has shown that ground screens can be a very cost effective way to improve the performance of both new and existing instruments.

Many well known radio telescopes including Effelsberg, Pico Veleta, Ohio State and Nancay have ground shielding. A ground screen 16 m high and 1 km long has been erected around the perimeter of the Arecibo telescope, as one of the major components of the upgrading program presently under way there. The improvement in performance is particularly effective with this 305 m diameter fixed spherical reflector, as the screen intercepts rays in the primary illumination pattern which have moved off the reflector at high zenith angles. Measurement of system temperature with a 21 cm line feed, carried out with and without the ground screen in place, show an improvement of 28K at the maximum zenith angle of 20 degrees.

The Gregorian subreflector, now under construction, will move the illumination pattern 15m downhill, further reducing the vignetting noise. With this offset, the measurements project a further 14K noise reduction. The system temperature increase with zenith angle for the 21 cm line feed system, prior to installation of the ground screen, was 47K. In contrast, the Gregorian system temperature is expected to increase by no more than 5K at maximum zenith angle, an order of magnitude improvement.

Receivers have improved to the point that they frequently contribute only a small fraction of the total system temperature, and further reductions must be sought elsewhere. Careful consideration of diffracted and scattered ray paths may identify cost effective shielding options. These can significantly reduce the system temperature contributed by the telescope's 300K environment.

J1-2
1400

REDUCING THE CONTRIBUTION OF INVERTED-Y SUPPORTING TRIPODS TO THE NOISE TEMPERATURE OF RADIO TELESCOPES

Fernando J. S. Moreira Aluizio Prata, Jr.*
University of Southern California
Dept. of EE-Electrophysics
Los Angeles, CA 90089-0271
Michael A. Thorburn
Jet Propulsion Laboratory
4800 Oak Grove Drive
Pasadena, CA 91109-8099

Depending on the geometry, the struts used to support subreflectors (or feeds, in single reflector systems) of radio telescopes can pick up a significant amount of thermal noise from the ground surrounding the antenna. Invoking the reciprocity principle to analyze the radio telescope as a transmitting antenna it can be established that, for large physical apertures operating at moderate elevation angles, the dominant strut-related ground-noise contribution is produced when the collimated wave leaving the antenna scatters on the strut. Furthermore, this dominant contribution comes primarily from the struts attached to the collimating-reflector upper half. Due to this fact, an inverted-Y supporting tripod geometry generally has less noise contribution than other commonly used alternatives. In this work the inverted-Y tripod is then considered and optimized to reduce its associated noise pickup.

In order to determine the ground-noise pickup of the inverted-Y configuration, a numerical analysis has been carried out assuming that the radio telescope operates transmitting energy. In this situation a near-plane wave illuminates the struts, and the corresponding scattered electromagnetic field has been determined with high accuracy using integral equation techniques. Also, advantage has been taken of the fact that, on electrically large apertures, the struts have an electrically large length and hence can be modeled as infinitely long. The obtained strut-scattering characteristics have then been used to calculate the strut relative noise temperature contribution, as a function of the antenna elevation angle. With this information the top-strut cross-section has been optimized to yield minimum ground-noise pickup.

The results obtained indicate that minimum strut-related ground-noise pickup is achieved with struts that have a sharp edge directed towards the collimating reflector. In particular, an optimum closed-form tear-drop cross section was derived for the inverted-Y top strut. As a final conclusion it has been determined that, depending on the radio telescope existing supports, retrofitting the strut cross section may yield a five times reduction of the strut-related noise-temperature.

J1-3
1420

NOISE SHIELDS AND FEEDS FOR THE GBT

S. Srikanth
National Radio Astronomy Observatory*
2015 Ivy Road
Charlottesville, VA 22903

The Green Bank Telescope (GBT) which is under construction at the National Radio Astronomy Observatory (NRAO) site in Green Bank, WV uses a double-offset geometry with its aperture completely free of any blockage. In the design phase of the telescope, comparisons were made between on-axis antennas and clear aperture antennas. The blockage-free design provides higher gain, reduced far-out sidelobes, lower system temperature and minimized standing waves as compared to an on-axis design. The GBT has an adjustable primary reflector of 100 meters projected aperture. A laser ranging system under development at NRAO will be used to adjust the primary to 0.009" rms and achieve precision pointing up to about 90 GHz. Rapid receiver selection and switching between prime focus and secondary focus operation will also be possible.

The illumination taper for the feeds was determined after optimizing for gain/system temperature. A few trade-offs have been made because of the size of the feeds at lower frequencies. In the absence of aperture blockage, a few effects considered minor in an on-axis telescope could become dominant and, efforts have been made to minimize such effects. For example, attention has been paid to minimize scattering from the gaps between surface panels and edge diffraction effects. The subreflector subtends a half-angle of 15 degrees from the secondary focus, and the antenna specification calls for a blockage-free region in the 15 to 30 degree radial range around the feed axis. However, structural members of the support arm that holds the subreflector and the feeds are present in this region. The cross-section of this structure subtends angles between 5 and 18 degrees in the circumferential direction in the 15 to 30 degree range. The spillover energy that strikes the structure in the above region gets scattered in different directions, while a portion of the energy strikes the hot ground resulting in increased antenna temperature. Noise shields have been designed to be installed in the region around the subreflector. These shields block the support arm structure and direct the energy into the main reflector. The spillover energy is then directed into the cold sky by the main reflector. This can be interpreted as the reduction of far-out sidelobes and an increase in near-in sidelobes of the antenna beam pattern. The reduction in system temperature is about 1.5 K at 1.15 GHz and 1 K at 4.90 GHz. Design of the noise shield and its effect on the sidelobes will be discussed.

*The National Radio Astronomy Observatory is a facility of the National Science Foundation operated under cooperative agreement by Associated Universities, Inc.

J1-4
1440

ANTENNA NOISE IN THE BERKELEY-ILLINOIS-MARYLAND ARRAY

J. B. Lugten* W. J. Welch J. L. Gibson
Radio Astronomy Lab.
University of California
Berkeley, CA 94720

The antennas of the Berkeley-Illinois-Maryland Association (BIMA) millimeter array have been designed to minimize the antenna contribution to system noise. One reason for their small noise contribution is that the tripod legs which support the subreflector pass outside the edge of the primary mirror and thus do not shadow large areas of the primary mirror. The tripod legs block only 1.4% of the antenna's geometrical area. Also, because of the tripod geometry, much of the light scattered by the legs into the receiver feeds originates from the cold sky rather than from the ambient temperature surroundings. A second important reason for the telescopes' low noise performance is that their optical design is very simple and clean; no additional mirrors intervene between the receivers and the secondary mirror. The use of additional mirrors between the receivers and the secondary mirror is avoided by placing the feeds for each of the (up to 4) frequency bands slightly off axis in the Cassegrain focal plane. The resulting coma is negligible. The telescope pointing must be offset slightly to switch frequency bands.

The total antenna noise is the sum of many small contributions; no single source dominates. Most of the total measured antenna noise is accounted for by the known noise sources. Some of the larger noise contributions are due to the ohmic losses of the primary and secondary mirror, the reflection losses from the membrane window of the receiver cabin, and the scattering of radiation into the feed horns by the subreflector tripod. The geometry of the tripod legs is such that much of the radiation scattered into the feeds by the legs comes from directions close to the primary beam, with smaller amounts arriving from directions further off axis. At the zenith, almost all of this scattered radiation comes from the cold sky; as the telescope elevation is decreased, progressively more radiation is coupled in from the ground, amounting to about 1.2 K at 15 degrees elevation. It is important to include this elevation dependence of the tripod scattering in the analysis of measured tipping curves.

An older antenna of the BIMA array has subreflector support legs which do not extend beyond the edge of the primary mirror. Its noise performance is somewhat worse than that of the current design.

J1-5
1520

OBSERVING THE COSMIC MICROWAVE BACKGROUND: NOISE REDUCTION IN THE OWENS VALLEY 5.5M TELESCOPE

T. Herbig
Princeton University Physics Department, Jadwin Hall Princeton, NJ 08544-0708

The 5.5 m radio telescope at the Owens Valley Radio Observatory is dedicated to observations of the cosmic microwave background radiation (CMB). With this instrument, observations of the Sunyaev-Zeldovich effect (SZE) were made in several nearby clusters of galaxies (T. Herbig *et al.*, *Astrophys. J.*, **449**, L5–L8, 1995; S. Myers *et al.*, in preparation) with 9σ to 16σ detections. Observations of the intrinsic anisotropy of the CMB on intermediate angular scales are ongoing and will continue this winter.

CMB observations require highly sensitive instrumentation, because the expected signals are on the order of tens of microkelvins; thus, the design had to combine the need for low-noise instrumentation with the requirement of small systematic effects.

The instrument is based on an existing on-axis Cassegrain telescope, as the cost of a clear-aperture system of this size would have been prohibitive. This means that the suppression of ground pickup had to receive particular attention. For instance, a redesign of the secondary support structure reduced the total ground pickup of the telescope from 27 K to 9 K (C. R. Lawrence, T. Herbig, and A. C. S. Readhead, *Proc. IEEE*, **82**, 763–767, 1994). Adding the contributions from the atmosphere and the CMB, the total system temperature at the zenith is 52 K. The receiver is a dual-feed system that operates at a frequency of 32 GHz with a bandwidth of 5.7 GHz and a receiver temperature of 33 K.

This paper assesses some the of the instrument aspects which improved the sensitivity of the system and some of the trade-offs which compromised it. The discussion includes receiver design, ground spillover, ground screens, and the control of systematic effects.

J1-6
1540

REDUCTION OF GROUND NOISE IN RADIO TELESCOPE ANTENNAS BY MODIFYING FEED STRUTS AND REFLECTOR EDGES

T.L. Landecker*
Dominion Radio Astrophysical Observatory
National Research Council of Canada
PO Box 248
Penticton, B.C., Canada V2A 6K3

Techniques are described for the reduction of ground noise received by a radio telescope reflector antenna. These techniques redirect energy from sidelobes in the back hemisphere to sidelobes in the front hemisphere and must be applied with care if antenna performance is not to be degraded.

Analysis of the measured radiation pattern of a 9-m prime-focus paraboloid indicates that 5K is contributed by scattering of ground radiation from the feed support struts into the aperture. This contribution is calculated, based on simple theory, and measurements verify the predictions. Feed struts of triangular cross-section can reduce antenna noise by 3 K.

A cylindrical shroud, attached at the rim of the reflector, can reduce noise from direct spillover. If the shroud is parallel to the reflector axis, it can reduce gain and have other deleterious effects on the radiation pattern. The bad effects can mostly be eliminated by using a shroud which is not parallel to the axis, but flares outwards. Calculations using a method of moments routine show that the effects of the shroud can be quite accurately predicted using geometrical optics. The energy redirected into the forward hemisphere can be spread over a large angle by shaping the shroud; this provides a method of controlling the peak sidelobe level.

Calculations for a prime-focus paraboloid of diameter 45 wavelengths show that a shroud of height 5 wavelengths reduces the contribution from ground radiation by 6 K.

Antennas of diameter about 10 wavelengths are very difficult to feed efficiently without unacceptable aperture blockage, and consequently have very high spillover. Shrouds can dramatically reduce spillover in such antennas.

J1-7
1600

SENSITIVITY COMPARISON OF POTENTIAL MMA ANTENNA DESIGNS

Peter J. Napier
National Radio Astronomy Observatory
Socorro, NM 87801

The Millimeter Array (MMA) is a proposed new radiotelescope consisting of 40 eight meter diameter antennas operating in the frequency range 30-350 Ghz. Two different antenna designs for the MMA have been studied. In this paper we compare the sensitivity of the two designs using the ratio gain/system temperature (G/T) as a figure of merit. Since the MMA will be located on a site with very low atmospheric absorption, and because it can be expected that on the time scale of the MMA millimeter wavelength receivers will have very low receiver temperatures, the impact of antenna noise on G/T is significant.

One of the antenna designs is a conventional symmetric paraboloid reflector on an elevation-over-azimuth mount. This design, which is based on the antennas used for the BIMA millimeter array, uses a minimum blockage quadrupod subreflector support. In this type of support the legs extend all the way to the edge of the primary reflector, removing the spherical wave blockage due to feed leg shadowing that is usually present at the edge of the primary reflector. This design has very good G/T performance.

The other potential antenna design is an offset reflector, not blocked by a subreflector support structure, mounted on a slant-axis-over-azimuth mount. In this type of mount the upper axis is not orthogonal to the azimuth axis and has some stiffness advantages over a conventional mount. The asymmetric geometry of the offset reflector causes the polarization and field-of-view to be degraded. This degradation can be cured by the addition of two reflectors to the optical path. Although small, the signal loss and added noise associated with these additional reflectors have a significant impact on G/T, thereby eliminating the sensitivity advantage of the clear aperture design.

0815-Wed:, MATH 100
PLENARY SESSION

0815 Introduction

Session A-1, 1335-Wed., CR1-40
ELECTROMAGNETIC FIELD METROLOGY
Chairperson: M. Kanda, National Inst. of Standards and Technology, Boulder, CO 80303

A1-1
1340

COMPLEX ANTENNA PATTERN MEASUREMENTS USING INFRARED IMAGING AND MICROWAVE HOLOGRAPHY

John E. Will, John D. Norgard, and Ronald M. Sega
University of Colorado
Colorado Springs, CO 80933
and
Carl F. Stubenrauch and Katie MacReynolds
National Institute of Standards and Technology
Boulder, CO 80303
and
Michael Seifert
Rome Laboratory (RL/ERST)
Griffiss AFB, NY 13441

Abstract

Complex (magnitude and phase) measurements of the radiating field at several locations over a known surface in the near field of a radiating antenna can be used to determine its far-field radiation pattern. Current infrared (IR) imaging techniques, which have been successfully used to rapidly map the magnitude of a radiating field at many locations (mXn camera pixels per image capture) over a surface, suffer from an inability to determine phase information. This paper discusses the progress made to date using the concepts of microwave holography to determine both magnitude and relative phase information from infrared imaging data; thus, enabling near-field measurements of antenna patterns using the IR thermal imaging technique.

A1-2
1400

EFFECTIVENESS OF FIBER OPTIC CONNECTOR FEEDTHROUGHS IN SHIELDING ELECTROMAGNETIC INTERFERENCE

Keith D.Masterson, David R.Novotny and Galen H.Koepke
Electromagnetic Fields Division
National Institute of Standards and Technology
Boulder, CO 80303

Commercially available fiber optic connector styles (ST, SC, and FC) used with bulkhead-adapter feedthroughs were tested to determine the extent they degraded the electromagnetic shielding of electronics enclosures. Metal, plastic, and ceramic components were included in the test matrix. We used a nested reverberation cell measurement technique [1] and covered a frequency range from 1 GHz to 16 GHz. The shielding effectiveness of our reference nested cell was approximately 90 dB and quite flat with frequency except for a slight resonance near 14 GHz. The results of our measurements show degradation in the shielding effectiveness due to the connector feedthroughs that ranged from only a few dB for an all metal FC style to a loss of more than 70 dB for a duplex SC style. We compared experimental measurements for shielding effectiveness for the small circular apertures required to mount the adapter barrels to theory in order to more accurately determine the Q of the nested cell and to adjust the effective cross sections that we calculate for the feedthroughs. The effective cross section can be used to estimate the degradation in the shielding effectiveness for enclosures other than our reference cell. In some cases, the feedthroughs coupled more energy into the enclosure than was coupled in through the empty hole in the mounting plate that was required for its installation. The extrapolation of the data to higher and lower frequencies is discussed.

1. D.A. Hill, M.T. Ma, A.R. Ondrejka, B.F. Riddle, M.L. Crawford, and R.T. Johnk, "Aperture Excitation of Electrically Large, Lossy Cavities," *IEEE Trans. Electromagn. Compat.*, vol. 36, pp. 169-177, 1994.

A1-3
1420

THE TIME-DOMAIN MEASUREMENT OF THE REFLECTIVITY OF A URETHANE / FERRITE COMPOSITE ABSORBER FROM 20-1000 MHZ

Robert T. Johnk
Arthur R. Ondrejka
Herbert W. Medley
Motohisa Kanda
National Institute of Standards and Technology Boulder, CO
and
Christopher L. Holloway
Institute for Telecommunications Sciences, U.S. Department of Commerce, Boulder, CO

During the past six years, there has been much interest at NIST in the time-domain measurement of pyramidal absorber reflectivity. Up to this point, the efforts at NIST have been primarily directed at the measurement of urethane absorbers. However, there have been tremendous advances in anechoic chamber technology, due to the availability of new absorbers as well as significant advances in efficient and accurate modelling techniques. In response to these developments, NIST has recently performed a series of measurements on a 1m x 1m sample of a state-of-the-art urethane/ferrite tile composite absorber. This type of absorbing structure is heavily used in the construction of EMC/EMI test chambers that operate in the 30-1000 MHz range, primarily for purpose of emissions testing.

The particular absorber sample that was evaluated was a layered structure consisting of a urethane absorber, ferrite tiles, plywood, and an aluminum back plate. Reflectivity data were obtained by illuminating the sample with a NIST-developed ultra wideband time-domain reflectometer system. This system is easy to implement with modest hardware and instrumentation requirements, and absorber reflectivity data can be obtained with this system over a wide frequency range in a short time. Reflectivity data are presented in the 20-1000 MHz range for ferrite tile panels and a ferrite tile/urethane composite structure. The results dramatically demonstrate the advantage of using composite absorbers in the construction of low-frequency anechoic chambers.

A1-4
1440

A STANDARD SOURCE METHOD FOR REDUCING ANTENNA FACTOR ERRORS IN SHIELDED ROOM MEASUREMENTS

Dennis Camell and Galen Koepke
Electromagnetic Fields Division
National Institute of Standards and Technology
Boulder, CO 80303

Calibration of a receiving antenna in the test environment that it is used will improve the accuracy and repeatability of the test. Test results from shielded rooms are often based on antenna factors (AFs) derived from outdoor sites. These AFs are determined from uniform, plane-wave electric-fields, which are unlike the environment in the shielded room. A method is developed which will measure the AF within the environment of the shielded room. This should improve the results obtained in the shielded room environment.

A well characterized standard source of electromagnetic radiation is used to calibrate the effects of shielded rooms on antenna factor. This source is a 10 cm spherical dipole with an optical fiber interface. The magnitude of the electric-field radiated from the spherical dipole is set by a transfer function. This transfer function was determined empirically from calibrations at the NIST open area test site (OATS) and anechoic chamber.

The calibration of the receiving antenna is performed in a shielded room and the results tested using MIL-STD 461/462 RE 102 emissions measurements with a simulated device-under-test (DUT). A fixed length dipole with a fixed CW source was used as the simulated DUT. Frequencies of interest are 30 to 1000 MHz. The measurements are performed at three different sites and the results compared. Results show that compensating for the room effects does improve test results.

A1-5 1520 AN IMPROVED TECHNIQUE FOR THE MEASUREMENT OF EMI GASKETS FROM 20 MHZ TO 2 GHZ

Arthur R. Ondrejka
Robert T. Johnk
Motohisa Kanda
National Institute of Standards
and Technology
Boulder, CO 80303

Several techniques are being used to evaluate the effectiveness of EMI shielding gaskets, and there are a variety of commercially available devices to perform these measurements. No one method has been satisfactorily accurate. The technique described here was developed to improve the accuracy of the measurement by combining the best features of the shielding effectiveness measurements and the trans-impedance method. It provides an incident rf field applied to the gasket which is a TEM mode of known amplitude.

The device used in this method is a terminated 5 ohm strip-line transmission line. Two similar gaskets are used, one on either side of the center conductor, shorting it to each of the two ground planes. The gasket is chosen to have a smaller dimension than the width of the center conductor and so forms a small cavity. The gasket becomes the perimeter of the cavity, while the center conductor and one of the ground planes form the top and bottom surfaces. A signal propagating down the transmission line is applied to the edge of the gasket, and the residual signal which penetrates into the cavity is measured by a 50 ohm probe.

The probe measures the voltage on the center conductor with and without the gaskets in place, and the ratio is a measure of the gasket shielding effectiveness. Alternatively, the current which is applied to the gasket can be estimated from a measurement of the net applied rf voltage and the impedance of the transmission line. A greater certainty in the accuracy results from a comparison of the two approaches. A Time-Domain measurement system is used for the voltage measurements in our experiments, and it provides significant insight into the characteristics of the gaskets, and the most likely modes of signal penetration.

A1-6
1540

PLANE-WAVE-SPECTRUM REPRESENTATION FOR FIELDS IN REVERBERATION CHAMBERS

David A. Hill
Electromagnetic Fields Division
National Institute of Standards and Technology
Boulder, CO 80303

Reverberation chambers (also called mode-stirred chambers) are experiencing increased use for radiated emissions and immunity measurements. They are large, multimode cavities that use either mechanical stirring (paddle wheel) or frequency stirring to create a statistically uniform field. A plane-wave-spectrum representation of the fields in a reverberation chamber will be described in this talk. The fields are described by an integral of propagating plane waves over the visible region (real angles), and the plane-wave coefficients are random variables with appropriate statistical properties (D.A. Hill, M.L. Crawford, M. Kanda, and D.I. Wu, IEEE Trans. Electromag. Compat., 35, 69-74, 1993). Ensemble averages of relevant quantities can be derived to predict measured quantities averaged over stirrer position (for mechanical stirring) or frequency (for frequency stirring).

The theory has been used to derive the following results for ensemble averages that are consistent with reverberation chamber measurements: (1) the squared magnitudes of the electric and magnetic fields are independent of position and are related by the square of the free-space impedance, (2) the power received by an antenna is independent of its directivity and polarization properties, (3) the power received by a test object (immunity measurement) is given by an average over all incidence angles and polarizations, and (4) and an emissions measurement gives the total power radiated over all angles. Some comparisons of theory and emissions and immunity measurements will be presented.

The theory has been used to derive an expression for chamber Q (J.M. Dunn, IEEE Trans. Electromag. Compat., 32, 53-58, 1990) that is consistent with cavity mode theory. The theory has also been used to derive the spatial correlation function (D.A. Hill, IEEE Trans. Electromag. Compat., 37, 138, 1995) that is consistent with theoretical results for cavity modes (T.H. Lehman, Interaction Note 494, 1993), radiative transfer (E. Wolf, Phys. Rev. D, 13, 869-886, 1976), and acoustic reverberation chambers (R.K. Cook, R.V. Waterhouse, R.D. Berendt, S. Edelman, and M.C. Thompson, J. Acoust. Soc. Amer., 27, 1072-1077, 1955).

A1-7
1600

TRANSIENT EVALUATION OF MODE-STIRRED CHAMBERS

John M. Ladbury, Robert T. Johnk, and Arthur R. Ondrejka
Electromagnetic Fields Division
National Institute of Standards and Technology
Boulder, CO, 80303

Electromagnetic reverberation chambers have become increasingly popular in recent years. They provide an excellent environment for immunity testing, and have recently been employed for emissions testing as well. Before any chamber can be used, it must be carefully evaluated, so that the field intensity inside the chamber as a function of input power can be estimated. It is therefore necessary to obtain an estimate of the chamber quality factor (Q). The quality factor is important because it measures the ability of a chamber to store modal energy in the form of high field strengths.

The traditional method for measuring chamber Q involves measurements of the net input power and received power at several positions of a large rotating paddle, and an average Q is calculated based on these values, as well as the chamber volume. This method suffers from a variety of problems. First, only simple chamber geometries with easily measured or estimated volumes can be evaluated. Second, the method is time consuming, and the measurement time can often be measured in days. Lastly, this method assumes perfect antennas, and does not include receive antenna mismatches or antenna efficiencies.

In this talk, we will present a method of rapidly measuring the average chamber quality factor over a broad frequency band, and at only a single paddle position, using time-domain techniques and time-frequency analysis. The impulse response of the chamber is measured, and the resultant waveform is processed using a short-time Fourier transform. The decay rate of the spectral components as a function of time is inversely proportional to the chamber Q. This method yields results which are independent of measurement antenna and chamber volume. The combination of all these advantages results in a method which is less complicated, faster, and more repeatable than the traditional measurement method, and also appears to be more accurate, as well.

A1-8
1620

NEW EMF PHOTONIC SENSORS

Hubert Trzaska Pawel Bienkowski*
EM Environment Protection Lab.
ITA, Technical University of Wroclaw
POLAND

EMF is represented by the electric (**E**) field vector, the magnetic (**H**) field vector and by the Poynting vector, the latter reflects the radiated power density. EMF measurements are performed in the far field and in the near field. EMC involvement of the authors focuses their attention on the near field EMF measurements. That kind of measurements limits methods that can be applied. Disturbance of the measured EMF distribution by a sensor and mutual interaction of the sensor and the source of the field are the main problems in this case. Every conducting body put into the field becomes the secondary radiator, that has important influence on the resultant field distribution. Because of this resistive transmission lines to connect the sensor with an indicator are commonly used.

An effective solution here is the use of an optic carrier and an optic fibre as the transmission line. This was the first, the most 'primitive', photonic application in the field. The second step here there was the use of a photonic EMF sensor with an electrooptical effect. Crystal, that is the most popular in practice is the Niobian Lithium $LiNbO_3$ (the authors use this crystal too).

There are two types of optical modulators widely applied: polarimeters and interferometers. In both of them tuning of optical bias angle is very important, but typically used methods don't enable to change fluently the bias angle or e.g. to minimaze a temperature drift. The authors have suggested somewhat new approach to this problem. The main idea is based upon an additional optical compensation element, which is tuned by DC voltage applied. Known photonic sensors, with no regard to their type, allow to measure fields (voltages) that cause phase (polarization) shift not exceeding $\pm\pi/2$. Presented solution enables not only continuous regulation but, by the use of a negative feedback and the compensation concept, the measurement of unlimited magnitudes.

A sensitivity is the only disadvantage of the present solutions of the photonic EMF sensors. Apart from the technological tries to work out new, more sensitive crystals the authors have worked out new circuitry that ensures increase of sensitivity. The first of them requires multiple access of an optic ray to EMF modulator. In practice it enlarges the optical length of the modulator and, as a result, it permits to increase the sensitivity almost in n-times. The second one is based upon the use of frequency modulation of a laser beam. The EM Environment Protection Lab. latter assures the sensitivity increase much above levels obtained till now.

Session B-2, 1335-Wed., CR2-6
ANTENNAS
Chairperson: T.S. Angell, Center for the Mathematics of Waves, Dept. of Mathematical Sciences, Univ. of Delaware, Newark, DE 19716

B2-1
1340

ASYMPTOTIC APPROXIMATIONS FOR OPTIMAL CONFORMAL ANTENNAS

Thomas S. Angell* Ralph E. Kleinman
Center for the Mathematics of Waves
Department of Mathematical Sciences
University of Delaware
Newark, DE 19716
Boris Vainberg
Department of Mathematical Sciences
University of North Carolina
Charlotte, NC 28223

In earlier work, we have given constructive methods to compute the surface currents on a conformal antenna which is required to radiate a maximal amount of energy into a predetermined sector of the far field. The resulting optimization problem was considered as a constrained optimization problem with constraints on the set of input currents which reflected certain physical limitations.

Recently, the authors have used asymptotic methods to compute approximate optimal surface currents in the time harmonic two–dimensional electromagnetic case (the Helmholtz equation with impedance boundary condition), for the case of high frequency. The analysis is complicated by the fact that we are dealing simultaneously with two large parameters, both the wave number k and the position $\mathbf{x}$. Moreover the radiation pattern is related to the current distribution through either the Dirichlet–to–Neumann or Neumann–to–Dirichlet map (depending on the polarization) on the antenna surface. In general these maps are not known explicitly. However our work effectively constructs these maps at high frequencies for convex surfaces.

The analysis involves defining a related time dependent problem which approaches the original problem for large time in a way very different from the Fourier transform of the frequency domain problem. The distinguishing feature of this new formulation is that the large time behavior corresponds to the high frequency behavior of the time harmonic problem rather than the low frequency behavior as is the case in the usual time dependent formulation. By applying the principle of limiting amplitude, we succeed in obtaining the high frequency characterization of the Green's function for the problem and then an explicit form for an approximation to the optimal current.

In the present work, we extend these asymptotic results to the full three–dimensional time–harmonic electromagnetic case with Leontovich condition. We obtain a representation of the suboptimal current which explicitly shows the dependence on the total curvature of the radiating structure at each point, $\kappa(\mathbf{x})$, and the surface impedance $\lambda(\mathbf{x})$. Specific computations are carried out for some canonical shapes.

National Radio Science Meeting (Boulder CO), Jan. 1996

B2-2
1400

VARIABLE BEAMWIDTH REFLECTOR ANTENNA WITH ARRAY FEED

David
A D Olver and J U I Syed
Queen Mary and Westfield College
Mile End Road
London E1 4NS
United Kingdom

The growing use of remote sensing from aircraft and satellites can benefit from the use of a variable beamwidth antenna so that the footprint of the antenna on the ground remains constant as height changes. Reflector antennas can be made to radiate a variable beamwidth by mechanically defocusing the feed. This leads to a phase taper across the aperture plane which defocuses the parabolic reflector and causes the radiated beam to spread in space and the on-axis gain to decrease. In this paper it is shown that the same outcome can be obtained by using a small array as the feed for a reflector antenna. This allows the phase taper to be controlled electronically.

Array fed reflector antennas have been widely studied, but not for the purposes of changing the beamwidth of a focused reflector. In order to investigate the potential of this antenna a study has been performed with both single and dual reflector antennas. This used simple array theory to predict the feed performance and then Physical Optics to predict the radiation characteristics of the complete antenna. Phase only control of the elements gives a good performance which is similar to that obtained when the feed is physically moved. Ideally a large array would be used, but there is insufficient space in the focal region of a practical reflector. It was found that a seven element planar array produced acceptable phase control.

A parametric study showed that the maximum phase taper depends on the reflector F/D ratio. The location of the array feed can be selected to give maximum variability of the beamwidth. It is not necessary to place the array directly in the focal plane because the phases of the array elements can be adjusted to compensate. The beamwidth can be changed by more than 200% (three times the focused beamwidth) as long as the commensurate gain loss is acceptable.

Experimental verification of the predictions has been provided by constructing a three element linear array of open-ended waveguides as the feed for a 30 GHz Cassegrain antenna with a main reflector diameter of 122λ and a subreflector diameter of 16λ. The focused -10 dB beamwidth was measured as 0.8°. By changing the relative phase of the outer elements of the array from 0° to 260°, the beamwidth increased to 2.8°. The relative on-axis gain loss was -11 dB. The measured results exactly confirmed the theoretical predictions.

Phases
phase center - moved
by cumulative
phase

Eap remains the same
but gain changes
due to HP change

Haven't looked at
spillover, but is included,

National Radio Science Meeting (Boulder, CO), Jan. 1996

B2-3
1420

GAIN ENHANCEMENT OF WIDE FLARE ANGLE HORN ANTENNAS USING METALLIC BAFFLES

Matthew A. Koerner, Robert L. Rogers
Applied Research Laboratories
The University of Texas at Austin
Austin, TX 78713-8029

Reduces length of pyr. horns.

The gain of a wide flare angle pyramidal horn antenna has been significantly increased by arranging simple geometric metallic structures inside the antenna. Field phase curvature at the antenna aperture, characteristic of horn antennas, was reduced when using these loading schemes. A gain improvement of 5.5 dB was achieved on a horn with a flare of 45 degrees and axial length of 5.3 lambda utilizing simple planar metallic baffles placed in the antenna. Experimental results were compared to numerical results using a moment method model of the antenna and loading structures. Both results were in close agreement, and numerical models were used to analyze the loaded antenna system. Economical, compact, high gain antennas can be produced by using these loading schemes.

MFIE code — Pulse-fit match along horn

2D E-plane MoM code compared well to 3D horn measurements

Measured 10.3 GHz

$\epsilon_{ap} = 45\%$

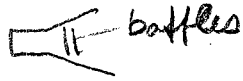

short horn

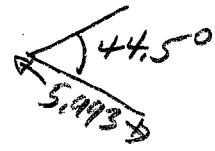

Comparison: Optimum gain

same aperture

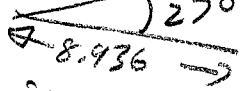

calculated and measured

Gain increased from 19 to 22 dB over optimum

Baffles act to reform spherical wave

all the way across in H-plane

Narrows bandwidth too

Tried baffles oriented 90° from above and it worked as well.

Tried one baffle and it didn't work.

needed to use finite thickness in models since used MFIE / Need to look at impedance matching

B2-4
1440

A RIGOROUS TECHNIQUE FOR SYNTHESIS OF OFFSET REFLECTOR ANTENNAS

Vladimir Oliker
Emory University, Atlanta, GA 30322
and
Matis, Inc., Atlanta, GA 30329

The geometric optics approximation may be used in design of offset single and dual nonaxially symmetric reflector antennas when it is required to control the field amplitude and/or phase on the far field or on the output aperture. In principle, the formulation of the problem is straight forward and consists of two steps: (a) using Snell's law one derives the ray tracing equations and (b) using the energy conservation law for the energy flow along each differential tube of rays one derives the relation between the primary feed and output power patterns. These relations are supplemented by boundary or initial like conditions.

In case of nonradially symmetric and noncoaxial reflectors the synthesis problem has a fairly long history that started in the early sixties with papers by B. Kinber in the former USSR and V. Galindo-Israel et al. in the USA. Later, the problem has been also studied by F. Brickell, B. Westcott, and their collaborators in England. In most of these studies the authors have to rely on specific numerical computations for some model cases in order to justify the validity of their approaches. Essentially, there have been no theoretical results establishing solvability of the problem. In fact, Kinber claimed that the problem does not have a solution. Several rigorous results establishing uniqueness and existence in special circumstances have been obtained by L. Marder in 1981 and V. Oliker in 1987.

The purpose of this talk is to explain a new theorem in geometrical optics established in 1994 by L. Caffarelli and V. Oliker and show that as a consequence of this theorem one can obtain a complete and rigorous solution of the synthesis problem for a single reflector antenna. If time permits we will also describe a new rigorous approach to the problem of synthesis of dual reflector antennas.

Cancelled

B2-5
1520

ANALYSIS OF ARBITRARY THIN-WIRE LOOP ANTENNAS AND SCATTERERS USING PERIODIC WAVELET EXPANSIONS

Gaofeng Wang, Bing-Zhong Wang*, and Deguang Feng
Tanner Research, Inc., 180 N. Vinedo Ave., Pasadena, CA 91107
*University of Electronic Science and Technology of China,
Chengdu, 610054, China

Recently, it has been found that making use of orthogonal wavelets as basis functions can speed up numerical solutions of the integral equations arising in electromagnetics (B.Z. Steinberg & Y. Leviatan, IEEE Trans., AP-41(5), 610-619). By using such a wavelet-based method to an integral equation, a sparse matrix equation can be obtained. There are several reasons that make the wavelets a good instrument for the numerical analysis of integral equations. First of all the wavelets have localization properties in both space and frequency. Using the wavelets as the basis functions generates strong de-correlation among the expansion coefficients and weakens the global coupling effects in integral equations. Moreover wavelet expansions allow to construct local high order schemes. Furthermore, a multiresolution analysis implemented by the wavelet expansions naturally provides multigrid schemes.

Originally, wavelets are bases on the whole straight real line. Some difficulties arise when applying such wavelets on the whole real line to problems in finite bounded domains. Moreover the real-world problems likely have curved solution domains instead of straight lines. To overcome the above difficulties, a hybrid wavelet expansion and boundary element method (HWBM) was proposed (G. Wang, IEEE Trans., AP-43(2), 170-178). It was demonstrated that the HWBM exhibits the advantages of sparse matrix, few unknown coefficients, and flexible and accurate model of curved surfaces.

The thin-wire structures are the simplest three-dimensional objects. In practice, lots of the real-world structures can be approximated as thin-wire structures. Moreover, since conducting surfaces can be modeled as wire grids, many general three-dimensional conductors can also be analyzed by a thin-wire code through wire-grid models. Here, a numerical analysis of arbitrary thin-wire loop antennas and scatterers using the HWBM concept is presented. The periodic wavelet expansions are applied to solve the thin-wire electric-field integral equation (EFIE). In this approach, each closed wire loop is mapped into the definition domain [0,1] of the periodic wavelets. Through these maps, periodic bases over the closed wire loops can be derived from the periodic wavelets. By Galerkin's method, a sparse matrix equation is yielded from the integral equation under study. The feasibility of this approach is demonstrated by numerical results for a variety of thin-wire loop antennas and scatterers, and its accuracy is verified by comparisons with other methods.

Cancelled

B2-6
1540

OPTIMIZED DUAL OFFSET SHAPED REFLECTORS FOR COMPACT ANTENNA TEST RANGE

Dr. Dai Zhongning Prof. Kooi Pang-Shyan Prof. Yeo Tat-Soon
Department of Electrical Engineering
National University of Singapore
10 Kent Ridge Crescent
Singapore 0511
Republic of Singapore

Dual offset shaped reflectors were proposed to the design of compact antenna test range for high efficiency and dynamic range(T. Harrison, Microwave Journal, 137-145, 1986). Synthesis theory and method through repeated computation for shaped reflectors are successively developed(V. Galindo-Israel, IEEE Trans. on AP, 39, 1007-1013,1991). In this paper, a simple optimization design method based on geometrical optics is realized.

By assumed aperture field, near field is calculated. According to the requirements for main polarization and cross polarization of near field, appropriate distribution of aperture field and requirement for cross polarization are determined.

A new method and a group of formulas for synthesis are advanced. The initial values are the far field pattern of feed and the amplitude function of the aperture field. Only circular aperture is discussed. The dual offset reflector system includes main reflector, subreflector and their relative position. On the concept of physics, the correction of subreflector is to realize amplitude distribution and the correction of main reflector is to realize equi-phase of the aperture. The differential equation of a parameter of main reflector is derived from the distribution of the aperture field of main reflector according to energy balance relation. From Fermat's principle, the differential equation of a parameter of subreflector is derived. Through total differential condition of subreflector, another differential equation is obtained. Then a series of results for the geometrical parameters of main reflector and subreflector can be obtained. For different result, the cross polarization of aperture is different. When layout is loose, the cross polarization of aperture is low. When layout is compact, the cross polarization is high.

Cross polarization is the main goal in the optimization of compact antenna test range. Through reflection theorem, a closed form formula for the cross polarization of aperture is obtained directly. After approximation, this simple expression is related to few geometrical parameters of reflectors. Thus it is not necessary to solve all the equations of reflectors in the optimization. Computation is simplified greatly. An optimized compact antenna test range is realized easily.

National Radio Science Meeting (Boulder, CO), Jan. 1996.

B2-7
1600

PERFORMANCE CHARACTERIZATION OF HANDHELD ANTENNAS FOR SATELLITE AND TERRESTRIAL WIRELESS COMMUNICATION SYSTEMS

Joseph S. Colburn Yahya Rahmat-Samii*
Department of Electrical Engineering
University of California, Los Angeles
Los Angeles, California 90095-1594

In recent years, personal wireless communications has been a very active area in terms of research effort and business activity. For terrestrial communication systems, one research goal has been the design of multiple antenna handsets for diversity reception, with emphasis on low profile, non-obtrusive antennas. For the satellite based personal communication systems, there is need for relatively small handset antennas that offer good circular polarization performance over broad frequency and angular ranges.

The use of numerical techniques for the design and simulation of handset antennas has been found to provide accurate and convenient tools. Two techniques extensively used for these applications are Finite-Difference Time-Domain (FDTD) and Method of Moments (MOM). The diversity of these two techniques offer a broad range of simulation capabilities. It has been found possible and important to accurately model the handset chassis and operator's presence to determine their affects on the radiation and circuit characteristics of the radiators.

In this presentation, many of the handset radiating elements studied for both terrestrial and satellite personal communications applications will be discussed: planar inverted F antennas (PIFA), helices, monopoles and curl antennas. Various configurations incorporating these antennas in the handset will be illustrated and performance characteristics, such as input impedance and far-field patterns, computed with the numerical tools for the geometries considered will be shown. Also measured results will be given, including the diversity performance of the dual antenna handset configurations designed. In addition, considerable attention will be directed to the issue of biological interaction with the handset radiators.

B2-8
1620

INTERFERENCE REDUCTION IN CELLULAR SYSTEMS USING SWITCHED BEAM SMART ANTENNAS

Carl B. Dietrich, Jr., Warren L. Stutzman, and William A. Davis
Antenna Group
Center for Wireless Telecommunications
Bradley Department of Electrical Engineering
Virginia Polytechnic Institute and State University
Blacksburg, VA 24061-0111

As the number of subscribers increases, cellular telephone systems will require increased capacity, especially in urban areas with high concentrations of users. Smart antennas, including switched beam and fully adaptive antennas, have the potential to increase the capacity of cellular and PCS communication systems. Two approaches to increasing capacity, interference reduction/ rejection and spatial division multiple access (SDMA), are briefly discussed. This work concentrates on the interference reduction/rejection approach using switched beam antennas.

Simulations of a cellular system using a switched beam antenna are presented. The simulations show the variation of carrier to interference ratio (C/I) levels with number of beams per sector, side lobe level, number of sectors per cell, frequency reuse factor, cell size and channel model. The influence of power control schemes on C/I is also investigated. These simulations employ idealized antenna patterns which can be generated for any number of beams per sector. The simulations were performed with and without considering multipath effects. Significant improvements in C/I are obtained as the number of beams per sector is increased. The minimum number of beams per sector required to reduce the frequency reuse factor for different sectorization schemes is developed, and the resulting increases in system capacity are determined.

Results of simulations using realizable antenna array patterns calculated from actual element patterns are compared with those using the approximate, idealized patterns. The need for more accurate approximate patterns is considered. Variations in realizable antenna patterns caused by the frequency difference between uplink and downlink are also modeled, and the effect of these variations on the C/I is evaluated.

D/B1-1
1400

FDTD ANALYSIS OF THE INTERACTION OF ULTRAFAST OPTICAL PULSES WITH GRATING SURFACES LOADED WITH EXCITED ATOMS

Richard W. Ziolkowski , Electromagnetics Laboratory
Department of Electrical and Computer Engineering
The University of Arizona, Tucson, AZ 85721
Office: (520) 621-6173 Fax: (520) 621-8076
ziolkowski@ece.arizona.edu

We are developing full-wave, vector Maxwell equation solvers for use in studying the physics and engineering of linear and nonlinear integrated photonics systems. Particular emphasis has been given to the interaction of ultrafast optical pulses with nonresonant and resonant optical materials and structures. Results will be presented that simulate the interaction of ultrafast optical pulses with corrugated surface sections (i.e., gratings of finite length) filled with materials exhibiting resonant loss or gain. In this presentation, we consider the gratings to be loaded with atomic media resonant at the frequency of the incident radiation. Interest in these problems follows from our desire to design micron-sized linear and nonlinear guided wave couplers, modulators, and switches.

These resonant problems pose interesting FDTD modeling issues because of the many time and length scales involved. To understand the physics underlying the small-distance scale and short-time scale interactions, particularly in the resonance regime of the materials and the associated device structures, a first principles approach is desirable. Thus, the results to be presented are based upon a quantum mechanical two-level atom model for the materials. An analogous three-level atomic system model is currently being developed; three-level modeling results will be presented if they are completed in time for the conference. The resulting Maxwell-Bloch model requires a careful marriage between microscopic (quantum mechanical) material models of the resonant material systems and the multi-dimensional, macroscopic Maxwell's equations solver. The FDTD numerical issues will be discussed. Examples will be given to illustrate the design and control of these resonant large scale optical structures. If the atoms are in their ground state, the medium will be highly absorbant. If they are in their excited state, the medium will be active and gain can ensue. The effect of these materials radically alters the grating's performance. The presentation will emphasize the far-field field distributions resulting from these two material configurations. Variations in the grating geometries within these material parameter choices will also be discussed.

D/B1-2
1440

HYBRID 2-D BPM-FDTD SIMULATION

Jeffrey S. Kallman
Lawrence Livermore National Laboratory
P. O. Box 808, L-156
Livermore, CA 94550

Beam propagation methods (BPM) (M. D. Feit and J. A. Fleck, Jr., J. Opt. Soc. Amer. B, 633-640, 1988) and finite-difference time-domain (FDTD) methods have both been used by the photonics community for a number of years. BPM can be used to simulate large problems in which light can be treated paraxially. FDTD can be used to simulate small linear problems when the full physics needs investigation. Hybridizing these methods allows the examination of large devices having small, physics-intense regions. An example of a problem requiring this treatment is a long stubbed taper (see figure). The BPM is capable of simulating the taper up to the stubbed end. The assumptions made by the BPM are violated at this point, and we use FDTD to determine the scattering from the stub. Beyond the stub we once again use the BPM.

To interface the BPM (a frequency domain method) to the FDTD algorithm, the output of the first BPM section is expressed as a sum of modes (both bound and continuum) of the FDTD cross section. Each mode has its own phase and amplitude, and is launched into the FDTD grid using a one-way launch algorithm.

Interfacing the FDTD output to the following BPM section is straightforward. After the FDTD section reaches steady state a time history is taken of a column of grid elements (which column is used depends on whether forward propagation or reflection is of interest). The time history can be made to yield the amplitude and phase of each grid point at the BPM frequency, and the final section BPM simulation is run using this as its input.

In its current implementation the hybrid method is restricted to simulating two dimensional, TE mode devices requiring only a single FDTD section. Future directions for development include using a vector BPM method or an eigenmode propagation method as the frequency domain part of the hybrid algorithm, extending the hybridization to three dimensions, and using multiple FDTD sections.

This work was performed under the auspices of the U.S. Department of Energy under contract W-7405-ENG-48.

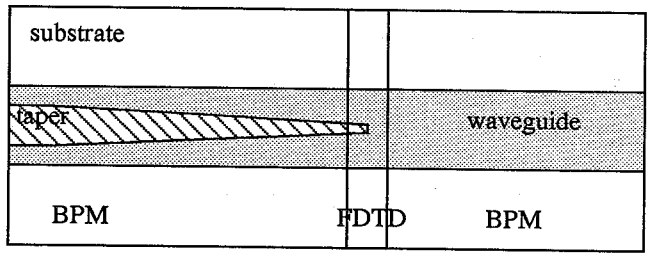

D/B1-3
1540

FDTD MODELING OF THE INTERACTION OF FOCUSED GAUSSIAN BEAMS WITH CAVITIES LOADED WITH LOSSY MATERIALS

David C. Wittwer and Richard W. Ziolkowski*
Electromagnetics Laboratory
Department of Electrical and Computer Engineering
The University of Arizona, Tucson, AZ 85721
Office: (520) 621-6168 Fax: (520) 621-8076
wittwer@ece.arizona.edu

We are developing full-wave, vector Maxwell equation solvers for use in studying the physics and engineering of the interactions of focused Gaussian beams with complex targets. Particular emphasis in our work has been given to the ultrafast time and ultrasmall distance scales associated with optical pulses. Focused optical beams have many applications from optical disk storage technologies to photolithography to inertial confinement fusion.

We will present our FDTD analysis of the interaction of focused Gaussian beams with open cavity structures loaded with lossy dielectric materials. The associated simulator has required the development of several novel FDTD source and diagnostic tools. The development of our Gaussian beam total field/scattered field source will be discussed. The ability of the simulator to focus and steer the Gaussian beam will be emphasized. Differences between traditional scalar models of the focused Gaussian beam and the more rigorous full-wave electromagnetic vector modeling of the focused Gaussian beam provided by the FDTD simulator will be highlighted. The need to measure the fill-time of the cavity and its relationship to the Q-factor of the cavity will be described. The energy stored in the cavity, particularly in the region of the lossy dielectric materials which represent the loading of the cavity, and its relationship to the energy coupled into the open cavity will also be illustrated with a variety of numerical results. Various types of cavity shapes and lossy linear dispersive dielectric materials have been considered. Examples of these results will also be given.

D/B1-4
1620

FDTD MODELING OF ELECTROMAGNETIC PACKAGING EFFECTS

Gary Haussmann* Jason Mix* Melinda Piket-May Eric Thiele
Department of Electrical and Computer Engineering
Campus Box 425
University of Colorado
Boulder, CO 80309

Previously we presented an interface between an FDTD electromagnetic simulation and a circuit simulator (SPICE). This provides a method for modeling lumped elements and linearly controlled sources within the FDTD grid using SPICE, without having to simulate the circuit elements in our internal FDTD code. Examples include a SPICE simulated resistor used in terminating a microstrip transmission line, and the embedding of a transmission line lumped element model (using SPICE) within an FDTD simulated microstrip.

The strength of this method is that it allows the definition of circuits more complex than simple lumped elements, allowing us access to all of the abilities available in SPICE, such as simulating larger circuits and modeling nonlinear devices such as BJT and FET elements. The relative simplicity of specifying devices to SPICE allows us to change the configuration and parameters of a complex circuit more quickly than modifying FDTD simulation code.

Here we present FDTD simulations using more complex SPICE circuit models, such as a transistor amplifier. We can study the viability of certain packaging configurations with such circuits; depending on the packaging geometry, certain undesirable effects, such as oscillation or instability, may be observed. Using these simulations, we hope to observe such undesirable effects and find configurations to avoid them. Specifically, we are looking for effects due to the more complex field interactions - effects that would not appear using only circuit simulations and simpler models (i.e., approximations on waveguide propagation using only lower order modes).

Session E/J-1, 1335-Wed., CR0-30
TECHNIQUES FOR RFI MONITORING, EXCLUSION, AND REMOVAL
Chairperson: A.W. Clegg, Naval Research Laboratory, Remote Sensing Division, Washington, DC 20375
Organizers: A.W. Clegg and D.J. Cohen, National Telecommunications and Information Administration, U.S. Department of Commerce, Annapolis, MD 21401

E/J1-1
1340

WARC 95 -IMPACT ON SPECTRUM UTILIZATION AND RFI

R. D. Parlow
National Telecommunications and
Information Administration Room 4099
U.S. Department of Commerce
14th and Constitution Avenue N.W.
Washington, D. C. 20230

The issues and results of the recently completed World Administrative Radio Conference (WARC 95) are reviewed. The principle issue at the WARC was the frequency allocations for the new global mobile communication satellite networks. Key issues involve feeder links, spectrum allocations for non voice systems and the removal of constraints on existing mobile satellite service allocations. The specific agenda items relating to facilitating the use of the frequency bands for mobile satellite services considered were:

(1) A review of the technical constraints associated with frequency bands below3 Ghz to mobile satellite services

(2) Review the following allocations 1980-2010 MHz and 2170-2200 MHz in Regions 1 and 3 and bands 1970-2010 and 2160-2200 in Region 2.

(3) Consider allocations and regulatory aspects for feeder links for the mobile satellite service taking into account possible interference to geostationary orbit satellite systems.

Other issues at WARC 95 were power limits for earth stations in the Space Science Service. The band of interest was the 2025-2110 MHz. Also the WARC 95 took action on the Voluntary Group of Experts Report pertaining to simplification of the Radio Regulations.

The key background spectrum management principles submitted to the WARC by the Conference Preparatory Group (CPM) and the Voluntary Group of Experts (VGE) were: (1) simplification of the Radio Regulations (2) flexibility and broadly defined allocations to support flexibility and (3) worldwide allocations.

Looking to the future a review is made of the expected issues and agenda for the future WARC 97.

E/J1-2
1400

RFI LESSONS AT AN OBSERVATORY

W. A. Baan
Arecibo Observatory
P.O.Box 995
Arecibo, PR 00613

The Arecibo Observatory is located within the second densest broadcasting region in the United States and is very vulnerable to interference because of its exposed observing platform. In order to preserve the usefulness of radio astronomy observing bands below 15 GHz, the Observatory depends strongly on efforts to encourage clean up existing neighboring services and to prevent new services from interfering. The identification of interfering signals is done with a spectrum monitoring and direction finding system. Some success stories will be presented of local coordination with broadcasting services and various fixed-mobile services. However, in general the interference identifications are followed by a lengthy (local) coordination process. Twenty-four hour monitoring results will be presented and some results of routine interference evaluations of actual telescope data. The telescope data evaluations show evidence of interference across large fractions of the RAS spectrum and in particular at lower frequencies. In practise the radio astronomers discards large (unknown) fractions of the data. It is important that the RFI situation at lower frequencies does not repeated at higher frequencies. The RAS bands would be much cleaner if good engineering practices are used by all spectrum users. The radio observatories would also benefit from tighter standards on unwanted emissions. Improvements in efficiency of spectral usage would benefit all spectrum users not only the radio astronomy community.

E/J1-3
1420

RADIO FREQUENCY INTERFERENCE MONITORING AT THE VLA AND VLBA RADIO ASTRONOMY OBSERVATORIES

C. Janes, National Radio Astronomy Observatory, Socorro, NM 87801
e-mail cjanes@nrao.edu
D. Jenkins and R. Jones, New Mexico Institute of Mining and Technology, Socorro, NM 87801
N. Lui, Polytechnic University, Brooklyn, NY 11201

Several radio frequency interference (RFI) monitoring projects are in place or planned for the Very Large Array (VLA) and Very Long Baseline Array (VLBA) radio astronomy observatories, both operated by the National Radio Astronomy Observatory (NRAO). RFI can corrupt the passive observations of very faint cosmological sources; and if strong enough, an interfering signal can cause gain compression of the telescope front end amplifiers.

RFI is being periodically measured and documented in the frequency bands from 304 to 348 MHz (P band) and from 1213 to 1771 MHz (L Band) at the VLA. Using the entire array and dedicated observing time, the tests are run once a month to provide an infrequent snapshot of RFI entering the sidelope of the antennas. The L band interference test, called SYSLQUIK (see L-Band RFI Survey at the VLA, B. Brundage et. al., URSI Program and Abstracts, January 1994), provides a resolution bandwidth of 390.625 kHz, while SYSPQUIK, the P band test, provides a resolution bandwidth of 12.207 kHz.

Intermediate frequency (IF) monitoring was initiated at the VLA in December 1994, by connecting a PC-controlled swept frequency spectrum analyzer to the IF output of a single VLA antenna. Though limited to measuring signals greater than some fraction of the system noise temperature and to bands commanded by the observing sequence, the IF monitoring was used to document dozens of incidents of intermittent interference in radio astronomy bands over the period December 1994 - June 1995.

Other monitoring tests are planned, such as one to continuously monitor the output of the P band and L band receivers at a single VLA antenna to measure RFI entering the antenna sidelobes across the entire receiver band independently from the observing schedule. Another test calls for identifying the source of external interference in the P and L bands by automatically recording the demodulated output of a scanning radio receiver. A third monitoring program will use independent antennas and amplifiers to monitor from 200 MHz to 1400 MHz for the VLA upgrade.

Monitoring at the VLBA sites has been limited to spot checks with a spectrum analyzer and occasional system temperature checks. The plan is to conduct interference tests periodically for all VLBA bands similar to the SYSLQUIK and SYSPQUIK tests at the VLA.

Finally, a digital spectrometer is being built at NRAO to autocorrelate the signal from a single antenna. Using the 1024 lag University of New Mexico Canaris chips, circuit boards from the Greenbank Radio Telescope (GBT) correlator, and a PC, the equipment is expected to provide up to 4096 lags for a resolution bandwidth of 12.2 kHz.

Plots of the results of the SYSLQUIK and SYSPQUIK interference tests at the VLA are available via the World Wide Web (WWW) NRAO home page at URL http://info.aoc.nrao.edu. The plan is to include results from other monitoring tests on the Web as data become available.

The National Radio Astronomy Observatory is a facility of the National Science Foundation operated under cooperative agreement by Associated Universities, Inc.

E/J1-4
1440

POTENTIAL INTERFERENCE ON LOW-FREQUENCY SPACE-BASED INTERFEROMETERS FROM TERRESTRIAL SOURCES

Marisa McCoy[1], Monte F. Taylor[2], John P. Basart[2], and Edward Rios[2]
1 Mobile Systems International, Inc.
1755 N. Collins Blvd., Ste. 400
Richardson, TX 75080
2 Department of Electrical and Computer Engineering
Iowa State University
Ames, IA 50011

Earth orbiting radio telescopes operating at low frequencies are subject to interference from terrestrially generated signals. In planning for an orbiting interferometer operating in the 1 to 30 MHz range it is appropriate to learn more about the nature of interfering signals originating from the earth that can propagate through the ionosphere. In late October 1994, a spacecraft, WIND, was launched to study the characteristics of the solar wind. Prior to moving to a point between the earth and sun, WIND completed a number of highly elliptical orbits around the earth. Signficant measurements of terrestrial interference were made over a three-week period when the sunspot number was low and the ionosphere relatively transparent.

The data collected by WIND indicate that commercial broadcast transmissions are the most intense component of the intereference in space in the low frequency range up to the 14 MHz upper limit of WIND. Eighteen second samples clearly show sharp rise and fall times, similar to that detected by the AMPTE receiver. Individual signals also appear to follow a set transmission schedule since many emissions turn on and off at half-hour increments. The worst case flux densities are 30 to 40 dB above the Galactic background at a distance of 20 Earth radii. This implies that for an interferometer in Earth orbit at an altitude of 40,000 km, the flux densities would be as high as 40 to 55 dB above the Galactic background. Additionally, the WIND data has illustrated the need to perform observations only while an interferometer is located on the Earth's day side. The night time ionosphere is so transparent that interference levels would "blind" the interferometer.

In modeling the ionosphere propagation, a transfer function approach (ICED ionsopheric model coupled with ray tracing) was used to determine whether the interference signals from a particular transmitter-receiver geometry would reach the orbiting receiver. Simulations for low (10), medium (60), and high (170) sunspot number show the transfer function is sensitive to gross changes in the state of the ionosphere. Smaller variations in sunspot number (<10) produced no discernible changes in the transfer function. The minimum breakthrough frequency was at about 6.5 MHz for the low sunspot number case. As the sunspot number was increased, the minimum breakthrough frequency increased to 17 MHz when the sunspot number was set to 170.

E/J1-5
1500

THE GEORGIA TECH SPACEBORNE TRANSMITTER DATABASE AND ITS USE DURING THE 1995 PROJECT PHOENIX L-BAND AND S-BAND CAMPAIGN

P. G. Steffes* D. R. DeBoer
School of Electrical and Computer Engineering
Georgia Institute of Technology
Atlanta, GA 30332-0250

To address the problem of space-based interference to SETI searches and radio astronomical observations, a database and search system has been developed and maintained which can predict the times, frequencies, and directions of intereference caused by spaceborne transmitters. This RFI Search System includes two databases. The first, known as GEOSAT was developed at Georgia Tech and includes 326 geostationary and 325 non-geostationary satellites (for a total of 651). The second database was developed by the Space Frequency Coordination Group (SFCG) and is called SSDB. SSDB is maintained by Dr. Luis Vadillo (INTA/Spain) and includes both deep-space and earth orbiting spacecraft which are governmentally owned. It includes 219 spacecraft and is non-overlapping with GEOSAT. Thus, a total of 870 spacecraft are included in the databases, with information on transmitted frequencies, power, bandwidth, polarization, beamshapes, and modulation type. The database also includes the longitudes of geostationary spacecraft and the two-line orbital elements for non-geostationary spacecraft (updated from the NASA/USSC database) so as to determine spacecraft positions.

Searches of the databases are conducted with a C language program called DBSEARCH. Search parameters consist of a sky window in right ascension/declination or in azimuth/elevation and a frequency range. The observer's location, as well as the date, time, and duration of the search are likewise entered. The spacecraft found to lie within the search space are written to an ASCII output file, along with the search parameters and spacecraft characteristics.

The RFI Search System was successfully used during the Project Phoenix deployment at the Parkes (Australia) Observatory. It both predicted and accounted for most all major sources of spaceborne RFI. Of special interest was the finding that because the radiation intensities of the spacecraft signals were 60-100 dB above the detection thresholds of the Project Phoenix system, interference occured whenever the spacecraft involved were above the horizon, and could not be eliminated by antenna pointing.

E/J1-6
1540

USING SIGNAL PROCESSING TO IMPROVE ADJACENT BAND SHARING

David J. Cohen
U.S. Department of Commerce
National Telecommunications and
Information Administration
179 Admiral Cochrane Drive
Annapolis, MD 21401

A number of new and different adjacent band channel sharing problems are of concern to the spectrum management community. Efficient and cost effective use of the spectrum requires that services utilizing adjacent bands operate successfully.

Initially, an overview is presented of the spectrum management regulatory approach to defining adjacent band sharing between services. The relevant technical parameters are necessary bandwidth, occupied bandwidth, emission bandwidth, spectrum masks and unwanted emissions (out of band and spurious emissions). A thorough understanding of these parameters is needed to identify which entity(ties) must take action to ameliorate an adjacent band interference problem.

The spectral characteristics of signals and receiver selectivity control adjacent band interference. Signal processing methods which can shape and make other adjustment to signal spectral characteristics are one means to facilitate adjacent band sharing. These signal processing methods are defined and explained.

Transmitter spectral filtering is one of the signal processing techniques which can be used to improve adjacent band sharing. At the transmitter premodulation filtering is an effective method to shape the transmitted power spectrum. Similarly filtering can also be included at the receiver. Heretofore, the private sector has not specified receiver standards. Examples of the absence of receiver standards effect on adjacent band interference are presented.

Another signal processing technique which can be utilized at the receiver is signal excision. Signal excision is an interference rejection technique which utilizing signal processing techniques to remove narrowband interference energy from a wider bandwidth desired signal spectrum.

E/J1-7
1600

THE FUTURE RFI ENVIRONMENT ABOVE 30 GHz

Andrew W. Clegg
Naval Research Laboratory
Remote Sensing Division
Code 7213
Washington, DC 20375-5351
clegg@funafuti.nrl.navy.mil

Encompassing 30 - 300 GHz, the millimeter wave (mmW) band offers relief from spectrum crowding at lower frequencies, large available bandwidth, favorable propagation characteristics for certain applications, and relatively high directivity with small antennas. The FCC has recently proposed regulatory changes to foster commercial development of the mmW band. Impending actions include:

• Designating the 46.7-46.9 GHz and 76-77 GHz bands for unlicensed vehicular radar systems. Potentially tens of millions of vehicles will be equipped with radars to provide "intelligent cruise control" capability and driver blind-spot warnings. Unwanted emissions from vehicular radar systems may produce harmful interference to passive systems operating in protected bands.

• Opening the 59-64 GHz band, in which propagation is limited to short distances due to high atmospheric attenuation, to general unlicensed devices. A likely application for this band is wireless local area computer networks. The neighboring bands of 58.2 - 59 and 64 - 65 GHz are allocated to the passive services.

Changes still under consideration include:

• Opening the 116 - 117 GHz band, co-located with an existing passive allocation, for licensed (116 - 116.5 GHz) and general unlicensed (116.5 - 117 GHz) devices.

• The opening (for licensed and unlicensed services) of nearly 5 GHz of additional spectrum space which neighbors passive allocations and poses a potential interference problem from out-of-band emissions.

The status of the FCC's actions concerning the mmW band will be updated. An attempt will be made to predict the RFI environment in the mmW band assuming the likely applications for each of the reallocated bands. Particular emphasis will be placed on the impact of the FCC's actions on current and planned remote sensing and radio astronomy operations.

E/J1-8
1620

PROPAGATION MODELS FOR MICROWAVE FREQUENCIES

George Hufford
Institute for Telecommunication Sciences
Boulder, CO 80303

One imagines that the received power from a radio source above 1 GHz should be easy to estimate: if the two terminals can see each other there is a large "free space" field, otherwise there is nothing. Unfortunately, actual measurements seem to say differently; diffraction and scattering, even at these frequencies, are still an important part of the electromagnetic phenomenon.

The ITM (Irregular Terrain Model, or the Longley-Rice model) and TIREM (Terrain Integrated Rough Earth Model) are two general purpose models that are supposed to calculate better estimates for frequencies up to 20 GHz. They are semi-empirical: while using fairly elementary electromagnetic background theory, they are also an empirical fit to measured data—the theory helps mostly when one wants to extrapolate from the measurements. At higher frequencies, it is almost standard now to use Liebe's MPM (Millimeterwave Propagation Model). This estimates molecular absorption caused by the oxygen and water vapor constituents of the atmosphere, and for these purposes it should be accurate up to 1 THz.

Radio field strengths vary with time. At the longer distances this variability can be considerable and is seemingly unpredictable. The ITM and TIREM try to describe such variability by estimating the cumulative distribution functions, and they are usually fairly accurate in the 5% to 95% range. But on high reliability circuits this is not enough and special techniques are often necessary to explore the tails of the distributions. For interference problems, atmospheric ducting and rain scatter are rarely occurring phenomena that must be considered. For example, Appendix 28 of the ITU "Radio Regulations" tries to guard against the situation that would arise if the beam from a satellite earth station intersected with the beam from a terrestrial system and if rain fell in the resulting common volume. In this way, one hopes to reduce interference to 0.01% of the time (1 hr/year).

E/J1-9
1640

BROADBAND SPECTRUM SURVEYS BY NTIA/ITS

Frank H. Sanders, NTIA/ITS.S2
325 Broadway
Boulder, CO 80303-3328

Broadband spectrum measurements are performed by the National Telecommunications and Information Administration (NTIA) and its Boulder laboratory, the Institute for Telecommunication Sciences (ITS), for the purpose of quantifying radio spectrum occupancy. NTIA spectrum surveys normally run across the frequency range of 100 MHz to 19.7 GHz, sometimes starting as low as 2 MHz. The NTIA/ITS spectrum survey results are available as NTIA Reports. The figure shows an example page from one such report (F.H. Sanders and V.S. Lawrence, NTIA Report 95-321, 1995). The three curves in the figure show maximum, minimum, and average activity in the 406-420 MHz spectral band during two weeks at the survey location.

Broadband spectrum surveys require the use of automated measurement systems that run continuously for approximately two weeks per survey. The NTIA/ITS facility that performs this work is the Radio Spectrum Measurement System (RSMS). The RSMS is a vehicularly mounted measurement system that features low-noise and high dynamic range. RSMS software is written entirely by ITS. Specialized algorithms are used on a band-specific basis during the each survey. Algorithms are tailored for measurements on such transmitters as mobile radios, fixed microwave links, and radars.

The NTIA Reports on these surveys represent the first attempt to publish this these measurements in the public arena. It is expected that spectrum survey information, used in conjunction with allocation and assignment information in databases, will be of assistance to spectrum managers nd engineers who are planning the introduction of new systems and technologies in the radio spectrum.

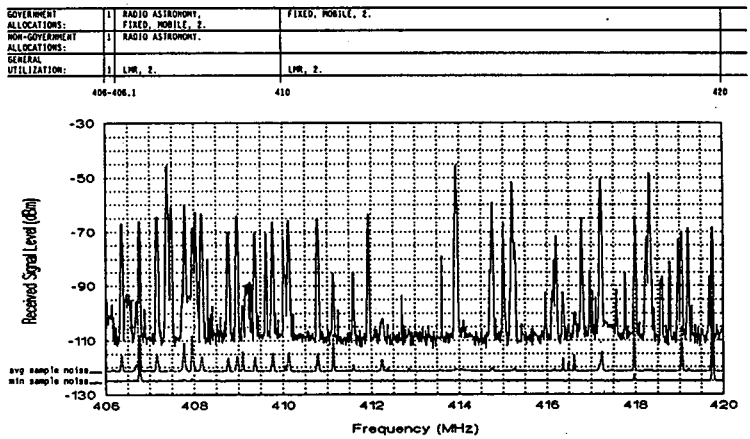

E/J1-10
1700

DIRECT DIGITIZATION OF THE RF IN RADIO RECEIVERS - HOW CLOSE ARE WE?

Jeffery A. Wepman, ITS.S3
U.S. Department of Commerce
Institute for Telecommunication Sciences
325 Broadway
Boulder, Colorado 80303

As advances in technology provide increasingly faster and less expensive digital hardware, more and more of the traditionally analog functions of a radio receiver will be replaced with software or digital hardware. The final goal for radio receiver design is to directly digitize the RF signal right after the receive antenna and hence implement all receiver functions in either digital hardware or software. The trends in receiver design have been evolving toward this goal by incorporating digitization closer and closer to the receive antenna for systems at increasingly higher frequencies and wider bandwidths. While radio receivers with analog RF front ends using digitization at baseband have been around for many years, the popularity of receivers using digitization at the IF is increasing rapidly. Digitization at the RF, without an initial downconversion, is currently used in only very restricted applications where the maximum frequency is relatively low and/or the spurious free dynamic range requirements are relatively low.

The key factors in radio receivers where digitization occurs at the IF or RF are analog-to-digital conversion and digital signal processing. Digital-to-analog conversion is also a factor for applications requiring analog output (such as voice). Because of the rapid advances in hardware development of analog-to-digital converters (ADCs), digital-to-analog converters (DACs), digital signal processors, and specialized integrated circuits (such as direct digital downconverters), development of radio receivers using digitization at the IF and in some cases at the RF is on the verge of a virtual explosion.

Hardware limitations of ADCs, digital signal processors, and DACs place constraints on digitization at the IF and RF in radio receivers. Digitization at the RF, in general, requires some sort of bandlimiting (filtering) and amplification before the actual digitization takes place. The required amount of filtering and amplification is quite application specific. Improvements in ADCs are announced often but typically one can get either high sampling rates or high resolution but not both simultaneously. ADCs with the high sampling rates required for wide bandwidth applications may not have sufficient spurious free dynamic range. Digitization at the RF is now being considered for satellite receivers since a large spurious free dynamic range is not a necessity, very high sampling rate ADCs already exist, and even faster ADCs are being developed. For receiver applications requiring a large spurious free dynamic range, such as HF communications, digitization at the IF is currently a more practical option.

Perhaps presenting an even greater limitation than ADCs, are digital signal processors. The speed, size, and cost of these processors are important for the particular radio receiver application. The requirement for real-time operation for many radio receivers places a heavy burden on these processors. It is difficult to discuss limitations of digital signal processing in general terms since a tremendous variety of algorithms can be implemented in radio receivers depending on the specific application. The amount of time that signal processing requires is a function of both the speed of the processor and the number and complexity of the algorithms required to perform the needed radio receiver functions.

F/B1-1
1340

Scattering Cross Sections of Composite Rough Surfaces With New Unified Full Wave Solutions

Ezekiel Bahar and Yuzhi Zhang
Department of Electrical Engineering
University of Nebraska-Lincoln
Lincoln, NE 68588-0511

Microwave remote sensing of rough surfaces has stimulated the need for a better understanding of the interaction of radar signals with composite (multi-scale) surfaces. This interaction is particularly important for the ocean surfaces where the like and cross polarized radar returns can yield information about the rough sea surface parameters. To this end, a new approach for evaluating the scattering cross sections for composite (multi-scale) random rough surfaces is presented based on the original full wave solution. Initially, the incoherent scattering cross sections are calculated, using the original full wave approach, for the entire radar footprint. The composite rough surface is regarded as a sum of individual pixels of arbitrary orientations. Extensive use is made of the full wave scattering cross section modulation to account for the large scale surface slopes. The incoherent scattering cross section of the composite rough surface is obtained by summing (averaging) the cross sections of the individual pixels over the slopes (in and perpendicular to the plane of incidence) of the mean plane of the pixels.

In this work, the rough sea surfaces are assumed to be characterized by the Pearson-Moskowitz spectral density function which accounts for the surface wind speed. The rough surface heights and pixel slopes are assumed to be characterized by Gaussian probability density functions.

It is shown that the value of the cross section for the composite rough surface is relatively stationary over a broad range of values of pixel size L_p.

The backscatter like and cross radar cross sections are evaluated for all angles of incidence (normal to grazing). The results, using the new full wave approach, are compared with the earlier full wave results as well as results based on a hybrid analysis of a two-scale model. This new full wave solution for the cross section reduces to the perturbation solution in low frequency limit, the physical optics solution in high frequency limit and to a single expression, that accounts for Bragg scatter and specular point scatter, for multi-scale random rough surfaces.

F/B1-2
1400

MULTIPLE SCATTER BY VERY STEEP ROUGH SURFACES: COMPARISON OF OPTICS AND EXACT METHODOLOGIES

Donald E. Barrick
CODAR Ocean Sensors
1000 Fremont Avenue
Los Altos, CA 94024

Optics formulations are convenient and insightful for analysis of large-scale smoothly curving rough surfaces. Geometrical optics calculates scatter via the divergence of rays striking a surface facet and reflecting in the specular direction; currents on the surface are thereby bypassed. Physical optics calculates scatter from an integral involving currents -- or tangential fields -- over the surface; the latter are directly proportional to the incident field. When the surface is precipitous (in addition to having large heights in terms of wavelength), single-bounce optics approximations no longer represent the total interaction process. Results become dependent on polarization, even for backscatter, owing to the double-bounce (and higher) contributions. Both geometrical and physical optics formulations can be patched up to include double interactions. The question arises: how far can these intuitive methods be pushed before they no longer produce realistic answers?

We treat this subject here by restricting attention to: (i) backscatter, from (ii) perfectly conducting, (iii) one-dimensional (iv) sinusoidal profiles (v) at vertical incidence, (vi) for both horizontal and vertical polarization. Examination of this very simple profile allows us to follow the physics of the interaction process as roughness steepens from smooth to very precipitous. Both optics results are compared to those from a simple, exact method (D.E. Barrick, Radio Sci., 30, 563-580, 1995). The scattered fields are examined vs steepness for all three approaches, while the currents on the surface are compared for the exact and physical-optics formulations.

Surface currents exhibit oscillations on the steepest parts of the surface; this is explained in terms of the interference between singly and doubly incident contributions. Physical optics better captures this oscillatory behavior: (i) for horizontal rather than vertical polarization; (ii) when slopes are less.

Geometrical optics predicts infinite backscatter when the reflecting facet's curvature is zero (it is flat); elsewhere, it works better in both the single and double-bounce regions: (i) when slopes are smaller; (ii) for larger surface radii of curvature; (iii) for horizontal polarization. Physical optics avoids these singularities, capturing the correct backscatter behavior a little better while exhibiting the same parameter dependences for good quality as enumerated for geometrical optics.

F/B1-3
1420

VARIATION ON UNIFIED MODAL METHOD NEAR GRAZING FOR COMPOSITE ROUGH SURFACES: MICROWAVE SEA SCATTER

Donald E. Barrick
CODAR Ocean Sensors
1000 Fremont Avenue
Los Altos, CA 94024

Increasing attention is being devoted to near-grazing microwave scatter from the sea. A number of anomalies have been noted that are not easily explained by classic composite surface models, including the spiky nature of horizontally polarized returns that often exceed the vertical echo, and the differences in spreads of the Doppler spectra seen on the two polarizations. It is accepted that Bragg scatter from short waves (half the radar wavelength) is responsible for the return, but modified by the presence of the long waves. Wave tilting is invoked at higher angles to interpret wave modulation transfer functions (generally derived from tower-measured data). This becomes problematic near grazing where the tilted short waves on the backsides of the long wave are optically shadowed; does one therefore neglect these occluded parts in attempting to develop scatter models?

An exact, computationally efficient, modal methodology was presented and used to study surface currents/fields excited by a near-grazing plane wave over a periodic ocean-like surface profile (D.E. Barrick, Radio Sci., 30, 563-580, 1995). When the surface roughness scales are large in terms of wavelength (e.g., moderate sea states at 4 GHz), only a few modes are needed to represent the surface fields due the sea's relatively small slopes. The scattered fields are another matter: far more modes are required here to describe near-grazing backscatter because the number goes as $\sim 2L_L/\lambda$, where L_L is the longest ocean wave's (swell) spatial period and λ is the radio wavelength. Short Bragg-backscattering ocean waves (with lengths $L_B = \lambda/2$) are the dominant contributors, and they are displaced spectrally by the factor $2L_L/\lambda = L_L/L_B$ from the fundamental long-wave region. Scatter from them is modified by the presence of the long waves, and these short waves at high mode numbers must be included properly in order to produce accurate results.

Direct inversion to solve for the relevant high-order scattered mode coefficients is impossible because of the poor condition number of the matrices involved. This is true both for our exact unified modal method and also for the Rayleigh formulation. We present here a spectral splitting process -- and establish its accuracy -- that involves only a small number of modes (or unknowns) in the matrix inversion: less than ~30. The higher Bragg-scattering surface spectral modes are then included in a stable, efficient matrix multiplication to get the backscattered fields. These fields are 'imaged' as a function of position on the long wave near grazing for VV and HH polarizations (as would be seen with a high-resolution radar), to study the spiky nature of HH polarized signals. Finally, Doppler spectra are calculated as the different surface spectral components follow the gravity-wave dispersion relation to describe their motions over time.

F/B1-4
1440

X-BAND POLARIZATION DEPENDENCY OF RADAR BACKSCATTER FROM THE OCEAN AT LOW GRAZING ANGLES

A. N. Keane
NOAA/ERL/Environmental Technology Laboratory
University of Colorado/CIRES
325 Broadway
Boulder, CO 80303
E. A. Skirta*
NRC and NOAA/ERL/Environmental Technology Laboratory
325 Broadway
Boulder, CO 80303

Experimental results, which were performed to investigate microwave scattering and emission from the ocean in X-band (R.A. Kropfli and S.F. Clifford, Proc. IGARSS'94, *v. IV*, pp.2407-2409, 1994) indicate several features of radar power returns and Doppler velocities at horizontal and vertical polarizations at low incidence.

Numerical analysis of grazing angle dependence of the time-averaged copolarized and cross-polarized power returns from SCOPE experimental data basis is presented at angles ranging from 8.5° to 3°. A theoretical solution (A.G. Voronovich, National Radio Science Meeting, 1996) developed for backscattering from a rough two-dimensional dielectric surface at low grazing angles, that includes curvature of undulating surface and wind spectrum, is applied to compare it with the results of the experimental observations, and to offer an additional argument for a dependence of the radar echo in the presence of spikes on curvature of sea surface.

An examination of angular dependence of normalized radar cross sections (NRCS) at different azimuth angles allowed us to find out that the cross sections observed are proportional θ^2 at low incidence, θ is being a grazing angle. We could conclude that the effect is wind speed and wind direction dependent, and more pronounced for vertical polarization than for horizontal. These data suggest that different scattering mechanisms are to be responsible for VV and HH polarizations and up- and downwind illuminations at small grazing angles.

Power returns and corresponding Doppler velocities, that determine the polarization ratio $\sigma_{hv} = \sigma_{hh}/\sigma_{vv}$ to be equal or exceed 0 dB in upwind direction, are investigated for various sea state conditions (stable and unstable) under low and moderate wind speeds ($v_{av} = 3.5 - 4.5$ m/s). The occurrence of super events with the polarization ratio greater than 0 dB provides a support to existence of different types of scattering sources. In downwind direction the vertical polarization returns are attenuated near the Brewster angle and may determine multipath scattering events which include a reflection at the Brewster angle.

F/B1-5
1520

COMPARISONS OF LONG-WAVELENGTH RADAR ECHOES OF THE MOON WITH LUNAR SURFACE COMPOSITIONS

Thomas W. Thompson
Jet Propulsion Laboratory
California Institute of Technology
Pasadena, CA 91109

Bruce A. Campbell
Center for Earth and Planetary Studies
National Air and Space Museum
Washington, DC 20560

B. Ray Hawke
University of Hawaii
Honolulu, HI 96822

We examined long-wavelength (70-cm and 7.5-meter) radar scatter from moon in order to gain some insight into the structure and chemical composition of the lunar surface. Radar backscatter values from the lunar maria were compared with models for (1) quasi-specular scattering from the surface-space interface, (2) echoes from a buried substrate, and (3) Mie scattering from surface and buried rocks. The 70-cm echoes agree best with our third model, Mie scattering from buried rocks. Depolarized radar echoes from the moon are likely due to a combination of single and multiple scattering events, although single scattering could account for the observed echo powers, based on a comparison with rocky terrestrial surfaces.

Although lunar radar backscatter strength in the Mie scattering model is controlled by loss tangent, we could not find a clear variation between the 70-cm echo powers and the mineral content of lunar soils. We compared the radar backscatter values with titanium and iron oxide contents inferred from optical observations. Although the radar image correlated well with the unit boundaries defined from optical color differences, the 70-cm backscatter values did not correlate well with titanium-oxide abundances derived from earth-based multispectral observations nor from iron abundances derived from Clementine spacecraft observations. However, the 7.5-meter backscatter values did correlate with iron contents suggesting that loss tangent at this wavelength is controlled by the abundance of iron oxide.

All of this suggests that radar and multispectral optical data can provide insights into lunar surface composition. For example, the low-radar echoes associated with cryptomare areas indicate changes in chemical composition with depth. The low-radar echoes associated with radar-dark halo craters indicate changes in chemical composition and/or subsurface rock populations.

F/B1-6
1540

TWO-SCALE MODEL AT LOW GRAZING ANGLES

A. Voronovich
NOAA/ERL/Environmental Technology Laboratory,
University of Colorado/CIRES
325 Broadway
Boulder, CO 80303

Two-scale model of scattering of electromagnetic waves from rough surface suggested first by Wright (J. W. Wright, *IEEE Trans. AP-* **16**, 217-223, 1968) is based on splitting the spectrum of sea roughness into long- and short wave components. For small and moderate grazing angles scattering is actually due to short waves. Those short waves are superimposed on undulating surface formed by long waves. It is important that undulating surface is usually assumed to be locally plane.

However, the last assumption is based on the tangent-plane (Kirchhoff) approximation which is valid if the parameter $t = kR\sin^3\theta$ is large enough (here R is radius of curvature of undulating surface , k is wavenumber of radiation, and θ is grazing angle. Due to strong dependence on the grazing angle the condition $t \gg 1$ can be easily violated for small enough θ. In this case diffraction of the incident field should be taken into account, and the results will depend on curvature of the undulating surface.

To estimate this effect scattering of electromagnetic waves from rough surface of dielectric cylinder with radius R has been investigated for two-dimensional problem. It is assumed that $Rk \gg 1$ and $kh \ll 1$, where h is typical amplitude of small scale roughness. Calculation of corresponding scattering process is quite similar to the case of planar undulating surface with Hankel functions used instead of plane waves. Backscattering amplitude has been calculated both for vertical and horizontal polarizations. If $t \gg 1$ corresponding formulae transform into well-known classical expressions. In particular, backscattering cross-sections σ_{HH} and σ_{VV} in this case are proportional to $\sin^4\theta$. However, for $t \ll 1$ the dependency of backscattering crosssection on grazing angle changes qualitatively and transforms into $\sigma \sim \sin^2\theta$ for both polarizations. Experimental data (in particular, obtained during SCOPE experiment (R. A. Kropfli and S. F. Cliffird, *Proc. IGARSS'94*, **4**, 2407-9, 1994)) show that such a dependency is observed in many cases (however, not always.) Theoretically predicted dependency of the ratio σ_{HH}/σ_{VV} on grazing angle matches experimental data reported in (P. H. Y. Lee et al , *Journ. Geophys. Res.*, **100**, C2 , 2591-611, 1995) for X-band if the value $R = .2$ m is used in numerical simulations.

F/B1-7
1600

RECONSTRUCTION OF SURFACE PROFILES FROM SCATTERING DATA

T. A. Leskova
Institute of Spectroscopy
Troitsk, Russia
A. A. Maradudin*
Department of Physics and Astronomy
University of California
Irvine, CA 92717
E. R. Méndez
CICESE
Ensenada, Baja California, Mexico

In a recent note Garcia and Nieto-Vesperinas (Optics Lett. **20**, 949 (1995)) have suggested that if the intensity of the electromagnetic field scattered from a one-dimensional rough surface defined by $x_3 = \zeta(x_1)$, where the region $x_3 > \zeta(x_1)$ is vacuum while the region $x_3 < \zeta(x_1)$ is the scattering medium, is integrated over all angles of incidence, the result, regarded as a function of x_1 for a fixed value of x_3, follows the profile function $\zeta(x_1)$ of the scattering surface closely, provided that the height x_3 is sufficiently close to the surface. In this paper we extend this suggestion in a simple way that formally yields the surface profile function itself. We denote by $F(x_1, x_3|\omega)$ either $H_2^>(x_1, x_3|\omega)_{sc}$ or $E_2^>(x_1, x_3|\omega)_{sc}$, the amplitudes of the scattered magnetic or electric fields in the case of p- or s-polarization, respectively, and denote by $I(x_1, x_3|\omega)$ the integral of $|F(x_1, x_3|\omega)|^2$ over the wave number k from $-\omega/c$ to $+\omega/c$, where k is the component of the wave vector of the incident light parallel to the unperturbed scattering surface ($\zeta(x_1) \equiv 0$), and ω is the frequency of the incident electromagnetic field, assumed to be a plane wave. To first order in $\zeta(x_1)$ the result has the form $I(x_1, x_3|\omega) = \text{const.} + \int_{-\infty}^{\infty} \zeta(x_1 - u) F(u; x_3) du$, where the function $F(u; x_3)$ depends only on the properties of the unperturbed scattering system. This integral equation of convolution form can be solved for $\zeta(x_1)$ by Fourier transform methods. We have applied this approach to obtain $\zeta(x_1)$ in the case of the scattering of s-polarized electromagnetic waves from a one-dimensional perfectly conducting surface defined by a deterministic surface profile function $\zeta(x_1)$. The reconstruction of this function from data for $I(x_1, x_3|\omega)$ obtained by an exact numerical approach is quite good.

F/B1-8
1620

SIGNAL FLUCTUATIONS IN A TRANSMISSION PATH OVER TREE TOPS AT MILLIMETER WAVE FREQUENCIES.

Robert L. Rogers
Applied Research Laboratories
The University of Texas at Austin
Austin, Texas 78713-8029

Signal fades and enhancements were observed at 27GHz over a 7km range across the top of a pine forest in the southern United States. Weather data including relative humidity, temperature, wind speed, wind direction, rainfall rate, and barometric pressure were recorded at the receiver location. Both signal fades and signal enhancements were observed during periods of high humidity and low air movement which occurred in episodes that were observed to last as long as an hour. As expected, fades were observed during periods of rain, but there were significant fluctuations in signal strength that occurred when no precipitation was reported in the area. The possibility of an rf duct formed at the transition from the top of the canopy to the air is explored.

G3-1
1400

IONOSPHERIC TOMOGRAPHY USING ITERATIVE CROSS-ENTROPY MINIMIZATION

Walter S. Kuklinski
Department of Electrical Engineering
University of Massachusetts Lowell
Lowell, MA 01851

Paul Fougere and John Klobuchar
Phillips Laboratory/GPIM
29 Randolph Road, Hanscom AFB
MA 01731-3010

The problem of reconstructing Ionospheric electron densities from ground-based receiver to satellite TEC (Total Electron Content) measurements is formulated as an underdetermined linear inverse problem. By assuming the Ionospheric electron density is constant in a fixed set of J spatial cells an (Lx1) vector of TEC measurements $\underline{c}$ can be related to a (Jx1) vector of electron densities $\underline{d}$ as: $\underline{c} = A\underline{d}$ where A is an (LxJ) matrix of ray path distances. The fact that the electron densities, TEC measurements, and ray path distances are all positive, coupled with the sparse nature of the A matrix has been utilized to implement a computationally efficient Ionospheric Tomography reconstruction algorithm.

The algorithm presented here utilized an iterative cross-entropy optimization technique described by Byrne (IEEE Trans. Image Proc., Vol. 2, pp 96-103 1993). In this technique the Kullback-Leibler distance between any two nonnegative vectors $\underline{a}$ and $\underline{b}$, $KL(\underline{a},\underline{b})$, is used to define a functional $G(\underline{x})=\alpha KL(P\underline{x},\underline{y}) + (1-\alpha)KL(\underline{x},\underline{p})$ that is minimized using an alternating projection iterative method. The method requires $\underline{x}$ and $\underline{y}$ be nonnegative vectors, related as: $\underline{y} = P\underline{x}$. P is further constrained to contain only nonnegative elements and have unity column sums. $\underline{p}$ is a prior estimate of $\underline{x}$ used to regularize the solution. α allows a tradeoff to be made between data consistency and regularization. Using a factored representation of $A = PD_C$ where, D_C is a diagonal scaling matrix with elements equal to the column sums of A, the Ionospheric Tomography problem can be transformed to satisfy the convergence criteria of the alternating projection iterative minimization technique.

This algorithm has been evaluated using TEC data corresponding to known incoherent scatter radar measurements of electron density. Maximum entropy reconstructions, which did not require a prior estimate of the electron density, and minimum cross-entropy reconstructions that utilized model electron density data as the prior vector $\underline{p}$ have been produced. The results, which where obtained using a 100 Mhz 80486 processor, required less than 20 seconds of CPU time and less than 8 Mbytes of RAM. The high quality of these reconstructions coupled with computational efficiency of this algorithm indicates the potential utility of this technique for real-time Ionospheric Tomography.

G3-2
1420

A LOCALIZED SPACE-FREQUENCY TECHNIQUE FOR IONOSPHERIC TOMOGRAPHY

C. Biswas* H. Na
Department of Electrical and Computer Engineering
4400 Engineering Building
University of Iowa
Iowa City, IA 52242

Ionospheric tomography has the potential for reconstructing two- and three- dimensional images of electron density distributions in the ionosphere. This system uses a satellite and a chain of ground stations to measure total electron content (TEC) data along various propagation paths. Ionospheric tomography algorithms then form estimates of the electron density distributions from a collection of TEC values. In this system, the range of angles of the propagation paths, along which TEC are measured, is restricted due to geometric constraints. As a result, reconstructions are degraded and the use of additional constraints or a priori information in ionospheric tomography algorithms is required for resolution enhancement.

The majority of current algorithms perform reconstruction in the spatial or image domain. These algorithms use a variety of additional constraints and a priori information for resolution enhancement. This paper presents a new space-frequency algorithm for ionospheric tomography that utilizes two unique features for resolution enhancement. First, the algorithm expands the measured data into a four-dimensional space-frequency domain in order to permit estimation of the image from localized spectral characteristics. Second, it utilizes feature extraction to select localized a priori information from a database of localized images for further enhancement. This emphasis on localized processing and localized a priori information not only provides image enhancement but enables the algorithm to be specialized for various regions of the ionosphere within a single image. This paper will present the complete algorithm and reconstructions of simulated ionospheres generated from the IRI-90 model. Characteristics of ionospheric spectra that make them suitable for feature extraction will be discussed. Finally, comparisons to reconstructions formed without localization will be detailed.

G3-3
1440

COMPARISON OF TOMOGRAPHIC AND CONVENTIONAL METHODS FOR RESOLUTION OF THE CONSTANT OF INTEGRATION

J. R. Austen*
Department of Electrical Engineering
Tennessee Technological University
Cookeville, TN 38505

Computerized tomography (CT) techniques can be used to produce a two-dimensional image of the electron density in the ionosphere (Austen et al., *Radio Science*, **23**, 299-307, 1988; Raymund et al., *Radio Science*, **25**, 771-789, 1990; Kronschnabl et al., *Radio Science*, **30**, 105-108, 1995). The necessary data are transionospheric satellite beacon total electron content (TEC) data recorded simultaneously at multiple ground stations.

The satellites with the most suitable orbit and signal structure are the navy navigation satellite system (NNSS) satellites. However, although the signal structure of these satellites provides for relatively simple TEC measurements, the true value of the TEC is corrupted by an additive constant. This constant must be determined for each receiver-transmitter pair and, because it arises from the inherent ambiguity in a phase measurement, it is different for each satellite pass and must be recomputed each time.

Traditional methods for solving the problem rely on assumptions about the state of the ionosphere; typically assumptions are that it is horizontally stratified or that a constant gradient exists throughout a region. These methods yield incorrect results when the state of the ionosphere is different than that assumed in the model.

Methods have been developed which incorporate the resolution of the constant of integration into the ionospheric tomography process. These methods will be reviewed and a comparison of results for several ionospheric models will be presented.

G3-4
1500

SENSITIVITY OF IONOSPHERIC TOMOGRAPHY TO THE QUANTITY OF GROUND STATIONS

L. Schueller* H. Na
Department of Electrical and Computer Engineering
4400 Engineering Building
University of Iowa
Iowa City, IA 52242

Ionospheric tomography is a technique for reconstructing two- and three-dimensional images of electron density distributions in the ionosphere from total electron content (TEC) data. The data acquisition system gathers TEC values along propagation paths lying between a satellite orbit and a chain of ground stations on the earth's surface. Considerable research has been devoted in this area to the development of reconstruction algorithms and the evaluation of these techniques on datasets acquired in experimental campaigns. Because of the geometry of the data acquisition system, images reconstructed using these techniques are not ideal. Therefore in order for ionospheric tomography to realize its full potential as an ionospheric measurement technique, it is critical that the resolving capability of ionospheric tomography and the factors that govern this resolution be fully understood.

This paper presents a study on the effect of the number of ground stations on ionospheric reconstructions with respect to two specific criteria: vertical resolution and horizontal resolution. The number of ground stations in the receiving chain is one of the most significant parameters in the data acquisition system. It directly impacts the sampling of the region of interest and the information contained in the resulting dataset. It is also one of the most easily controlled parameters of the system.

The study presented in this paper was performed on a series of simulated images of two and four peaks. The spacing between these peaks was systematically varied to enable a controlled analysis of the vertical and horizontal resolution. TEC data was simulated for systems with three to twelve ground stations which is the typical range used in experimental campaigns. Images were then reconstructed using the Recursive Correction Method and evaluated using several different image resolution measures. This paper presents the results of this study and characterizes the effect of the number of ground stations on each of these resolution measures.

G3-5
1540

TOMOGRAPHIC IMAGING OF THE POLAR-CAP IONOSPHERE

L. Kersley S.E. Pryse M.J. Williams
Department of Physics
University of Wales
Aberystwyth, SY23 3BZ
UK.

The imaging of field-aligned structures in electron density in the ionosphere at high latitudes is discussed. Results are presented from a preliminary experimental campaign conducted in December 1994 on Svalbard. Two receiving stations were set up at Ny Alesund and Longyearbyen monitoring transmissions from the polar NNSS satellites to measure the ionospheric electron content by the differential carrier phase technique. Data from the intersecting ray paths have been used in a reconstruction algorithm to create two-dimensional images of electron density in a height versus latitude plane. The successes and the limitations are discussed of such a basic tomographic experiment at high latitudes, where ionospheric structures follow the nearly vertical field lines. Sample results are presented illustrating various characteristic features of the electron density in the vicinity of the polar cap. A satellite pass around magnetic noon yielded a field-aligned feature in the electron density possibly associated with soft-particle precipitation into the cusp region. Very low densities were measured on flux tubes corotating in the winter darkness. Patch-like enhancements were found in the afternoon sector at high latitudes with the plasma caught in the anti-sunward convective flow across the polar cap. Very low electron densities on flux tubes in the polar hole, stagnating in the dawn convective cell, were seen at high latitudes after magnetic mignight. Plans, made on the basis of these preliminary results for a more comprehensive tomographic experiment at European polar latitudes, will be discussed.

G3-6
1600

TOMOGRAPHIC RECONSTRUCTIONS OF THE IONOSPHERIC RESPONSE TO THE NOVEMBER 1993 MAGNETIC STORM

G. S. Bust* T. D. Raymund G. Kronschnabl
Applied Research Labs
The University of Texas at Austin
P.O. Box 8029
Austin, TX 78713

The November 1993 magnetic storm was a severe magnetic storm ($kp \sim 7$) with after effects observed for several days. During this storm an unprecedented number of observations were made by different scientists from around the world. The observations include solar measurements and measurements of the magneto-sphere, atmosphere and ionosphere. the ionospheric measurements include incoherent scatter data from Millstone Hill and data from three separate ionospheric tomography campaigns. A collaborative effort is under way to integrate these observations and our understanding of the physical processes into one coherent description of the storm event. Measurements of the ionospheric response to the storm onset, and its subsequent behavior over the storm period provide information on the solar-magnetosphere-ionosphere coupled system. In addition, knowledge of the ionosphere dynamics over the entire storm period will provide new insight into predictive modeling of storm events. During the storm period Applied Research Laboratories, the University of Texas at Austin (ARL:UT) had an array of ionospheric tomography receivers deployed between Pierre, South Dakota and Pharr, Texas. Typically during a twenty-four hour period, eight to twelve good quality data reconstructions were obtained from the satellite data sets. Tomographic reconstructions of the ionosphere have been computed for all good satellite passes during the storm period (November 3rd through 11th). The morphological features of the ionospheric response to the storm have been studied through analysis of the tomographic reconstructions. Results from these studies will be presented. In particular, the characteristics of the night-time mid-latitude trough over the storm period will be discussed. Other features of interest that will be presented include observed secondary 'depletion' regions equatorwards of the main trough, and the apparent increase in irregular behavior of the mid-latitude ionosphere as the trough moved equator-wards.

G3-7
1620

IONOSPHERIC TOMOGRAPHY USING MAXENT ON RATE DATA DURING A LARGE MAGNETIC STORM

Paul F. Fougere
Phillips Laboratory/GPIM
29 Randolph Road
Hanscom AFB
MA 01731-3010

The Russian American Tomography Experiment (RATE) ran from Oct 29 to Nov 4, 1993. On the American side, we had dual-frequency receivers set up at four locations on the Eastern edge of North America: Block Island, Rhode Island; Hanscom AFB, Massachusetts; Jay, Vermont; and Roberval, Canada. Using the dual-frequency (140 and 400Mhz) beacon on the Navy Navigation Satellite System (NNSS), with a nominal altitude of 1000 km, a tomography pass would typically last about 20 minutes from horizon to horizon. Over thirty passes have been analyzed using the MaxEnt method described by Fougere (Radio Sci. 30, 429,444 1995), which determines the average vertical profile in the form of an analytical Chapman profile, as well as a set of electron density contours .

On Nov 3, the index of magnetic activity (Kp) climbed rapidly from 0 to 7$^-$ in a little over one day. (The quasi-logarithmic Kp index ranges from a low of 0 for very calm conditions to 9 for the most intense magnetic storms). During the course of this magnetic storm, the Ionospheric response was studied using data collected and analyzed in 23 passes. The results of this intensive study, using contour charts of electron density as well as the three important parameters of the average Chapman profile: the maximum density, the altitude of maximum and the scale height will be presented.

The Russian tomography experiment, which utilized the same four locations, as well as the incoherent scatter radar results obtained by the Haystack Observatory group, will be discussed at a later date.

G3-8
1640

IMPROVED TOMOGRAPHY OF THE IONOSPHERE USING A COMBINATION OF ULTRAVIOLET AND RADIO BEACON MEASUREMENTS FROM ROCKETS OR SATELLITES

P. A. Bernhardt* K. F. Dymund
Plasma Physics and Space Science Divisions
Naval Research Laboratory
Washington, DC 20375
C.M. Cotton S. Charkrbarti
Center for Space Physics
725 Commonwealth Ave
Boston University
Boston, MA 02215

Computerized tomography (CT) can be used to analyze total electron content (TEC) data to yield two-dimensional maps of ionospheric electron density. TEC is determined by detecting the differential phase between two or more radio waves transmitted from a space borne radio beacon. The TEC data are recorded by a chain of receivers on the ground in a line parallel to the orbit of the radio beacon transmitter. Because the observations are obtained along integration paths from either a high altitude rocket or a satellite to a ground receiver, none of the integration paths through the ionosphere are horizontal. Consequently, with only vertical or oblique integration paths through the ionosphere, the information is insufficient to uniquely reconstruct the electron densities in the ionosphere.

Several techniques have been used to overcome the limited angular coverage problem in ionospheric tomography. First, measurements of the vertical electron profile using ionosondes or incoherent scatter radars have been used supplement the TEC data base for CT. Second, knowledge of the general shape of the ionosphere has been used constrain the reconstruction results.

Another approach to accurate reconstructions with ionospheric radio tomography is to add instruments on the satellite or rocket to provide the missing data required for unique reconstructions. An extreme ultra-violet (EUV) photometer or spectrograph can be used to provide altitude profiles 83.4 and 91.1 nm emissions that are produced by radiative recombination of O^+. In the F-region the O^+ and electron densities are equal. The combination of EUV observations in the horizontal direction and radio beacon measurements in the near vertical direction provide enough data to uniquely characterize the F-region electron densities. This techniques will be tested using the NASA sponsored TERRIERS satellite or the NRL sponsored CERTO program.

Session A-2, 0835-Thurs., CR1-40
TIME DOMAIN, ANTENNA, AND MATERIAL METROLOGY
Chairperson: S.M. Riad, The Bradley Dept. of Electrical Engineering, Virginia Polytechnic Inst. and State Univ., Blacksburg, VA 24061

A2-1
0840

A TEM-HORN ANTENNA WITH DIELECTRIC LENS FOR FAST IMPULSE RESPONSE

Dr. John F. Aurand
Sandia National Laboratories
High-Power Electromagnetics Dept. 9323
P.O. Box 5800, MS-1153
Albuquerque, NM 87185-1153

We recently designed and built a TEM-horn antenna with a dielectric aperture lens in order to achieve faster transient pulse response. The antenna consists of a conventional TEM-horn configuration (two flat, long triangularly-shaped conducting plates with a constant separation angle), and an additional solid Teflon™ lens placed at the aperture end of the plates.

TEM horns are commonly used for wideband time-domain work because they offer minimum dispersion as a traveling-wave endfire structure (which can be made fairly nonresonant). However, even carefully designed TEM horns have an inherent pulse smearing effect due to spherical wavefront propagation within the structure. A dielectric planar-spherical aperture lens is used to compensate for this plane-wave to spherical-wave conversion. The idea is simply to collimate the wavefront between the plates in order to improve the impulse response.

A 91-cm-long antenna was designed and built. Two different schemes were employed for the plate configuration: the first version utilizes single-sided etched copper traces on low-loss printed-wiring boards (PWB), and the other version utilizes solid copper plates. The PWB configuration is designed with stepped resistive loading at the aperture end of the traces in order to minimize ringing antenna currents, and a custom transition from the parallel-plate antenna structure to coaxial feedpoint. The solid-plate configuration was then developed because the impulse response of the PWB topology wasn't good enough. The resulting step-equivalent risetime (10-90%) of the solid-plate version is 24 ps, the fastest TEM-horn we have designed and built. In both configurations, expanded polystyrene is employed as a solid structural material between the plates, and the dielectric planar-convex lens is located at the aperture end of the plates.

This paper describes our antenna design for both plate configurations, and measurements of the resulting performance for two nominally-identical antennas. This type of antenna offers very good short-pulse operation, and is highly recommended for wideband time-domain antenna work.

This work was supported by the U.S. Dept. of Energy under Contract DE-AC04-94AL85000.

A2-2
0900

ADAPTATION OF LENS AND REFLECTOR IRAS FOR VARIOUS APPLICATIONS

Carl E. Baum
Phillips Laboratory
3550 Aberdeen SE
Kirtland AFB, NM 87117-5776

The TEM horn is an antenna which can be used for radiating (or receiving) fast electromagnetic transients. However, it presents an open circuit to the transient source (pulser) which can sometimes be a problem. This is relieved by adding a resistive termination connecting the two horn conductors. The placement of the path(s) for the current in this termination is important in that it significantly affects the low-frequency antenna performance. By routing these currents behind the horn, the associated magnetic dipole moment can be oriented to combine with the electric dipole moment to orient the low-frequency radiation in the forward direction, the same direction as the high-frequency radiation. Other features of such an antenna can include a lens at the horn aperture to make a lens IRA, and a ground plane to suppress the creation of an undesirable common mode at the connection to the horn (the horn apex), effectively making the pulser exterior conductors part of the ground plane. As an added feature, one need not have the ground plane flat as one goes behind the horn apex. How far one should extend the ground plane before truncation or other (downward) bends in the conductor is a complex question. One can truncate the ground plane at the horn aperture if desired, with recognition of the fact that the antenna aperture radiates down as well as up (i.e., the image of the aperture below the ground plane is missing in that case).

The reflector IRA has a design based on a conical-transmission-line feed launching a fast-rising spherical TEM wave into a paraboidal reflector focused at infinity. Various alterations can be made to the basic antenna design to accommodate mounting on conducting structures. By utilizing one of the symmetry planes of a circular reflector IRA one has half the reflector IRA on a ground plane with the beam (direction of transmission or reception) parallel to this ground plane. By use of an offset feed, this is further generalized to other beam directions. For cases that one may wish to make the reflector effectively part of a conducting surface (local ground plane) with transmission and/or reception approximately perpendicular to this surface, one can make the reflector as a well in the ground plane. Various options concerning the feed-arm locations (recessed or protruding) are also available.

A2-3
0920

MEASUREMENTS OF SHORT-PULSE PROPAGATION THROUGH CONCRETE WALLS

Dr. John F. Aurand
Sandia National Laboratories
High-Power Electromagnetics Dept. 9323
P.O. Box 5800, MS-1153
Albuquerque, NM 87185-1153

We recently performed a series of experimental measurements of short-duration electromagnetic propagation through two different concrete walls. Several different pulse shapes were used for the incident radiation, with frequency content from VHF to 20 GHz. Both walls were 30 cm thick, with 3 layers of reinforcing steel bars inside. For this set of data, the incident wave polarization was vertical linear only. Corroborating swept-frequency measurements were made with a vector analyzer.

The transmitter portion of the wideband time-domain measurement system consisted of a very fast low-voltage commercial pulse generator and a wideband TEM-horn antenna with dielectric aperture lens. The receiver consisted of an identical TEM-horn antenna and a wideband sampling oscilloscope. In terms of characterizing the propagation through a wall or other lossy dielectric layer, the most straightforward configuration is a free-space transmission measurement, in which a radiated EM wave is launched by a transmitting antenna, propagates through a material layer of some thickness, and is captured by a receiving system. The material layer under test is modeled as a two-port device, with an overall transfer function which relates the output pulse to the input excitation pulse. This transfer function can then be used to unfold or determine the dielectric constant and loss tangent of the material layer.

Two different transmission measurements are made in order to form the layer transfer function. One is a free-space reference measurement, representing the measurement system response. The other is the through measurement, in which the pulse is actually measured through the layer of interest. The transfer function is then given by the frequency-domain ratio of the processed received waveforms.

This paper describes the propagation measurements through the two different walls, and examines the transfer function, dielectric constant, loss tangent, attenuation constant, and time-domain impulse response of these walls. The attenuation increases steadily with frequency, and is a strong function of moisture content (as expected) within the concrete.

This work was supported by the U.S. Dept. of Energy under Contract DE-AC04-94AL85000.

A2-4
0940

CHARACTERIZATION OF CONCRETE MATERIAL USING TEM HORN ANTENNAS

Wansheng Su, Raqibul Mostafa
Sedki. M. Riad, and Imad L. Al-Qadi*
The Bradley Department of Electrical Engineering
Virginia Polytechnic Institute and State University
Blacksburg, Virginia 24061-0111
Phone: +1-540-231-4463, Fax: +1-540-231-3531
email: sriad@vt.edu

This paper presents the work performed at Virginia Tech to investigate the electrical properties of concrete materials over a wide frequency range from 100 kHz to 10 GHz. The main purpose of this research is to establish a data base for evaluating concrete materials.

The EM characterization of the concrete material is to allow the investigation of its physical condition. This is based on the fact that the mechanical, physical and chemical properties of concrete materials are correlated to their electrical properties, such as permittivity and permeability.

To examine the properties in the microwave frequency range, a pair of TEM horn antennae, are used to perform the characterization. The selection of TEM horn antennae is due to their extremely wide operating frequency band and good time domain performance. The concrete samples were cast in the form of 2' x 2' x 4" slabs. Steel rebars were used to reinforce the slab structure close to its perimeters only in an effort to further them from the measurement region in the center of the slab. Measurements were performed at different times during its curing period as well as with varying environmental conditions.

Two antennae are used to perform both reflection and transmission measurements which enable us to extract complex permittivity and/or permeability of the concrete material under test. Measurements are performed using both time domain and frequency domain network analyzers. A simple response calibration procedure, short circuit for reflection and through for transmission, is used to calibrate the measurement system. Obtained results from both time domain and frequency domain measurements demonstrate a good agreement.

A2-5
1020

CALIBRATED TIME-DOMAIN NETWORK ANALYSIS FOR INTERCONNECT AND DEVICE MEASUREMENTS

Donald C. DeGroot and Roger B. Marks
National Institute of Standards and Technology
Microwave Metrology Group
325 Broadway
Boulder, CO 80303-3328

In competitive electronic markets, the price of RF devices is critical, and amortizing the cost of expensive test equipment can significantly increase component cost. Currently, time-domain network analysis (TDNA), the acquisition of frequency-domain network parameters using time-domain reflection/transmission (TDR/T) instrumentation, is emerging as a practical, cost-effective alternative to traditional frequency-domain network analyzers (FDNA). Though the concept was proposed nearly three decades ago (A. M. Nicolson, IEEE Trans. Instrum. Meas., 17, 395-402, 1968), recent advances in instrumentation (D. A. Smolyansky *et al.*, 44th ARFTG Conference Digest, 56-62, 1994) and calibration techniques (R. B. Marks, *et al.*, 44th ARFTG Conference Digest, 47-55, 1994; W. Su, and S. M. Riad, IEEE Trans. Instrum. Meas., 42, 157-161, 1993) have made the application of TDNA to rf and microwave measurements practical today. Until recently, there have been few demonstrations of fully-calibrated TDNA device measurements. Consequently, there has been little guidance in establishing appropriate parameters and instrument settings for automated TDNA systems.

In this presentation, we will demonstrate the application of calibrated TDNA to on-wafer measurements of coplanar waveguide transmission lines and test devices and provide a comparison to accurate FDNA measurements of the same devices. As in automated FDNA, the TDNA user must choose a number of suitable instrument settings before collecting accurate data. This presentation will also show how sample density, window size, and waveform averaging affect the accuracy of calibrated TDNA results. Although this study used on-wafer measurements to demonstrate calibrated TDNA and the effects of instrument settings, the techniques are generally applicable to other implementations, such as fixtured device and packaging measurements.

A2-6
1040

DETERMINING COMPLEX PERMITTIVITY USING TIME DOMAIN NETWORK ANALYSIS

Jeffrey A. Jargon and Michael D. Janezic
National Institute of Standards and Technology
Electromagnetic Fields Division
325 Broadway, Boulder, CO 80303 USA

Recently, time domain network analyzers (TDNA) have emerged as a viable alternative to conventional frequency domain network analyzers (FDNA) (R.B. Marks, D.C. DeGroot, and J.A. Jargon, "High-Speed Interconnection Characterization using Time Domain Network Analysis," *Advancing Microelectronics*, Nov.-Dec. 1995). Here, we apply this concept to the determination of complex permittivity with the transmission/reflection (TR) method (J. Baker-Jarvis, E.J. Vanzura, and W.A. Kissick, "Improved Technique for Determining Complex Permittivity with the Transmission/Reflection Method," *IEEE Trans. Microwave Theory Tech.*, **38**, 1096-1103, Aug. 1990). The TR technique applies a robust algorithm and avoids the ill-conditioning at frequencies corresponding to integer multiples of one-half wavelength in the sample. We apply the multiline through-reflect-line (TRL) calibration (R.B. Marks, *IEEE Trans. Microwave Theory Tech.*, **39**, 1205-1215, Jul. 1991) to TDNA since this method permits calibration over a wide frequency band and fully characterizes the calibration lines.

To carry out the measurements, an unknown sample, whose complex permittivity we wish to determine, is placed in a section of coaxial line and measured with a time domain network analyzer. Coaxial calibration standards are measured at the same test ports. Off-line, the time records of the samples and the calibration artifacts are converted to frequency dependent scattering parameters using a fast Fourier transform, and a calibration is performed. The calibrated scattering parameters of the unknown sample are then used to determine the complex permittivity.

Figure 1 illustrates the results showing the real part of the permittivity of a sample of polytetrafluoroethylene (PTFE) in 7 mm coaxial line using TDNA and FDNA.

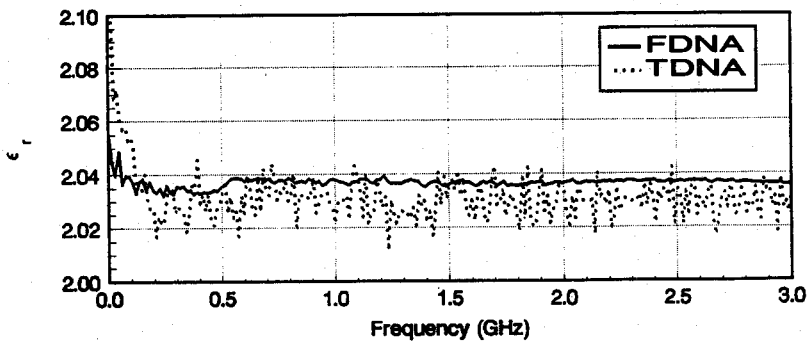

A2-7
1100

USE OF FULL SHEET RESONANCE FOR DIELECTRIC SUBSTRATE MEASUREMENT

Richard L. Lewis
Electromagnetic Fields Division
Electronics and Electrical Engineering Laboratory
National Institute of Standards and Technology
325 Broadway
Boulder CO 80303

Full sheet resonance (FSR) techniques (L. S. Napoli and J. J. Hughes, IEEE Trans. MTT, 19, 664-665, July 1971) have been available for a number of years for measuring the relative dielectric constant of copper clad substrates. Measurement of the cavity's Q enables the measurement to be corrected for wall and radiation loss (J. Q. Howell, IEEE Trans. MTT, 21, 142-143, March 1973). FSR measurements are used to assure quality control of dielectric substrate production (G. I. Woolaver, Microwaves & RF, 29, 153-158, August 1990). A measurement program has been undertaken at NIST using an automatic network analyzer to evaluate the FSR method, and preliminary results have produced consistent relative dielectric constants using this technique. The transmission method for measuring Q (D. Kajfez and P. Guillon, ed., Dielectric Resonators, Artech House, 1986) is employed using capacitive coupling at the substrate corners to optimize resonant mode excitation. Capacitive coupling is achieved by positioning the dielectric substrate's corners just inside the opening of two coaxial waveguide connectors (P. H. Ladbrooke, M. H. N. Potok, and E. H. England, IEEE Trans. MTT, 21, 560-562, August 1973). Noise reduction is achieved by allowing the substrate's upper copper cladding to touch the center conductor of one coaxial connector and allowing the substrate's bottom copper cladding to touch the outer conductor of the other coaxial connector. A critical factor in analyzing results is the accurate assignment of mode numbers to resonant frequencies. To clarify the confusion of multiple modes, a mode table of resonant frequencies is generated, so that the material's dielectric constant is obtained using an iterative procedure. Identification of resonant frequencies is complicated by the possibility of false resonances and frequency pulling due to the proximity of multiple resonances. Consequently, the lower order modes provide the most accurate measurement of the cavity's Q, while the higher order modes help assure accurate mode number assignment. Our discussion will include a description of how coupling is achieved and how the results compare to other methods.

A2-8
1120

THIN-FILM FERROELECTRIC COPLANAR-WAVEGUIDE PHASE SHIFTERS OPERATING AT ROOM TEMPERATURE

Daniel S. Stotz, Huey-Daw Wu, Jack Thiesen, Scott Ruth,
and Frank S. Barnes
Department of Electrical Engineering
University of Colorado at Boulder
Boulder, CO 80309-0425

Electronically-controlled phase shifters using $Ba_{0.6}Sr_{0.4}TiO_3$ (BST) ferroelectric thin film and coplanar waveguide (CPW) structure have been designed, fabricated, and characterized for operation at room temperature. The large variation of the dielectric constant of the BST with DC bias voltage makes this material suitable for the construction of phase shifters which can be used in the feed system of the electronically steerable phase array antennas. The $Ba_{0.6}Sr_{0.4}TiO_3$ material has a Curie temperature of around 280 K so that at room temperature it is operated in the paraelectric region where the loss tangent drastically reduced while still maintaining sufficient tunability of its dielectric constant. A CPW structure was chosen for two reasons. First, the main line and the ground planes of CPW are on the same surface of the dielectric substrate, which simplifies the device fabrication. Secondly, by properly choosing the center conductor and gap widths of a CPW, a 50 Ω line is achievable even though the dielectric constants of the substrate and the BST thin film are substantially high. As a result, we can make the gap width small to have large DC bias field and the center conductor width large to reduce the conductor loss while still keeping the impedance at a reasonable level.

A 0.5 μm BST thin film was deposited on the $LaAlO_3$ substrate using the pulsed laser deposition. A 1.62 cm long Ag/Au CPW meander line with a 100 μm center line and a 25 μm gap was patterned on the BST layer with the lift-off metallization technique. The microwave performance of the phase shifters was measured using the HP 8510 network analyzer and the Cascade Microtech probes. The calibration was made with the Cascade Microtech LRM impedance standard substrate. We have obtained a phase shift of ~100° at 10 GHz by applying a DC bias voltage of 100 V between the center line and the ground planes. The insertion losses without DC bias and with 100 V are measured to be 11.4 dB and 7.4 dB, respectively. Because of the low impedance (~22 Ω) of the CPW, significant amount of power dissipation is caused by the reflection loss due to impedance mismatch; which can be overcome by tapering the two ends of the meander line into 50 Ω CPW lines.

The conformal mapping technique for the analysis of two-layer CPW structures enables us to extract the material parameters of the BST thin film from the measured scattering parameters of the phase shifters. By neglecting the radiation loss of the device, the insertion loss has been separated into the conductor loss, the dielectric loss, and the reflection loss. Several techniques to reduce the conductor loss of the CPW structure and the dielectric loss of the ferroelectric material will be presented.

Session B-3, 0855-Thurs., CR1-9
HYBRID TECHNIQUES
Chairperson: A.F. Peterson, School of Electrical and Computer Engineering, Georgia Inst. of Technology, Atlanta, GA 30332
Organizer: D.R. Wilton, Dept. of Electrical and Computer Engineering, Univ. of Houston, Houston, TX 77204

B3-1
0900

EFIE-MFIE ITERATIVE TECHNIQUE: A CURRENT-BASED HYBRID METHODOLOGY

Richard E. Hodges Yahya Rahmat-Samii*
Department of Electrical Engineering
University of California, Los Angeles
Los Angeles, California 90095-1594

Hybrid analysis techniques represent a useful approach for the difficult problem of intermediate frequency regimes which are too large for numerically exact methods such as the Moment Method (MM) and are not amenable to pure asymptotic approximations. Hybrid methods may either be ray-based, such as GTD-MM, or current-based. This paper presents a general current-based hybrid method suitable for electrically small antennas ($\sim \lambda$) mounted on a comparatively large structure. The method uses a hybrid combination of the Electric Field Integral Equation (EFIE) and Magnetic Field Integral Equation (MFIE) in which the EFIE and MFIE are applied to geometrically distinct regions of an object. The Hybrid EFIE-MFIE (HEM) formulation can model arbitrary three-dimensional metallic structures comprised of wires and both open and closed surfaces. This approach is "hybrid" in a dual sense: (1) Fredholm integral equations of the first and second kind are applied to separate regions of an object, and (2) two distinct solution methods are used to solve the coupled integral equations.

A double iterative method, HEM iterative (HEMI), is used to solve the HEM equations. This technique uses the Moment Method (MM) in the EFIE region with an iterative Neumann series technique in the MFIE region. Since physical optics (PO) is an approximation of the HEM formulation, this technique provides a practical method to utilize the PO current. In addition, it offers a general and systematic mechanism to correct the inherent error in PO. Consequently, it overcomes the limitations of the Physical Optics Hybrid Method (POHM). The HEM solution method is also naturally suited to parallel processing computer architectures such as Multiple Instruction Multiple Data (MIMD) machines. Accurate solution of relatively large problems is achieved by efficient use of the large distributed memory available on a parallel machine.

A general model of radiation from a system of metallic wires and surfaces is presented in order to demonstrate the method. Numerical results comparing MM, POHM and HEMI are given for representative examples, including wire antennas mounted on a cylindrical structure and a complex cavity antenna. The computed results verify that HEMI is an effective method to improve the POHM calculations, and the HEMI results are in good agreement with MM calculations and experimental data.

B3-2
0920

Three-dimensional Scattering Using the Integral Equation – Asymptotic Phase Method

Keith R. Aberegg and Andrew F. Peterson*
School of Electrical & Computer Engineering
Georgia Institute of Technology
Atlanta, GA 30332-0250

A hybrid numerical/asymptotic procedure called the integral equation – asymptotic phase (IE–AP) method was recently developed for scattering from perfectly conducting two-dimensional cylinders (K. R. Aberegg and A. F. Peterson, "Application of the integral equation – asymptotic phase method to two-dimensional scattering," *IEEE Trans. Antennas Propagat.*, vol. 44, pp. 534-537, May 1995). The IE–AP approach employs an asymptotic solution to predict the relatively rapid phase dependence of the unknown current distribution, in order to leave a slowly-varying residual function that can be represented by a coarse density of unknowns. Results suggest that the use of the physical optics approximation as the asymptotic solution can often reduce the required unknown density to as few as one per wavelength on average in 2D problems without a significant loss of accuracy, even for scatterers with edges.

In the present investigation, the IE–AP formulation is extended to treat 3D conducting bodies. The surface current density appearing within the combined-field integral equation is replaced by a product of the physical optics current and an unknown residual function. In order to increase the electrical size of the cells without incurring unnecessary error, the residual function is represented by novel mixed-order vector basis functions defined on curved triangular patches. The specific basis functions we employ provide a linear normal component and a quadratic tangential component of the vector surface current along the patch edges, and maintain normal continuity between patches in order to produce a finite surface divergence. They can be thought of as an extension of the Rao, Wilton, and Glisson triangular rooftop basis functions to a higher polynomial order.

The 3D IE–AP formulation will be described, and results for simple three-dimensional scatterers including spheres and cone-spheres will be presented to illustrate the accuracy of the procedure. Results will be compared with numerical solutions obtained using the lower-order Rao, Wilton, and Glisson triangular rooftop functions and other solutions obtained from body-of-revolution formulations. It appears that the incorporation of the asymptotic phase function can reduce the required number of unknowns by an order of magnitude compared with traditional solutions.

B3-3
0940

HYBRID COMBINATION OF NUMERICAL AND ASYMPTOTIC TECHNIQUES FOR ANALYSIS OF HIGH FREQUENCY RADIATION/SCATTERING BY GENERIC AIRCRAFT/MISSILE SHAPES

M. Hsu P.H. Pathak H.T. Chou R.J. Burkholder*
The ElectroScience Laboratory
Department of Electrical Engineering
The Ohio State University
1320 Kinnear Road
Columbus, Ohio 43212

An important EM phenomenon that needs to be predicted efficiently and accurately is the radiation/scattering of EM waves by electrically large aircraft/missile configurations. A hybrid combination of numerical and asymptotic high frequency methods is proposed to achieve this objective in a tractable fashion. The motivation for the development of this hybrid approach stems from the fact that brute force integral equation as well as partial differential equation based numerical solutions of such electrically large complex structures becomes highly inefficient and perhaps even intractable, and that purely asymptotic high frequency based solutions cannot handle electrically small parts of the complex structure which can nevertheless in many instances be potentially important contributors to the overall radiation/scattering. Also, analytical asymptotic high frequency solutions may not be presently available for handling some of the electrically large portions of the complex structure. Thus, an integral equation-based formulation whose solution can be obtained via the moment method (MM) is proposed in which the kernel (Green's function) of the integral equation is chosen to a priori asymptotically satisfy the EM conditions on a large portion of the object such as on the basic generally convex aircraft/missile fuselage shape through the use of appropriate UTD solutions. This leaves the unknown induced currents to be found, using the MM procedure, only over the remaining parts (e. g., control surfaces/fins, etc.) of the aircraft/missile geometry, thereby drastically reducing the number of unknowns to be solved in this hybrid MM-UTD approach in comparison to those required to be solved in the other purely numerical solution techniques. Of course an aircraft structure contains, in addition to the fuselage and control surfaces/fins, other large or small perturbations such as antennas, antenna windows, jet inlet cavities, gaps, etc. These important additional effects can be incorporated by extensions of this basic hybrid MM-UTD scheme via a super hybrid procedure which combines other numerical methods (e.g., FEM) best suited for antennas, gaps, etc. and asymptotic methods (e.g., modified iterative physical optics) for jet engine cavities. These general ideas will be discussed along with the current status of the proposed hybrid method, and an example of the basic hybrid MM-UTD will be illustrated with numerical results. The super-hybridization will also be discussed along with immediate future goals to obtain a super hybrid solution for analysis of radiation/scattering from generic aircraft/missile configurations.

B3-4
1020

NEW DEVELOPMENTS OF HYBRID FINITE ELEMENT METHODS FOR SCATTERING AND RADIATION BY COMPLEX TARGETS

J. Jin* N. Lu S. Ni
Department of Electrical and Computer Engineering
University of Illinois at Urbana-Champaign
Urbana, IL 61801-2991

A robust hybrid technique is developed for computing electromagnetic scattering by large targets with cracks and cavities on their surfaces. The technique employs the field equivalence theorem to divide the original problem into two problems. The first is the scattering by the large bodies with the cracks and cavities filled with perfect conductors, and is computed efficiently using a high-frequency method, such as the shooting-and-bouncing-ray (SBR) method. The second problem is the field generated by a surface magnetic current inside the cracks and cavities with their openings covered with perfect conductors, and is solved accurately using the finite element–boundary integral (FE-BI) method. The field continuity conditions are then employed to combine these two methods, resulting in an efficient and accurate technique for computing the scattering by large targets with cracks and cavities on their surfaces.

This hybrid technique is then extended to characterize the radiation patterns of conformal microstrip patch antennas and arrays on a large complex body. For this problem, the FE-BI method is first used to analyze the microstrip patch antennas and compute an equivalent magnetic current on the aperture of the microstrip patch antennas. The SBR method is then employed, in conjunction with the reciprocity theorem and edge diffraction, to calculate the radiated field in the presence of the complex body. Comparison with measured data shows that the technique is accurate and efficient.

To further expand the capability of the hybrid technique, a new method is developed to lift the bottleneck of the FE-BI method, which is the full submatrix generated by the boundary integral equation (BIE). This method employs the recently developed fast multipole method (FMM) to achive a fast evaluation of the boundary integral. In this method, the surface, over which the BIE is applied, is first divided into several groups, each containing a number of elements. For elements within the same or nearby groups, their electromagnetic interaction is calculated individually in a traditional manner through a direct integration. However, for elements within different groups that are far apart, their interaction is calculated collectively by first translating the scattered field of different elements within a group into the group center, then transmitting this field to the center of another group, and finally redistributing it to the elements within that group. Doing this, both the memory requirement and computing time is reduced, thus improving the capability of the hybrid technique.

B3-5
1040

A HYBRID HIGH-FREQUENCY/FDTD METHOD FOR COMPUTING THE RCS OF LARGE OPEN-ENDED WAVEGUIDE CAVITIES

T.-T. Chia R.J. Burkholder* R. Lee
The ElectroScience Laboratory
Department of Electrical Engineering
The Ohio State University
1320 Kinnear Road
Columbus, Ohio 43212

A hybrid approach which combines high-frequency asymptotic methods with low frequency numerical methods has recently been introduced to analyze the electromagnetic (EM) scattering from the interior of large open-ended waveguide cavities with complex terminations (T.-T. Chia, R.J. Burkholder & R. Lee, *IEEE Trans. Antennas Propagat.*, **43**, 1082-1090, 1995). A primary application is the computation of the radar cross-section (RCS) of jet inlet and exhaust cavities. The method takes advantage of the efficiency of high-frequency asymptotic ray and physical optics methods for finding the EM coupling into the cavity via the open end and the propagation inside the smoothly varying duct (waveguide) section up to a cross-section immediately in front of the termination. The reflection (interior scattering) from the termination, which may be a complex engine face, is found via numerical analysis using the fields incident from the duct section. Then, a specially formulated termination reciprocity integral (P.H. Pathak & R.J. Burkholder, *IEEE Trans. Microwave Theory Tech.*, **41**, 702-707, 1993) is used to find the externally scattered fields by integrating the incident duct fields with the fields reflected by the termination over the cross-section in front of the termination.

In this paper, we describe the implementation of this approach using the Finite Difference Time Domain (FDTD) method to numerically characterize the complex termination. The EM modeling of the waveguide duct and termination sections of the cavity are decoupled so that the two sections can be analyzed independent of one another. This is accomplished by expanding the fields in the cross-section between the two sections (which is assumed to be circular) into waveguide modes, and using FDTD to characterize the scattering from the termination in terms of a modal reflection matrix. A great advantage of using FDTD instead of a frequency domain method is that a short pulsed time variation may be used to obtain multiple reflection matrices for a wide range of frequencies from a single FDTD run. Representative results will be shown which use the FDTD method combined with four different high-frequency methods for analyzing the duct section, including shooting and bouncing rays (SBR), the generalized ray expansion (GRE), iterative physical optics (IPO), and a waveguide modal reference solution.

B3-6 Roundtable Discussion
1100

D2-1
0840

ANALYSIS OF INJECTION-LOCKING OF MICROWAVE OSCILLATORS USING NONLINEAR TRANSISTOR MODELS

J. Dixon* Z. B. Popović
Department of Electrical and Computer Engineering
Campus Box 425
University of Colorado
Boulder, CO 80309

Injection-locking is often used in oscillators for reducing phase noise and improving stability of a high-power oscillator. Existing commercial microwave circuit analysis software does not have the capability to analyze nonlinear injection-locking transistor oscillator behaviour. In the literature, injection locking of microwave oscillators was analyzed using Van der Pol oscillator models, which do not correspond to transistor nonlinear device models. In this paper, we will first discuss the deficiencies of the Van der Pol model when applied to microwave transistor oscillators. We will then present a time-domain analysis technique which uses a more complicated nonlinear Curtice-cubic transistor model and can analyze behaviour of free-running and injection-locked oscillators.

The turn-on transient of free-running oscillators is shown to exhibit chaotic behaviour for some types of loads. Analysis results, including time-domain waveforms, phase plots and spectra, using several different commercial transistors will be presented. The injection-locking analysis allows us to observe the behaviour of the oscillator as a function of injected signal power and frequency. Again, for some cases of injected signals, the obtained signal content suggests chaotic behaviour, which can be observed experimentally in the oscillator spectra. The theoretical approach will briefly be presented and experimental results on a 0.5-GHz lumped element transistor oscillator discussed.

D2-2
0900

PARAMETER EXTRACTION FOR QUASI-OPTICAL AMPLIFIER ARRAYS

N. J. Kolias R. C. Compton*
School of Electrical Engineering
Cornell University, Ithaca, NY 14853
A. Alexanian R. A. York
Department of Electrical and Computer Engineering
University of California at Santa Barbara, Santa Barbara, CA 93106

Quasi-optical amplifier arrays provide a possible alternative to the tube-base amplifiers currently used in applications requiring significant millimeter-wave power (J. C. Wiltse ed., *Millimeter and Microwave Engineering for Communications and Radar*, 80-88, 1994). In several amplifier array approaches, each unit cell consists of orthogonally oriented input and output antennas which are connected by a transmission line, with gain achieved by placing an amplifier in the line. The array is designed to couple power from a focused, incident beam, amplify it, and then re-radiate it out in the orthogonal polarization. To achieve optimal amplifier performance, one would like to know the input and output s-parameters on either side of the transistor amplifier in order to design an optimal amplifier for the array. In this paper we present a technique for calculating these s-parameters.

The parameter extraction technique works as follows. The array is first modeled as a 4-port, where port 1 is vertically polarized waves on the input side of the array, port 2 is horizontally polarized waves on the input side of the array, port 3 is vertically polarized waves on the output side of the array and port 4 is horizontally polarized waves on the output side of the array. With the amplifiers replaced with straight through transmission lines, 4-port s-parameters for the passive array can be readily obtained either experimentally or theoretically using 3D-FDTD analysis (A. Alexanian et.al., submitted to *IEEE Microwave and Guided Wave Letters*, Sep. 1995). For passive arrays which are reciprocal and polarization independent (i.e. $s_{22} = s_{11}$, and $s_{33} = s_{44}$), the passive 4-port may be modeled as two identical 3-ports which are connected together by the unit cell's transmission line. The s-parameters for these identical 3-ports may be determined theoretically from the 4-port s-parameters of the passive array. Calculating the s-parameters looking into the 3-port from the transmission line, allows us to match the transistor amplifier and optimize the array performance.

Acknowledgement: This work was supported by the Army Research Office.

D2-3
0920

A DIELECTRIC SLAB WAVEGUIDE LENS REALIZED FROM YAGI-UDA SLOT ARRAY ANTENNA ELEMENTS AND MICROSTRIP DELAY LINES

Alfred Richard Perkons and Tatsuo Itoh
University of California, Los Angeles
Electrical Engineering Department
School of Engineering and Applied Science
405 Hilgard Avenue
Los Angeles, CA 90024-1594

The hybrid dielectric slab-beam waveguide (HDSBW) is well suited as a transmission medium for mm and sub-mm wave quasi-optical circuits (F. K. Schwering and J. W. Mink, 1993 URSI Radio Science Meeting, p. 26, June 28 - July 2, Ann Arbor Michigan). A quasi-optical amplifier using Vivaldi antennas and conventional dielectric lenses in a HDSBW configuration was recently reported (J. Harvey etc., 1995 IEEE MTT-S Digest, pp. 921-924). A HDSBW lens realized from Yagi-Uda slot array antenna elements and microstrip delay lines has advantageous characteristics and a passive version has been fabricated. Active devices can be easily incorporated into the HDSBW lens microstrip delay lines to form a quasi-optical amplifier/power combiner. A one-way combining efficiency of 65% has been measured at X-band.

Directive excitation of the HDSBW was achieved with a microstrip fed Yagi-Uda slot array with one reflector and one director. The slots were etched in a common ground plane separating the HDSBW and microstrip substrates. Truly planar excitation, compatible with planar fabrication technology, of the HDSBW has been achieved. Coupling into the HDSBW substrate was maximized by choosing the thickness to be such that the center operating frequency corresponds to 90% of the cutoff frequency of the second order TM mode; slot excitation of the first order TE mode is negligible. Initial dimensions for the Yagi-Uda slot array antenna were selected using guidelines available in the literature (T. Itoh etc., 1981 IEEE MTT-S Digest, pp. 5-7). Experimental optimization of the antenna dimensions resulted in a design with a SWR<2.0 and front-to-back ratio greater than 10 dB over a 5% bandwidth.

Two linear arrays of the above described Yagi-Uda slot array antennas connected by microstrip delay lines comprise a passive HDSBW lens. Delay line length is analogous to thickness of a conventional dielectric lens. A ten element lens with focal length to diameter ratio of 0.43 had a total measured loss of 4.3 dB at X-band. This translates to a one-way combining efficiency of 65%; independent of the number of array elements. An active version of such a lens should be useful as a HDSBW solid state repeater or as an amplifier/power combiner at mm and sub-mm wavelengths.

D2-4
0940

AN X-BAND QUASI-OPTICAL ISOLATOR

S. Hollung* M. Marković Z. B. Popović
Department of Electrical and Computer Engineering
Campus Box 425
University of Colorado
Boulder, CO 80309

A number of active quasi-optical components, such as oscillators, amplifiers, multipliers, mixers and beam-control grids, have been presented in the past decade (*IEEE MTT Trans. Special Issue, October 1994*). The purpose of developing such components is to achieve higher power levels at millimeter-wave frequencies from a very large number of low-power solid-state devices. Quasi-optical sources are essentially active antenna arrays, and can therefore be used as the source and radiating structure of an analog transmitter or receiver front end. In high-power transmitters, isolators are placed at the output of the last amplifier stage in order to protect the transmitter from possible reflected high power levels. Here we present a quasi-optical isolator which can be placed at the output of a quasi-optical oscillator or amplifier. The isolator does not use nonlinear magnetic materials and consists of a set of six cascaded printed grids loaded with lumped elements (resistors and capacitors).

For communication applications, it is often useful to use circularly polarized waves: they are unaffected by the ionosphere and also are less sensitive to multipath fading. However, most quasi-optical amplifiers intended for use in transmitters use orthogonal linear polarization for input and output waves, mainly for stability reasons. The isolator we present in this paper has a dual purpose: it converts the linearly polarized wave at the output of a quasi-optical amplifier to a circularly polarized wave with less than 2 dB loss at X-band, and also provides isolation of around 10 dB. The linearly polarized input wave first passes unattenuated through a polarizing grid cascaded with another grid loaded with resistors. In the latter, the resistive strips are perpendicular to the electric field vector, and the resistive grid has a very small effect on the input wave. The wave then passes through a CP polarizer consisting of 4 capacitively-loaded grids and is right-hand circularly polarized at the output. A reflected wave is left-hand circularly polarized, and upon transmission through the polarizer is absorbed in the resistive grid. This paper will discuss the design and characterization of the described X-band quasi-optical isolator.

D2-5
1020

ELECTROMAGNETIC WAVE EFFECTS ON MODFETs

S. M. Sohel Imtiaz, M. A. Alsunaidi, M. A. Megahed, and S. M. El-Ghazaly
Department of Electrical Engineering
Arizona State University, Tempe, AZ 85287-7206

When the semiconductor device operates in the millimeter-wave range, with the device width comparable to the electromagnetic wave length and the short wave period may be comparable to the electron relaxation times, the conducting electrons interactions with the electromagnetic wave cannot be neglected. In this work, Maxwell's equations are used in conjunction with a 3D hydrodynamic model to develop a powerful and accurate simulator for high frequency devices, using the finite difference time domain (FDTD) method. The electromagnetic forces on the electrons are derived from Maxwell's equations and the electron transport characteristics are obtained from the hydrodynamic model. This novel approach has been utilized in millimeter-wave semiconductor modeling. It is a very powerful tool for analyzing the behavior of submicron gate MESFETs (M. A. Alsunaidi and S. M. El-Ghazaly, 1995 IEEE MTT-S Digest, pp. 1257-1260, May 1995).

To demonstrate the potential of this simulator, it is used to analyze the millimeter-wave performance of **M**odulation **D**oped **F**ield **E**ffect **T**ransistors (MODFET). At first, the DC analysis is done for MODFETs. The output characteristics, the transconductance, and the cut-off frequency are in good agreement with those of Shawki et al. (T. Shawki, G. Salmer and O. El-Sayed, IEEE Trans. Electron Devices, vol. 37, pp. 21-30, Jan. 1990). The AC analysis is also performed. The electron-wave interaction can be described by examining the input and the output voltage waves, for different device widths. The output voltage wave takes a finite time to respond to the input voltage wave. At first, the input wave decreases in magnitude as it moves along the device electrodes. This is due to the EM energy loss to the conducting electrons. As the output wave develops, the coupling between the input and the output waves, enhances the input wave. The output wave increases as it moves along the device width. The reason is that the EM energy is propagated along the device and the wave amplitude increases. The DC and the AC analysis are also done for MESFETs of similar dimensions and are compared with those of MODFETs.

D2-6
1040

HIGH-EFFICIENCY SWITCHED-MODE MICROWAVE AMPLIFIERS

T. Mader E. Bryerton* M. Forman Z. B. Popović
Department of Electrical and Computer Engineering
Campus Box 425
University of Colorado
Boulder, CO 80309
Reza Tayrani
Compact Software
Patterson, New Jersey

By increasing the efficiency of a 50% efficient amplifier to 90%, the dissipated heat power is reduced by a factor of nine for the same output power. Increasing the efficiency of high-power circuits decreases their size (reduced heat sink) and power consumption, and increases their output power, reliability and lifetime. High-efficiency amplifiers in the microwave region can be made by using switched-mode topologies borrowed from lower frequencies, and modifying them to suit microwave circuit fabrication technology. We investigate in particular two classes of switched-mode operation: class E and class F. Experimental results and comparison between class E and F circuits, using the same Siemens CLY5 MESFET will be presented in this paper.

In switched-mode amplifiers, the amplifying device is used as a switch. At high frequencies, transistors are not ideal switches, mainly due to the device on-resistance and output capacitance. In addition, lumped elements, especially high-Q inductors, are hard to realize. We present a simplified design procedure for switched-mode transmission-line microwave amplifiers. The design procedure is well suited for computer-aided synthesis. Validation of circuit synthesis is presented on several amplifiers which use commercial transistors at frequencies between 0.5 and 5 GHz. Power-added efficiencies as high as 80% at 0.5 GHz and 73% at 5 GHz with around 1 W of corresponding output power will be discussed. Comparison of experimental class A amplifiers to class E and F amplifiers will be given. Some improvements in nonlinear transistor models for switched-mode operation will be suggested.

D2-7
1100

EXTRINSIC PARAMETERS MODELING OF HIGH FREQUENCY SEMICONDUCTOR TRANSISTORS

M. A. Megahed and Samir M. El-Ghazaly
Department of Electrical Engineering
Arizona State University, Tempe, AZ 85287-7206

Traditionally, the design and characterization procedures for high frequency devices and circuits have relied on measurements. Measured small-signal s-parameters and DC data are frequently used in association with equivalent circuits. In these equivalent circuits, element values are obtained by fitting the model terminal characteristics to the measured data. This emperical approach requires extensive experimental efforts to establish a solid foundation for design. Moreover, the predicted equivalent circuits can not easily accounted for the extrinsic parasitics associated with the transistors.

Conventionally, physical modeling of semiconductor devices employs a solution of Poisson equation to update the electric field inside the device. When semiconductors devices are operated at high frequencies, the semiconductor transport physics and consequently the device modeling problem become more involved. In such cases, quasi-static semiconductor device models fail to accurately represent the effects of the extrinsic parasitics.

A full-wave three-dimensional simulation model is used to predict the extrinsic parameters of high frequency semiconductor transistors. Maxwell's equations are blended with the hydrodynamic systems of the active device. The resulted system of equations are solved using the finite difference technique. The current denisties inside the transistor are updated using the time varying electric field, which is obtained form the full-wave model.

National Radio Science Meeting (Boulder, CO)
Jan. 1996

Session F-3, 0835-Thurs., CR1-42
MOBILE AND PERSONAL ACCESS RADIO PROPAGATION
Chairperson and Organizer: W.J. Vogel, Electrical Engineering Research Laboratory,
The Univ. of Texas at Austin, Austin, TX 78758

F3-1
0840

INTO BUILDING FADING AT L- AND S-BAND FOR SATELLITE PCS

W. J. Vogel, G. W. Torrence, and H.-P. Lin
Electrical Engineering Research Laboratory
The University of Texas at Austin
10100 Burnet Road, Austin, TX 78758-4497
E-mail: (Wolf_Vogel, Geoff_Torrence)@mail.utexas.edu,
hplin@spoke.ece.utexas.edu

Selected results from L- and S-Band slant-path fade measurements into six different buildings (a tiltwall concrete structure, a brick wall building, a wooden farm house, a suburban house, a motel, and a store) employing a tower-mounted transmitter and dual-frequency receiver are presented. The objective of the measurements was to provide information for personal communications satellite design on the correlation of fading inside buildings between frequencies near 1620 and 2500 MHz. Fades were measured along horizontal directions with 5 cm spacing. The measurement system consists of a dual-frequency sweeping transceiver located in a van, a 20 m crank-up transmitter tower mounted to the van, and a remote receiving antenna, filter, and preamplifier mounted on a linear positioner.

Fade differences between L- and S-Band exhibited a normal distribution with means usually near 0 dB and standard deviations from 7.2 to 8.2 dB. However, after spatial averaging over a few wavelenghts, the correlation between L- and S-Band was significantly improved. Time variations are small if there is little wind and the receiver and transmitter are stationary. This means that for satellite communications systems with fade margins less than about 15 dB, time variations of mobile terminal power at the satellite will be spatial variations converted to time variations primarily by user motion and secondarily by satellite motion. Simultaneous swept measurements over 160 MHz spans showed that the standard deviation of the power levels as function of frequency increased linearly with average fade depth from a minimum of about 1.3 dB and increased by .2 dB per 1 dB of fade. Fade slopes were also a function of fade level, with LMSS-Band averages in the range of 1 to 2 dB/MHz for 10 dB fades and increasing to about 3 to 4 dB/MHz at a 30 dB fade.

F3-2
0900

A SIMPLE MODEL FOR PREDICTING INDOOR RECEIVED LEVELS OF SATELLITE TRANSMITTED SIGNALS

Matthew Aprea and Charles W. Bostian
Center for Wireless Telecommunications
Virginia Polytechnic and State University
Blacksburg, Virginia 24061-0111
E-mail bostian@vt.edu

The indoor performance of hand-held terminals for low-earth orbit-satellite (LEOSAT) communications is important to users and operators of those systems. Measurements by W.J. Vogel and G.W. Torrence (*IEEE Transactions on Antennas and Propagation*, 41: 954-961, July 1993) provide a wealth of experimental data and a statistical model for the gross behavior of LEOSAT signals as received inside a variety of buildings.

In an effort to develop a simple deterministic prediction tool for indoor LEOSAT reception, the authors investigated a lossy cavity model and several ray tracing approaches. We obtained best results with a vector three-ray model that includes a direct ray, a ray arriving via a single reflection from the floor, and a ray arriving via one reflection from the floor and one reflection from the ceiling. Required input data are ceiling height, antenna height above the floor, whether there exists a line of sight path through a window, and the satellite elevation angle. The model tracks the polarization and phase of each ray and includes the polarization, amplitude, phase, and direction of arrival dependencies of the antenna response. Its predictions for received signal level versus frequency from 700 to 1500 MHz agree reasonably well with measurements.

The received signal is sensitive to receiving antenna location. A user can usually maximize the received signal by moving no more than half a meter. Relatively small changes in frequency (from 880 to 990 MHz, for example) can also improve typical signal levels for a particular building by as much as 10 dB.

National Radio Science Meeting (Boulder, CO)
Jan, 1996

F3-3
0920

AN EXTENDED EMPIRICAL ROADSIDE SHADOWING MODEL

Vegetative shadowing

Julius Goldhirsh[1], Wolfhard J. Vogel[2]
[1]The Johns Hopkins University, Applied Physics Laboratory
Johns Hopkins Road, Laurel, Maryland, 20723-6099
[2]The University of Texas at Austin
10100 Burnet Road, Austin, TX, 78758-4497

A revised empirical roadside shadowing (EERS) model has been derived which extends the previous empirical roadside shadowing (ERS) model such that it is now applicable to frequencies as high as 20 GHz and as low as 870 MHz. The previous model was limited to approximately 3 GHz. The EERS may now be applied to percentages from 1% to 80% and to elevation angles ranging from 7° to 60°. The ERS model was limited to probabilities below 20% and to elevation angles above 20°. The model is representative of a median distribution which deviates from the measured distributions generally less than ±5 dB at elevation angles above 20°.

The new model employs the following three additional extensions: (1) A logarithmic formulation relating the attenuation at 20% probability to higher values up to 80%, corresponding to an average zero fade condition. (2) A multiplying exponential containing a difference in frequencies term relating the 1.5 GHz fade to attenuations at frequencies as high as 20 GHz. (3) The extended model assumes that at elevation angles smaller than 20° (down to 7°), the fade is relatively invariant to elevation angle and is, on average, equal to the 20° attenuation. The rationale for the latter assumption is that at 20°, the Earth-satellite path is already passing through the lower part of the tree canopies. Reducing the path elevation angle is likely to result in attenuation caused by tree trunks which may tend to mitigate the path attenuation. On the other hand, at lower elevation angles, attenuation effects may increase because of fading from those tree canopies which are further offset from the road. These two opposing conditions create, on average, an invariance in attenuation with reducing path elevation angle. The above model assumes the absence of terrain blockage, multiple tree attenuation, and multipath effects. Because these effects may be present, the deviation of actual measurements relative to the EERS model may be substantially larger than ±5 dB (at the smaller elevation angles) as borne out by comparative measurements in Alaska.

path ⊥ to travel direction

National Radio Science Meeting (Boulder, CO), Jan. 1996

F3-4
0940

A METHOD TO DERIVE SATELLITE DIVERSITY FOR LEO PCS

Riza Akturan and Wolfhard J. Vogel
Electrical Engineering Research Laboratory
The University of Texas at Austin
10100 Burnet Road, Austin, TX 78758-4497
E-mail: (Riza_Akturan, Wolf_Vogel)@mail.utexas.edu

Low-Earth-Orbit (LEO) satellite systems are now being designed to provide global hand-held communications. The performance of these systems is limited (apart from system parameters) by propagation effects such as shadowing from trees or blockage by buildings. A potentially powerful method to overcome some of these effects is satellite diversity, a scheme in which more than one satellite at a time can be available to a particular user. Predicting the effectiveness of diversity is difficult, however, as no multiple satellite systems have been deployed and measurements with multiple airplane-borne transmitters are expensive.

We developed a prediction method for satellite diversity gain based on image processing of fish-eye lens pictures taken in urban Japan. Normally, 3-state fade simulation uses Ricean, Rayleigh and/or lognormal density functions. We obtained a better fit to measured data (Y. Karasawa et al., Proc. PIERS 1994) by using triangular basis functions. To derive satellite diversity gain at different locations, we placed the ground location at a northern, mid, and equatorial latitude and employed a hypothetical 48-satellite constellation. Finally, we calculated satellite diversity gain for both combining and hand-off diversity schemes at the three different latitudes. Most diversity gain is obtained in blocked and heavily shadowed fade regions of the CDFs, and this shows that satellite diversity is especially effective in densely built-up urban environments.

blocked ⇒ building
shadowed ⇒ vegetation

National Radio Science Meeting (Boulder, CO)
Jan. 1996

F3-5
1020

Propagation Model for LEO Satellites

Kent Penwarden
Globalstar
3200 Zanker Road
San Jose, CA 95164-0670
E-mail: penward@gstar1.globalstar.loral.com

A low-earth orbit (LEO) satellite system providing mobile satellite service (MSS) must provide communication connectivity on (1) the service links between mobile earth stations (MES) and satellites and (2) the feeder links between land earth stations (LES) and satellites. An MES and its associated LES must have co-visibility of at least one satellite for a communication link to be established (if satellite-to-satellite cross links are not employed). This study included satellite diversity, where alternate paths are provided should the initially-selected path be blocked.

The purpose of the study was to determine the geographical area served by a LES. This was accomplished by simulating the relationship of the LEO satellite constellation to both the LES and the MES. The propagation environment surrounding a MES was depicted as a skyline profile of elevation versus azimuth angles. For each simulation run, a skyline profile was chosen to be representative of an environmental classification (e.g., urban, suburban, and rural). The set of environments used for this study was chosen from a larger collection of computer image-processed photogrammetric field data.

This simulation has been used to predict a number of different results, such as the circumstances in which the availability of placing and completing a 3-minute call can be 98% or better. By identifying those environments where calling might be more difficult, the simulation aids in the placement of the LES. By recording the identification of the successive satellites through which the MES and LES communicate, satellite hand-off activity is quantified to aid in the design of switching and routing circuits within the LES.

National Radio Science Meeting (Boulder, CO) Jan. 1996

F3-6
1040

ELEVATION ANGLE DEPENDENCE OF FADING FOR SATELLITE PCS IN URBAN, SUBURBAN AND RURAL ENVIRONMENTS

Riza Akturan, Hsin-Piao Lin, and Wolfhard J. Vogel
Electrical Engineering Research Laboratory
The University of Texas at Austin
10100 Burnet Road, Austin, TX 78758-4497
E-mail: (Riza_Akturan, Wolf_Vogel)@mail.utexas.edu,
hplin@spoke.ece.utexas.edu

still photos

Images of urban Japan taken vertically through a 180° fisheye lens were analyzed to obtain, as a function of elevation, the fraction of sky that is clear, shadowed by trees, or blocked by buildings (R. Akturan and W.J. Vogel, *El. Let.*, **31**, 1125-1126, 1995). At 32° elevation, the resulting cumulative fade distribution matches the one derived directly from satellite measurements (Y. Karasawa et al., Proc. PIERS 1994). Using a 3-state fade model, we predict for the first time the elevation angle dependence of mobile satellite fading for elevation angles from 5° to 85°. We also derived similar results in other types of environments. In the talk, we will present our method to derive the elevation dependence of mobile satellite fading and discuss the results.

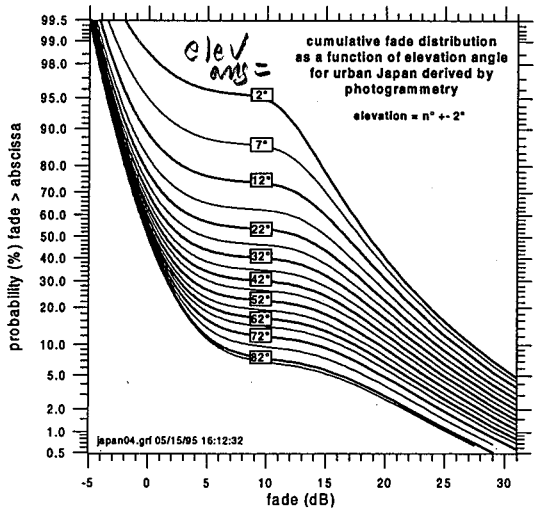

0.2 dB/deg elev between 15 & 25 dB @ 10%

Cumulative fade distributions for urban Japan as a function of elevation angle, derived using photogrammetry combined with 3-state modeling.

National Radio Science Meeting (Boulder, CO)
Jan. 1996

F3-7
1100

Propagation Channel Simulation for LMSS and Satellite PCS

Hsin-Piao Lin, Riza Akturan, and Wolfhard J. Vogel
Electrical Engineering Research Laboratory
The University of Texas at Austin
10100 Burnet Road, Austin, TX 78758-4497
E-mail: hplin@spoke.ece.utexas.edu, (Riza_Akturan, Wolf_Vogel)@mail.utexas.edu

A new propagation simulator for both vehicular and portable satellite communication services is introduced. In this research project, a simulated time-domain received signal for both amplitude and phase is generated based on photographic images taken with a 180° field-of-view fisheye lens camera combined with specified characteristics of the receiving system and location. Therefore, the propagation properties of a typical scenario in satellite communication systems can be predicted without conducting actual field measurements in advance.

A series of state sequences is generated by the photogrammetric method (R. Akturan and W.J. Vogel, *El. Let.*, **31**, 1125-1126, 1995) based on classifying environments into 3 states: clear, shadowed, or blocked. According to these state sequences, a modified Rayleigh fading channel and random number generators for each state's appropriate representative distribution function are used to simulate the received signal in both amplitude and phase. The simulator works up to the system level, includes the Doppler effect and makes the prediction of phase information and bit-error-rates possible. The output from the simulator is a timeseries signal containing both amplitude and phase information. The simulation has been validated using experimental data that were taken in Pasadena, California in different types of environments. A comparison between the simulated signal and measured data in amplitude and phase sequences, first-order statistics (probability density function, cumulative density function), second-order statistics (level crossing rate, fade duration), and bit-error-rate will be presented during the talk.

2055 MHz cw from TDRS 21° elev angle at Pasadena, Cal 1 minute of data
Time series agreed approximately
Statistics agreed well

1 minute of data using fisheye lens, 30 frames per second

To be published in VTC in Atlanta

National Radio Science Meeting (Boulder, CO) Jan. 1996

F3-8
1120

ON THE USE OF DIRECT SEQUENCE SPREAD SPECTRUM MODULATION TO REDUCE MULTIPATH FADING FOR MOBILE COMMUNICATIONS IN URBAN AREAS

Mobile Satellite

Mr. Jeffrey Jenkins
New Mexico State University
Department of Electrical and Computer Engineering
Box 30001 Dept 3-O
Las Cruces, NM 88003-3001

Fading due to shadowing and multipath is an important problem in the design of mobile communication systems. While little can be done to combat shadowing, the use of spread spectrum modulation has been suggested for reducing multipath fades. In theory, it can be shown that the time delays associated with the multipath signals allow the spread spectrum receiver to reject the multipath, improving the performance of the receiver. While this view has been widely held, there has been no side-by-side comparison of the fade performance of spread and unspread modulation systems in a *typical* mobile multipath environment.

This paper describes such an experiment conducted by researchers at New Mexico State University. The null hypothesis states that in typical multipath environments, the time delay associated with the multipath signals is insufficient to gain practical improvements in the fade performance of the system. The alternate hypothesis is that the delays are sufficiently large to see a significant improvement in the performance of the spread system. The experimental approach was to collect sufficient simultaneous samples with both types of systems to determine if the null hypothesis could be rejected.

A dual beacon S-Band transmitter was carried aboard a Cessna 172, consisting of a direct sequence spread spectrum beacon operating at an 8 Mhz chip rate centered at 2120 MHz, and a CW beacon operating at 2112 Mhz. The mobile receiver was driven through the downtown areas of El Paso, Dallas, and San Antonio, Texas. The fade statistics accumulated from the two beacons reveal that the spread modulation system does indeed have a significant improvement in performance over the narrowband system. Fade statistics are presented for these three areas at elevation angles of 15, 30, and 45 degrees. The performance improvement of the spread system increases as the elevation angle between transmitter and receiver is reduced from 45 degrees to 15 degrees. Time domain plots of the received signal strength shows differential fading, where the CW channel experienced severe fades while the spread signal did not.

How about rural data where LMSS systems are used?

National Radio Science Meeting (Boulder, CO)
Jan. 1996

F3-9
1140

PCS MODELING EFFORTS AT ITS

Robert O. DeBolt, Electronics Engineer
Department of Commerce, NTIA/ITS
325 Broadway, ITS.S1
Boulder, CO 80303

The Institute for Telecommunication Sciences, TA Services group, is developing a suite of models in the GIS environment for a wide variety of applications including personal communication systems (PCS). A GIS efficiently captures, stores, updates, manipulates, analyzes and displays all forms of geographically referenced information. The use of GIS has grown substantially over the past several years and it is now common for business, government and academia to employ GIS in many and diverse applications. As a result, databases necessary for telecommunication system analysis are now becoming available in forms easily imported into the GIS environment. These databases include terrain, roads, communications infrastructure, building locations and footprints, land type and use, and many others. These databases can be maintained in commonly used and available relational database management systems (RDBMS) which can be connected to the GIS or they can be placed into the GIS RDBMS. This greatly reduces the amount of database development necessary in PCS model development. Information which is not commonly available but which is needed for high frequency models is building heights and vegetation. Some city and county governments are beginning to enhance their GIS databases to include this data and this trend is expected to continue. Software is available and under development which allows the user to import digital stereo photographs taken from aircraft at relatively low altitudes or even spacecraft. With sufficient photo quality, this data can be used to create three dimensional surfaces for the GIS with accuracies on the order of a meter. This will greatly reduce the cost of developing databases with the accuracies necessary to ensure good analysis results. This presentation will focus on the PCS modeling efforts currently under development at ITS.

F3-10
1200

A SIMPLIFIED MODEL FOR CALCULATING THE DELAY SPREAD OF THE IMPULSE RESPONSE FOR INDOOR WIRELESS COMMUNICATIONS

Christopher L. Holloway
Institute for Telecommunication Sciences
U.S. Department of Commerce
325 Broadway, Boulder, CO 80303

In designing wireless telecommunication systems it is very important to control the intersymbol interference (ISI) or more importantly the bit error rate (BER). The ISI is directly related to the multipath phenomena resulting from objects (i.e., walls and furniture for indoor applications) in the propagation path between the transmitter and receiver. The delay spread of the impulse response of the propagation channel is a measure of the multipath effects. In this paper we introduce a simplified model for calculating both the impulse response and the delay spread for indoor propagation.

For years, the acoustic community has been estimating the decay rates (or reverberation time) of acoustic cavities and rooms (Morse and Bolt, Reviews of Modern Physics, 16(2), pp. 69-150, 1944) by estimating the cavities quality factor (Q). Recently these concepts have been used to analyze electromagnetic anechoic test chambers (DeLyser, Holloway, Johnk, Ondrejka, and Kanda, submitted to IEEE Trans. on EMC, 1995). By extending this work, it is possible to show that the average impulse response (IP) of a room can be expression in terms of the Q-factor and the operating frequency:

$$\mathrm{IP}(t) = \exp^{(-\frac{\omega}{Q}\ t)}$$

where the Q factor is a function of the volume of the room, the surface area of the room, the amount of energy absorbed into the wall, the energy loss through doors and windows, and energy absorbed into objects in the room. This type of representation of the IP leads to a RMS delay spread given by $\mathrm{RMS}_{ds} = \frac{Q}{\omega}$.

Comparisons between a measured impulse response and this model for two different room sizes have been made, and good agreement was demonstrated. If this technique can successfully be used to estimate IP inside rooms, then it is possible to analyze the coupling of energy into adjacent rooms and through entire building with the use of coupled mode and aperture theory. The advantage of the technique discussed here is that it is based upon simple assumptions, such that the IP can be calculated in a matter of seconds on a PC.

G4-1
0900

IONOSPHERIC CORRECTIONS METHODS TEST '95

G. Kronschnabl* J. Cook T. D. Raymund C. Vasicek G. Bust
Applied Research Laboratories
University of Texas at Austin
P.O. Box 8029
Austin, TX 78713-8029

The Ionospheric Corrections Methods Test '95 was conducted from mid-January 1995 through mid-February 1995. The Applied Research Laboratories, The University of Texas at Austin (ARL:UT), deployed a dual-chain network of eight Transit satellite receivers in approximately two parallel lines in the western half of the U.S. The two chains were roughly centered at longitudes of 105W and 118W and spanned over 1000 km. The eastern chain consisted of stations located at Las Cruces, NM (32.1N, 106.8W), Raton, NM (36.56N, 104.5W), Cheyenne, WY (41.0N, 104.8W), and Miles City, MT 46.2N, 105.9W). The western chain consisted of stations located at San Diego, CA (32.4N, 116.9W), China Lake, CA (35.3N, 117.3W), Winnemucca, NV (40.7N, 117.8W) and Pendleton, OR (45.5N, 118.8W). In addition, three ARL:UT developed GPS-TEC systems were deployed at Grand Junction, CO, Monterey, CA, and Pendleton, OR.

Initial CIT analysis of the Transit TEC data has produced over 60 reconstructions. As a point of comparison, synthetic ionograms were computed from the reconstructions and compared to ionograms obtained from ionosondes located at Boulder, CO, China Lake, CA, and San Diego, CA. This paper presents CIT reconstructions representative of a variety of ionospheric conditions.

In addition, we present and discuss the new concept of fusing CIT reconstructions and GPS-TEC measurements into a three-dimensional (3D) volume of electron density. The strengths and weaknesses of such a "full-spectrum" 3D ionospheric volume are discussed, including potential applications which could exploit the 3D volume. Finally, potential methods about including time-varying effects in the 3D volume are presented.

G4-2
0920

INITIAL RESULTS FROM A DUAL CHAIN COMPUTERIZED IONOSPHERIC TOMOGRAPHY CAMPAIGN: THE IONOSPHERIC CORRECTIONS METHODS TEST '95

T. D. Raymund* G. Bust J. Cook G. Kronschnabl C. Vasicek
Applied Research Laboratories
University of Texas at Austin
P.O. Box 8029
Austin, TX 78713-8029

An ionospheric tomography campaign was recently carried out by the Applied Research Laboratories, University of Texas at Austin (ARL:UT). The campaign, called the Ionospheric Corrections Methods Test '95, deployed in the western United States with a unique configuration: two chains of tomography receivers were placed in parallel such that both chains could observe the same Transit satellite simultaneously. The eastern chain consisted of stations located at Las Cruces, NM (32.1N, 106.8W), Raton, NM (36.56N, 104.5W), Cheyenne, WY (41.0N, 104.8W), and Miles City, MT (46.2N, 105.9W). The western chain consisted of stations located at San Diego, CA (32.4N, 116.9W), China Lake, CA (35.3N, 117.3W), Winnemucca, NV (40.7N, 117.8W) and Pendleton, OR (45.5N, 118.8W). The chains operated from year day 24 through year day 46 of 1995 (24 January through 15 February). The configuration of the experiment yielded a unique data set which allows new insights into the evolution of variations in the ionosphere over longitude.

Several different tomographic methods were applied to the data; the discussion includes comparisons of the techniques. Various features, longitudinal variations and particular artifacts present in the reconstructions will be compared and contrasted. In addition, the ease-of-use, cost and consistency of performance are evaluated. Several ionosondes provided simultaneous independent information about the ionosphere which is used for comparison. (Ionosondes were located at China Lake, CA, San Diego, CA, and Boulder, CO.)

In addition to algorithm comparisons, several particularly interesting high Kp cases are also discussed. For example, the Kp for day 29, hours 2100-2400 UT was 6+. The discussion focuses on special features and their evolution.

In addition to the tomography receivers, ARL:UT GPS/TEC receivers were also located in the region (Pendleton, OR, Grand Junction, CO, and Monterey, CA). These receivers collected high quality GPS TEC data using Ashtec Z12 receivers. Relevant initial results will be included.

G4-3
0940

A METHOD OF INCLUDING GPS-TEC MEASUREMENTS INTO THE GENERATION OF COMPUTER IONOSPHERIC TOMOGRAPHY DERIVED THREE-DIMENSIONAL IONOSPHERIC VOLUMES OF ELECTRON DENSITY

C. Vasicek* C. Coker T. L. Gaussiran II G. Kronschnabl
T. D. Raymund
Applied Research Laboritories
The University of Texas at Austin
P.O. Box 8029
Austin, TX 78713

The Ionospheric Corrections Method's Test '95, an ionospheric tomography campaign, was conducted from mid-January 1995 through mid-February 1995 by the Applied Research Laboratories, University of Texas at Austin (ARL:UT). The campaign consisted of eight Transit satellite receivers deployed in parallel chains in the western half of the United States. The two chains were roughly centered at longitudes of 105W and 118W and spanned over 1000 km. The eastern chain consisted or stations located at Las Cruces, NM (32.1N, 106.8W), Raton, NM (36.6N, 104.5W), Cheyenne, WY (41.0N, 104.8W), and Miles City, MT (46.2N, 105.9W). The western chain consisted of stations located at San Diego, CA (32.4N, 116.9W), China Lake, CA (35.3N, 117.3W), Winnemucca, NV (40.7N, 117.8W), and Pendleton, OR (45.5N, 118.8W). Additionally, three ARL:UT developed GPS-TEC systems were deployed at Pendleton, OR, Monterey, CA, and Grand Junction, CO.

The unique design of this experiment has enabled Computerized Ionospheric Tomography (CIT) reconstructions to be generated along both lines of receivers using TEC data from the same Transit satellite. This paper presents a method and examples of including GPS-TEC measurements into a process that generates a three-dimensional (3D) volume of electron density between the parallel two-dimensional (2D) CIT reconstructions. Finally, an example of using this same method to include the time-varying effects between reconstructions is presented.

G/H1-1 0900 **COMPOSITION OF TIDAL ION LAYERS IN THE E REGION**

K. L. Miller and M. Lemon
Center for Atmospheric and Space Sciences
Utah State University
Logan, Utah 84322-4405

Incoherent scatter radar observations of descending tidal ion layers in the upper E region were made using the 430-MHz radar at the Arecibo Observatory. A tidal ion layer was observed on the night of April 30, 1994, which descended from the base of the F region to an altitude of about 130 km between 20:59 and 21:49 AST. The column electron density of the layer was determined for this study by integrating the density between the minimum background density above and below the layer. The height-integrated loss rate was derived from the change in column density during the time between successive profiles. The time development of the layer was simulated assuming continuity arguments and the presence of two molecular species, NO^+ and O_2^+, in a layer of the same density as the measured layer. Appropriate reaction rates and the initial measured electron density were used to model the change in the electron density at each height. Column densities and loss rates were calculated for the simulated two-species layer in the same manner as for the measured data. The measured and modeled column-integrated loss rates are used to test two hypotheses about the composition of the layer. First, the assumption is made that the longevity of the layer is due to a high percentage of metallic ions in the layer. The mixing ratio of metallic ions is derived from the ratio of the measured and the simulated loss rates. The derived mixing ratio in the simulation decreases with time and is inconsistent with the slow recombination of metallic ions and the fast recombination of molecular ions. Second, the assumption is made that transport of surrounding ionization into the layer is the main ionization source. Vertical ion convergence required to maintain the layer is presumably caused by a vertical shear in the horizontal neutral wind. A comparison of height-integrated loss rates derived from the measured layer and the simulated layer shows that the layer can be supported by the transport of ionization. The comparison shows that the vertical velocities that are associated with the ion flux required to maintain the observed layer are within acceptable values.

G/H1-2
0920

NEUTRAL WIND AND TIDAL ION LAYER OBSERVATION AT E-REGION HEIGHTS ABOVE ARECIBO

Qihou Zhou*
Arecibo Observatory
National Astronomy and Ionosphere Center
Cornell University
Arecibo, PR 00613

We report neutral wind and tidal ion layer observational results at E-region heights obtained from the Arecibo incoherent scatter radar during January 20-30, 1993. Both of the zonal and meridional winds were small in comparison with previous observations for winter condition at Arecibo. Nevertheless, spectral analysis shows the superposition of at least two wind systems at any given altitude from 90 km to 130 km. Of particular interest is a strong planetary wave with a period of two days below 110 km. The amplitude of the 2-day wave, 40 m/s at 102 km, was comparable with that of the diurnal tide, which is normally the dominant tide below 110 km. The vertical wavelengths of the diurnal tide and the 2-day wave are estimated to be 25 km and 60 km respectively. Between 110 and 130 km, the most consistent tidal oscillation was semi-diurnal although the diurnal component was as strong as the semi-diurnal one at some heights. The vertical wavelength of the semi-diurnal tide was about 35 km.

The ion layers observed during this period, in general, appeared to be consistent with the neutral winds observation. Corresponding to the above mentioned two-day wave system, an ion layer was observed to appear every other day below 95 km. We believe that this is the first time that an once-every-other-day ion layer has been unequivocally identified at Arecibo or anywhere else. The regularly observed diurnal layer below 100 km also appeared to be modulated by the two-day wave. Between 100 and 115 km, three layers were often observed to be confined in a very narrow altitude range, reflecting the complicated interaction of the semi-diurnal, diurnal tides and the two-day wave. Although intermediate layers were often present above 115 km, they were usually very weak and showed great variability.

G/H1-3 0940 OBSERVATIONS OF THIN E-REGION STRUCTURES AT SONDRESTROM, GREENLAND

Brenton J. Watkins and David F. Bedey
Geophysical Institute, University of Alaska
Fairbanks, AK 99775

We report progress of an observational program at Sondrestrom, Greenland that uses incoherent-scatter radar to study the occurrence and morphology of thin sporadic-E layers. The radar has been operated in an elevation-scanning mode to map the north-south extent and altitudes of these layers that are typically about 1-2km thick and occur at altitudes from about 100 to 140km.The radar has been operated with a pulse scheme that interleaves a coarse resolution long pulse, with a high-resolution (300 or 600m) Barker-coded multi-pulse.

Two-dimensional north-south maps of high-resolution electron density fields are used to define the thin-layer structures, and the corresponding long-pulse data derived from the F-region is used to derive the electric field structure as a function of latitude. Attempts to use the high-resolution spectral data for velocity and ion mass determinations is also underway and some preliminary results will be presented.

At high latitudes the strong electric fields that are typicaly present play the major role in formation of these thin structures that are probably composed primarily of metallic ions. This is the motivation for constructing an experimental mode that can derive the vector electric fields as well as density data.

A number of examples will be shown to illustrate the wide variety structure types, and the dynamic nature of their formation and dissappearance.

G/H1-4
1000

OBSERVATIONS OF LAYERING IN THE POLAR LOWER IONOSPHERE

J. D. Mitchell, C. L. Croskey and D. J. Walter
Communications and Space Sciences Laboratory
Department of Electrical Engineering
The Pennsylvania State University
University Park, PA 16802

Rocket-launched probes from the Andøya Range, Norway (MAC/EPSILON Campaign), and Esrange, Sweden (NLC-86 and NLC-91 Campaigns), have provided evidence for small-/large-scale structure in electron and ion parameters, along with in situ measurements of electric field. Nose tip probe measurements of electron current and associated number density fluctuations demonstrate layering in identified PMSE (polar mesosphere summer echo) and NLC (noctilucent cloud) regions between 80 and 90 km. An NLC-associated decrease in electron density determined for NLC-91 appears to be about 25%, with a more dramatic depletion (about an order of magnitude) observed during NLC-86. Electron density structure also was detected in the nose tip probe current data for PMSE regions, consistent with the on-site CUPRI 50-MHz radar. An examination of the Gerdien condenser positive ion measurements during NLC-91 suggests the existence of very small mobility values ($k_{o+} \sim 0.1$ cm^2/V-s) for the 80-90 km region, which are thought to indicate the presence of charged aerosols. While the altitude resolution for our ion measurements is relatively limited, the only height where the concentration of low-mobility charge species exceeds the number density of more mobile (molecular) positive ions is in the region of PMSE identified by CUPRI. The low-mobility ion presence for 80-90 km was also observed to cause a drop in positive ion conductivity, an effect previously noted for the MAC/EPSILON Campaign.

Observation of an AC vertical field associated with an NLC layer has previously been reported by Penn State (C. L. Croskey et al., Asilomar Chapman Conference, 1992) and others (R. Pfaff, 10th ESA Symposium, 1991; A. M. Zadorozhny et al., Geophys. Res. Lett., 20, 2299-2302, 1993). Zadorozhny et al. suggest local generation of the AC fields is due to impact ionization as the payload electrodes collide with the (massive) NLC particles. From a re-examination of our NLC-86 measurements, we find evidence for two generation mechanisms. At some AC frequencies the electric fields are present both above and below the layer and become larger within the layer. These fields are probably the result of global Schumann resonances, the amplitudes becoming larger due to the lower electrical conductivity within the NLC layer. At other AC frequencies electric fields are not evident above or below the NLC layer but become relatively large within the layer. The narrow-band nature of these local (impact) generated fields implies a fairly ordered structuring in the underlying matrix of the NLC particles.

G/H1-5
1040

SHEARS IN THE LINE-OF-SIGHT DOPPLER VELOCITY OF QUASI-PERIODIC RADAR ECHOES OBTAINED WITH THE MU RADAR

R. T. Tsunoda,[1] W. O. J. Brown,[2] S. Fukao,[3] M. Yamamoto[3]
[1] Geoscience and Engineering Center, SRI International
Menlo Park, California 94025
[2] Dept. Atmospheric and Oceanic Sciences
McGill University
Montreal, Quebec, Canada H3A 2K6
[3] Radio Atmospheric Science Center, Kyoto University
Uji, Gokanosho, Kyoto 611, Japan

Radar backscatter measurements from nighttime sporadic E layers in the midlatitude ionosphere have revealed that both the echo power and the mean Doppler velocity can have quasi-periodic patterns as functions of space and time. The measurements are puzzling not because their wavelike characteristics resemble those of atmospheric gravity waves but because the values of the Doppler velocity indicate the occasional presence of varying electric fields that can be anomalously large. Line-of-sight mean Dopple velocities in excess of 300 m/s have been reported to be associated with these magnetic-aspect-sensitive echoes, a velocity that is several times larger than the bulk ionospheric motion expected at midlatitudes. In an attempt to explain this behavior, Tunoda et al. [1994] (R. T. Tsunoda, S. Fukao, and M. Yamamoto, "On the origin of quasi-periodic radar backscatter from midlatitude sporadic E," Radio Sci., 29, 349, 1994) suggested that a polarization process may be operating under those conditions. To better understand the physical processes underlying the formation of quasi-periodic echoes, we used the MU radar in Japan to obtain high-resolution backscatter measurements of these quasi-periodic echoes. The radar was operated with a range resolution tha ranged from 150 to 600 m and with spaced-antenna reception to obtain information about the distribution of backscatter power and the nature of the Doppler spectra as functions of space and time. We show, in this paper, that there exist variations (that s, shears) in the mean Doppler velocity (along the radar line of sight) that have spatial scales that vary from a few tens of kilometers down to the resolution limit set by the operating parameters. We show that these results are indicative of complex dynamo processes that probably include the altitude-varying tidal wind field, the altitude modulation pattern imposed on the sporadic E layer, and possibly, the dynamo contributions from the electrically coupled F region.

G/H1-6
1100

SIMULTANEOUS OBSERVATIONS OF SPORADIC-E LAYERS BY COHERENT AND INCOHERENT SCATTER RADARS

José M. Rosado-Román* Clark A. Miller Wesley E. Swartz Donald T. Farley
School of Electrical Engineering, Cornell University Ithaca, NY 14853.

Our data were taken by the 430 MHz incoherent scatter radar at the Arecibo Observatory (AO-ISR) and by the Cornell University Portable Radar Interferometer (CUPRI) operating at 46.9 MHz during the 1992 NASA-CRRES El Coqui campaign. The CUPRI was located at Sprat Hall, St. Croix, US Virgin Islands, ($17.74°N$,$-64.89°E$) and looked northwest at low elevations in order to direct the beam perpendicular to the magnetic field in the E-region above and slightly to the north of the AO-ISR ($18.35°N$, $-66.75°E$). This allowed CUPRI to function as a coherent scatter radar (CSR). Interferometry was possible in both vertical and horizontal baselines. The CUPRI operated on St. Croix from May 30 to July 12, 1992. Coincident data between the CUPRI and the AO-ISR is available for several hours during several different days in the month of June.

Data from the AO-ISR for the night of June 19, 1992, reveal a strong plasma density enhancement with some minor altitude perturbations just after 1948 LT. Coincident data from the CUPRI reveal an extended range over which echoes are received. The echoing region over the AO-ISR is approximately 250 kilometers range from the CUPRI site. The strongest CUPRI echoes received from over the AO-ISR coincide with the appearance of the strong plasma density enhancement. The relatively weak SNR, the near zero mean radial velocity, and relatively broad spectral widths are suggestive of a gradient drift type instability.

Interferometric study of the CUPRI data reveals high coherence confirming that the echoes come from relatively narrow height bands while the altitude of the scatters appears to be nearly independent of range. The echoes come from regions where the beam is perpendicular to the magnetic field. Spatially small changes in layer shape and density observed by the AO-ISR, suggest a trigger mechanism for the onset of the CUPRI echoes. In a previous experiment at St. Croix, in 1982, (Riggin et al., J. Geophys. Res., 91,8011,1986). observed velocities close to the acoustic limit. During El Coqui such saturated velocities were not seen. Spectra are similar to type II spectra from the equatorial electrojet which correspond to instabilities generated by the gradient drift mechanism.

Aspect widths were found to be as small as $0.2°$ in the vertical during the more intense events, values which are similar to those reported at the Chung Li radar (Huang et al., submitted to J. Geophys. Res., 1994.). The horizontal aspect widths on the other hand are generally $1.0°$ broad but can be as small as $0.5°$. The narrowness of the aspect widths clearly demonstrates that the events are highly localized within the beam of the radar.

G/H1-7
1120

HIGH-RESOLUTION STUDIES OF ATMOSPHERE-IONOSPHERE COUPLING AT ARECIBO, PUERTO RICO

F. T. Djuth[1], M. P. Sulzer[2], V. B. Wickwar[3], B. Isham[2], C. O. Hines[1], and J. H. Elder[1]
[1]Geospace Research, Inc., 550 N. Continental Blvd., Suite 110, El Segundo, CA 90245
[2]Arecibo Observatory, Arecibo, Puerto Rico 00613
[3]Utah State University, Center for Atmospheric and Space Sciences, Logan, UT 84322

A variety of aeronomic problems involving the coupling of the neutral atmosphere to the ionosphere can be addressed by applying the so-called coded long-pulse (CLP) radar technique [Sulzer, *Radio Sci., 21,* 1033, 1986] to plasma line echoes created by daytime photoelectrons [Djuth *et al., Geophys. Res. Lett., 21,* 2725, 1994]. At Arecibo Observatory, extremely accurate measurements of absolute electron density (0.01 to 0.03 % error bars) are readily achieved with an altitude resolution of 150 m and a temporal resolution of ~2 s. In addition, the CLP technique provides information about electron density structure within a 150-m altitude cell and yields parameters from which the energy spectrum of photoelectrons ($\geq$ 5 eV) can be deduced and electron-neutral collision rates can be determined.

In the lower thermosphere above Arecibo, background gravity waves couple to the ionospheric plasma, typically yielding 1-3% electron density "imprints" of the neutral waves. These imprints are present in all observations; they are routinely detected 30-50 standard deviations above the noise. Complementary analysis and modeling efforts indicate that important information about gravity waves in the lower thermosphere can be derived from the measurements (e.g., altitude profiles of vertical wavelength, horizontal velocity, and perhaps vertical energy flux). The neutral wave structures are also evident when the frequency difference between the downshifted plasma line peak and the upshifted peak is viewed as a function of altitude (i.e. versus range cell). This may be indicative of ion heating by the neutral wave. Finally, recent observations made with improved altitude coverage clearly reveal the propagation of neutral waves from the lower thermosphere (~110 km altitude) to very high altitudes (~500 km). The electron density imprints become very small at the highest altitudes, presumably because the associated neutral waves are dissipated by viscous effects (molecular/hydromagnetic viscosity).

When the absolute plasma line amplitude (κTp) is plotted versus electron phase energy [e.g., Carlson *et al., Geophys. Res. Lett., 12,* 565, 1977], sharp amplitude reductions at well-defined phase energies are often observed. These dips are believed to be caused by inelastic scattering of electrons by the neutral gas. Many of the features in the phase energy spectrum are currently being examined as part of a comprehensive study of electron thermal balance in the *F* region. Revisions in scattering cross sections may be required to explain several of the observations.

G/H1-8
1140

APPARENT ELECTRODYNAMIC COUPLING OF ION LAYERS IN THE 90-270 KM ALTITUDE REGION ABOVE ARECIBO.

J. D. Mathews*
Communications and Space Sciences Laboratory
The Pennslyvania State University
316 Electrical Engineering East
University Park, PA 16802

High-resolution (150 m and 10 s in range and time, respectively) 430 MHz Incoherent Scatter Radar (ISR) evening and night-time observations of the 90-270 km altitude region of the Arecibo ionosphere have revealed the presence of apparent electrodynamic co upling between the base of the F layer and the underlying intermediate Tidal Ion Layer (TIL) as well as between the intermediate TIL and underlying TIL and sporadic E layers. Specifically, a quasi-periodic "rain" of ionization lasting over many hours has been observed extending from the F region to the underlying intermediate TIL. The apparent period of this ion "rain" is near 10 minutes with–assuming 50 m/s mean winds– a corresponding 30 km horizontal periodicity. Additionally, onset of large oscilla tions in the intermediate TIL correspond in phase to the ion "rain" and also appear to be tied to the onset of sporadic E or Complex Layer Structure (CLS) events in the 90-105 km region. Possible mechanisms for the proposed electrodynamic coupling are di scussed. These mechanisms include "local" electric fields generated by gradient-drift instabilities in the intermediate TIL and/or Perkins-like instabilities in the F region. An additional mechanism is proposed whereby these electric fields in combinati on with existing tidal wind fields "trigger" at least one manifestation of sporadic E. It is also argued that these structures are related to the quasi-periodic structures observed by VHF radar at MU (e.g., Tsunoda et al., *Radio Science*, **29**, 349-365, 1994) and at Arecibo (e.g., Riggin et al., *J. Geophys. Res.*, **91**, 8011-8024, 1986).

Session G/H-2, 1015-Thurs., CR2-26
IONOSPHERIC MODIFICATION WITH HIGH POWER RADIO WAVES
Chairperson and Organizer: P.A. Bernhardt, Plasma Physics Division, Naval Research Laboratory, Washington, DC 20375

G/H2-1
1020

PROPAGATION OF INTENSE ELECTROMAGNETIC WAVES IN SELF-INDUCED TURBULENCE

D.F. DuBois*
Los Alamos National Laboratory
Los Alamos, NM 87545
H.A. Rose
Lodestar Research Corp.
Boulder, CO 80301
A. Hanssen
University of Tromso, Tromso, Norway

In HF modification of the ionosphere and in laser plasma interactions a pump wave reflected from the critical surface can form a standing wave pattern. Near critical density the ion acoustic decay instability and the related purely growing instability will be most strongly excited near the peaks of the standing wave. Locally a saturated state of Langmuir turbulence is excited whose correlation lengths and times are small compared to the macroscopic scales of the standing wave pattern. This separation of scales permits a mesoscale approach wherein the ponderomotive pressure of the induced turbulence, which is usually much greater than that of the pump alone, is locally computed using homogeneous plasma simulations. This allows us to compute the time evolution of the self consistent pump, turbulence, and density profiles as a function of position in an initially inhomogeneous plasma profile. Here we present preliminary 1D results which can be compared to time and altitude resolved observation of induced ionospheric turbulence. Dramatic dynamical effects are observed even for moderate incident pump powers. The standing wave pattern drops to lower altitude in a quasi periodic fashion because the half wave length induced density depletion grating inhibits the propagation of the pump until these depletions relax. Generally the initial standing wave profile is disrupted on the time scale of and ion acoustic transit time across a pump maximum.

G/H2-2
1040

A MACRO-KINETIC THEORY OF NONLINEAR PLASMA PHYSICS*

J. Huang and S. P. Kuo
Weber Research Institute
Polytechnic University
Farmingdale, NY 11735

Nonlinear plasma physics is on the cutting edge of the plasma physics research. Important nonlinear plasma phenomena include nonlinear wave-wave interaction (e.g., parametric instabilities and nonlinear scattering), nonlinear wave-particle interaction (e.g., nonlinear Landau damping and plasma maser instability), self-focusing and formation of solitons and cavitons. Study of nonlinear plasma physics can be done using either fluid equations or kinetic (Vlasov) equations. The former reveals a clear physical picture of the nonlinear coupling mechanism (e.g., beating current, ponderomotive force, and thermal pressure force), while the latter retains detailed kinetic information at the expense of extensive analytical or numerical work.

The usual way to take the advantage of both approaches, in the analysis of parametric instabilities for example, is to first obtain the set of coupled mode equations and nonlinear dispersion relations from the fluid approach and then substitute the fluid susceptibilities for the kinetic ones. This substitution does not have a fundamental theoretical basis, and the range of the validity of this method is not clear. On the other hand, one can also insert the ponderomotive potential in the Vlasov equation to obtain a similar dispersion relation in certain simple cases. This insertion is based on the physical insight in the nonlinear potential, and is hence phenomenological.

In the present work, a novel way of analyzing kinetic (Vlasov) equations for the study of nonlinear plasma phenomena, including parametric instabilities, nonlinear Landau damping, and strong Langmuir turbulence, is presented. The approach uses moment expansion for the perturbed distribution function in the nonlinear coupling terms. Since the proposed theory incorporates fluid variables into the kinetic framework, it is termed macro-kinetic theory (MKT). This macro-kinetic formulation is in principle exact if all the moments in the expansion are taken into account. The formalism provides a theoretical basis for previous phenomenological results. Moreover, direct numerical simulation of the macro-kinetic equation can be very useful for the study of strong Langmuir turbulence.

* Work supported by NSF.

G/H2-3
1100

SIMULATIONS OF CONVECTIVE LANGMUIR GROWTH AND SATURATION DURING HF MODIFICATION OF AN ARTIFICIAL Ba^+ IONOSPHERE‡

D. L. Newman* M. V. Goldman
APAS Department
Campus Box 391
University of Colorado
Boulder, CO 80309,
B. B. Afeyan
Lawrence Livermore National Laboratory, L-418
Livermore, CA 94551,
E. Fedutenko
4 Svobody Sq.
Kharkov State University 310077
Ukraine

The CRRES AA 2 Barium release experiment over Arecibo (F. T. Djuth et al., *J. Geophys. Res.*, **100**, 17,347, 1995) produced an "artificial Ba^+ ionosphere" with a short ($\sim$ 5 km) density scale length. One consequence of this short scale length is that the density inhomogeneity cannot be neglected when considering linear parametric instabilities driven by an HF heater. This is in contrast to the case for HF modification of the F-region in the natural ionosphere, where a weaker density gradient justifies a locally homogeneous evaluation of parametric growth rates.

The observations reported by Djuth et al. (1995) are of particular interest because of unusual asymmetries observed at early times in the relative intensities of up- and downgoing heater-induced Langmuir waves, as probed by incoherent scatter radar (ISR) reflected off the Langmuir turbulence. A previous analysis based on ray optics and linear convective growth theory (M. V. Goldman, et al., *J. Atmos. Terr. Phys.*, submitted, 1994) was able to account for key features of the ISR spectrum, including the observed asymmetries.

We present here the results of numerical simulations of wavepacket evolution in an inhomogeneous heated plasma (both with and without an external magnetic field) using a wave-optics formulation based on a linearization of the Zakharov equations for coupled Langmuir and ion-acoustic waves. A Galerkin approximation is employed, in which the wavevector component perpendicular to the density gradient is held fixed. Including the influence of the geomagnetic field in the Langmuir dispersion relation is significant because, for certain geometries, it permits multiple classical (WKB) turning points in the Langmuir-wave trajectory.

‡Supported by NSF and DOE (LLNL contract W-7405-ENG-48)

G/H2-4
1120

PLASMA WAVES OBSERVED IN THE IONOSPHERIC FOCUSED HEATING EXPERIMENT**

P. Rodriguez* C. L. Siefring P. A. Bernhardt M. M. Baumback
Plasma Physics Division, Code 6755
Naval Research Laboratory
Washington, DC 20375

In the Ionospheric Focused Heating (IFH) experiment, the ionosphere was modified by the release of an electron-attachment chemical from a sounding rocket to create a large scale depletion, while being continously illuminated by the Arecibo heating radar at 5.1 MHz. Onboard the sounding rocket a wave diagnostics payload measured plasma waves inside and outside the ionospheric depletion. On the upleg trajectory electron density structuring and associated low-frequency electric field fluctuations were observed. It appears that the structuring is associated with the standing wave pattern caused by reflection of the 5.1 MHz pump from the critical density region above. Such structuring has been observed with ground-based measurements. The IFH in situ measurements indicate that the structuring occurs over a wide altitude range. Coincident with these low frequency measurements, the upgoing pump wave is observed to be frequency-shifted to lower frequency by about 30 Hz while the reflected downgoing pump wave is shifted to higher frequency by the same amount. Such frequency shifts are caused by the Doppler effect and the change in the k-vector of the pump wave. These observations provide detailed diagnostics of the pump wave interactions with the ionosphere before the chemical release.

**Work supported by ONR and NASA.

G/H2-5
1140

RESULTS FROM 1995 HEATING EXPERIMENTS AT EISCAT

B. Isham*
Arecibo Observatory
Arecibo, PR 00613
C. La Hoz
The Auoral Observatory
University of Tromsoe
N-9037 Tromsoe, Norway

The incoherent scatter chirp technique was simultaneously operated on the EISCAT UHF (931-MHz) and VHF (224-MHz) radar systems for the first time in April 1995 and was successfully used to observe simultaneous daytime HF-enhanced plasma lines on both radars in addition to the natural plasma line on the UHF radar. Additional dual-radar observations are planned for November 1995. The radar programs contains several data channels in addition to the chirp, including multipulse spectra with 1-kHz frequency and 300-m range resolution, standard and 300-m resolution power profiles, and long pulse ion line acf measurements, as well as UHF remote site measurements. The remote site measurements are of particular interest as they provide addition k vectors for the observations, putting additional strong constraints on the nature of the observed phenomena.

This type of data is important for answering questions concerning the nature of both the usual and the "outshifted" HF-enhanced plasma lines. The outshifted line is sometimes seen during UHF observations, appearing downshifted (upshifted) from the heating frequency in the downshifted (upshifted) plasma line spectrum with a shift of 100 to 300 kHz. Comparison of UHF data with simultaneously collected VHF data takes advantage of the k-vector difference between the two radars, which can translate into a difference in the frequency offset of the outshifted line as seen by the two radars. The difference between the frequencies of the photoelectron- enhanced plasma line (PEPL) and the HF-enhanced plasma line (HFPL) observed in past EISCAT and Arecibo heating experiments exhibits this same k-vector dependence. At EISCAT the frequency difference also varies with ionospheric conditions, and the new possibility of simultaneous observations of the PEPL and HFPL with both the EISCAT VHF and UHF radars promises to put strong constraints on possible explanations of this behavior. The latest results will be presented.

J/F1-1
0840

TIMESCALES AND CALIBRATION REQUIREMENTS FOR PHASE CORRECTION USING WATER VAPOR RADIOMETRY

O. P. Lay*
Division of Physics, Math. and Astronomy
California Institute of Technology 105-24
Pasadena, CA 91125
D. P. Woody
Owens Valley Radio Observatory
P.O. Box 968
Big Pine, CA 93513

The correction of phase fluctuations due to tropospheric water vapor is an important goal for both existing and future millimeter and submillimeter arrays. Many groups are developing correction methods based on water vapor radiometry, where the emission from water vapor in the antenna beams is measured and used to estimate the required phase correction.

Our work shows how the standard theory of atmospheric fluctuations can be used to predict the temporal phase power spectrum measured by an interferometer, accounting for the orientation of the baseline with respect to the wind direction and the thickness of the turbulent layer. This theory is compared to observations made at Owens Valley Radio Observatory.

The effects of these fluctuations are determined for the traditional scheme of phase calibration (no radiometry), where observations of the target source are interleaved with a calibrator source that is used to remove instrumental drifts. It is shown that, in addition to the rapid fluctuations that cause decorrelation during integrations, there is substantial phase power in slow fluctuations (period exceeding 10 minutes) that eludes the calibration correction.

The impact of radiometry on reducing the fluctuations is assessed. There are two levels on which radiometry corrections can be applied. The first corrects only the fluctuations within each on-source period. The demands on the precision of the radiometers are modest ($\sim 1\%$), but this method leaves a significant fraction of the phase power uncorrected. The ideal approach requires that the phase corrections for the target source are referenced correctly to those on the calibrator. For existing arrays, it is shown that this requires the sensitivity of the radiometers to water vapor to be the same to within $\sim 0.1\%$. Two possible methods of calibration to achieve this are outlined.

J/F1-2
0900

WVR-BASED TROPOSPHERE DELAY CALIBRATION OF VLBI OBSERVATIONS ON A 20 KM BASELINE

L.P. Teitelbaum* S.J. Keihm M.J. Mahoney R.P. Linfield
G.M. Resch
Jet Propulsion Laboratory
California Institute of Technology
4800 Oak Grove Drive
Pasadena, CA 91109-8099

Dual frequency (S/X band) Very Long Baseline Interferometry (VLBI) observations over a 20 km baseline at Goldstone, CA were conducted in order to demonstrate the troposphere delay calibration capability of current generation Water Vapor Radiometers (WVRs). Analysis of data taken in June and September 1994, employing a new 34 m beam waveguide antenna at one end of the baseline, is complete.

Data were taken both for single long scans ($\sim$ 2000 s) of transiting sources at nearly fixed elevation angles and for multiple short scans ($\sim$ 150 s) of sources distributed over the sky over $\sim$ 15 hr time scales. For scans when WVRs were copointed with the VLBI antennas to better than 1° at both ends of the baseline, and for appropriate detrending of the data, extremely strong correlations were exhibited between the VLBI post-fit residual delay and WVR station-differenced wet path delay, over all time scales. The deviations between the wet tropospheric delays inferred from the VLBI and WVR data can be accounted for quantitatively, indicating that the error budget for WVR calibration of a short baseline VLBI experiment is understood. Applying the WVR delays as a calibration to the VLBI delay model, before the parameter estimation step in the processing, resulted in a nearly factor of three reduction in the post-fit, root mean square delay residual. This is believed to be the most dramatic example of successful troposphere calibration reported to date.

JPL is developing an advanced WVR to serve as the critical element in a troposphere calibration system required to support the Cassini Gravitational Wave Experiment. A brief summary of the status of the advanced WVR project will also be presented.

J/F1-3
0920

WVR RETRIEVAL ERROR FOR DELAY RATE MEASUREMENTS

R. P. Linfield*
Jet Propulsion Laboratory
California Institute of Technology
Pasadena, CA 91109

The use of Water Vapor Radiometers (WVRs) for calibrating line-of-sight tropospheric wet delays at microwave frequencies has been extensively studied. A much less well-studied problem is the use of WVRs for calibrating changes in the line-of-sight wet delay over short time scales (*e.g.* delay rates). A calculation has been made of the expected WVR retrieval error for delay changes on time scales of 100–10000 s. The term 'retrieval error' is defined narrowly here, and refers to the uncertainties in converting changes in WVR brightness temperature to changes in line-of-sight delay, due to uncertainty in the line-of-sight temperature profile and the shape of the line-of-sight water vapor density profile. Accurate calibration of line-of-sight tropospheric delay changes will be needed for science experiments that utilize the radio link between the earth and spacecraft. Examples of such experiments include measurements of the gravity fields of planets and their satellites, and the search for low frequency gravitational radiation during the cruise phase of a planetary mission.

The model used for these calculations assumed that the spatial spectrum of water vapor fluctuations was Kolmogorov in nature, with convection of these spatial fluctuations past the observer. In addition, constant and time-variable uncertainties in the vertical temperature profile were included.

The calculated retrieval error (expressed as an Allan Standard Deviation) due to water vapor fluctuations was 3%–4% of the total delay fluctuation level at 100 s, and 1%–3% at 10000 s. The retrieval error due to plausible levels of constant (*i.e.* time-independent) temperature profiling errors was quite small. However, if the temperature profiling error has nonlinear time variations ≥ 0.1 K/km on time scales of a few hundred seconds, WVR calibration capability would be limited to $\geq 10\%$ of the total delay fluctuation level.

The time-dependent accuracy of temperature profilers (*e.g.* passive Microwave Temperature Profilers and active Radio Acoustic Sounding Systems) needs to be better quantified.

J/F1-4
0940

TROPOSPHERIC PHASE STRUCTURE FUNCTIONS FROM SPACECRAFT DOPPLER TRACKING

Jessica Sidman
Scripps College
Claremont, CA 91711
J. W. Armstrong*
JPL
Pasadena, CA 91109

We have measured temporal radiowave phase structure functions for time lags 10-100 seconds using Doppler tracking data of the Mars Observer spacecraft. These X-band observations were made for 19 days in March-April 1993 using 34-m antennas at the three NASA/JPL Deep Space Network tracking complexes (California, Spain, Australia). Elevation angles ranged from 17 to 74 degrees; hydrogen maser frequency standards controlled the transmitter and receiver. The observations were made in the "two-way" tracking mode (transmitted signal coherently transponded back to earth), which allows us to distinguish propagation and instrumental noises based on their differing transfer functions to the observable. Data were taken when Mars Observer was in interplanetary cruise with a sun-earth-spacecraft angle of about 100 degrees and an earth-spacecraft distance of about 500 light seconds.

After removing systematic effects due to spacecraft trajectory and motion of the spacecraft antenna relative to center-of-mass, we obtained residual Doppler frequency time series. These frequency residuals were integrated to produce phase time series from which structure functions were calculated. The structure functions thus obtained were approximated by power-laws, $D(\tau) = const\tau^{\alpha}$. We characterize $D(\tau)$ by its level at $\tau = 100$ seconds and its powerlaw index, α, measured between 30 and 100 seconds.

Powerlaw indicies varied between 0.67 and 1.6, averaging 1.2. The lower envelope of a plot of structure function level versus elevation angle showed a weak elevation angle dependence, but large positive excursions were observed. Any dependence on local time between about 1600-0300 hours was weak. A histogram of structure function level shows more relatively low values and fewer relatively large values. There were small systematic variations in the structure function level between the sites, with the Australian site having larger levels in our sample. Assuming frozen flow, our structure function levels can be compared with spatial measurements made at the VLA (R. A. Sramek, "Atmospheric Phase Stability at the VLA", URSI/IAU Symposium on Radio Astronomical Seeing, Beijing, 1989). We found the median inferred rms path delay (averaged over all sites and converted to a spatial separation of 1km using an assumed 5 m/sec transverse wind speed) to be about 3 times larger than the median of the VLA summer night rms path delays. We discuss some implications for precision Doppler tracking observations, particularly as they refine the noise model for low-frequency gravitational wave searches.

J/F1-5
1020

ATMOSPHERIC PHASE CORRECTION AT THE PLATEAU DE BURE INTERFEROMETER WITH DUAL FREQUENCY RECEIVERS

R. Lucas, M. Bremer, S. Guilloteau
IRAM 300 rue de la Piscine
28406 Saint Martin d'Heres
FRANCE

With the installation of new dual frequency receivers on the Plateau de Bure Interferometer, we have started to study the correlation between the total power fluctuations at 230 GHz and the phase noise induced by atmospheric water vapor. This is an important step to extend the total amount of available observing time, because the performance of the interferometer in general and especially at longer baselines and higher frequencies depends critically on the variation of the amount of water vapor along the line of sight, which fluctuates with time scales down to a few seconds. At IRAM, the previous mixer generation was not sufficiently stable to isolate the atmospheric component from the total power fluctuations, but the new receivers showed promise that the necessary requirements could be met. The dual frequency capabilities allows to use the spectral region around 230 GHz for the water vapor estimation, and to correct the phase at both frequencies in real time. First encouraging results in this direction were shown in the IRAM Newsletter (May 1995). We will summarize the status of this project after several months of tests in both summer and winter conditions.

J/F1-6
1040

INTERFEROMETER PHASE CORRECTION FROM RECEIVER TOTAL POWER MEASUREMENTS

R. Plambeck* R. Forster B. Frye J. Lugten W. Welch
M. Wright
Radio Astronomy Lab
University of California
Berkeley, CA 94720

The Berkeley-Illinois-Maryland Array allows observations at millimeter wavelengths with antenna separations of up to 1.2 km. At such long baselines the array sensitivity is limited by atmospheric phase fluctuations – due largely to tropospheric water vapor – with time scales of a few seconds to tens of minutes. The same molecules of water vapor which cause the phase delays also emit radiation; hence it is possible to monitor variations in the atmospheric path length by measuring changes in the sky brightness at each antenna. This is done most simply by monitoring the receiver total powers at the observing frequency.

The conversion factor from sky brightness to phase delay depends on the observing frequency and the altitude distribution of water vapor. At 100 GHz, a 1 K increase in sky brightness typically corresponds to 200° of phase delay. Thus, in order to determine the atmospheric phase delay with an accuracy of 10°, one must measure the sky brightness with an accuracy of 0.05 K. This is only 3×10^{-4} of the typical DSB system temperature of 150 K, requiring that the receiver gains be stable to this level. Very good temperature stabilization of all components is required to achieve such gain stability. Tests of the BIMA receivers show that a fractional gain fluctuation of 10^{-4} is produced by the following temperature changes:

SIS mixer operating at 3.8 K	0.002 K
1.8 GHz HEMT amplifier at 14 K	0.012 K
amplifier chain and detector at 300 K	0.008 K

In lab tests we have succeeded in stabilizing temperatures to these levels, and find that the receiver total power fluctuations are then approximately 4×10^{-4} on time scales of 1–1000 sec, 2×10^{-3} on time scales of a day. If this level of gain stability can be achieved routinely on the telescopes, it should be possible to compensate for many of the atmospheric fluctuations at long baselines.

J/F1-7
1100

A 22 GHZ WATER LINE MONITOR FOR INTERFEROMETER PHASE CORRECTION

D. P. Woody*
Owens Valley Radio Observatory
California Institute of Technology
100 Leighton Lane, Big Pine, CA 93513

A new radiometer system has been developed for monitoring the 22 GHz water vapor emission line with the sensitivity and stability required for correcting the tropospheric phase variations above the Owens Valley millimeter interferometer array. The goal of this project is to correct for the water vapor induced path length variations to a precision of .05 mm on time scales from 1 to 1000 sec using Water Line Monitors (WLM's) mounted on the six antennas in the array. The WLM's will sample the same path through the lower troposphere as the astronomical signal by utilizing the antenna's secondary and primary with a beam offset of 10 arcmin.

The 22 GHz water vapor line offers the advantage that it is unsaturated and the conversion from emission temperature to delay at the "hinge points" in the line profile is only weakly dependent upon the amount and distribution of the water vapor in the atmosphere. These "hinge points" have been used to good advantage in previous water vapor radiometers and it is important to minimize the dependence upon the details of the atmospheric model when applying phase corrections in real time. In addition the continuum emission from liquid water, ice, and antenna spillover can be rejected by measuring the contrast between the emission near the center of the line and the wings.

The principle changes from the previous generation of water vapor radiometers is the use of a single 18-26 GHz RF receiver for both the line and continuum emission, the use of wider channel bandwidths and a "Dicke switching" system between the channels. These changes improve the sensitivity and ability to differentiate between continuum and line emission. They also reduce the effect of drifts in the RF gain, detectors, and dc electronics. Laboratory tests of two prototype WLM's indicate that the required sensitivity and stability has been achieved. The next step is to verify their performance using the 100 m baseline 12 GHz satellite phase monitor on loan from the Center for Astrophysics. These tests will explore the feasibility of real time phase correction and the variability of the conversion from emission temperature to path delay.

J/F1-8
1120

WATER VAPOUR MEASUREMENTS USING THE 183 GHz LINE

M. Wiedner* R. E. Hills
Mullard Radio Astronomy Observatory
Cavendish Laboratory
Cambridge
England CB3 0HE

The JCMT and the CSO are now used regularly as an interferometer with a baseline of 164 metres operating at frequencies above 300 GHz. Even under good conditions the phase fluctuations are dominated by atmospheric effects. In the middle of the day there is often strong decorrelation on integration times as short as 10 seconds. We are building two 183 GHz radiometers which will be used to measure the difference in the water vapour content of the atmosphere above the two telescopes and thus correct the phase. The goal is to obtain the path difference to better than 30 microns on timescales of 1 second.

The emission from the sky will be picked off from the incoming beam by a mirror some distance in front of the Cassegrain focus and a few arc minutes off axis. This results in a beam that is slightly displaced from the astronomical beam and somewhat out of focus, but these effects are small in the crucial lowest kilometre of the atmosphere. The advantages are that the radiometer can remain in the same position whatever receiver and polarization is being used for the astronomical observations and also that confusing signals from astronomical sources will not normally be seen.

The radiometers use uncooled subharmonic mixers with the LO at 91.65 GHz - exactly half the line frequency. The mixers have a wide IF bandwidth - 0.1 to 10 GHz - and the conversion is double-sideband. Three sub-bands centred at 1.2, 4.2 and 7.8 GHz are separated out from the IF band by a second down-conversion and then amplified, filtered and detected. A "flip-mirror" together with hot and ambient loads provides calibration. The sensitivity should be better than 0.1 K with 1 second of integration.

The major advantage of using the 183 GHz line is that the emission is relatively strong: at an offset of 1.2 GHz from the line centre, we expect to see about 15 K of emission for each millimetre of additional path. This compares to about 2 K per mm at 225 GHz and 0.4 K at 22 GHz. The optics is also of more manageable size than at 22 GHz. The disadvantage is that the centre of the line becomes optically thick at relatively low values of total water vapour. It is for this reason that we use three IF channels with different offsets from the line centre. We plan to record both the absolute sky brightness in these channels and the short term fluctuations. We have carried out modelling which shows that accurate estimates of the atmospheric path can be obtained from these data over a wide range of atmospheric conditions. The highest frequency channel serves mainly to monitor the emission from clouds.

J/F1-9
1140

CANCELATION OF ATMOSPHERIC EMISSION FOR MILLIMETER WAVELENGTH CONTINUUM TOTAL POWER OBSERVATIONS

M.A. Holdaway* F.N. Owen
National Radio Astronomy Observatory
1003 Lopezville Rd
Socorro, NM 87801 D.T. Emerson
National Radio Astronomy Observatory
Campus Building 65
949 North Cherry Ave
Tucson, Arizona 85721

Fluctuations in the water vapor in a telescope's line of site lead to both interferometric phase errors and to variable atmospheric emission which is observed in total power. We use the Chilean phase monitor data to estimate the total power error made in subtracting the atmospheric emission for beam switched and on-the-fly (OTF) continuum total power observations. When the error in atmospheric subtraction is less than the system noise per switching interval, the total power observations will not be limited by the atmosphere. Even if the atmospheric noise dominates, it should average down if a systematic atmospheric trend is removed by double beam switching or by OTF scanning.

On the Chilean site, switching at 1 Hz typically increases the noise by only about 50%. Switching at 5 Hz will almost never be limited by the atmosphere. It is possible that next generation of radio antennas, such as the Millimeter Array (MMA), will be be able to *position switch* by a few arcminutes at 1 Hz. With slew speeds of $\sim$ 1 degree/s, OTF continuum observations of sources up to $\sim$2 degrees across will rarely be limited by atmosphere. Hence, it is possible that a nutating subreflector will not be required for the MMA antennas. Since OTF mapping does not suffer from the sensitivity losses of beam switched observations on large sources, this may be a fundamental breakthrough in imaging very large structures at millimeter wavelengths.

Session B-4, 1335-Thurs., CR1-9
THEORETICAL ELECTROMAGNETICS
Chairperson: A.D. Yaghjian, Rome Laboratory, Hanscom AFB, MA 01731

B4-1
1340

SHADOW-BOUNDARY ILDC'S FOR PERFECTLY CONDUCTING SMOOTH CONVEX SURFACES

A. D. Yaghjian* R. A. Shore M. B. Woodworth
Rome Laboratory
Hanscom AFB, MA 01731, USA

To find useful shadow-boundary ILDC's for perfectly conducting smooth convex surfaces, uniform high-frequency approximations are determined for the scattered and PO far fields of perfectly conducting circular cylinders illuminated by normally and obliquely incident TE and TM plane waves. For each of the four cases (TE and TM incidence for the scattered and PO far fields), a single general expression is found that involves only simple trigonometric and exponential functions (no integrals) and remains a valid approximation over the full 360 degrees in the far field. The far-field approximations are derived by combining geometrical optics, Kirchhoff integrals, stationary-phase evaluations, and creeping-wave analyses. Special attention has to be given to the PO far fields for an obliquely incident TE plane wave. In that case, unlike the other three cases, the far fields do not remain transverse electric and the solution for oblique incidence cannot be obtained directly from the solution for normal incidence.

By subtracting the approximate PO far fields from the approximate scattered far fields, and separating the resulting fields into contributions from the top and bottom of the cylinder, a uniform high-frequency approximation (PTD coefficient) is obtained for the fields radiated by the non-uniform current (total minus PO current) at a single shadow boundary of the cylinder. Shadow-boundary PTD incremental length diffraction coefficients are then determined by substituting these high frequency approximations for the non-uniform fields into the expressions derived in Shore and Yaghjian (*IEEE AP Trans.*, **36**, 55-70, 1988) and Hansen and Yaghjian (*IEEE AP Symp. Digest*, London, Ontario, Canada, 794-797, 1991).

Numerical results are shown that compare the exact scattered and PO far fields, computed from the eigenfunction solutions and the PO integrals, with the far fields computed from the approximate expressions. Good agreement is seen between the exact and approximate scattered and PO far fields, and notably, between the differences of the PO and scattered far fields (that is, the non-uniform far fields), for cylinders as small as one wavelength in diameter.

The uniform PTD shadow-boundary incremental length diffraction coefficients are integrated around the shadow boundary of a perfectly conducting sphere illuminated by a plane wave, and the resulting fields are added to the computed PO far fields of the sphere. Comparisons with the exact eigenfunction solution of the sphere show that the ILDC shadow-boundary fields significantly enhance the accuracy of the PO far fields, especially for large bistatic scattering angles.

B4-2
1400

ON THE CHARACTER OF THE ZEROS OF POLYNOMIALS RELEVANT TO THE SMALL CURVATURE APPROXIMATION IN ASYMPTOTIC DIFFRACTION THEORY

Ronald J. Pogorzelski
Jet Propulsion Laboratory
California Institute of Technology
4800 Oak Grove Drive
Pasadena, CA 91109

In dealing with the problem of estimating the high frequency coupling between two antennas mounted on a non-metallic aircraft skin, one is faced with approximation of the spectral integrals representing the propagation of rays along the geodesics of the surface between the antennas. When the antennas are sufficiently separated, the integrals can be conveniently represented as a rapidly convergent residue series. On the other hand, when the antennas are in close proximity, the residue series fails to converge rapidly and a power series representation proves to be efficacious. [Paknys and Wang, IEEE Trans. AP-35(3), 1987, 293-298] When the effective surface impedance is not small, an intermediate region of separation appears in which neither the residue series nor the power series is effective. Recently, an asymptotic formalism was presented [Pogorzelski, National Radio Science Meeting, Boulder, CO, January 1995] which extends the earlier work of Bremmer [IRE Trans. AP-6, 1958, 267-272] and Wait [J. of Res. of NBS, 56(4), 1956, 237-244] describing a "small curvature approximation" to the case of general (non-azimuthal) ray directions on the surface of a cylinder (excluding only axial propagation). Based on the formulation of Pearson [Radio Sci. 21(4), 1986] this asymptotic formalism provided a means of approximating the spectral integrals in the intermediate region of separation.

In applying the above generalized small curvature approximation technique, one is faced with obtaining the zeros of high degree polynomials. This arises from the necessity of obtaining a partial fraction expansion of the approximated integrands. Ordinarily, this would be a computationally limiting factor in the efficiency of the overall technique. However, due to the somewhat convenient character of these polynomials, the zeros may be easily estimated analytically. These estimates are sufficiently close to the true zeros that numerical iteration based on Newton's method produces the desired zeros very accurately in very little computation time. Having analytical estimates of the zeros also provides insight into the effect of increasing the number of terms retained in the approximations used in the integrands. The estimation of the zeros and the implications of their locations are discussed in detail and example computations are described.

B4-3
1420

TARGET SYMMETRY AND THE SCATTERING DYADIC

Carl E. Baum
Phillips Laboratory/WSR
3550 Aberdeen S.E.
Kirtland AFB, NM 87117-5776

This paper considers the impact of reciprocity and geometrical symmetry of a target on the associated scattering dyadic. Reciprocity makes the backscattering dyadic symmetric and gives reflection and two-fold rotation symmetries to the bistatic scattering dyadic. The target geometry (including it's constitutive parameters) may also have various symmetries, such as characterized by the point symmetry groups (various combinations of rotations and reflections). By orienting various rotation axes and reflection planes of the target in special ways with respect to both incidence and scattering directions, various symmetry-associated simplifications in the scattering dyadic can be made to occur. For special cases of back and forward scattering the various point symmetry groups are considered with preferred axes and planes now aligned according the common axis defined by incidence and scattering directions, giving a rich structure to the scattering dyadic. In forward scattering inversion symmetry is sufficient to give a symmetric scattering dyadic for all directions of incidence (like backscattering without geometrical symmetries). This forward-scattering property also applies if the target has symmetry axes or planes appropriately oriented with respect to the direction of incidence. For low frequencies (electrically small target) further simplifications occur, leading to further symmetries (including invariance to reversal of incidence and scattering directions) in the scattering dyadic, without invoking geometrical symmetries. In this case, it is the electric and magnetic polarizability dyadics that are important. The presence of geometrical symmetries introduces symmetries in the polarizability dyadics, which in turn introduce further symmetries in the low-frequency scattering dyadic.

B4-4
1440

THE ANGULAR SPECTRUM REPRESENTATION AND THE SHERMAN EXPANSION OF PULSED ELECTROMAGNETIC BEAM FIELDS IN LOSSY, DISPERSIVE MEDIA

Kurt Edmund Oughstun
College of Engineering and Mathematics
University of Vermont
Burlington, Vermont 05405-0156

The angular spectrum of plane waves representation of a pulsed electromagnetic beam field propagating in a lossy, dispersive medium that occupies the half-space $z > z_0$ expresses that wavefield throughout that half-space as a superposition of both homogeneous and inhomogeneous plane waves. A generalization of the Sherman expansion for source-free wavefields in lossless media (G.C. Sherman, J. Opt. Soc. Am. 59, 697-711, 1969) to the lossy, dispersive medium case is used to derive a spatial series representation of a pulsed, source-free electromagnetic beam field from its angular spectrum representation. This spatial series representation explicitly displays the temporal evolution of the pulsed beam-field through a single contour integral that is of the same form as that obtained in the description of a pulsed plane wave field that is propagating in the positive z-direction in the lossy, dispersive medium. In general, the temporal pulse evolution is found to depend upon the transverse spatial position in the beam field through the derivatives of the field boundary values. The dynamical evolution of the temporal field structure for an ultrawideband pulse may then be completely described by modern asymptotic techniques (K.E. Oughstun and G.C. Sherman, Review of Radio Science, 1990-1992 Oxford U. Press, 1993, pp. 75-105) whose quantitative accuracy has been firmly established.

This research is supported, in part, by the U.S. Air Force Office of Scientific Research under Grant # F49620-94-1-0430.

B4-5
1520

SOME PROPERTIES AND APPLICATIONS OF THE GREEN'S FUNCTION FOR FLOQUET-PERIODIC DOMAINS

Jay W. Parker*
Jet Propulsion Laboratory
4800 Oak Grove Drive
Pasadena, CA 91109-8099

Computing the transmission and reflection of an oblique plane wave impinging on an infinite periodic region is a well-known first step in predicting the response of a frequency selective surface. We consider how to exploit a formalism that supports response prediction, as well as yielding information about an unknown array from the response, the inverse problem. One general analysis technique uses a source-type domain integral equation, leading to consideration of the Green's function for a Floquet-periodic domain. This Green's function corresponds to the field produced by an infinite-periodic phased array of point current elements, one such element per period, with phase changing by a constant increment from each period to the next. It also corresponds to the point-current response within a finite-width domain, with a boundary condition at the opposing surfaces that ties the field values with a phase-increment relationship. This Green's function may be applied to a region of inhomogeneous penetrable material, providing a relationship between internal fields, local material constants, and a corresponding radiation problem due to an equivalent current distribution. A straightforward linear transformation of the equivalent current distribution produces the complex reflection and transmission for an arbitrary incoming wave.

Computation of near-field patterns from equivalent current sources appears to require $(NM)^2$ operations where N is the total discretization rank in the transverse directions, and M is the total discretization of the cell in its finite dimension. In the limit of a large number of discrete transverse domain elements, this may be reduced to $M^2 N \log N$ by utilizing fast Fourier transforms in the transverse directions. We show how this advantage may be exploited in the analysis problem (filling the system matrix), analysis of solution sensitivity, and a cost-function Frechet derivative that constitutes an element of a versatile optimization technique. Applying such inverse problem techniques to Floquet-periodic domains may lead to insights in crystallography, characterization of patterned structures on planetary surfaces, and improved optimization for frequency selective surface designs.

B4-6
1540

Electromagnetic Fields Scattered from Irregular Layered Media

Ezekiel Bahar and Robert D. Kubik
Department of Electrical Engineering and Center for Electro-Optics
University of Nebraska-Lincoln
Lincoln, NE 68588-0511

Full wave solutions are derived for the vertically and horizontally polarized electromagnetic waves scattered by irregular stratified media. The interface, $y = h_{01} = h(x, z)$, between free space, (the uppermost medium containing the source and receiver) medium (0), and the overburden or coating film (intermediate medium) is assumed to be a continuous function of the lateral variables x and z. The interface between the intermediate medium (medium 1) and the substrate (medium 2) is assumed to be planar, $y = h_{12} =$ constant.

The work presented here is based on the full wave approach to scattering from irregular multi-layered structures. A physical interpretation is given to each term of the full wave solution. This provides a basis for the construction of physical models for diffuse scattering in complex irregular layered structures. The full wave expression for the scattered field accounts for the following:

(a) Scattering upon reflection $D_{00}(\vec{k}_0^f, \vec{k}_0^i)$ from above the interface $y = h_{01}$.

(b) Multiple reflections $(O_{RRi})^{q-1}(q = 1...\infty)$ in the intermediate layer (medium 1) at the incident angle before it is scattered upon transmission across the interface $D_{01}(\vec{k}_0^f, \vec{k}_1^i)$.

(c) Multiple reflections $(O_{RRf})^{p-1}(p = 1...\infty)$ in the intermediate layer (medium 1) at the scattered angle after it is scattered upon transmission across the interface $D_{10}(\vec{k}_1^f, \vec{k}_0^i)$.

(d) Multiple reflections $(O_{RRi})^{q-1}(q = 1...\infty)$ in the intermediate layer (medium 1) at the incident angle before it is scattered upon reflection from below the upper interface $D_{11}(\vec{k}_1^f, \vec{k}_1^i)$ and multiply reflected $(O_{RRf})^{p-1}$ $(p = 1...\infty)$ in the intermediate layer (medium 1) at the scatter angle.

The 2×2 matrices D_{ab} (that account for cross and co-polarized scattering) are dependent on the summation integers p and q. The physical interpretation of the matrices $D_{ab}\,(a, b = 0, 1)$ are given. The 2×2 matrices O_{RRi} and O_{RRf} account for the round trips the waves undergo in medium 1, before and after they are scattered (upon reflection D_{00}, D_{11} and transmission D_{01}, D_{10} across the rough interface) at the incident (i) and scatter (f) angles.

B4-7
1600

RADIATED FIELD FROM THIN HALF-WAVE UNCOUPLED ORTHOGONAL DIPOLES EXCITED BY FINITE-CYCLE SINUSOIDS

Ajit K. Choudhury
Department of Electrical Engineering
Howard University
Washington, DC 20059

Eric L. Mokole
Suren N. Samaddar
Radar Division (Code 5340)
Naval Research Laboratory
Washington, DC 20375-5336

The intent of this work is to ascertain through analytical means whether a circularly polarized radiated field is possible for ultrawideband (UWB) input signals to some antenna. Consequently, the behavior of the radiated electric field from thin, half-wave, electromagnetically uncoupled, orthogonal dipoles in free space that are excited by a finite number of cycles of a sinusoidal voltage is investigated. A coordinate frame is chosen so that the x-axis and z-axis point along the axes of the dipoles. The frequency f_0 of the input voltage is the frequency associated with the dipoles' length, and the input to the dipole along the x-axis is a time-delayed version of the input to the dipole along the z-axis. To obtain closed-form expressions for the field, a zero-order approximation of the current along each dipole in the frequency domain is used.

The time-domain radiated field is extended in time with respect to the input signal's duration N/f_0, where N is the number of cycles of the input $\sin(2\pi f_0 t)$. In particular, if the time delay between inputs is $.25/f_0$ and if the feed network is perfectly matched to the dipoles, then the duration of the field is slightly less than $(N + .75)/f_0$, except at broadside where equality occurs. This temporal extension arises from radiations that occur at the ends of each dipole, as well as from delayed radiations at the feed points that are caused by current being reflected from the ends of the dipoles. At broadside, the field is initially vertically polarized for $.25/f_0$, is elliptically polarized with two different orientations for a total time of $.5/f_0$, is circularly polarized for time $(N - .75)/f_0$, is elliptically polarized again for $.5/f_0$, and finally is horizontally polarized for a time of $.25/f_0$. For a single-cycle sine $(N = 1)$, the radiated field's duration is 1.7 times the duration of the input, and circular polarization occurs for only one-quarter of the period of the input signal. As one allows the number of input cycles to increase, circular polarization is predominant. Usually when someone speaks of circular polarization, they are considering a CW signal and do not bother with the beginning and ending of that signal. Our results indicate that the so called CW field has a start and finish and that observations of circularly polarized fields are made in the interval between the transient leading and trailing edges. These results establish the feasibility of radiating circularly polarized fields in the broadside direction.

B4-8
1620

GREEN'S FUNCTION THEORY FOR PLANAR AND PERIODIC DEFECT ARRAYS IN PHOTONIC BAND STRUCTURES

Arthur R. McGurn
Department of Physics
Western Michigan University
Kalamazoo, Michigan 49008 U.S.A.

The defect modes associated with a plane or a periodic array of line defects in a two-dimensional photonic band structure are studied using exact Green's function methods. Specifically, we consider the above described defect problems created in a pure photonic band structure system which models an experimental system recently investigated by McCall et al (S.L. McCall, et al. Phys. Rev. Lett. 67, 2017-20, 1991). This is a square lattice array of cylindrical rods formed of linear dielectric material with $\epsilon = 9$ surrounded by vacuum and of filling fraction $f = 0.4488$. In one study a plane of rods is replaced in the photonic band structure by a plane of impurity rods which may be of either linear or nonlinear dielectric material, and conditions are determined for the existence of impurity modes, associated with the impurity array, in the photonic band gap. The electric fields of the impurity modes are computed for impurity modes in the gaps. In a second study a two-dimensionally periodic array of line defects is introduced into the photonic band structure such that the periodicity of the defect array may or may not coincide with the periodicity of the original photonic band structure. The defect rods are treated in both the case for which the impurities are formed from linear and nonlinear dielectric materials, and the conditions necessary for defect modes to exist in the photonic band gaps are determined. In both the cases of impurity planes of impurity rods and of two-dimensional arrays of impurity rods, examples are shown for the dispersion relations of the gap impurity mode frequencies as functions of appropriate wavevectors. These dispersion relations for gap impurity modes are found to exhibit themselves various gaps in both frequency and wavevector.

Session D-3, 1335-Thurs., CR2-28
MICROMACHINING FOR MICROWAVES
Chairperson: Z.B. Popović, Dept. of Electrical and Computer Engineering, Univ. of Colorado at Boulder, Boulder, CO 80309
Organizers: Z.B. Popović; and G.M. Rebeiz, EECS Dept., The University of Michigan, Ann Arbor, MI 48109

D3-1
1340

SWITCHING OF MICROWAVE SIGNALS USING METALLIC MICROMECHANICAL MEMBRANES

Chuck Goldsmith, John Randall, Tsen-Hwang Lin, Susan Eshelman, Bill Norvell, David Denniston, Bill Powers, and Delfin Nacilla
Texas Instruments Incorporated
P.O. Box 655474 M/S 245
Dallas, Texas 75265

During the past few years, developments in microelectromechanical systems (MEMS) have enabled exciting developments in the fields of sensors (accelerometers and pressure sensors) and actuators (motors and pumps). Today, the technologies of bulk and surface micromachining facilitate the fabrication of high quality integrated circuit control components such as optical and microwave switches. These switches possess distinct performance advantages over similar components fabricated from standard semiconductor devices.

The switches discussed in this presentation use a thin metallic membrane actuated by a DC electrostatic potential. Actuation of the membrane causes the switch to make or break contact with the RF signal path. Selecting the proper materials and dimensions for the membrane and electrodes allows these devices to switch high frequency signals with low loss and reasonable switching voltages. Currently, the design of these devices at Texas Instruments centers on capacitive microwave switches where movement of the membrane alters the switch capacitance by a factor of 100 or more. This eliminates many of the problems associated with dry-contact switching and exhibits high on-off impedance ratios with low parasitics at microwave frequencies. Additionally, these devices require no DC bias current nor recessed or separate bias electrodes. These devices are currently fabricated on both high resistivity silicon and gallium arsenide. This allows the possibilities of integration with silicon CMOS drive circuitry or GaAs microwave amplifiers.

In this presentation, we will describe the surface micromachining techniques used to fabricate the devices, electrical and electromechanical modeling methods for estimating their performance, and overall high frequency performance of these capacitive membrane switches. Various membrane circuit configurations and applications will also be discussed.

D3-2
1420

MICROMACHINED MICROWAVES AND MILLIMETER-WAVES AT THE UNIVERSITY OF MICHIGAN

Gabriel M. Rebeiz and Linda P. B. Katehi
EECS Department
The University of Michigan
Ann Arbor, MI 48109-2122

The talk will present the research effort on the development of low-loss microwave components and micropackaging modules using micromachining techniques. Using this technology, we have fabricated and investigated a family of high-speed, low-dispersion transmission lines and components. The transmission lines are suspended on a thin dielectric membrane and therefore do not suffer from dispersion effects and from losses due to substrate modes. The dielectric membrane is composed of a silicon nitride/silicon dioxide layer and is only 1.0-1.5 microns thick. Several geometries such as the microshield transmission line, the air-strip line, the shielded air-microstrip line, and the standard coplanar waveguide line will be presented. These lines have shown excellent propagation characteristics up to Terahertz frequencies.

Based on this technology, novel conductor-loss limited stripline resonators and interdigitated filters with 5-40% bandwidth and an insertion loss of 0.5-1.5 dB at 15-20 GHz will be presented. New millimeter-wave bandpass filters, based on a suspended microstrip line and the microshield line, such as a 5% bandpass filter at 94 GHz with an insertion loss of 2.5 dB and the first-ever planar micromachined filter at 250 GHz with a measured insertion loss of 1.5 dB are also presented. Also, low-loss Wilkinson couplers at 30 GHz and wideband Lange couplers at 20 GHz will be presented. An 18 GHz SSB mixer requiring only 1 mW of LO power and resulting in a 30 dB image rejection response is also built using this technology. Finally, some micropackaging modules built using this technology and suitable for low-cost millimeter-wave radiating systems will be presented.

D3-3
1500

MICROMACHINED SILICON WAVEGUIDE CIRCUITS

W.R. McGrath[1], J. Wright[2], S. Tatic-Lucic[2], Y.-C. Tai[2], C. Walker[3], M. Yap[2]

[1]Center for Space Microelectronics Technology, Jet Propulsion Laboratory, California Institute of Technology, Pasadena, CA 91109

[2]Dept. of Electrical Engineering, California Institute of Technology, Pasadena, CA 91125

[3]Dept. of Astronomy, University of Arizona, Tucson, AZ 85726

Rectangular waveguides are commonly used as circuit elements in remote-sensing heterodyne receivers at millimeter wavelengths. The advantages of waveguides are low loss and mechanical tunability. However conventional machining techniques for waveguide components operating above a few hundred GHz are complicated and costly. Waveguides micromachined from silicon however would have several important advantages including low-cost; small size for very high frequency (submillimeter wave) operation; high dimensional accuracy (important for high-Q circuits); atomically smooth walls, thereby reducing *rf* losses; and the ability to integrate active and passive devices directly in the waveguide on thin membranes, thereby solving the traditional problem of mounting thin substrates.

We report on the development of silicon micromachining techniques for fabricating silicon-based waveguide circuits which can operate up to several THz. Both WR-10 (75 GHz - 115 GHz) and WR-4 (170 GHz - 260 GHz) waveguides have been fabricated from (110) silicon wafers. A potassium hydroxide solution is used to etch the waveguide channels. The high etching ratio of the (110):(111) crystal planes in silicon allow for channels with vertical sidewalls. Waveguide channels both with and without thin ($\approx 2\ \mu m$) silicon nitride membranes in the E-plane have been produced. Low-temperature selective metallization techniques based on electroless plated nickel have been developed which coat the silicon waveguide walls but leave silicon nitride membranes untouched. Insertion loss measurements have been made up to 260 GHz using a broadly tunable backward wave oscillator. The results show performance comparable to conventional metal waveguide (within $\pm$ 0.25 dB). These techniques will allow for the fabrication of complex, high-frequency waveguide components which would be practically impossible by conventional techniques.

The research described in this abstract was performed by the Center for Space Microelectronics Technology, Jet Propulsion Laboratory, and the Department of Electrical Engineering, California Institute of Technology, and was jointly sponsored by the National Aeronautics and Space Administration, Office of Space Access and Technology, and the JPL Director's Research and Discretionary Fund.

D3-4
1540

Micromechanical Tuning Elements for Submillimeter Wave Integrated Circuits

Victor M. Lubecke,[1] William R. McGrath,[1]
and David B. Rutledge[2]

[1] Jet Propulsion Laboratory,
California Institute of Technology,
Pasadena, CA 91109, USA

[2] Department of Electrical Engineering,
California Institute of Technology,
Pasadena, CA 91125, USA

Monolithic integrated circuit technology promises a practical means for realizing reliable and reproducible planar millimeter and submillimeter wave circuits. Planar circuits are fabricated through photolithographic techniques, which allow for the cost-effective production of intricate designs not possible with waveguide technology. Such circuits however, do not typically allow for post-fabrication optimization of performance. This can be a critical problem for the millimeter and submillimeter band, where device parasitics and fabrication tolerances are difficult to control and characterize. A micromechanical tuning element suitable for integration in a variety of monolithic millimeter and submillimeter wave circuits has been developed. It is called a *sliding planar backshort* (SPB) and it can be fabricated as an integral part of a dielectric-coated coplanar transmission line. The SPB forms a movable short-circuit over a useful bandwidth, which allows for the variation of the transmission line's electrical length. A semiempirical approach was employed in its design. Measurements at 2 GHz have shown $|s_{11}|$ for the SPB to be better than -0.5 dB over a bandwidth of at least 50% on both coplanar strip and coplanar waveguide transmission lines, and photolithographically fabricated SPB's have been successfully demonstrated as discrete components at frequencies up to 100 GHz. A technique for fabricating a micromechanical version of the SPB as an integrated component has also been developed. Two such SPB's, fabricated as integral parts of a quasi-optical 620 GHz monolithic integrated circuit, have been used to vary the measured response of a thermoelectric detector over a range of almost 15 dB. Such tuning elements can be used for characterizing developmental circuits, and for optimizing the in-use performance of various millimeter and submillimeter wave integrated circuits.

D3-5
1600

APPLICATIONS OF MICROMACHINED MMIC TECHNOLOGY

P. Bauhahn*
Honeywell Technology Center
3660 Technology Drive
Minneapolis, MN 55418 D. Ferguson
Systems and Processes Engineering Corporation,
Austin, TX 78746

Micromachining technology has moved from the development of basic processes to the application of the technology in products and systems. The Honeywell Technology Center has recently developed a microelectromechanical switch compatible with Gallium Arsenide microwave monolithic integrated circuit (MMIC) fabrication processes. This micromachined MMIC switch offers much better electrical performance than current semiconductor switches and enables applications which would not be practical using existing technology.

The micromachined switch has been fabricated and tested on wafer. The insertion loss varied from less than 0.1 dB at 1 GHz to approximately 0.6 dB at 40 GHz. The isolation of a single series switch ranged from -15 dB at 40 GHz to better than -20 dB below 20 GHz. The insertion loss and isolation varied monotonically with frequency as a consequence of the simple structure. Preliminary reliability tests have shown more than 1×10^9 operations with no visible change in device characteristics for related structures.

The purpose of this paper is to describe the switch's basic construction, electrical performance and outline the application of the switch to products and systems under consideration.

D3-6
1620

MICROMACHINED RF SWITCH FOR MICROWAVE APPLICATIONS

J. Jason Yao
Rockwell Science Center
1049 Camino Dos Rios
Thousand Oaks, CA 91360
e-mail: jjy@risc.rockwell.com

As an enabling technology, MicroElectroMechanical Systems (MEMS) technology has been continuously providing new and improved design paradigms for commercial applications. Here we describe a MEMS application to microwave circuits in the form of a miniature switch that is capable of handling GHz signal frequencies while still providing an excellent electrical isolation in the Off-state and a minimal insertion loss in the On-state. The lack of the dynamic range in On/Off impedances for frequencies beyond 1 GHz is one of the major problems for conventional transistor-based switches (typical values are 1 dB insertion loss and -25 dB isolation at 4 GHz). Our micromachined miniature RF switch is made with a MEMS technology using a suspended silicon dioxide micro-beam as the cantilevered arm, a platinum-to-gold electrical contact, and an electrostatic actuation as the switching mechanism. Figure 1 shows a topview micrograph of a miniature switch design. In this presentation, we describe the device design, the fabrication method, and the switch results including both RF performances and device mechanics and dynamics. Specifically, micro fluid dynamics around the RF switch's moving cantilever contributes heavily to the switch's dynamic performance. Air resistance caused by the squeeze film damping effect of the film (air) underneath the switch's moving cantilever can slow down the switch's transient response significantly. A numerical simulation of the switch's fluid dynamics coupled with the electrostatic simulation has been carried out and will be presented in this meeting. The prototype RF switch has an electrical isolation of -42 dB and an insertion loss of 0.1 dB at 4 GHz, as illustrated in Fig. 2. The switch's closure time is on the order of 30 μs, and it requires a minimal actuation voltage of 28 Volts. All characterizations were performed in atmospheric ambient. The silicon dioxide cantilever has been stress tested for a total of sixty five billion cycles (6.5×10^{10}) and no fatigue problem was observed. The maximum current handling capability for the prototype switch is 250 mA with the cross sectional dimensions of the narrowest gold line being 1 μm x 20 μm. The fabrication process uses five photo-masks and a low temperature budget of 250 °C. The micromachined miniature switches will have applications in signal routing for microwave and millimeter wave IC design, in MEMS impedance matching networks, in band-switched tunable filters for frequency-agile communications, and in telecommunications in general.

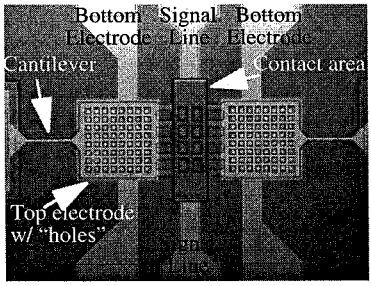

Figure 1: A micrograph showing the RF switch.

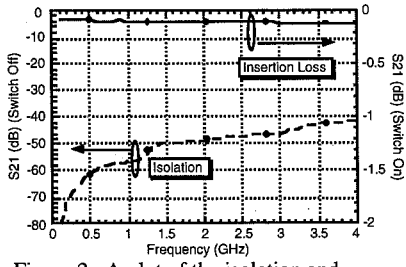

Figure 2: A plot of the isolation and insertion loss of the RF switch as a function of the signal frequency.

D3-7
1640

MEM ANTENNA SYSTEMS: CONCEPTS, DESIGN AND SYSTEM IMPLICATIONS

J.J. Lee D. Atkinson
Hughes Aircraft Company
J.J. Lam* L. Hackett R. Lohr L. Larson R. Loo
M. Matloubian G. Tangonan
Hughes Research Laboratories
H. de Los Santos R.Brunner
Hughes Space and Communications Company

We report on recent advances in micro-electro machined (MEM) microwave switches and their applications in antenna systems. The fabrication and performance characteristics indicate that MEM switches are far superior than pin diode switches and can be manufactured using silicon processing technology. Specifically, the MEM switches have a broadband ultra-low insertion loss (0.5 dB) from 2-45 GHz and very high isolation (35 dB) over the same spectral region. The MEM switches can be used to result in low-loss phase-shifter phased-array/active antenna applications. Also, MEM switches can replace PIN diodes in focal-plane multi-element receivers for low-cost collision avoidance automotive applications at 76-78 GHz. The fabrication steps consist of well-known semiconductor processing of 5 distinct but simple steps. These last attributes imply that the MEM switches can be produced at very low cost. We explore the implications of the performance, cost and weight on the design of current and future microwave communication systems. In specific, we will outline the impact of the MEM based antenna systems in both the commercial and defense electronics arena.

Session F-4, 1335-Thurs., CR1-42
ACTIVE REMOTE SENSING OF THE OCEAN
Chairperson and Organizer: D. Thompson, The Johns Hopkins Univ., Applied Physics Laboratory, Laurel, MD 20723

F4-1
1340

HIGH FREQUENCY WAVE HEIGHT SPECTRAL IMPLICATIONS FROM TOPEX CROSS SECTION DATA

Gary S. Brown
ElectroMagnetic Interactions Laboratory
Bradley Department of Electrical Engineering
Virginia Polytechnic Institute & State University
Blacksburg, Virginia 24061-0111

Much of our current understanding of the scattering from randomly rough entended surfaces derives from the dependencies suggested by the two-scale or composite surface scattering model. It is well known that for near normal incidence backscatter, this model predicts that the level of scattering will be proportional to a product of the Fresnel reflection coefficient at normal incidence, a factor associated with the attenuation of coherent em energy reflected from a planar surface having small scale roughness only, and the probability density function of the large scale slopes evaluated at zero slope. The Fresnel reflection coefficient at normal incidence depends on the em frequency and the electrophysical properties of the surface. The other two elements in the above description for the surface cross section involve both artificial and real quantities. For example, the coherent attentuation factor depends on the radar frequency and the second moment of the small scale height which, also, is due to the division of the roughness spectrum into large and a small scales of roughness relative to the em wavelength. Similarly, the slope probability density function depends on the slopes of the large scale structure on the surface which can be envisioned as resulting from a filtering of the true surface by a low-pass filter which eliminates only the small scale high frequency waves. The classic implementation of such a mathematical operation is the use of an oil slick to damp the high frequency waves on a surface.

While the composite model has been used to describe radars' response to clutter, predict sensitivities to surface characteristics, and suggest new remote sensing concepts little if any effort has gone into using radar data to invert the scattering model. This is primarily due to our inability to design such a comparison which involves as few surface unknowns as possible. The two TOPEX radar altimeters having much different frequencies provide this opportunity. With calibrated measurements of the backscattering cross section of the ocean surface at normal incidence at both C– and Ku–bands, it is possible to infer information on the part of the surface height spectrum that is most important in determining the large scale slope characteristics. In this paper, the two frequency cross section data will be compared and the implied surface height spectral behavior will be determined based on an assumed power law spectrum in the spectral region about the point of spectral division. Using the assumptions about the small scale height that are implicit to the two-scale model, it will be shown that the over-ocean data imply a spectral rolloff exponent that is less than the Phillip's equilibrium range value of 4 ! Also, it will also be shown that some over-land data produce an even smaller exponent. This is consistent with the land being rougher than the ocean surface in the spatial frequency range of the two radars. The primary implication of an exponent smaller than 4 is that both the land and ocean surfaces may be, as recent publications have suggested, fractal.

F4-2
1400

ON THE JHU/APL MODEL FOR THE COMPLEX FIELD BACKSCATTERED FROM THE OCEAN

B. L. Gotwols, D. R. Thompson, and R. D. Chapman
Johns Hopkins University
Applied Physics Laboratory
Johns Hopkins Road
Laurel, MD 20723

It has been known for many years that high resolution microwave signals backscattered from the ocean surface exhibit a first order amplitude probability density function (pdf) which does not obey the Rayleigh distribution. The spiky nature of the signal causes an excess in the distribution tail. A number of authors have postulated various probability density functions such as lognormal, Weibull, and K-distributions to fit the near grazing incidence data. However, for the moderate incidence angles (20° - 70°) which are generally used for microwave scatterometers, Synthetic Aperture Radars (SAR), and Real Aperture Radars (RAR), none of the aforementioned distributions fit the measured data over the full range of amplitude. Until recently the situation was even worse for the phase of the backscattered signal, where, to our knowledge, there was no published model available.

Recently a model for the amplitude pdf of the microwave field backscattered from the ocean surface was proposed (D.R. Thompson and B.L. Gotwols, JGR, 99, 9725-9739, 1994; B.L. Gotwols and D.R. Thompson, JGR, 99, 9741-9750, 1994) that fits the data at all amplitudes. The same model has also been used successfully to compute the phase (R.D. Chapman, B. L. Gotwols, and R. E. Sterner II, JGR, 99, 16293-16301, 1994). The model described in this trio of papers successfully describes the statistics of the complex backscattered field based on sound physical principles, without the need for an ad hoc assumption of the underlying statistical distribution. The cornerstone of the proposed model is based on the observation that the backscattered field is locally normally distributed. By this it is meant that for a given long wave slope (wavelength greater than the radar footprint) the complex field is normally distributed, but with a variance that depends on the underlying slope. One might say that as the long waves propagate through the footprint, the amplitude distribution "breathes".

Comparison of the model with 150 Gbytes of data collected during the SAXON FPN experiment shows exceptionally good agreement at wavelengths ranging from 2 - 20 cm, for both amplitude and phase. SAXON FPN was conducted in the North Sea during autumn because of the large variation expected in wind and wave conditions. Wind speeds to 20 m/s, and significant wave heights to 7 m were encountered. Over 1000 five minute runs at mid incidence (~45°) were analyzed at each wavelength and polarization. All runs where the wind direction was within ±45° of the radar look direction (to avoid effects due to the tower legs) were fit to the model and compared with environmental parameters such as wind speed, atmospheric stability, and long wave swell.

It will be interesting to see how far out in incidence angle this model will work. To this end, we constructed a short pulse, dual polarized X-band radar which will be fielded for the first time during the COPE experiment in Sep. - Oct. 1995. The results from COPE will be discussed in a companion paper.

F4-3
1420

MODERATE-TO-NEAR GRAZING ANGLE X-BAND RADAR BACKSCATTER FROM THE OCEAN AS MEASURED DURING COPE

R.D. Chapman, B.L. Gotwols, and M. J. Jose
Johns Hopkins university
Applied Physics Laboratory
Johns Hopkins Road
Laurel, MD 20723

The Coastal Ocean Probing Experiment (COPE) was a joint program between NOAA and DOD to examine radar scattering phenomenon in near coastal environments. The experiment involved a number of shore-based radars, several aircraft, a blimp, a small survey vessel, and the Research Platform Flip all brought together for a three week deployment off the Oregon coast. Our contribution to this multi-component experiment was the deployment of a small research radar from the research vessel Flip. This X-band radar is a coherent, dual- polarized radar with a pulse length of 20 ns. This new radar has low power (50 W peak) and is compact, making it easy to deploy from Flip. The goal of our efforts is to examine the statistics of moderate-to-near grazing angle radar backscatter in an oceanic environment. In particular we want to identify the scattering phenomenon particular to near-grazing angles by comparison of these data with the JHU/APL radar scattering model which has proven successful at moderate incidence angles. In support of this goal we acquired approximately 500 Gbytes of data during three weeks of continuous operations. This talk will describe the data that we acquired and present early results of our analysis, highlighting the differences between moderate and near-grazing angle scattering.

F4-4
1440

MEASUREMENTS OF COHERENT MICROWAVE SEA RETURN FROM AN AIRSHIP

William J. Plant
William C. Keller
Vahid Hesany
Kenneth Hayes
Andrew Jessup
Applied Physics Laboratory
University of Washington
Seattle, WA 98105-6698

In a series of flights extending over three years, we have measured microwave cross sections, Doppler offsets, and Doppler bandwidths at X and Ku-bands from a manned, powered airship. The airship was leased from the US/LTA Corporation of Eugene, Oregon and the measurements were made off the coast of Oregon. Data have been collected over a range of incidence angles from 10 to 70 degrees, at both HH and VV polarization, and under a variety of atmospheric and oceanic conditions.

During the first two years, coherent, CW and interrupted CW, X-band systems collected HH and VV polarized return simultaneously. Wind and wave measurements were obtained from a platform suspended below the airship while sea surface temperature was measured from the platform and imaged from the gondola of the blimp. The results show how microwave signatures depend on wind conditions, swell and sea surface temperature in the measurement area.

In the most recent measurements, completed in October of this year, we operated a coherent, rotating, short-pulse, X-band system which collected sea return over a range of incidence angles from about 30 to 70 degrees during each pulse. HH and VV returns were measured at different times during this experiment and surface conditions were obtained from the research vessel FLIP which operated in the area. The rotating could be stopped in flight so that maps of cross section, Doppler offset and Doppler bandwidth could be made over areas of about 300 m by 10 km. Measurements in the rotating mode indicated the possibility of measuring wind, wave, and current conditions simultaneously. The mapping mode successfully mapped surface features such as lines of surface convergence and surf zones yielding measurements of surface velocities and velocity spreads of these features as well as their roughness.

F4-5
1500

X-BAND SIGNAL MODULATIONS FROM PROPAGATION THROUGH A DISTURBANCE ON THE MARINE INVERSION

R.A. Kropfli and R.J. Zamora
NOAA Environmental Technology Laboratory
Boulder, CO 80303

Images of the ocean surface were made with an X-band (9.3 GHz) radar at an elevated site on San Clemente Island during the San Clemente Island Ocean Probing Experiment (COPE) in September, 1993. Occasionally, unusual images were produced that were not explainable by scattering from extraordinary ocean wave conditions; the ocean was undisturbed during these radar observations. The most notable of these images taken at grazing angles near 5° consisted of a stationary, wave-like pattern having a wavelength of about 2 km and 15 dB modulations in signal strength. The structure was roughly parallel to the long axis of the island and located on its leeward side.

Several hypotheses employing standing ocean waves were put fourth and discarded because 1) the ocean was fairly calm with no unusual swell or other wave conditions existing at the time, 2) it seemed unlikely that ocean waves reflecting off the island and/or the Southern California shore 60 miles away could produce such a strong effect, 3) the patterns were seen equally strong at horizontal and vertical polarizations, and 4) there was an absence of corresponding disturbances in the Doppler velocity field. The observations during this particular event, as well as others, were accompanied by strong marine inversions below the level of the radar, 573m MSL.

The hypothesis that was confirmed by the results of calculations reported here was based on a standing wave on the strong Southern California marine inversion in the lee of the island causing variations in grazing angle at the surface as well as causing local enhancements (focussing) of incident energy at the surface. The wind was normal to the axis of the island and the stationary pattern in the radar image. A ray trace calculation was performed with a modeled 2D field of modified refractive index that was based on a nearby sounding. A 50 M unit notch in the profile was modeled with a linear variation plus a Gaussian curve matched to the observed sounding and the notch was varied sinusoidally in height with a 1 km wavelength and with only a ±10 m variation in height.

The ray trace through this refractivity field produced periodic variations in local grazing angle by .4°, sufficient to account for the 15 dB signal strength variations in the image.

F4-6
1540

ALONG-TRACK INTERFEROMETRY: TECHNIQUES AND OCEAN APPLICATIONS

Richard E. Carande
Vexcel Corporation
2455 55th St
Boulder, CO 80301

Synthetic Aperture Radar (SAR) has been used extensively by the ocean remote sensing community to probe the surface of the ocean on a moderate to high resolutions scales. Observations which have been made include those on wave spectra, internal waves, current effects, wind effects to name but a few. Interferometric SAR can in many cases improve these measurements, but of possibly more importance and interest, can provide data which may be used to make new measurements. In this paper the Along- Track Interferometer (ATI) technique is described, followed by several examples of oceanographic applications of the technique using data acquired with an L-Band ATI system. Examples include measurements of currents, modulation of Doppler shifted means by local winds, wave height estimations and surface coherence time. Techniques involving multiple baselines for estimating ocean surface coherence times are compared to techniques which rely upon a single baseline. Prospects for future improvements which will allow true vector measurements of the oceans response to the interferometer will be discussed.

Finally, the potential development of a spaceborne along-track synthetic aperture radar system is examined and the unique challenges associated with the ATI technique from space are discussed. The possibility of designing a dual-use platform capable of acquiring both along-track and across-track interferometric data is presented. This two platform interferometric SAR can provide both the oceanographic community with interferometric SAR data in the along-track mode for ocean applications, and the land mapping community with accurate height models using cross-track interferometric acquisition techniques.

F4-7
1600

MEASUREMENTS OF OCEAN WAVES AND MARINE SURFACE WINDS USING HIGH-FREQUENCY DOPPLER RADAR

Hans C. Graber(1), Donald R. Thompson(2), Brian K. Haus(1) and Robert E. Jensen(3)

(1)Division of Applied Marine Physics
Rosenstiel School of Marine and Atmospheric Science
University of Miami, Miami, Florida 33149, USA
(2)Applied Physics Laboratory
The Johns Hopkins University
Laurel, Maryland, 20723, USA
(3)Waterways Experiment Station, U.S. Army Corps of Engineers
Coastal Engineering Research Center
Vicksburg, Mississippi 39180, USA

A high-frequency (25.4 MHz) ground-wave ocean surface current radar (OSCR) was deployed for two experiments of the North Carolina coast covering a domain of about 1000 km^2. The spatial resolution of the radar was about 1 km and provided real-time maps of surface vector currents at 20 minute intervals. The Doppler spectrum was also recorded along each beam of the phased antennae receiving array which produced 700 cells within the domain. From the sets of radial Doppler spectra time series of surface vector currents, wind speed and direction and ocean wave heights are determined at each cell. During the High Resolution Remote Sensing Experiment (HIRES-II) which took place off Cape Hatteras in June 1993, two directional wave buoys were moored within the OSCR domain measuring atmospheric parameters and directional wave spectra. The winds were generally low with occasional bursts originating from summer thunderstorms. The wave field was dominated by westward propagating swell with a small, locally generated windsea. In contrast, the nearshore wave and sediment transport experiment, DUCK94, was carried out in October 1994 which experienced several storm systems during the 30 day deployment of OSCR. In particular, a mid-month Nor'easter brought winds in excess of 15 m/s to the region for several days and generated wave heights above 6 m. A linear pressure gauge array in 8 m water depth and a directional wave buoys over the inner shelf measured directional wave spectra. Coincident observations of directional wave spectra, near-surface currents and marine surface winds from the buoys are used to evaluate the capability of the HF radar to provide not only surface vector currents, but also mean parameters of the directional wave spectrum and the surface wind vector. The comparison will quantify the accuracy of the radar derived sea state and boundary-layer wind parameters for a wide range of wind and wave conditions.

F4-8
1620

SURFACE WIND SIGNATURES IN SPACEBORNE SAR

Robert C. Beal
The Johns Hopkins University
Applied Physics Laboratory
Johns Hopkins Road
Laurel, Maryland 20723
email: r.beal@jhuapl.edu

Spaceborne SAR is potentially a high resolution imaging scatterometer. Through spatial modulation of the surface scatterers, SAR ocean surface signatures contain clear manifestations of: 1) the surface wind field, 2) surface current and/or thermal boundaries, and 3) the spatial evolution of surface waves. These surface signatures are seldom directly linked to geophysical quantities of interest. For example, the wind signature can be masked by atmospheric instability. Auxiliary information is often necessary to determine the backscatter directional dependence, although sometimes the imagery itself reveals this dependence. Surface current or thermal signatures can be displaced from the subsurface current. In the higher altitude SAR satellites, such as ERS-1/2 and Radarsat, surface wave imaging is distorted by Doppler remapping of the moving scatterers.

To extract useful information from spaceborne SAR, the distinguishing signatures of the various geophysical quantities must be recognized: how they interact, how they might be separated and partitioned, and how certain types of signatures can be irrepairably distorted or confused. Spaceborne SAR imagery can be significantly enhanced by blending it with other data sources, such as infrared imagery, conventional scatterometers and altimeters, and various in situ estimates. In many cases, especially at lower winds, the stability of the atmospheric boundary layer plays a significant part in determining the backscatter. Using ERS-1 imagery collected over the North Atlantic during April and May 1992, this paper will present some of thepotential and limitations of spaceborne SAR for ocean applications, especially emphasizing its high resolution wind monitoring capabilities.

F4-9
1640

ANALYSIS OF MARINE ATMOSPHERIC BOUNDARY LAYER PHENOMENA FROM SYNTHETIC APERTURE RADAR SIGNATURES

George S. Young and Todd D. Sikora
Department of Meteorology, Pennsylvania State University

Synthetic aperture radar (SAR) imagery of the ocean surface frequently contains pronounced signatures of atmospheric phenomena in addition to the signatures of a variety of oceanic phenomena (T.W. Gerling, J. Geophys. Res., 91, 2308-2320, 1986). These atmospheric signatures result from local variations in the wave field caused by corresponding variations in the surface stress. Thus, the atmospheric signatures result from the distribution of turbulence within the atmospheric boundary layer. This relationship can be used to determine the nature of the turbulence-modulation phenomena present within the marine atmospheric boundary layer (MABL) from the form of their SAR signatures. Moreover, quantitative estimates of such useful parameters as MABL depth and stability can be made from the SAR imagery via existing similarity theories relating the horizontal scale and degree of the turbulence modulation to the fundamental scaling parameters of MABL turbulence.

Modulation of the surface stress by boundary-layer spanning convective cells results in a mottling of the SAR image with high backscatter being associated with the more intense surface stress under high-momentum convective downdrafts (T.D. Sikora et. al, Mon. Wea. Rev., in press). Boundary layer depth can be diagnosed from the horizontal scale of these SAR signatures as mixed layer similarity theory dictates that the convective cells' horizontal dimensions scale with the boundary layer depth Quantitative estimates of this horizontal scale are made by two-dimensional spectral analysis. The boundary layer depth is then estimated as 2/3 of the wavelength of the spectral peak (J.C. Kaimal et al, J. Atmos. Sci., 33, 2152-2169, 1976).

Mixed layer similarity theory can be applied to other aspects SAR convective signatures to estimate MABL turbulence intensity and quantify the related MABL stability. This approach relies on the links between SAR backscatter, surface stress, and surface wind speed. Two meteorological factors complicate these relationships. First, the wind direction must be known to reasonable approximation to achieve an unambiguous relationship between SAR backscatter and surface stress. Second, the MABL stability must be known quantitatively as it controls the relationship between wind and stress.

The signatures' orientation provides information on the mean boundary layer wind direction. This orientation can be determined from two-dimensional spectral analysis. Quantifying the MABL stability requires a more complicated iterative approach. The basis of this approach is the Monin-Obukhov atmospheric surface layer similarity theory relating the variability (standard deviation) of wind speed to the mean wind speed. The MABL surface layer stability is the controlling parameter in this similarity relation as it is in the relation between wind speed and surface stress (and thus, via the scatterometer equations, SAR backscatter). This set of equations is solved iteratively as follows. First, SAR statistics are related via stability-dependent scatterometer equations to the wind speed and its variability and then these quantities are used in turn to improve the estimate of the MABL stability to be used in the next iteration of the SAR scatterometer equations.

F4-10
1700

AIRBORNE ALTIMETRY EXPERIMENTS OVER THE GREENLAND ICE SHEET

Rudolf A. Pawul* Prof. Calvin T. Swift
Microwave Remote Sensing Laboratory
Knowles Engineering Bldg.
University of Massachusetts
Amherst, MA 01003
Dr. Ellen J. Ferraro
System Design Laboratory
Raytheon Company
430 Boston Post Rd.
Wayland, MA 01778

The Advanced Airborne Flight Experiment (AAFE) altimeter is a Ku-band pulse compression radar altimeter originally built by Hughes Aircraft and later refurbished by the Microwave Remote Sensing Laboratory at the University of Massachusetts. During 1991, 1993 and 1994, the AAFE altimeter participated in the NASA sponsored Arctic Ice Mapping Experiments over the Greenland ice sheet. It was installed, along with NASA laser altimeters, in a NASA P-3 aircraft under similar conditions for each of the three years. Also aboard the aircraft were Global Positioning System (GPS) receivers which allowed several flight lines from the first year to be accurately repeated. In addition, the GPS receivers calculated the aircraft's altitude above the ellipsoid, a reference around the surface of the earth. Thus, using the AAFE altimeter's results to determine the altitude of the aircraft above the ice sheet, we are able to investigate annual variations in surface elevation which may be attributed to a growth or decay of the ice sheet during the available time period.

This paper will contain a description of these field experiments as well as a study of the results from the AAFE altimeter for repeated flight lines over the three year period. The Greenland ice sheet consists of different diagenetic zones, which all have varying scattering properties. A section will also be devoted to the effect of these zones on the waveform retracking algorithm. Moreover, we will examine measurements from the accompanying NASA Airborne Oceanographic Lidar (AOL), a scanning laser altimeter, and compare results with the AAFE altimeter where they are applicable.

G/H3-1
1400

GENERATION OF IONOSPHERIC DENSITY STRIATIONS AT THE TEN-METER SCALE BY THE ARECIBO HF HEATER*

S. P. Kuo and J. Huang
Weber Research Institute
Polytechnic University
Farmingdale, NY 11735
M. C. Lee
Plasma Fusion Center
Massachusetts Institute of Technology
Cambridge, MA 02139

Generation of ionospheric density irregularities by high power HF waves has been investigated extensively in the so-called ionospheric heating or modification experiments. In the early heating campaign, these density irregularities were detected by ground-based HF/VHF/UHF radars or by scintillation measurements of beacon satellite signals. HF/VHF/UHF backscatter radars can only measure density irregularities with small to medium scale sizes that are half the wavelengths of radar signals. By contrast, scintillation measurements detect large-scale density irregularities with a broad spatial spectrum, typically with scale lengths ranging from hundreds of meters to a few kilometers.

During the recent El Coqui heating campaign at Arecibo, Puerto Rico, rocket probes were used to perform in-situ measurements of HF heater wave-induced density irregularities in the ionospheric F-region. It was surprisingly found that density irregularities have filament-like structures along the geomagnetic field line with spacing around 15 meters. This filament structure of density irregularities has a very large ratio of the parallel to perpendicular scale lengths. The amplitudes of these density irregularities were estimated to have a mean value of 6% of the background plasma density.

In the present work, parametric excitation of the heater-induced intense Langmuir waves into ion Bernstein waves and daughter Langmuir waves is investigated. It is used to explain the formation of the above-mentioned ten-meter scale ionospheric density striations. We have found that the nonlinear beating current plays a dominant role in the source mechanism to produce ion Bernstein waves, forming ionospheric density striations. Analysis of thresholds and growth rates shows that ten-meter scale ion Bernstein modes can be preferentially excited in agreement with the rocket experiments in the El Coqui Campaign.

* Work supported by NSF.

G/H3-2
1420

REMOTE SENSING OF THE THERMOSPHERE USING OPTICAL EMISSIONS PRODUCED BY HIGH POWER RADIO WAVES

M. Wong P. A. Bernhardt*
Beam Physics Branch
Plasma Physics Division
Naval Research Laboratory
Washington, DC 20375
L.S. Wagner J.A. Goldstein
Information Technology Divison
Naval Research Laboratory
Washington, DC 20375
C.A. Selcher
Physics Department
West Virginia University
Morgantown, WV 26506

Optical emissions excited using high power radio waves in the ionosphere can be used to measure a wide variety of parameters in the thermosphere. Powerful high frequency (HF) radio waves produce energetic electrons in the region where the waves reflect in the F-region. These hot or suprathermal electrons collide with atomic oxygen atoms to produce localized regions of metastable $O(^1D)$ and $O(^1S)$ atoms. These metastables subsequently radiate 630.0 and 557.7 nm, respectively, to produce artificial airglow clouds. The shapes of the airglow clouds are determined by the structure of large-scale ($\approx$ 10 km) plasma irregularities that develop during ionospheric heating. When the HF wave is operated continuously, the motion of the airglow clouds follows the ExB drift of the plasma. When the HF wave is turned off, the airglow clouds expand by decay by collisional quenching and radiation, expand by neutral diffusion and drift in response to neutral winds. By monitoring the evolution of artificial airglow clouds under conditions of continuous and switched radio wave heating, the electric fields, neutral wind vectors, diffusion coefficients and neutral densities in the upper atmosphere may be measured. This technique is illustrated using data that were obtained in March of 1993 and 1995 at the ionospheric modification facility near N. Novgorod, Russia. Analysis of artificial airglow clouds yields zonal plasma drifts of 70 m/s eastward at night. The zonal neutral wind speed is estimated to be 96 m/s and the $O(^1D)$ diffusion coefficient was determined to be between 0.8 and 1.4 x 10^{11} cm^2/s at 260 km altitude. The quenched lifetime of the $O(^1D)$ was determined to be 29.4 seconds. From the diffusion and quenching rates, the atomic and molecular concentrations in the thermosphere can be determined.

G/H3-3
1440

THE EFFECTS OF PLASMA HEATING ON THE BROAD UPSHIFTED CONTINUUM IN THE SPECTRA OF STIMULATED ELECTROMAGNETIC EMISSIONS

L.S. Wagner* J.A. Goldstein
Information Technology Divison
Naval Research Laboratory
Washington, DC 20375
P. A. Bernhardt
Beam Physics Branch
Plasma Physics Division
Naval Research Laboratory
Washington, DC 20375
C.A. Selcher
Physics Department
West Virginia University
Morgantown, WV 26506
V.L. Frolov, E.N. Serveev
Radiophysical Research Institute, N. Novgorod, USSR

Ionospheric heating experiments were conducted in March and April of 1995 at the SURA research facility of the Radiophysical Research Institute of Nizhniy Novgorod, in Russia. These experiments, using between 100 and 200 MW effective radiated power between 4.3 and 6.0 MHz, were designed to investigate stimulated electromagnetic emission (SEE) observed from the ground. The SEE spectra contained both broad upshifted and downshifted continuum when the heating frequency was near the third harmonic of the electron cyclotron frequency. If the O- mode pump frequency (f_0) was slightly higher than the nth gyro harmonic (i.e., n f_H), then the primary SEE feature was the broad upshifted maximum or BUM. Effects due to the interaction of two or more O-mode pump frequencies were recorded as well as self-interaction involving a single O-mode pump frequency. The observations indicated that the BUM was suppressed by either a second O-mode or X-mode pump. The elevation of the electron temperature by radio wave heating may be responsible for the reduction of the BUM amplitude. In addition, the BUM amplitude and spectral shape are dependent upon the pump frequency and the pump power. We have also observed early time transient effects and their inhibition by ionospheric preconditioning. These observations of SEE may be connected with small-scale, field-aligned irregularities produced by thermal parametric instabilities. The magnitude of preconditioning on the SEE features could be a measure of the lifetime for irregularities and elevated temperatures in the ionosphere.

G/H3-4
1500

DETECTION OF ARTIFICIAL PLASMA INHOMOGENEITIES IN THE LOWER THERMOSPHERE AND MESOSPHERE ABOVE HIPAS

F. T. Djuth[1], K. M. Groves[2], J. H. Elder[1], J. Villasenor[3], J. M. Quinn[2], A. Y. Wong[3]
[1]Geospace Research, Inc., 550 N. Continental Blvd., Suite 110, El Segundo, CA 90245
[2]Phillips Laboratory, GPIA, Hanscom Air Force Base, MA 01731
[3]Department of Physics, HIPAS Observatory, University of California, Los Angeles, CA 90024

Results from recent experiments aimed at establishing the feasibility of using high-powered, high-frequency (HF) radio waves to probe the lower thermosphere/mesosphere are presented. The measurements were made at the High-Power Auroral Stimulation (HIPAS) Observatory located near Fairbanks, Alaska. The principal objective was to use artificial electron density perturbations created in the auroral environment to determine the properties of the background neutral gas between ~70 km to ~140 km altitude. Observations of this nature have been previously reported from the midlatitude SURA facility near Nizhny Novgorad, Russia [e.g., Belikovich *et al., Radiophys. Quantum Electron., Engl. Transl., 21,* 985, 1978; Belikovich *et al., Geomag. Aeron, 26,* 705, 1986]. The measurement technique relies on the production of so-called "artificial plasma inhomogeneities" (API) in the altitude region(s) of interest. These induced irregularities are thought to be horizontally stratified and conform to the standing wave pattern produced by the reflection of the powerful HF wave in the ionosphere. In the lower ionosphere (*D* and *E* regions) electron thermal forces are believed to drive the electron density irregularities.

Information about the neutral atmosphere in the auroral region is obtained by measuring the relaxation time of the induced irregularities and the Doppler shift of the backscatter echoes. By monitoring the relaxation characteristics of the API backscatter at altitudes ≥ 80 km, altitude profiles of the ambipolar diffusion coefficient can be constructed (from which neutral density/neutral temperature profiles can be deduced). At lower altitudes, electron attachment processes become important, and the interpretation of the results is more complex. Doppler measurements of vertical motion yield information about the gravity wave spectrum and mean vertical wind in the lower atmosphere. In the initial HIPAS experiments presented here, independent altitude profiles of the relaxation time constant and echo Doppler shift are made every 30 s.

In general, the observations confirm that artificial plasma inhomogeneities can be an effective diagnostic of neutral gas motion, neutral density, and/or neutral temperature. The location of HIPAS in the auroral region makes such measurements very interesting from a geophysical perspective.

G/H3-5
1540

STEREOGRAPHIC IMAGING OF IRREGULARITIES ASSOCIATED WITH HEATED REGIONS IN THE IONOSPHERE

Gary S. Sales and Arjang Noushin
Center for Atmospheric Research
University of Massachusetts Lowell
Lowell, MA. 01854

The Digisonde, operating in the "drift" mode inbetween ionograms, using the Doppler interferometry technique developed at the Center for Atmospheric Research, is able to identify and locate individual reflecting sources within the ionospheric structure. Normal operation involves a single sounder operating in the vicinity of structured ionospheric irregularities such as polar patches, ionospheric modification regions and equatorial airglow depletion bands. The effort, here, is concentrated on probing artificially heated regions of the F-region of the ionosphere where electron density irregularities in the plasma are generated by processes that transfers energy from the high power pump into the formation of irregularities.

This paper describes a stereographic imaging technique that makes it possible to determine the location of the irregular structures and the distribution of velocities associated with the ionospheric irregularities formed during the heating process. The simulations carried out here involves two sounders separated spatially by about 90° in azimuth and each some 50 to 100 km from the high power pump site.

The spatial extent of the pump wave in the F-region of the ionosphere is determined, basically by the "heater" antenna pattern. For these simulations it was assumed that the heater illuminates a 100 km x 50 km area in the F-region at an altitude of 250 km; the long axis is in the N-S direction. The energy in the pump wave is coupled to the ionospheric plasma and stimulates the growth of ionospheric irregularities with scales from the order of kilometers down to meters.

The study presented here is aimed at simulating HF sounding and HF/VHF radar probe experiments to better plan the operation and better understand the results. Using a simple model of the heated region of the ionosphere; i.e., assuming it contains a full spectrum of irregularities and together with a three dimensional ray tracing code, calculations are carried out to simulate both vertical soundings as well as oblique HF and VHF (up to 50 MHz) radar probing.

For the situation when the irregularities are produced by high power heater, the velocities are expected to be relatively random and spatially restricted. The proposed stereographic technique allows the "same" irregularities to be observed from different directions and a resultant horizontal velocity component uniquely determined for each source. Then the distribution of sources leads to the characterization of the Doppler spectrum spreading of the scattered signal.

G/H3-6 1600

HF RADAR AND DOPPLER SPECTRUM INVESTIGATIONS OF AIT (PRELIMINARY RESULTS)

Yu.M. Yampolski, V.S. Beley, S.B. Kascheev, and A.V. Koloskov,
Institute of Radio Astronomy
National Academy of Sciences of Ukraine
4 Chervonopraporna Street
310002 Kharkov, Ukraine
D. Hysell,
Clemson University, Department of Physics and Astronomy
Clemson, SC 29634-1911
B. Isham,
Arecibo Observatory
Box 995, Arecibo PR 00613-0995 Puerto Rico
and V.G. Somov,
Kharkov State University,
4 Svobody Square,
310077 Kharkov, Ukraine

Results from radar measurements of Artificial Ionospheric Turbulence (AIT) in the HF band are presented. The experimental campaign was carried out in March, 1995. The AIT was stimulated by the powerful Sura HF ionospheric modification facility (located near Nizhni Novgorod, Russia) transmitting in the 4 to 9 MHz frequency range. The probe signal was provided by a special transmitter at the Kharkov State University Observatory, with an operating frequency of about 15-20 MHz. The receiving site was located approximately 40 kilometers from the transmitter at the RINAN observatory. The bistatic radar was characterized by high frequency stability, which allowed measurements of the Doppler frequency shift, and high spatial selection, implemented in the pulsed mode through the proper choice of the pulse parameters and the use of the large receiving antenna array of the UTR-2 (Ukrainian T-shaped Radio Telescope 2), whose T-shaped antenna aperture is 1 by 2 kilometers in size. The average distance between UTR-2 and the Sura HF transmitter was about 1000 km. The time-delay resolution was 100 mcs (spatial pulse length 15 km). The angular resolution and accuracy of the Doppler frequency measurements were about 0.7 degree and 0.025 Hz, respectively. An eight-channel coherent receiver allowed investigating the radar signal scattered by the artificial turbulence simultaneously within different beams of the multibeam pattern of UTR-2. It enabled analyzing the fine structure of the AIT both in the horizontal and vertical plane. In all about 100 hours of observations of artificial ionospheric turbulence have been carried out.

The main results obtained during the campaign are as follows:

1. Large-scale spatial splitting of the AIT domain during steady-state HF modification was observed.
2. Quasi-periodic variations of the spatial and time characteristics of the AIT are likely due to natural wave processes in the ionosphere such as internal gravity waves and Pc pulsations.
3. Splitting of the Doppler spectra during steady-state HF modification and during the relaxation stage may be caused by radial drift of the turbulence.
4. Repeated periodic bursts of the scattered probe signal intensity sometimes occur during the AIT relaxation stage. A possible cause of this behavior is the generation of artificial Pc III geomagnetic pulsations.
5. The data allowe us to estimate the AIT relaxation time.

G/H3-7
1620

HEATER-MAINTAINED SPREAD F PHENOMENA OVER ARECIBO

M.J. Starks* M.C. Lee
Plasma Fusion Center
Massachusetts Institute of Technology
Cambridge, MA 02139

Our recent experiments at the Arecibo Observatory have indicated a possible link between gravity wave-seeded spread-F and subsequent maintainance of the resulting ionospheric plasma density structures by HF heating. Specifically, in two heating experiments during August 1992 spread-F was observed via Digisonde profiles to appear after tens of minutes of heating. This spreading persisted until the heating was suspended, whereupon it rapidly disappeared. The effect could not be reproduced on either night by reapplication of the RF despite hours of heating.

Time plots of density contours over the observatory suggest the presence of acoustic gravity waves during the heating campaign. It is proposed in this work that gravity waves may seed the Perkins' instability (F. Perkins, *J. Geophys. Res.*, **78**, 218, 1973) as described in Huang, *et al.* (*Radio Sci.*, **29**, 395, 1994). Structures with wave vectors oriented perpendicular to the magnetic meridian plane are not detectable by ionosonde (Kuo *et al., Radio Sci.*, **20**, 546, 1985). These seeded spread-F structures may be initially undetected as a result of such an orientation. HF heater waves could then reorient and maintain the structures via a mechanism such as the thermal filamentation instability (Lee and Kuo, *Radio Sci.*, **20**, 539, 1985), even after the seeding gravity wave departs.

No electric field data exists to verify the correct ambient conditions for operation of the Perkins' instability during our 1992 heating campaign. Our new heating experiments at the Arecibo Observatory are scheduled for late January 1996 and will attempt to observe the electric field configuration, the presence of gravity waves, and the formation and amplification of spread F structures (Lee *et al.*, 1995, scheduled Arecibo experiments in Jan. 1996). Analysis of heater-wave interactions with the spreading process will provide estimates of growth rates and the extent of amplification.

Session G/H-4, 1355-Thurs., CR2-6
MID-LATITUDE IONOSPHERIC INEQUALITIES
Chairperson and Organizer: A.R. Jacobson, Space and Atmospheric Sciences Group, Los Alamos National Laboratory, Los Alamos, NM 87545

G/H4-1
1400

MILLSTONE HILL OBSERVATIONS OF MID/LOW-LATITUDE TRANSIENT TROUGHS

J. C. Foster
Atmospheric Sciences Group
MIT Haystack Observatory
Westford, MA 01886

Meridian-plane elevation scans with the Millstone Hill incoherent scatter radar provide evidence of a strong perturbation of the coupled magnetosphere-ionosphere system during the early phases of the November 4, 1993 magnetic storm. This event is the subject a detailed study under the National Space Weather initiative. The mid and auroral-latitude ionosphere was greatly perturbed as high-density solar plasma, embedded in a high speed solar wind stream, impacted the magnetosphere late on Nov. 3, 1993. A narrow ionospheric trough formed at L=3.5 in the pre-midnight sector and particle precipitation produced elevated electron temperatures and enhanced ionization immediately poleward of the trough. The most pronounced radar signature was a brief (20-min) uplifting of the *F* region equatorward of the trough, such that the peak altitude increased with distance away from the trough. A similar signature had been observed under similar circumstances on March 20, 1990 and in that event a second, low-latitude (L=2), ionospheric trough, co-located with a discrete region of sunward plasma convection, was observed by the radar and the DMSP F9 satellite. During the November 4, 1993 event, the DMSP F10 satellite observed narrow, magnetic conjugate regions of strong horizontal and upward plasma velocity (> 1500 m/s) at L=1.25 at 00:30 UT, the time of the uplifting of the mid-latitude *F* region observed by the radar. These observations were confined to longitudes near the South Atlantic magnetic anomaly and the ionospheric perturbation was temporally coincident with a severe perturbation of the energetic particle population in the inner magnetosphere.

The observed plasma drift characteristics suggest that the low-latitude troughs are related to supersonic equatorial bubbles, triggered at a somewhat higher latitude by the upward **ExB** drift associated with the storm-induced occurrence of an eastward electric field which is also responsible for the observed uplift of the *F* layer.

G/H4-2
1420

TOMOGRAPHIC INVERSION OF MIDLATITUDE AIRGLOW STRUCTURES

J. Semeter* M. Mendillo
Boston University Center for Space Physics
725 Commonwealth Avenue
Boston, MA 02215

Photometers, spectrometers, and imagers comprise the traditional optical diagnostic components of aeronomic science. As passive detectors of line-of-sight emissions they describe integrated characteristics of a region under study. The CEDAR Optical Tomographic Imaging Facility (COTIF) represents a natural evolution for ground based aeronomy. Using CCD-based measurements of optically thin emissions from multiple locations, two dimensional volume emission rate profiles can be reconstructed [ε(height, Long/Lat)] through tomographic inversion. Determination of the altitude-dependence of optical emissions will contribute to our understanding of the physical processes governing diffuse aurora, discrete auroral arcs, Stable Auroral Red (SAR) arcs, gravity waves, equatorial spread-F plumes, and active experiments.

The first field test of COTIF was conducted during Winter-Spring 1995 and targeted midlatitude airglow structures at 6300Å. Four meridional imaging spectrographs were placed along a line extending from Block Island, RI to Carribou, ME (roughly demarcating the midlatitude trough region). A reconstruction algorithm has been developed to address the limited angle nature of these observations. The technique involves optimizing Chapman-like production profiles at discrete latitudes and subsequently refining the volume emission rates using maximum entropy. The first six months of COTIF observations produced several interesting test data sets for this technique. We present here two examples of reconstructed volume emission rate profiles: a SAR Arc observed on 5 March 1995, and diffuse aurora, ambient aiglow, and the main trough observed on 2 May 1995.

G/H4-3
1440

MU RADAR OBSERVATIONS OF MIDLATITUDE F-REGION TID'S, GRADIENTS, AND IRREGULARITIES

W. L. Oliver
National Center for Atmospheric Research
P. O. Box 3000
Boulder, CO 80307-3000
S. Fukao
Radio Atmospheric Science Center
Kyoto University
Uji, Kyoto 611 Japan

By observing the ionospheric F region simultaneously in four different beam directions with the MU radar, we have been able to track the passage of TID's, measure the horizontal gradients that they cause in the F layer density, and deduce the propagation characteristics of the neutral-atmosphere gravity waves causing these effects. It appears that the ionosphere is essentially always awash in gravity waves detectable by the MU radar. These ever-present waves have wind perturbations of less than 10 m/s and produce electron density perturbations of about 3%. Statistically they show a slight preference for southward travel, but on a given day can come from any direction, and usually come for hours on end from a constant source direction. They only infrequently show a pattern of rotation of travel azimuth throughout the day as might be expected if the waves experience filtering according to the direction of the background wind. The wave fronts are slanted vertically with a downward component of phase propagation (upward energy propagation) below 300 km altitude but then gradually steepen and become vertical above 400 km altitude owing to viscous disipation. The wave speed is about 200 m/s and largely independent of wave period within the range of periods 60 to 130 minutes in the lossless region below 300 km altitude. There is little variation in this speed with time of day, season, or solar or magnetic activity, although winds on disturbed summer mornings, when the F region neutral density is lowest, do show a slightly higher speed.

Ocassionally waves with much larger amplitudes appear in conjunction with sudden storm commencements at high latitudes.

These gravity waves are thought to seed the F region instability structures observed with the MU radar on summer nights at solar minimum. The gravity-wave undulations are thought to grow by the Perkins mechanism to form instabilities, the growth rate for which is greatest when the neutral density is smallest.

G/H4-4 1500 EVENING, SUMMER TOTAL-ELECTRON-CONTENT DISTURBANCES IN THE GRAVITY-WAVE FREQUENCY RANGE

Abram R. Jacobson
Space and Atmospheric Sciences Group
Mail Stop D466
Los Alamos National Laboratory
Los Alamos, NM 87545

The Los Alamos satellite-beacon array comprises nine radio-interferometer stations illuminated by 136-MHz carriers from several geosynchronous satellites. The instrumental noise level corresponds to less than 10^{13} m^{-2} in TEC, so even very weak disturbances, not just the dominant TIDs due to thermospheric gravity waves, can in principle be detected and characterized. In practice, the limitation on detecting weak non-TID irregularities is imposed not by instrumental noise, but rather by signal competition from the TID background level. Thus, during winter daytime, when thermospheric gravity waves are most in evidence, it is impractical to observe other sorts of disturbances unless they are significantly higher in frequency than the 0.3 - 1.5 milliHz band of maximum TID TEC disturbances. We see high-frequency (> 2 milliHz) disturbances and have shown that they are due to field-aligned irregularities in the plasmasphere, but we have not during winter daytime been able to see if the plasmaspheric irregularities also appear at lower frequencies.

On the other hand, during Summer, the TID background is relatively weak, and it is possible to observe a clear continuum between the still-present high-frequency disturbances, and a lower-frequency (<1.5 milliHz) extension which has very similar properties. This lower-frequency disturbance is common in evening, peaking at 16-21 h local time. We will present the observational evidence about these lower-frequency TEC disturbances and will show how they are likely not thermospheric gravity waves, despite their gravity-wave frequency range. Rather, they appear to be low-altitude manifestations of plasmaspheric irregularities, and thus to be moving with an $\mathbf{EXB}/B^2$ drift as do the entire fluxtubes on which the irregularities reside.

G/H4-5
1540

ELECTROBUOYANCY WAVES: THE PERKINS ELECTRODYNAMICS RESPONSE TO THERMOSPHERIC GRAVITY WAVES

Clark A. Miller*
Center for Science and International Affairs
John F. Kennedy School of Government
79 John F. Kennedy St.
Cambridge, MA 02138
Michael C. Kelley
School of Electrical Engineering
304 Engineering and Theory Center
Cornell University
Ithaca, NY 14853

Most observers and theorists of traveling ionospheric disturbances (TIDs) have assumed TIDs to be passive ionospheric responses to atmospheric gravity waves. Gravity wave winds simply push the ionospheric plasma up and down the Earth's magnetic field lines. In this paper, we argue that this assumption is simply wrong. By moving the ionospheric plasma along the Earth's magnetic field lines, gravity waves alter the conductivity of the ionosphere and, as a result, produce an essential electric field response. This electric field response occurs for both resonant and non-resonant gravity wave / ionosphere interactions and acts to damp some disturbances and enhance others. The azimuthal filter produced by the interaction is identical to that observed in a wide variety of studies of nighttime, medium-scale traveling ionospheric disturbances at mid-latitudes. Additionally, the existence of electrodynamically driven propagating disturbances has been confirmed by observations.

G/H4-6
1600

SUPERDARN OBSERVATIONS OF TRAVELING IONOSPHERIC DISTURBANCES

W. A. Bristow
The Johns Hopkins University Applied Physics Laboratory
Johns Hopkins Rd
Laurel MD, 20723-6099

Traveling ionospheric disturbances (TIDs) have been studied using the Goose Bay HF radar since the original work by Samson et al. (Geophys. res. Lett., 16, 875-878,1989). Samson demonstrated that power enhancements and decreases propagating through the radar's field of view were caused by gravity waves perturbing iso-electron density contours of the F-region ionosphere. These perturbations focus and defocus the HF radar waves causing power enhancements and decreases that propagate with the gravity wave phase fronts. The large spatial field of view of the Goose Bay radar allowed the first observations of gravity wave phase fronts over a continuous extended area.

We have extended the Goose Bay observations using the radars that comprise the SuperDARN radar network. The radar network provides a new opportunity to observe gravity wave propagation over a large spatial area. At the time of this writing, data were available from four northern hemisphere radars: Goose Bay, Labrador; Saskatoon, Saskatchewan; Kapuskasing, Ontario; and Stokkseyri, Iceland. With these four radars we observe waves over approximately an 80 degree longitude sector, from about -30 degrees east longitude to about -110 degrees east longitude between about 50 degrees and 80 degrees magnetic latitude.

Although the SuperDARN radars are located at high latitudes, the observed TIDs often propagate southward toward middle latitudes. Many of the mid-latitude TIDs observed by other experiments may have a high-latitude source, and in fact may be some of the same waves observed by SuperDARN. In this presentation, SuperDARN TID observations will be reviewed and the wave characteristics will be discussed. Implications for mid-latitude TID observations will be discussed.

G/H4-7
1620

MIDLATITUDE RESPONSE TO GEOMAGNETIC ACTIVITY — RED-LINE INTENSITIES AND WINDS AT BEAR LAKE OBSERVATORY

Vincent B. Wickwar[(1)], Ian K. Monson[(1)], David Rees[(1,2)]
(1) Center for Atmospheric and Space Sciences
Utah State University
Logan, UT 84322-4405
(2) Hovemere, Ltd., Bromley, Kent, UK

An extremely sensitive Fabry-Perot interferometer has been used since 1991 to observe the thermospheric O(^{1}D) emission at 630-nm above Bear Lake Observatory (41.9° N, 111.4° W, 50 Λ). These observations have yielded detailed results on the relative intensity and the neutral wind. The most prominent feature of these observations has been a large response to geomagnetic activity, i.e., for Kp ≥ 4. (1) There is a large increase in the relative intensity that starts in the N and NE, and can extend equatorward over much of the sky—a range of approximately 10 Λ. (2) There is a large neutral wind from the east toward the west, which in the evening sector is indicative of a strong westward ion velocity or, equivalently, a large northward electric field. These effects are strongest in the north, but can extend over most of the sky: the winds can reach 500 m/s. (3) There is a large meridional neutral wind toward the south that again is strongest in the north and can cover much of the sky. The elements of this response do not fit with our current knowledge of the behavior of the equatorward boundary of the auroral oval, and hence of particle precipitation, or our current knowledge of SARarcs (even with the SAID extension). We will present the observations, and compare and contrast them with possible explanations.

G/H4-8
1640

DESCENDING LAYERS, SPORADIC E, AND QUASI-PERIODIC RADAR ECHOES

R. T. Tsunoda,[1] S. Fukao,[2] M. Yamamoto[2]
[1] Geoscience and Engineering Center, SRI International
Menlo Park, California 94025
[2] Radio Atmospheric Science Center, Kyoto University
Uji, Gokanosho, Kyoto 611, Japan

Three features have often been observed in the nighttime midlatitude ionosphere: descending layers, sporadic E, and quasi-periodic radar echoes from field-aligned irregularities. These features are interesting because the source mechanism for each phenomenon is not well understood and, as a group, they appear to be interrelated. That is, descending layers have been observed to form at the base of the F layer and to move downward into the E region where they often take the form of sporadic E layers. And quasi-periodic echoes have been shown to arise from irregularities imbedded in sporadic E layers. Using incoherent scatter and magnetic-aspect sensitive backscatter measurements obtained with the MU radar (located in Japan), we show that the ionospheric electric field appears to play a major role in the occurrences of all three phenomena. We show that a descending layer could be produced by the accumulation of metallic ions by the electric field during the course of a day. Because of this gathering process, the descending layer turns out to be the primary supply of metallic ions that are delivered to the E region where sporadic E layers can form from tidal wind shears. Quasi-periodic radar echoes are then a consequence of the above features that have been altitude modulated by an atmospheric gravity wave. Electric field control of the metallic-ion supply, which appears as a descending layer at deterministic times, is shown through ion trajectory simulations using the electric field measured by the MU radar as the input. We show that this control can account for the seasonal and diurnal variations found in the morphology of sporadic E, features that cannot be accounted for by simply invoking wind-shear theory. Given that descending layers, which evolve into sporadic E layers, lead to the production of quasi-periodic radar echoes, we can use this scenario to search for a source mechanism(s) responsible for deep altitude modulation of sporadic E layers and the development of a polarization electric field

Session J/F-2, 1335-Thurs., CR0-30
RADIO FREQUENCY PHASE SHIFTS CAUSED BY THE TROPOSPHERE
Chairperson and Organizer: D.P. Woody, Owens Valley Radio Observatory, Big Pine, CA 93513

J/F2-1
1340

COMPARATIVE MEASUREMENTS OF TROPOSPHERIC PHASE STABILITY

Simon J. E. Radford* Mark A. Holdaway
National Radio Astronomy Observatory
949 North Cherry Avenue
Tucson, AZ 85721-0665

Variations in the electrical path length caused by inhomogeneously distributed tropospheric water vapor present natural limits to the sensitivity and resolution of astronomical observations, particularly at millimeter and submillimeter wavelengths. Although active techniques can correct these phase errors to some degree, it behooves planners of a new instrument to choose a site with the best possible limits.

To evaluate possible sites for NRAO's proposed Millimeter Array, we constructed small aperture interferometers to directly measure the tropospheric phase stability. Similar to earlier designs (Ishiguro et al., 1990, in *Radio Astronomical Seeing*, ed. Baldwin & Wang, p. 60; Masson, 1994, in *Astronomy with Millimeter and Submillimeter Interferometry*, ed. Ishiguro & Welch, p. 87), these instruments observe an unmodulated beacon broadcast from a geostationary satellite and measure the phase difference between the signals received by two antennas 300 m apart. Although the beacon frequency is around 11.5 GHz, the results can be scaled to millimeter and submillimeter wavelengths because the atmosphere is non-dispersive away from line centers. Novel design features include a local oscillator phase locked to the received signal and digital correlation of the downconverted signals with a personal computer.

Two instruments have been deployed, one in 1994 September at 3720 m near the VLBA antenna on Mauna Kea, Hawaii, and the other in 1995 May at 5000 m near Cerro Chajnantor in northern Chile. This site is near the village of San Pedro de Atacama, about 275 km ENE of Antofagasta. Both instruments are operated in conjunction with adjacent 225 GHz tipping radiometers. With identical instruments operating simultaneously, we can directly compare the phase stability at the two sites. We have also compared our data with archival data for other sites, notably "millimeter valley" near the summit of Mauna Kea (Masson 1994).

Initial results for Mauna Kea indicate the phase stability distributions are similar at the VLBA site and at millimeter valley, but the best conditions occur at different times at these two locations. We confirm the pronounced diurnal variation in the phase stability on Mauna Kea. At Cerro Chajnantor, the phase stability is substantially better than on Mauna Kea. The diurnal variation is less pronounced and conditions of good phase stability occur two to three times more often.

.The NRAO is a facility of the National Science Foundation operated under cooperative agreement by Associated Universities, Inc.

J/F2-2
1400

FAST SWITCHING PHASE CALIBRATION FOR THE MILLIMETER ARRAY(MMA)

M.A. Holdaway* F.N. Owen
National Radio Astronomy Observatory
1003 Lopezville Rd
Socorro, NM 87801

Phase errors caused by inhomogeneously distributed tropospheric water vapor will often limit observations performed by millimeter wavelength interferometers unless we actively correct for them. Imaging simulations allow us to investigate the level of phase error which still permits good imaging. Using a new technique which deconvolves the statistical effects of phase errors from the corrupted image, we demonstrate 35 degree rms phase errors permit excellent imaging, and 70 degree errors permit good imaging.

There will be combinations of baseline, observing frequency, and atmospheric conditions which result in larger phase errors. Traditionally, a phase calibrator is observed by an interferometer every ~20 minutes, but most of the power of the phase fluctuations is on shorter timescales. In order to effectively remove the atmospheric fluctuations during poor atmospheric conditions, calibration must be performed on timescales of ~5 s, observing calibrators within ~1 degree of the target source. How well will *fast switching* phase calibration work?

Based on 90 GHz observations of 1500 sources, there are ~200 sources >1 Jy and ~5000 sources >0.1 Jy. Assuming standard MMA system temperatures, 2 GHz bandwidth, and 2 deg/s slewing, Monte Carlo simulations of calibrator distributions consistent with the source counts indicate phase errors on arbitrarilly long baselines after fast switching calibration will be the same as the phase errors on 20-40 m baselines without calibration. The distributions of phase errors from site test interferometers complete the picture, indicating the atmosphere above Mauna Kea will result in phase errors of 35 degrees or less on 20-40 m baselines (or on all baselines if fast switching is used) about 75% of the time.

J/F2-3
1420

MONITORING ATMOSPHERIC PHASE FLUCTUATIONS AT POTENTIAL MILLIMETER ARRAY (MMA) SITES WITH A 225 GHZ WATER VAPOR RADIOMETER

Scott M. Foster* M.A. Holdaway F.N. Owen
National Radio Astronomy Observatory
1003 Lopezville Rd
Socorro, NM 87801

Atmospheric phase errors are presumed to result from inhomogeneously distributed water vapor above the antennas of interferometric arrays. Since this water vapor also produces emission, we can obtain information about the phase fluctuations by making radiometric observations of the fluctuations in the sky brightness temperature.

NRAO 225 GHz site testing radiometers currently measure fluctuations in the sky emission every 3.5 hours at both the Mauna Kea VLBA site and the potential MMA site at Chajnantor, Chile. Since both of these sites also have site testing interferometers, which measure phase fluctuations on a 300 m baseline, we are able to calibrate the conversion from brightness fluctuations to phase fluctuations. We can use the atmospheric velocity inferred from the interferometer to convert the radiometer's temporal phase structure function into a spatial phase structure function. The spatial phase structure function inferred from the radiometer provides phase stability information out to much longer baselines than can be measured with the site test interferometer: the structure function's power law exponents remains nearly constant out to a few kilometers, where it turns over to a flat or less steeply rising power law. We may be seeing the outer scale of turbulence.

Our confirmation of the correlation between the rms brightness temperature fluctuations and the rms phase fluctuations is pparticularly relevant as the OVRO and BIMA millimeter observatories are designing radiometric phase correction schemes for their instruments. In addition, the radiometer's compact size and low power requirements make it very convenient for monitoring remote sites.

J/F2-4
1440

VLBA PHASE REFERENCING AT 15 GHZ

A. J. Beasley*
National Radio Astronomy Observatory
PO Box 0
Socorro NM 87801 USA

Residual geometric and propogation errors in VLBI data limit the minimum source flux density capable of being imaged using standard reduction techniques such as self-calibration or fringe fitting. Using regular observations of nearby strong extragalactic calibrators (a technique referred to as phase referencing), the residual phase errors in the VLBI data for a target source can be significantly reduced or removed, leading ultimately to improved image sensitivity and astrometric accuracy. Tropospheric and ionospheric effects are (to first-order) removed by the phase referencing process, however the temporal and spatial structure of these two error components can severely constrain observational parameters such as the maximum time between calibrator observations (switching time) and the allowable angular distance between target and calibrator (switching angle). At the present time, the variations in allowable switching times and angles are unknown. In this talk I will discuss the results of a on-going program of 15 GHz VLBA wide-bandwidth observations made during 1995 to examine the effects of tropospheric fluctuations on phase-referenced data. These observations consisted of long (six to twelve hour) observations switching every two or three minutes between various pairs of strong extragalactic sources with varying angular separations. An examination of the phase structure function derived from these observations places useful limits on preferred switching times and angles. A brief discussion of the use of GPS worldwide TEC measurements and dual-frequency observations to calibrate ionospheric effects in VLBA data will be given. In 1996, NRAO will begin to outfit the VLBA with 90 GHz receiver systems; schemes for calibrating mm-VLBI data will be reviewed.

J/F2-5
1520

ON THE FEASIBILITY OF USING COMMON IR SPECTROMETERS TO CORRECT FOR FLUCTUATING RADIO PATH DELAY DUE TO THE INHOMOGENEOUS WET TROPOSPHERE

Jay W. Parker*
Jet Propulsion Laboratory
4800 Oak Grove Drive
Pasadena, CA 91109-8099

Experiments relying on the phase of microwave interplanetary communication links suffer from a substantial source of phase noise due to the total refractivity fluctuations of water vapor in the troposphere. Many radio science experiments involving space vehicles will use Ka band in the near future, notably the Cassini mission to the Saturnian system. Cassini will exploit the Ka-band link to perform measurements of gravity fields around Saturn and its moons, attempt detection of gravitational waves, and measure solar General Relativistic effects near solar conjunction. In two-way Ka-band links, wet troposphere fluctuation dominates over space plasma and ionospheric fluctuations, and exceeds anticipated time-standard uncertainties. To approach theoretical performance of such radio science experiements requires real-time measurements of the tropospheric moisture fluctuations on time scales of minutes to hours. Others have demonstrated that high- resolution spectrometers measuring downwelling radiance are sensitive to the relevent moisture content, and can be the basis of temperature and water-vapor profiling along an arbitrary line of sight, with limited yet substantial vertical resolution. These spectrometers may be easily designed to have a beamwidth closely matching the volume of troposphere that affects large space-communications antennas.

We show through simulation using a line-by-line radiative transfer model that the information content of spectra measurable with inexpensive instruments is adequate for integrated refractivity measurements that reduce the impact of uncalibrated fluctuations by roughly a factor of ten. Initial field experiments result in plausible (but unverified) water and temperature profiles, and demonstrate that leading limitations of the method at present include errors in the HITRAN 1992 data base for pure-rotational and ν-2 water lines of moderate strength, and suggest inadequacy in models for the water vapor continuum in the thermal IR band (where intensity and detector performance are particularly favorable). Techniques for overcoming these limitations are proposed.

J/F2-6
1540

AN EVALUATION OF GPS-BASED ESTIMATES OF PRECIPITABLE WATER VAPOR FOR A VARIETY OF DATA LATENCY TIMES

Yoaz E. Bar-Sever*
Mail Stop 238-600
Jet Propulsion Laboratory, California Institute of Technology
Pasadena, CA 91109

Low operational cost and high temporal resolution make GPS estimates of zenith path delay (ZPD) and zenith precipitable water vapor (ZPWV) highly attractive in many applications. The effectiveness with which GPS-based techniques can replace or augment the more established technologies of water vapor radiometers (WVR) and radiosondes is application dependent. Applications such as climatology, weather prediction and media calibration for radio science vary in their demand for accuracy, product delivery schedule and in their need for zenith properties or line of sight properties.

The accuracy of GPS-based estimates of ZPWV at a given sight depends on the data latency time. One can identify three general types of data processing scenarios based on decreasing levels of data latency: post-processing, near real time processing and real time processing. Post-processing utilizes data from a global network of ground stations and it supports the highest solution accuracy for the GPS orbits, clocks and media calibration, including ZPD. The time delay involved in collecting and processing data from a global network of receivers (say, a subset of the IGS network) can be one or two days. In near real time processing, a delay of several hours in processing may be needed in order to bring in a station with a good clock that can serve as a reference. In real time processing only data from the target station is processed. Each data processing scenario requires a special estimation strategy to address its unique problems associated with the quantity, quality and sour! ce of data.

This paper reviews the data processing strategies that can be employed for different latency times. The quality of the GPS-based ZPWV estimates is measured by comparing them to estimates from more established technologies like WVRs and radiosondes and by formal error analysis. The accuracies that are currently achievable with each strategy are presented together with an outline of possible future improvements.

J/F2-7
1600

FIRST OBSERVATION OF THE EARTH'S ATMOSPHERE WITH THE NASA/JPL GOLDSTONE SOLAR SYSTEM RADAR

J. Y. N. Cho*
Arecibo Observatory
P.O. Box 995
Arecibo, PR 00613 R. F. Jurgens M. A. Slade
NASA/Jet Propulsion Laboratory
4800 Oak Grove Dr.
Pasadena, CA 91109

One of the outstanding scientific problems in middle atmosphere dynamics is the role that stratospheric turbulence plays in the vertical transport of minor constituents such as ozone, water vapor, and aerosols from volcanic eruptions and supersonic jet planes. Because the turbulence occurs in extremely thin layers (due to the high convective stability of the stratosphere), its observation has been difficult. A stratosphere-troposphere (ST) radar typically has a maximum range resolution of 150 m, but stratospheric turbulence often has finer scale features on the order of tens of meters.

To overcome the range-resolution problem the Arecibo bistatic S-band planetary radar with its capacity for very fast phase modulation was used to study the stratosphere (R. F. Woodman, *Radio Science*, **15**, 423-430, 1980; H. M. Ierkic et al., *Radio Science*, **25**, 941-952, 1990). However, that system is currently not in operation.

We have applied the same technique and used, for the first time that we are aware of, the Goldstone planetary radar to study the Earth's atmosphere. The S-band system was operated in a bistatic mode using a 70-m diameter dish for transmission and a 26-m dish for reception. A CW mode with a 1023-length, 0.125-μs-baud pseudorandom binary phase code was used with an average transmitted power of up to 400 kW. The altitude resolution of 20 m and a time resolution as short as 4 s are the best that we know of and are only rivaled among ST radars by what was achieved using the old Arecibo system.

We present the initial observations of stratospheric turbulent layers made by this system and discuss their impact on the current understanding of turbulent layers in a stratified region. We will also discuss the limitations of the current Goldstone configuration, and talk about plans for the future.

J/F2-8
1620

STRUCTURE IN THE SOLAR CORONA INFERRED FROM RADIO SCATTERIING MEASUREMENTS

R. Woo
JPL-Caltech
Pasadena, CA 91109

For over four decades, electron density irregularities in the solar corona have been investigated with scattering measurements using natural radio sources as well as spacecraft radio signals as they passed behind the Sun. Examples of these measurements include angular broadening, phase/Doppler scintillation and spectral broadening.

Despite the success in establishing many properties of the density irregularities, the nature of the irregularities and their relationship to solar features have not been fully understood. For example, two notable characteristics of the density irregularities have remained unexplained. The first is the abrupt rise in anisotropy of the density irregularities inferred from angular broadening measurements near the Sun, especially when conducted with longer baseline interferometers. The second is the break near 1 Hz in the inverse power-law density spectrum inferred from phase scintillation and spectral broadening measurements. For frequencies lower than the break, the density spectrum is Kolmogorov (spectral index of 5/3), while for frequencies that are higher, the spectrum is flatter (spectal index near 1).

In this paper, we show that these characteristics can be interpreted in terms of a corona that is permeated by a hierarchy of ray-like structures with the smallest size being about 1 km at the Sun. Within these structues, the density variations are represented by random irregularities that are convected along with the solar wind. The emerging picture of a corona that is highly structured unifies results from widely varying radio propagation measurements, and demonstrates how structures observed in white-light are related to those in the radio propagation measurements.

J/F2-9 Discussion
1640

Thursday Evening, 11 January, 1900-2200

Special Session, 1900-Thurs., CR2-28
DON SPAULDING MEMORIAL SESSION
Organizer: George Hagn

Session B/C/J-1, 0855-Fri., CR0-30
PHASED ARRAY FEEDS IN RADIO ASTRONOMY
Chairperson: J.R. Fisher, NRAO, Green Bank, WV 24944
Organizers: J.R. Fisher and D. Thomson, NRAO, Green Bank, WV 24944

B/C/J1-1
0900

PHASED ARRAY FEED DESIGN CONSIDERATIONS

J. R. Fisher*
NRAO
P.O. Box 2
Green Bank, WV 24944

Phased array feeds for radio astronomy reflector antennas must simultaneously provide very low spillover and beam spacing as small as the sampling theorem allows. This requires that array elements be physically small to fully sample the reflector focal plane and that the spillover be controlled by the array pattern rather than the pattern of individual elements. The maximum element spacing for a hexagonal array is set by the appearance of grating lobes and is given by

$$S_h = \frac{\lambda}{(1+\sin\theta_0)\cos 30^\circ}, \qquad (1)$$

where θ_0 is the half-angle of the illuminated reflector. This, with the minimum spacing limit of about 0.5λ set by mutual coupling, implies a bandwidth limit between 1:1.3 and 1:2, depending on F/D.

Aperture efficiency is limited only by the number of elements used to form one beam and can be greater than the taper efficiency of one element. Full off-axis efficiency can be maintained as long as the array size grows to intercept all of the power that as been redistributed by reflector aberrations. The array can be well away from the conventional reflector focal plane as long as it intercepts all of the reflected energy. There is no efficiency penalty for very close beam spacings. However, beams spaced closer than the sampling theorem limit will be partially correlated.

The receive-only application permits the use of correlation techniques to reduce the signal processing requirements for forming many beams simultaneously. Still, the processing load is enormous for even modest array sizes. Approximately $N_E N/2$ correlators and $N_E^2 N_B/2$ complex-weight multipliers are required, where N is the total number of elements in the array, N_E is the number of elements needed to form one beam, and N_B is the number of beams formed. N_E is typically between 19 and 100. Spectral line observations require each correlator to be a multi-lag device. Direct combination of element signals can be less expensive than cross-correlation when the number of beams formed is small. In any case, this application is a good candidate for new correlation and signal processing technology.

Need $A_e \sim \lambda^2/3$

Cancelled

B/C/J1-2
0920

A METHOD USING FOCAL PLANE ANALYSIS TO DETERMINE THE PERFORMANCE OF REFLECTOR ANTENNAS

Paul W. Cramer and William A. Imbriale
California Institue of Technology/Jet Propulsion Laboratory
Pasadena, CA 91109 USA
and
Sembiam R. Rengarajan
California State University
Northridge, CA 91330 USA

Array feeds for reflectors have a number of important uses which include 1) generating contour coverage patterns, 2) correction for reflector distortions, and 3) improved wide angle scan. Typical methods for optimizing the array feed for each of these applications are very efficient when a fixed array geometry is utilized and only the feed excitation coefficients are optimized since only one set of radiation integral evaluations is needed. For most existing methods, an optimization which allowed the element type, spacing, and size to vary would be extremely time consuming since a radiation integral evaluation would now be required for each feed element at each step of the optimization process.

A new method for computing the performance of reflector antennas with array feeds is presented that obviates the need to recompute the reflector radiation fields when the feed element type, size, or spacing is varied. This allows the optimization techniques to efficiently include size and spacing as parameters.

The mathematical formulation is based upon the use of the Lorentz reciprocity theorem, which convolves the focal plane distribution of the reflector system with the feed element aperture field distribution to obtain the element response. The antenna gain can then be obtained from both these responses and the array gain. Thus the time consuming reflector system radiation integral evaluation is only done once for a given scan direction or reflector surface distortion for all array feed geometries considered. The study was restricted to the case where the antenna is illuminated by an incident plane wave and thus the performance evaluation was restricted to only one observation direction. Optimizing shaped antenna patterns would require making the correct transformation between the far-field pattern and the focal plane distribution.

Examples are given using this technique to design an array feed for the correction of gravity-induced distortions of a large dual-shaped ground antenna, both conventional and beam waveguide (BWG), as well as the design of an array feed for improved wide-angle scan.

National Radio Science Meeting (Boulder, CO)
Jan. 1996

B/C/J1-3
0940

INVESTIGATION OF FREQUENCY VARIATIONS OF SINUOUS ANTENNAS

J. M. Bowen and P. E. Mayes
Electromagnetics Laboratory
University of Illinois
Urbana, IL 61801

P. G. Ingerson
Antenna Systems Laboratory
TRW Space and Defense
Redondo Beach, CA 90278

The logarithmic spiral antenna has many favorable qualities such as wideband performance, circular polarization, and low profile. These qualities have made the logarithmic spiral antenna useful in direction finding, electronic countermeasure, and communication applications. In 1987 DuHamel (R. H. DuHamel, U. S. Patent 4,658,262, April 14, 1987) patented the sinuous antenna which is related to the logarithmic spiral antenna and shares many of its qualities. In addition, the sinuous antenna is sensitive to orthogonal senses of polarization which makes it an attractive alternative to the logarithmic spiral antenna in certain applications. However, for certain design parameters half-power beamwidth variations were noted both in numerical modeling (J. M. Bowen and P. E. Mayes, IEEE Antennas and Propagation Society International Symposium Digest, June 1994) and in experimental measurements (P. G. Ingerson, P. M. Ingerson, and D. C. Senior, Proceedings of the Antenna Applications Symposium, Sept. 1991) of a sinuous antenna. The frequency-independent performance of a multi-arm logarithmic spiral can be inferred from its continuously self-scaling and self-complementary structure. The sinuous antenna is not continuously self-scaling, so frequency-independent performance is not guaranteed. In fact, the sinuous antenna may be self-scaling only for a discrete set of scale factors, i.e. when the geometry is log-periodic. However, the patent description of the sinuous antenna allows for design parameters which do not produce log-periodic geometry. It is such a set of parameters that yields an antenna with a minimum of variation in beamwidth across a log-period in frequency.

This paper will describe numerical modeling of sinuous antennas with different design parameters. The minimal beamwidth variations will be illustrated for a certain design that is not log-periodic. The paper will also describe some experimental measurements on sinuous antenna reflector feeds.

Supported by TRW
FERM code
Sami Rao at Calif. Microwave built antennas

National Radio Science Meeting (Boulder, CO)
Jan. 1996

B/C/J1-4
1000

THE SINUOUS ANTENNA -- A DUAL POLARIZED ELEMENT FOR WIDEBAND PHASED ARRAY FEED APPLICATIONS

Kamaljeet S. Saini
Department of Electrical Engineering
University of Virginia
Charlottesville, VA 22903

Richard F. Bradley
National Radio Astronomy Observatory*
Charlottesville, VA 22903

Typical radio astronomy applications require wideband antenna elements to provide large observable radio spectrum without the need to change feeds. Polarization measurements require the antenna to possess the capability of distinguishing between two orthogonal senses of polarization in the received signal. Some other conventional applications, like the direction finding systems, require similar antennas. The sinuous antenna element described here is one such element suited to these kinds of applications. It is compact, has a good E- and H-plane radiation pattern congruence, and possesses an input impedance which is essentially independent of frequency. Also, its phase center shows little variation over the designed band of operation. The structures corresponding to the two polarizations "fold" into each other, conserving space, and creating a compact antenna. Several of such antennas can be stacked close together to sample the far-field radiation pattern closely enough to be configured as a phased array. Few other candidate elements possess all these properties satisfying the requirements for similar and related applications.

We present the construction and performance of one such element designed for the 1.0 GHz-2.5 GHz band. The design was carried out with the log periodic scale factor, $\tau = 0.75$, to minimize the frequency dependence of the radiation pattern, while the self complementary four arm structure guaranteed a frequency independent input impedance of about 240 Ω.

The 3 dB radiation pattern was approximately 80°, a good number for efficient illumination of a parabolic dish from its prime focus. The circumferential nature of current distribution, arising out of the physical geometrical shape of the element, provided a good E- and H-plane pattern uniformity. The polarization wobble was measured to be less than ± 5° in the 1.0 GHz-2.0 GHz frequency band. The measured SWR (at the balun input) of about 2.0 in this band was close to the value of 1.7, which was theoretically expected with a balun designed to transform a 140 Ω impedance to 50 Ω. The cross-polarization rejection was better than -25 dB throughout the 1.0 GHz-2.0 GHz frequency band.

old number, actually used 240Ω to 50Ω balun and saw 15 dB RL

*The National Radio Astronomy Observatory is a facility of the National Science Foundation operated under cooperative agreement by Associated Universities, Inc.

National Radio Science Meeting (Boulder, CO) Jan. 1996

B/C/J1-5 1040

A PROTOTYPE ARRAY FEED - DESIGN AND CONSTRUCTION

Richard F. Bradley
National Radio Astronomy Observatory*
Charlottesville, VA 22903

Kamaljeet S. Saini
Department of Electrical Engineering
University of Virginia
Charlottesville, VA 22903

J. Richard Fisher
National Radio Astronomy Observatory*
Green Bank, WV 24944

A prototype phased array feed, based on the 5" diameter sinuous antenna, is currently being constructed for evaluation at the prime focus on the 140-foot radio telescope in Green Bank. This proof-of-principle design will cover the 1.16-1.62 GHz frequency band and will consist of 19 sinuous antenna elements located on the vertices of regular hexagons forming five rows having 3, 4, 5, 4, and 3 elements, respectively. Calculations indicate that an acceptably small grating lobe response up to 1.62 GHz is possible using this sinuous antenna with a fixed-element spacing. These calculations use the measured radiation pattern of the planar sinuous antenna backed by a metal ground plane. Coupling between adjacent elements is -15 dB at 1.0 GHz and better than -30 dB at 2.0 GHz, as measured using a 5-element linear test array. In principle, the 19-element array could support dual linear polarization, but to reduce the cost, it will be designed initially for single polarization.

The prototype array will operate at ambient temperature and each element should have a noise temperature of under 200 K. Each element consists of a 1.0-2.0 GHz sinuous antenna fed by a tapered balun to a low-noise MMIC-type amplifier. A FET-type switch matrix, functioning as a commutator, will select the signals from the 19 amplifiers into four pairs of RF channels. The number of channels is set by the existing spectral processor which can cross-correlate only four element pairs at one time. The eight output channels from the switch matrix (four pairs) are mixed down to the 70-500 MHZ IF band, further amplified, and then sent down the telescope via coaxial cable to the spectral processor where the cross-correlation occurs between pairs of channels. Full array correlation will be done by time-sharing the four correlators between the 171 element pairs using the switch matrix.

Once the array concept has been verified experimentally, the next step will be to construct a truly low-noise element. Approaches being considered include compact and low cost cryogenic systems that cool to 70 K and special balanced amplifiers.

*The National Radio Astronomy Observatory is a facility of the National Science Foundation operated under cooperative agreement by Associated Universities, Inc.

B/C/J1-6
1100

CORRELATOR REQUIREMENTS FOR A FOCAL PLANE ARRAY

R. P. Escoffier
National Radio Astronomy Observatory*
2015 Ivy Road
Charlottesville, VA 22903

A study of the correlator requirements for a radio telescope with a focal plane array is presented.

The requirement for a focal plane array correlator is to take the outputs of many feeds in the focal plane of a telescope and process them so as to form many narrow directed beams on the sky. Such an approach increases the utilization of the telescope which normally produces only a single large beam on the sky.

A set of appropriate parameters for a practical focal plane array is assumed, and corresponding hardware for the correlator is proposed.

Two approaches are studied. First, a phased array technique is presented where the antenna outputs are used to form weighted sums to construct directed beams on the sky. The weighting stage is performed in RAM to allow loading of weights unique to a given beam pattern but later summation stages are done in ROM for simplicity. Complex sum weights are used.

The second approach is to calculate the lag function for each array element and do the beam forming weighted sums in the lag domain. This approach has the advantage of being able to perform the weight multiplication after some integration time.

The two methods are compared to find the optimum approach.

*The National Radio Astronomy Observatory is a facility of the National Science Foundation operated under cooperative agreement by Associated Universities, Inc.

B/C/J1-7
1120

OPTIMALITY OF COMBINED MATCHED AND NULL STEERING BEAMFORMERS FOR FADING CHANNELS

Alfred O. Hero and Ronald Delap,
Department of Electrical Engineering and Computer Science
The University of Michigan
1301 Beal Avenue
Ann Arbor, MI 48109-2122

Rayleigh fading is characteristic of optical and radio frequency tropospheric and ionospheric propagation, land, sea, and free-space radar backscatter, multipath propagation in mobile radio channels, and volume and surface reverberation in underwater acoustic channels. While statistical models for fading signals have been available for some time, including for example the Rayleigh, Rician, and Nakagami models, they are generally intractible in terms of developing optimal beamformer structures for DOA estimation or signal detection. In this paper we derive optimal beamsummers under a simplified model which is based on a slow fading assumption: amplitudes are coherent over space but incoherent over time with unknown mean and variance. We derive optimal beamformers under two different adaptation criteria: (1) maximization of a detectability index for detection; and (2) minimization of a monotone function of the CR lower bound for DOA estimation. These lead to optimal beamformers which can be implementated as a split beam adaptive algorithm. The algorithm controls and combines a signal nulling beam, which has intrinsically high angular resolution, and a signal enhancement beam, which has intrinsically high gain robustness. We show experimental results which indicate that our split beam adaptive array comes close to the performance of a clairvoyant maximum likelihood algorithm implemented with an Akaike signal selection criterion.

B/C/J1-8
1140

ADAPTIVE SPACE-TIME MOUNTAINTOP RADAR PROCESSING

Lloyd J. Griffiths
Department of Electrical and Computer Engineering
University of Colorado
Boulder, CO 80309-0425

Interference that is observed in airborne radar systems that is produced by one or more jamming signals consists of two components. The first is the direct-path, or line-of-sight signal that is incident on the receiving array from the direction of the jammer. Adaptive array processing has been shown to be particularly effective in the elimination of the direct-path jamming signal. The second component, which is not so easily removed consists of the multiplicity of terrain scattered interference components that arrive at the receiving array from a cone of angles.

In airborne radar systems that operate in the VHF (30MHz-300MHz) region, the terrain below the receiver can act as an effective scattering mechanism over relatively wide spatial regions. Data have been collected in the Mountaintop Program that illustrate the nature of this terrain-scattered interference, which is also known as hot clutter. Figure 1.0 illustrates the eigenvalues obtained from Mountaintop data with a 14 element linear horizontal array using five successive data samples from each element. The signals were collected after normal radar doppler processing. A single strong interference was incident on the array and the direct-path component was absent for this data set. This result shows that signficant energy exists over 10 dimensions and that as many as 43 dimensions may be important in cancellation of the hot clutter. Equivalently, at least three time taps must be used in each of the doppler-space processors.

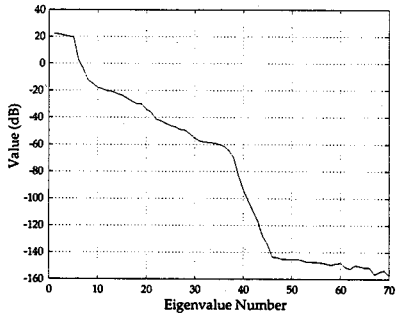

Figure 1.0: Hot clutter eigenvalues for 14 element array with five time taps.

This paper illustrates the results obtained with the use of simultaneous adaptation in both space (element number) and time (successive samples) in the Mountaintop radar environment. Data collected under conditions in which a time-varying jamming source was generated using Learjet flights will be described. The advantages of adapting with and without successive time samples is discussed. The paper describes the use of multiple linear constraints in the adaptive processing. Advantages of the linearly-constrained approach in comparison with the single steering vector method are presented.

Session D/A-1, 0855-Fri., CR2-28
HIGH FREQUENCY PACKAGES
Chairmen and Organizers: S. El-Ghazaly and G. Pan, Telecommunication Research Center, Arizona State Univ., Tempe, AZ 85287

D/A1-1
0900

THE CHALLENGES IN ELECTROMAAGNETIC MODELING OF HIGH SPEED ELECTRONICS PACKAGING

Samir El-Ghazaly Guangwen Pan*
Telecommunication Research Center
Campus Box 877206
Arizona State University
Tempe, AZ 85287

Mixed signal modules (MSM) have potential applications for digital UHF and X-band radars, Micro-GPS, NASA's remote sensing GLAS, synthetic aperture radars (SAR), etc. The MSMs have unique features that the analog signals are narrow-banded with very low amplitudes, while the digital signals are wide-banded with large swings. As a system, the MSM spans a large spectrum from nearly D.C. to tens of GHz, and the MSM covers a huge dynamic range of 120 dB or greater. Thus, the design and development of the MSMs are of great challenges. These challenges include, but not limited to:

1. impedance mismatching and discontinuities,
2. digital signal distortions due to dispersion,
3. crosstalk from large digital signals to very low level analog signals,
4. coupling through imperfect power and ground planes,
5. power/ground noise,
6. undesired resonance due to large gain of analog amplifies, and positive feedbacks of passive structures,
7. electromagnetic interference (EMI).

The fore-knowledge of these effects are critical for successful system designing and optimizing performance. Unfortunately, most commercial CAD tools available to date for the design and simulation are based on the Quasi-TEM, or Quasi-static assumption, which is only the low frequency approximation of the Maxwell equations. The QSA is simple in mathematics and efficient in programming, but it can not address many of the aforementioned high frequency issues. On the other hand, the assumption of zero conductor thickness and the traditional impedance boundary condition, which are widely used in the MMIC area, may not be applicable for the MSM problems.

As a result, these challenges form a new topic in the modeling and simulation of high-speed, high density and high-performance systems.

D/A1-2
0920

ANALYSIS OF MULTIPLE CROSSOVERS IN A GROUNDED TWO-LAYER DIELECTRIC

Gaofeng Wang*
Tanner Research, Inc., 180 N. Vinedo Ave., Pasadena, CA 91107
Bing-Zhong Wang
University of Electronic Science and Technology of China
Chengdu, 610054, China

Crossover structures are commonly found in modern electronic packages such as printed circuit boards (PCBs) and multiple-chip modules (MCMs). The previous approaches for studying the crossover structures include quasi-static analysis, iterative algorithm, transverse resonance analysis, full wave analysis. Among these approaches, the quasi-static analysis is the simplest and fastest one yet gives sufficiently accurate results for most circuit designs.

The quasi-static analysis of a microstrip crossover in a dielectric substrate was previously presented (S. Papathodorou, R. F. Harrington, & J. Mautz, *IEEE Trans.*, **MTT-38(4)**, 135-140, 1990). However, the formulas were devised only for a single microstrip crossover. To study a structure consisting of multiple crossovers, the formulas must be generalized to take account of the mutual couplings among the multiple crossovers.

In this work, the quasi-static analysis for a single microstrip crossover is generalized and applied to study multiple crossovers. A set of integral equations suitable for studying multiple crossovers has been derived. By making use of the moment method, the set of integral equations is solved for the charge densities. Both the distributed capacitances and lumped excess capacitances can be computed by using this scheme. A circuit model for multiple crossovers is built and the coupling effects among the multiple crossovers have been included in this model. Numerical examples are provided to validate this approach and illustrate its feasibility and efficiency.

D/A1-3
0940

A NOVEL RESONATOR APPROACH FOR CHARACTERIZATION OF ELECTRONIC MATERIALS USED IN MCM PACKAGES

Sedki M. Riad, Aicha Elshabini-Riad*
Wansheng Su, and Fred Barlow
Time Domain Laboratory
The Bradley Department of Electrical Engineering
Virginia Polytechnic Institute and State University
Blacksburg, Virginia 24060-0111, USA
Phone: +1-540-231-4463, FAX: +1-540-231-3531
email: sriad@vt.edu

Complete information concerning material properties at various frequencies are critical to the performance of electronic packaging and multichip modules (MCMs). This paper presents a novel resonator approach to accurately characterize electronic materials using stripline resonators.

As the conventional stripline resonator, the resonant frequencies are determined by the dielectric constant of the substrate and the quality factors are determined by the loss tangent of the substrate and the conductor loss due to the resonator line and top and bottom ground. For the traditional approach, the launchers are at the same plane as the resonator line section. Two problems exist for that configuration. First, since the launchers are in the middle of the substrate, it is hard to access electrically and mechanically. Second, the signal energy coupled to the resonator line is determined by the ends of both the launchers and the resonator line. Once the sample is made, there is no way to change it. Most serious problem is that the required gaps between launchers and resonant line are too small to be processed in order to obtain a proper amount of signal coupling.

In order to solve these two problems, coplanar line launchers are developed to move the stripline launchers from the middle to the top plane (Patent pending). This unique design makes the launchers accessible both mechanically and electrically. Adjusting the center line of the coplanar line of the coplanar line or the overlap length of the launchers and the resonator line enables the control of the signal coupling. Even the sample is done, the coupling still can be adjusted by laser trimming the center line of the coplanar line.

Numerical simulation has been performed to evaluate the coupling between the new launcher and the resonant line. Test samples are fabricated and measured. Both simulation results and measurement data are presented and compared to validate the method.

D/A1-4
1020

A TECHNIQUE FOR MODELING AND SIMULATION OF HIGH SPEED SYSTEMS

O. A. Palusinski*
Department of Electrical and Computer Engineering
Building 104
University of Arizona
Tucson, AZ 85721

Modeling of high speed communication hardware is so complex that there are no analytical design methods for many system components. Computer aided design support is not yet fully developed. Consequently design of high speed communication circuits and packages often involves experimentation with hardware. A design of RF power amplifier for portable equipment is an example illustrating this situation. Such an amplifier operates with varying load conditions (usually specified by a range of VSWR) and it is known that at certain loads the amplifier may significantly distort the output signal. This undesirable amplifier behavior occurs at both very low and very high load impedances due to the mismatch between the output line and load. The frequency spectrum of output signal exhibits components with frequencies lower than that of input excitation, aperiodic behavior is also observed. Experimentation in hardware with various design options is expensive and time consuming. It is therefore desirable to utilize computer support and simulation to minimize the number of bench experiments. However, existing methods and associated computer design tools appear to be inadequate in such applications as they were built for digital circuits or for analog circuits with periodic solutions. In addition, modeling of active and passive elements is limited to built in libraries of elements. A new software system is being built at the University of Arizona to resolve these problems. This software utilizes a spectral method (O. A. Palusinski et al., *IEEE Trans. MTT*, **37** 127-138, 1989) for computation of transients in fast, non-linear systems and will have facilities for convenient definition of new models of active and passive elements. The paper will present spectral technique based on series of Chebyshev polynomials and its application to simulation of non-linear RF circuits where the interest is in the circuit transient behavior. The proposed method offers advantages in the form of excellent error estimates and error control particularly suitable for analog systems. The method is also known for its high numerical efficiency. This efficiency is achieved due to several numerical properties of Chebyshev polynomials. These properties are very well documented in literature and are utilized in the simulation code. Modeling of passive elements such as digitized capacitors, inductors and resistors with the use of database concept will also be discussed.

D/A1-5
1040

A NEW FUNCTIONAL ANALYSIS OF DISPERSIVE 3D STRUCTURES

Guangwen Pan* Jilin Tan
Telecommunication Research Center
Campus Box 877206
Arizona State University
Tempe, AZ 85287

A new functional is rigorously derived based on the 3D analysis for the dielectric lossy and conductor lossy guided wave structures. The adjoint field is judiciously selected to meet the physical symmetrical requirement of the structure interested. Systematically, the boundary conditions of the first kind, second kind, and the third kind as well, are all incorporated with the new functional. The impedance boundary condition at the interface between the anisotropic material and the imperfect conducting ground plane is proposed. The computation domain includes the cross section of the lossy conducting line, in the case where the size of the cross section has the same order as the skin depth and the impedance boundary condition is no longer held.

The vector element analysis procedure, with the subspace iteration method, is then used to find the partial or the total system modes according to the requirement. All the spurious modes are totally suppressed by this procedure in the frequency of interested and and all the frequency dependent circuit parameters, such as R, L. C, G are extracted from this full wave analysis. Therefore, this method is especially suitable for the CAD design and packaging simulation and modeling.

Numerical examples of anisotropic dielectric image waveguide, PTEE bilateral fin line, and coupled asymmetrical dual lossy transmission lines with finite conductivity and finite thickness are presented as illustrations. Agreement with previous publications wherever available are observed.

D/A1-6
1100

A NETWORKING ANALYSIS OF H-MESHED-STRIP LINES BY FDTD METHOD

Bing-Zhong Wang*
University of Electronic Science and Technology of China
Chengdu, 610054, China
Gaofeng Wang
Tanner Research, Inc., 180 N. Vinedo Ave., Pasadena, CA 91107

High-speed electrical equipment systems demand new packaging technology to meet high propagation speed, high wiring density, and high frequency pulse requirements for a multichip substrate. Due to the high wiring density in high-speed multilayered digital integrated circuits, the number of interconnection through holes increases. Therefore, it is necessary for the ground plane to use a mesh pattern. The electrical properties of the meshed-strip line have been studied by measurement (O. Shimada, K. Ito, T. Miyagi, S. Kimijima, & T. Sudo, *Proc. IEEE CHMT'89 Japan IEMT Symposium*, 121-127, 1989) (A. Sasaki & Y. Shimada, *IEEE Trans.*, **CHMT-15**, 56-62, 1992).

Here, a full-wave analysis of the transmission properties of H-meshed-strip line is presented. The FDTD method, in combination with network concept, is used to analyze the transmission properties of the H- meshed-strip line. In view of the periodicity of the structure along the propagation direction, the H-meshed- strip line can be considered as a network consisting of a number of the same cascaded unit elements. To save computation time and computer memory, only one unit element is analyzed by the FDTD method. After getting the S-parameters of the unit element, the transmission matrix of the unit element can be readily obtained by a simple conversion. Then the total transmission matrix of the full length H-meshed-strip line can be computed by a cascade network formula. Finally, the total S-parameters of the full length H- meshed-strip line can be attained from the total transmission matrix by another simple conversion. Numerical examples are provided to demonstrate the validation and merits of this approach.

Session E-1, 0835-Fri., CR1-46
HIGH POWER ELECTROMAGNETICS
Chairperson: R.L. Gardner, USAF Phillips Laboratory, WSM, Albuquerque, NM 87117
Organizers: C.E. Baum and R.L. Gardner, USAF Phillips Laboratory, Kirtland AFB, NM 87117

E1-1
0840

SYSTEM LETHALITY - A HIGH POWER MICROWAVE PERSPECTIVE

R. L. Gardner*
USAF Phillips Laboratory, WSM,
3550 Aberdeen SE
Albuquerque,NM 87117-5776

Once a high power microwave (HPM) weapon has been demonstrated successfully on a particular system, there remains the problem of ascertaining what that success really tells you. One would like to believe that a test that shows damage or disruption means that systems similar to the test system are vulnerable as well. Unfortunately *similar* is not well defined in this context and it is very difficult to define *electromagnetic similarity in lethality* rigorously. This paper attempts to set some limits on electromagnetic similarity. We use a simple system that contains only a fuse and demonstrate the addition of a diode can change the lethality conclusion in either direction. This negative information provides some guidelines on extending our ability to define lethality classes. Simple circuit differences also show limits on the use of enumeration (derivation of statistics by counting failures) to draw conclusions about lethality. Further, it is shown that the system of interest for a fielded HPM weapon is not the system used to test the weapon. That system likely was designed perhaps decades after the test system.

The narrow lethality classes lead to the argument for analysis techniques that, in turn, can expand the region of applicability of the test results. Earlier work in electromagnetic pulse (EMP) and related disciplines has shown that strictly numerical models of systems are impractical. Three relatively new fields are discussed as promising to gain insight into the system lethality problem. The first of these is topological decomposition in which the system is decomposed into a number of more tractable problems. Next, the advances in numerical analysis and parallel processing has increased the complexity of problems that can be addressed compared to the approaches in the EMP era. Finally, the basis of statistical electromagnetics is discussed. Statistical electromagnetics is a combination of statistical laws with Maxwell's Equations and sets up boundaries for the results of svstem lethality experiments.

E1-2
0900

COMPARATIVE SYSTEM RESPONSE TO RESONANT AND UNIPOLAR WAVEFORMS

Carl E. Baum
Phillips Laboratory
3550 Aberdeen SE
Kirtland AFB, NM 87117-5776

In maximizing the interaction of incident electromagnetic waves with electronic systems one is faced with a problem of great complexity. While it is extremely difficult to calculate the response from first principles , one can use electromagnetic theory to characterize the *form* that the response takes and rely on measurements to evaluate the parameters in the appropriate models. The appropriate model is the singularity expansion method (SEM) which explicitly exhibits the various resonances as poles in the complex-frequency plane. Particularly for signals which reach deep into the system to the circuit level there are, in general, many resonances associated not only with the exterior envelope of the system, but also with the transfer functions through cables, cavities, etc. to the interior. An incident plane wave has a typical or canonical response which rolls off below some frequency related to the largest dimensions of the system. Above some frequency (of the order of a Ghz) related to resonant dimensions of apertures, small antennas, and certain internal equipment, the response also rolls off for "backdoor" or unintended interaction paths.

The maximum system response is usually achieved by selecting the incoming waveform as an approximate sinusoid of enough cycles to "ring up" the resonant response. A question of interest concerns what happens if one illuminates a system with a pulsed sinusoid which is not so tuned to a resonance. Perhaps one did not know what was the optimal choice of frequency and guessed incorrectly. In such an event is such a choice of waveform still appropriate, or does another temporal shape give stronger interaction with the system? So here let us consider a more impulse-like waveform (decaying exponential) and compare the response to this waveform to that due to the pulsed sinusoidal waveform. For comparing these responses, the various excitation and response waveforms are evaluated in norm sense in order to assign simple positive scalars which can be readily compared. The ∞-norm corresponds to the peak of the waveform and is appropriate for failure due to voltage breakdown or upset due to the level comparable to or exceeding the normal operating signal level. The 2-norm is proportional to the square root of the energy in the waveform, appropriate for burnout, except in cases where the energy in the system (associated with power-supply voltage) is triggered by the response waveform to deposit energy into various electronic devices.

E1-3
0920

CAVITY FIELD REDUCTION TECHNIQUES

C. E. Baum
Phillips Laboratory, WSR
3550 Aberdeen Ave SE
Albuquerque, NM 87117-5776
Donald P. McLemore*
Kaman Sciences Corp.
6400 Uptown Blvd., NE
Albuquerque, NM 87110

Recent high frequency coupling analyses (G. I. Hoffer, et. al., "Analysis of F-16 Low Power Coupling Data," Phillips Laboratory Report PL-TR-93-1057,1993) have suggested that coupling to circuit nodes inside electrical boxes follows the averagecavity fields inside an aircraft as a function of frequency with a constant relationship between the power observed at the circuit node and the power which would be coupled to an electrically long cable immersed in the cavity field. As a consequence, high frequency hardening strategies should include the reduction of these local fields.

This paper examines the effectiveness of both traditional and non-traditional cavity field reduction techniques on a testbed aircraft. Experiments for this comparison were conducted during the months of April and May, 1994, at the Large Electromagnetic System Level Illuminator (LESLI) facility on Kirtland AFB. The effect of adding the traditonal field reduction material, carbon embedded styrofoam, in the cavity was investigated in a cumulative fashion. Four separate sections of absorber sheets were added to the cavity and the effectiveness of each was evaluated. Measurements of a transfer function of the z-directed magnetic free field in the cavity and the skin current on the nose of the aircraft demonstrated that the field reduction capability of absorber material comes into play only when the mode density in the cavity becomes appreciable at the higher frequencies (near 1 GHz).

A number of other absorber-like concepts for hardening were also evaluated. One hardening technique was to line the walls of the cavity with ferrite loaded silicon tiles to reduce magnetic fields near the walls of the cavity and, in turn, to reduce cavity skin currents. All four x-y and y-z walls were covered (not the top and bottom of the cavity) with the tiles. Another idea was to load the cavity with resistor lattices (rectangular boxes of resistors approximately 2 inches on a side all connected together in a long parallelpiped) to reduce both the magnetic and electric fields. All of these techniques show approximately a 20 dB reduction in the field levels over ost of the frequency band, which is comparable to the carbon-loaded oam reductions at high frequencies. This new hardening hardware, however, shows significant reduction of the fields at the lower frequencies, which was not observed for the carbon loaded foam absorber.

E1-4
0940

OPTIMIZATION OF TRANSIENT RADIATION

Carl E. Baum
Phillips Laboratory
3550 Aberdeen SE
Kirtland AFB, NM 87117-5776

In designing antenna with pulsed sources for radiating transient pulses, one is faced with the problem of deciding what one wants. What is it about the far radiated fields that one wishes to optimize, and what does optimize mean (total energy, peak field, peak spectral content across some band of frequencies, particular polarization, etc.)? There is also the question of what constraints one wishes to impose on the antenna (e.g., physical dimensions) and pulser(s) (e.g., voltage, energy, peak and average power, etc.).In recent years this has led to the class of pulse radiators known as impulse radiating antennas (IRAs). With this technology expanding into various types of pulse radiators, it is important to understand which is better for a given application. There may be various "optimum" solutions, depending on the problem at hand. Norm concepts are introduced in a systemic way to extend the definitions of antenna gain and radiation pattern to apply to radiated temporal pulses. By considering reciprocity in the time domain the definitions are made to apply to both transmission and reception, allowing for the additional time derivative in transmission, or equivalently the additional time integral in reception. Norms of vector temporal waveforms are considered in terms of norms over the frequency spectrum of the two-sided-Laplace/Fourier transform of such waveforms. This leads into concepts of comparing waveforms via norms in the frequency domain which include weighting functions which emphasize portions of the spectrum of the pulse which are deemed important for the problem at hand.

E1-5
1020

IMPULSE RADIATING ANTENNAS WITH TWO REFRACTING OR REFLECTING SURFACES

Everett G. Farr*
Farr Research
614 Paseo Del Mar
Albuquerque, NM 87123

Carl E. Baum
Phillips Laboratory
3550 Aberdeen SE
Albuquerque, NM 87117

We consider here a new class of Impulse Radiating Antenna (IRA) that uses two surfaces to redirect the aperture field rays into a plane wave. Normally, IRAs use either a single reflector or a single lens to redirect rays into a planar wavefront. However, by using both a reflector and a lens, or two reflectors, one can achieve interesting antenna characteristics with respect to input impedance, structural stability, and antenna size.

The first antenna we consider is a Reflector/Lens IRA, or ReLIRA. In its simplest form, the ReLIRA uses a conical feed and a flat reflecting plate, all embedded in a dielectric material. The exit to the dielectric material is in the shape of a prolate reflector with a planar interface, or a hyperboloidal reflector with a prolate spheroidal lens. Also considered is form of Cassegrain antenna, which we call a CasIRA. This is a technique for confining a hyperboloidal subreflector with a large paraboloidal main reflector.

These designs can have a number of advantages over classical reflector or lens IRAs. They can be more compact, for a given level of high-frequency performance. They can also be shock resistant, since they are embedded in a solid material Finally, these designs can provide more options for matching to a source impedance, because the dielectric constant can be varied.

All of these designs can be split in half with a ground plane, resulting a split IRA, or SPIRA. This may be useful in cases where both transmit and receive antennas are required in the same aperture. Since the input impedance of half an IRA is typically 100Ω, if the dielectric material has a dielectric constant of 4, the resulting input impedance is conveniently 50Ω on each channel.

E1-6
1040

SLOW WAVE TRANSMISSION LINES FOR HIGH POWER MICROWAVE SOURCES

A. W. Biggs*
109 South Emerson Ave.
Wenathee, Washington 98801

Vircators, relativistic magnetrons, backward wave oscillators (BWO), Cerenkov masers, and magnetically insulated transmission line oscillators (MILOS) are a few of the slow wave high power microwave (HPM) sources with extended interactions between electron beams and electric fields in slow wave structures. The vircator, or virtual cathode oscillator, is designed with relativistic electron beams injected into drift tubes in excess of space charge limiting current (Child-Langmuir relation) to form virtual cathodes.

Relativistic versions of linear magnetrons are MILOs, where electron flow is confined or insulated by its own magnetic field. One unique modification of these MILOs is matching slow to fast waves with Chebyshev and binomial transformers, and then using mode converters to feed antennas. The slow wave structure of a plasma loaded BWO has controlled plasma background where a relativistic electron beam is injected into the structure. Another example of interaction between fields and electron beams in slow wave structures is seen in a relativistic multiwave Cerenkov generator, where two slow wave structures interact with hollow electron beams.

MILO slow wave guides are coaxial guides with corrugated outer conductors and smooth inner conductors. The rectangular corrugations are radial, short circuited, parallel plate cavities, like those in TWTs. Generated slow waves propagate with phase velocities proportional to serration depth.

Four analytical models include parallel plate guides, surface wave guides, coaxial guides, and circular guides. ω-β curves are similar for parallel plate and coaxial guides, and for surface and circular guides, as radii increase.

E1-7
1100

THE GENERATION OF LIME BY LASER PRODUCED PLASMA SPARKS

Robert Koslover William Page*
Phillips Laboratory/WST
3550 Aberdeen SE
Albuquerque, NM 87117-5776

LIME (Laser Induced Microwave Emissions) may be produced by many processes during the absorption of laser light. One relatively efficient process is by the production of plasma sparks by a focused, laser beam modulated or pulsed at RF frequencies. Available experimental data for this form of LIME will be discussed along with predictions from analytical models of the RF produced. The radiation of RF is associated with the dipole moment formed variously by: (1) high energy electron production and emission; (2) the motion of photo electrons at the expanding plasma shock front; and (3) photoemission from adjacent material irradiated by the UV light emitted from the plasma spark .

Experimental data has been obtained at the USAF Phillips Laboratory on UV radiation from plasma sparks and at Textron Defense Systems on both the production of high energy electrons and the overall RF production during the spark formation process. These data will be reviewed and compared with analytical models for the production of RF. Particular attention will be given to the effects of varying pulse repetition rate, temporal duration, pulse shape, and laser wavelength. The effects of varying pressure in air and other gases relative to vacuum conditions will be considered in the discussion of the efficiency (laser power to RF power).

In the case of secondary photoemission by spark-produced UV radiation, experimental data on the temporal and spectral characteristics of the UV will be presented. The electromagnetic interior boundary value problem when the UV is aborbed in an inclosure, thus producing a dipole layer, will also be discussed.

E1-8
1120

A NOVEL CHARACTERIZATION OF THE NOISE PERFORMANCE OF RECEIVING SYSTEMS WITH APPLICATION TO THE PREDICTION OF OPERATING NOISE TEMPERATURE

Derrick T. Copeland, Principal Investigator
Richard B. Wendt, Sr. Systems Engineer
Applied Data Trends, Inc.
Huntsville, AL 35815-4445

Accurate prediction of receiving system operating noise temperature in real operating environments requires a method which includes the effect of ambient operating temperature. Standard techniques for predicting operating noise temperature, based on measured effective input noise temperature or noise figure, ignore the dependence on ambient operating temperature (IRE Subcommittee 7.9, Haus (chair), et al., Proc. IEEE, 436-443, 1963). To overcome this deficiency, we develop a method for determining a fundamental noise characterization.

A novel characterization of noise performance is presented which enables a more accurate prediction of operating noise temperature at any ambient temperature. This paper gives the theory for the noise performance of receiving systems that combines the antenna load temperature (external noise) and effective composite receiver input temperature (system noise). We model the operating noise temperature using a linear relationship with the ambient temperature: $T_{op} = T_{ant} + (S_T * T_{amb} + T_{fi})$, where the ambient temperature sensitivity factor, S_T, and the fundamental composite input temperature, T_{fi}, are the characteristic receiving system constants. Candidate approaches for measurement are also presented. We apply the theory to the prediction of operating noise temperature based upon indoor measurements. Standard definitions are reviewed and limiting assumptions discussed in relation to the theory.

Session F-5, 0835-Fri., CR1-42
PASSIVE REMOTE SENSING OF THE ENVIRONMENT
Chairpersons and Organizers: E.R. Westwater, NOAA/ERL, Boulder, CO 80303; and A. Gasiewski, Laboratory for Radioscience and Remote Sensing, School of Electrical and Computer Engineering, Georgia Inst. of Technology, Atlanta, GA 30332

F5-1
0840

DESIGN AND PERFORMANCE OF A SPINNING FLAT REFLECTOR FOR MILLIMETER-WAVE RADIOMETRY

Mark D. Jacobson[1] and William M. Nunnelee[2]
[1] NOAA/ERL/ETL, R/E/ET1, 325 Broadway
Boulder, CO 80303
[2] NOAA/NWS, 920 Armory Road
Goodland, KS 67735

From late January through late March 1994, the National Oceanic and Atmospheric Administration operated two collocated dual-channel millimeter-wave radiometers at the Platteville, Colorado, site as part of the instrumentation for the Winter Icing and Storm Project along Colorado's Front Range. The two radiometers are identical, with the exception that one radiometer uses a spinning flat reflector while the other one uses a fixed flat reflector. The spinning reflector was designed to shed precipitation particles, thus improving the radiometer's performance during precipitating conditions. The spinning reflector speed is 300 revolutions per minute.

The two systems continuously made measurements of vertically downwelling brightness temperatures at 20.60 and 31.65 GHz, vertically integrated water vapor, vertically integrated liquid water, and vertical attenuation values during a variety of weather conditions. The data show several wet-weather periods with sereve data contamination for the fixed reflector radiometer, while the spinning reflector radiometer exhibited far less contamination during the same time period. These contaminated periods produce a larger variability in the data from the fixed reflector radiometer and lower correlation coefficients between the two instruments. A specific rain and wet snow event is analyzed in detail. Four Cross-chain Loran Atmospheric Sounding System (CLASS) radiosondes were launched at the radiometer site during this particular event, and the results show that the rotating reflector made it possible to measure precipitable water-vapor content of the atmosphere when the radiometer with the stationary reflector failed. Furthermore, other measured and derived radiometer parameters from the rotating reflector were affected much less during this event than the same radiometric parameters from the stationary reflector. The data suggest that the rotating reflector made it possible to measure accurately precipitable water vapor, vertically integrated liquid-water content, and zenith attenuation at 20.60 and 31.65 GHz, when a similar radiometer with a stationary reflector failed.

F5-2
0900

SMALL SLOPE EXPANSION FOR THERMAL AND REFLECTED ATMOSPHERIC RADIATION FROM THE OCEAN SURFACE

V.Irisov
University of Colorado at Boulder/CIRES
NOAA/ERL/Environmental Technology Laboratory
325 Broadway, Boulder, CO 80303.

One of the most important aspect of the thermal microwave radiometry of the ocean is a capability to calculate the radiative and reflective characteristics of the rough surface. For a long time a dominant model for such calculations was so-named two-scale approximation [*J.Geophys.Res. 1972 77, 5917-29*]. This model is a combination of the Kirhgoff and small perturbation approximation. Another approach, based on an expansion over small slopes, was developed by prof. A.G.Voronovich [*Sov.Phys.JETF, 1985, **62**, 65-70*]. In most cases the slopes of the sea waves don't exceed 10-15 deg., which makes this approximation very attractive for the ocean scattering and radiation modeling.

We consider the two main components of the microwave radiation from a sea rough surface - thermal radiation and reflected atmospheric radiation. Thermal radiation can be found as an absorption of an auxiliary plane electromagnetic wave. We develop both the small perturbation expansion and small slope expansion for the absorbed power. The comparison shows their identity, consequently the small perturbation expressions can be used to obtain small slope expansion for the emissivity of a rough surface.

Comparison of the same expansions for the atmospheric radiation reflected from a rough surface also shows that small perturbation expansion has features of the small slope expansion. In this case the variations of the downwelling atmospheric radiation are important and small perturbation formulae can be applied only for smoothly varying sky radiation.

Applicability of the small perturbation theory instead of the small slope approximation for microwave thermal radiation modelling simplifies calculations compare with two-scale and small slope approaches.

F5-3
0920

The Sensitivity of Simulated Passive Polarimetric Wind-Direction Signatures to Ocean-Wave Asymmetry, Foam, and Background Radiation

D. B. Kunkee and A. J. Gasiewski
School of Electrical and Computer Engineering
Georgia Institute of Technology
Atlanta GA, 30332-0250

An asymmetric-wave geometrical optics (AWGO) model of the upwelling thermal radiation over the ocean has been used to investigate passive polarimetric wind-direction signatures and their relation to wind-driven surface features such as wave asymmetry and foam, and the background (downwelling) radiation. Wind-direction signatures at 19 and 37 GHz were calculated using a Monte-Carlo ocean surface simulation in which the shapes of the simulated ocean features were controlled by incorporating both amplitude and phase spectral information into each realization. A geometrical optics (GO) model was used to calculate the upwelling radiation from each surface realization. The validity of the GO model is supported by calculations of the mean curvature of a wind-driven ocean surface and laboratory measurements of polarimetric emission at 92 GHz from small amplitude water waves.

Azimuthal wind-direction signatures were calculated under the following surface conditions: (1) all foam concentrated on the leeward side of breaking waves and (2) foam distributed over the leeward and windward slopes of breaking waves. The total foam coverage was the same under both conditions. Similarly, calculations were performed for various degrees of wave asymmetry as determined by slope statistics accumulated during each surface realization. The studies show that at angles near the SSM/I observing angle, T_h and T_U are sensitive but T_v is insensitive to wave asymmetry. However, T_v was found to be sensitive and T_U insensitive to the placement of foam on the waves. The study will help identify the optimal uses of T_v, T_h and T_U for remote sensing of ocean surface wind-direction. AWGO model simulations have also shown that the wind-direction signature is influenced slightly by the background radiation profile. Calculations using different atmospheric temperature and water vapor profiles indicate that, in general, the wind-direction signature in the first three Stokes parameters depends on the downwelling brightness profile.

F5-4
0940

A SCANNING 60 GHz RADIOMETER TO MEASURE AIR SEA TEMPERATURE DIFFERENCE: RECENT RESULTS DURING COPE

Yuri G. Trokhimovski
NRC Resident Associate
NOAA/ERL/ETL
325 Broadway
Boulder, CO 80303

Ed R. Westwater & Yong Han
CIRES
University of Colorado/NOAA
325 Broadway
Boulder, CO 80303

Vladimir Ye. Leuskiy
Astro Space Center
Lebedev Physical Institute
Russian Acad. of Sciences
Profsoyuznaya St. 84/32
Moscow, 117810, Russia

On of the basic parameters in the study of air/sea interaction is the air/sea temperature difference. Although this parameter can be measured by in situ sensors, the measurement of water temperature at a depth of 1 - 2 m is not always representative of the temperature at the boundary- the so-called skin temperature. A single-channel scanning 5-mm radiometer has been developed for shipboard applications to measure air/sea temperature differences and lower-atmospheric temperature profiles. Previous comparisons with in situ air and water temperature measurements, dropsonde temperature data, and radiosonde data have shown that the technique based on 5-mm measurements determines the air-skin water (skin depth of 0.3 mm) temperature difference with an accuracy of the order of 0.1 K. In addition, the temperature lapse rate is derived with good accuracy for altitudes below 300 m. Radiometrically-derived conditions of neutral, weakly stable and unstable have shown interesting correspondences with VV Ku-band sidelooking radar images.

The scanning radiometer will be operated during the Coastal Ocean Probing Experiment (COPE) that will be conducted of the coast of Oregon during September/October 1995. It will be deployed on the research oceanographic vessel FLIP that is operated by the Scripps Institute of Oceanography. Other instruments on FLIP that will provide comparison data include infrared radiometers to measure sea surface temperature (SST), high-resolution dropsondes, conventional bulk SST measurements, and air temperature at two levels. Additional ground truth will be available from a tethersonde that will be raised and lowered from a blimp in the vicinity of FLIP. Preliminary data from this experiment will be shown.

Prior to deployment during COPE, the scanning radiometer was operated at the Boulder Atmospheric Observatory (BAO). Here, the radiometer operated at several levels on the 300 m tower and its output was compared with in situ data from: (a) radiosondes; (b) hand-held meteorological instruments on the moving tower carriage; and meteorological measurements at fixed levels on the tower. Measured and calculated antenna temperatures agree to better than 0.1 K for the portions of the scan where the radiometer is viewing the sky. Initial results also indicate that the scanning radiometric technique could be applied from a low-flying aircraft.

F5-5
1000

PASSIVE SUBMILLIMETER-WAVE SENSING OF CIRRUS CLOUD PROPERTIES

K. Franklin Evans*
Program in Atmospheric and Oceanic Sciences
University of Colorado
Boulder, CO 80309-0311

The inability to remotely sense the global distribution of cirrus ice mass from satellite is a major problem for observing the climate system. While some optical properties of ice clouds can be measured from space currently, these are only indirectly related to ice water path (IWP), which is needed for climate model validation. Recently a new technique for remotely sensing cirrus IWP and characteristic particle size was proposed (Evans and Stephens, *J. Atmos. Sci.*, **52**, 2041-2072, 1995). This method relies on the scattering of upwelling radiation by ice crystals, reducing the brightness temperature from clear sky values. Submillimeter wavelengths are sensitive enough to detect cirrus of moderately low visible optical depth. Two radiometer frequencies can be used to obtain information about particle size, which is required to calibrate the relationship between brightness temperature depression and IWP.

Results of new scattering and radiative transfer calculations concerning the capabilities of the technique will be shown. Frequencies above 400 GHz are superior to lower ones because of their greater sensitivity to cirrus and lessened dependence of brightness temperature depression on particle size. Water vapor absorption prevents these frequencies from sensing the surface and boundary layer, yet the transmission from space to upper tropospheric ice clouds is high for well chosen frequencies. The ability to retrieve cirrus IWP and particle size are illustrated with a simple two frequency technique. This method is based on the computation of the scattering properties of eleven realistic ice particle shapes and hundreds of size distributions with the discrete dipole approximation. Upwelling and downwelling brightness temperatures at typical research aircraft altitudes are computed with a polarized radiative transfer model for several atmospheric profiles. In terms of their radiative effect, observed cirrus particle size distributions are shown to be equivalent to theoretical gamma size distributions. At submillimeter wavelengths two frequencies can unambiguously determine the characteristic particle size, while two polarizations can give some information about particle shape. The error in retrieved cirrus IWP is quantified in terms of uncertainties in particle shapes and variations in the background radiation, and is shown to depend on the characteristic particle size.

An update will be given of the development at the Jet Propulsion Laboratory of a prototype cloud ice radiometer. The instrument will measure two linear polarizations at 500 and 630 GHz with a scanning geometry. Flights on the NASA DC-8 are planned for the summer of 1996.

F5-6 1040 OBSERVATIONS OF WATER VAPOR AND CLOUD LIQUID FROM AN AIRBORNE DUAL-FREQUENCY RADIOMETER DURING THE VORTEX '95 EXPERIMENT

L.S. Fedor, E.R. Westwater, & Yong Han
CIRES
University of Colorado/NOAA
325 Broadway
Boulder, CO 80303

Yuri G. Trokhimovski
NRC Resident Associate
NOAA/ERL/ETL
325 Broadway
Boulder, CO 80303

The fine-scale horizontal variations of water vapor and cloud liquid water are of importance to climate, meteorology, and satellite validation/calibration. The Environmental Technology Laboratory of NOAA has developed a dual-frequency upward- (and downward-) looking radiometer at 23.87 and 31.65 GHz to measure the integrated amounts of water vapor and cloud liquid above an aircraft. Currently, the Airborne Microwave Water Substance Radiometer is certified to fly on the NOAA P3 and NOAA Twin Otter. Technical details of the instrument are given by Jacobson et al. (Microwave Journal 37 , 24-39, 1994).

Two experiments involving the NOAA P3 were conducted in the Oklahoma-Texas region during April 1 to June 15, 1995. The first, the Verification of the Origin of Rotation in Tornadoes EXperiment, focused on obtaining detailed observations of mesocyclones and their potential for developing into tornadoes. The second, sponsored by the Department of Energy's Atmospheric Radiation Program, was to obtain detailed aircraft observations of cloud liquid and water vapor to correlate with short- and long- wave radiation measurements. The almost mutually exclusive goals of the two experiments allowed shared use of NOAA P3 aircraft throughout the entire April-June period.

During VORTEX, the AMWSR was operated on all P3 flights; of particular interest were several flight flown in zig zag flight patterns through mesoscale moisture fronts known as "dry lines". Through the sharp boundaries of dry lines, strong horizontal gradients in moisture can occur. Several of the dry line cases were observed, and examples will be shown.

In addition, flights were made over all five stations of the DOE's Cloud and Radiation Testbed Site in Central Oklahoma to compare observations with ground-based radiometers and special radiosonde releases. We will present data taken during spiral ascents and descents about the central CART facility at Lamont, OK, and well as observations of stratus clouds obtained during "porpoise" ascents and descents of the aircraft.

F5-7
1100

EVALUATION OF SATELLITE RETRIEVAL ALGORITHMS FOR WATER VAPOR AND CLOUD LIQUID USING ISLAND-BASED MICROWAVE RADIOMETER DATA

D. A. Hazen[1], J. B. Snider[2], and W. B. Madsen[1]
[1]NOAA/ERL/Environmental Technology Laboratory
Boulder, Colorado 80303
[2]Cooperative Institute for Research in
Environmental Sciences (CIRES)
University of Colorado/NOAA
Boulder, Colorado 80309-0449

A one-year's data base of continuous ground-based microwave radiometric measurements (20 and 31 GHz) of precipitable water vapor, integrated cloud liquid, infrared cloudbase temperature, and shortwave solar irradiance was obtained at Porto Santo Island (33°N, 16.4°W), Madeira Islands, Portugal, from July 1992 through June 1993. Additional data for shorter periods of time were obtained from a ship operating in the North Atlantic Ocean during June 1992, and from New Ireland Island (2.6°S, 150.8°E), Papua New Guinea, during January and February 1993. The data base represents a unique set of ground-truth data which is being used to improve the quality and accuracy of liquid and water vapor retrievals from Special Sensor Microwave Imager (SSM/I) satellite millimeter wave brightness data. Ultimately, this work will improve NOAA's capability in global monitoring of atmospheric water.

We summarize an investigation of current statistical retrieval algorithms reported in the literature by comparing water vapor and liquid water retrieved from SSM/I data with the ground-based microwave measurements. In order to account for the widely different fields of view of the satellite and ground-based radiometers, we examine the effects upon retrieval accuracy of different spatial and temporal averaging. For example, we find that the "best" retrievals are obtained by limiting satellite data to within 5 km of the ground-truth site and by using 60 min averages for the surface data.

Using the form of the most promising algorithms from the literature, a sub-set of the ground-truth data was used to derive "new" statistical algorithms for water vapor and cloud liquid. We present a comparison of satellite data retrieved using the "new" algorithms with ground-based measurements for the remainder of the data base. We conclude by presenting preliminary findings on the relative performance of statistical and physical retrieval methods.

F5-8
1120

CONTRIBUTION OF ATMOSPHERIC WATER VAPOR TO THE TOTAL GPS SIGNAL DELAY

Daniel Wolfe
NOAA/ERL/ETL
325 Broadway
Boulder, CO 80303

Russell Chadwick and Seth Gutman
NOAA/ERL/FSL
325 Broadway
Boulder, CO 80303

Peng Fang and Yehuda Bock
Scripps Institution of
Oceanography
U.C. San Diego
LaJolla, CA 92093-0225

Michael Bevis and Steven
Bussinger
University of Hawaii at Manoa
2525 Correa Road
Honolulu, HI 96822

GPS radio signals are slowed by the Earth's atmosphere resulting in a delay in the arrival time of the transmitted signal from that expected if there were no intervening media. It is possible to correct for the ionospheric delay, which is frequency dependent, by using a dual-frequency GPS receiver. The delays due to the neutral atmosphere are not frequency dependent, but depend on the constituents of the atmosphere that are a mixture of dry gasses and water vapor. The total signal delays introduced by these components are referred to as the hydrostatic or "dry" delay (DD) and the "wet" delay (WD), respectively. In practice, the total signal delays measured by the GPS receiver from all satellites in view are mapped to the vertical using the function 1/sin(elevation angle of the satellite), and combined to give the "Total Zenith Delay" at an observing site. Total zenith delay (ZTD) due to the neutral atmosphere has a magnitude of approximately 250cm at sea level, to which the hydrostatic and wet components contribute about 97% and 3%: approximately proportional to the ratio of the total mass of dry air to water vapor in the atmosphere.

Comparisons with radiosondes and radiometers demonstrate that the WD can be directly related to total precipitable water vapor (TPW) above the GPS antenna through a factor that is related to the mean temperature of the atmosphere. The mean air temperature is currently estimated with a high degree of confidence from a surface temperature measurement and the climatological history of the temperature profile for that region based on radiosonde data.

NOAA's Environmental Research Laboratory maintains 7 continuously operating GPS receivers and surface meteorological sensors as part of its efforts to develop an operational surface-based GPS water vapor monitoring system. The ZTD is calculated using software originally developed for geodetic surveying that has been modified to account for the atmospheric parameters. A record of the total delay, surface pressure, surface temperature, and TPW is available at each site every 30-minutes. In this presentation, we will describe the temporal and spatial variability of TPW, as well as the contribution that water vapor makes to changes in the ZTD. This evaluation was conducted using data acquired over a 30-day period in April-May, 1995, at three widely spaced locations. Analyses indicate that the changes in TPW account for nearly all of the variability in the total delay, under both moist and dry conditions. The correlations between pressure, dry delay, and ZTD over periods exceeding 12 hours may be either positive or negative since pressure and water vapor are not independent variables, but are governed by the meteorological factors associated with differing air masses.

F5-9 RECENT RESULTS IN DERIVING WATER VAPOR PROFILES
1140 FROM COMBINED REMOTE SENSOR OBSERVATIONS

Yong Han and Ed R. Westwater
Cooperative Institute for Research in Environmental Sciences (CIRES)
University of Colorado/NOAA
325 Broadway, Boulder, CO 80303

The remote sensing of water vapor profiles by a single instrument during all weather conditions remains an illusive goal. The best observations of vapor profiles are currently provided by Raman lidar, which measures mixing ratio with a vertical resolution of 75 m and a temporal resolution of 1 min up to a range of about 9 km at night. However, the Raman lidar is severely limited during daytime conditions, and, like most optical and infrared instruments, does not penetrate most liquid-bearing clouds. At the present time, the most promising techniques for obtaining nearly-continuous profiles of water vapor combine observations from several remote and in situ sensors.

At the Department of Energy's Cloud And Radiation Testbed Central Facility in Lamont, Oklahoma, several remote sensors are currently operated continuously. These instruments include a dual-channel microwave radiometer, a Fourier Transform Infrared Radiometer, several ceilometers, Radio Acoustic Sounding Systems at 915 and 50 MHz. Recently, Han and Westwater *(J. Atmos. Oceanic. Tech.* 12, October 1995, in press) developed and applied a technique to microwave, RASS, and ceilometer data that achieved accurate results in cloudy conditions. This mathematical technique can be extended to incorporate soundings from Raman lidar as well. During clear nighttime conditions, the soundings are little changed from those of the Raman; however, during cloudy and daytime conditions, the impact of the remaining sounders is substantial. We illustrate our results from the FIRE II experiments that were held in Coffeyville, KS during November-December 1992. In addition, data from Intensive Operating Periods at the CART site during 1994 and 1995, will also be presented.

F5-10
1200

REMOTE SENSING OF VEGETATION TEMPERATURE AND ITS LINKS TO GLOBAL WARMING

James A. Smith*
Laboratory for Terrestrial Physics
Code 920
NASA Goddard Space Flight Center
Greenbelt, MD 20771
Narinder Chauhan
Department of Electrical Engineering and Computer Science
George Washington University
Washington, DC 20052

Remote sensing data, aided by Global Circulation Modeling, are being used to detect signatures of greenhouse effects. Of primary interest in these studies is a possible warming trend in the Earth's temperature that can either be estimated from direct remote sensing observations or can be derived from an analysis of the Earth's radiation budget. Land surface temperature/emissivity products are currently being derived using a variety of techniques to correct for atmospheric transmission, emissivity variations and spatial heterogeneity. But surface temperature observed from a satellite platform is a function of sensor view/solar zenith angle, vegetation type and structure, and in addition contains a mixture of soil and vegetation temperature. Accurate predictions of greenhouse effects require accurate estimates of the temperature distribution and the partitioning of radiative forcing into sensible and latent heat over land and vegetated surfaces and also a correction for the viewing geometry.

The present paper is focussed on quantifying the uncertainties in land surface temperature and energy budget arising from the variation in sensor view/solar zenith angle. Secondly, the role of vegetation structure on these estimates will be investigated. Thermal modeling and energy budget techniques (J. A. Smith and S. M. Goltz, *IEEE Transactions on Geoscience and Remote Sensing* , **32**, 1060-1066, 1994), will be used to assess the sensitivity of land surface temperature to the above parameters. The model treats fully leafed canopies as discrete ensembles of leaves partitioned into slope angle and height classes. The steady state energy budget equations incorporate sensible and latent heat fluxes in addition to other short and long wave energies. The model has recently been updated to include the stomatal conductance formulation presently being used by the Simple Biosphere Model (SiB2) (P. J. Sellers, et al., *Journal Climate.*, Accepted, 1996). This study can provide guidelines for correction to temperature data obtained through remote sensing means.

Session G/H-5, 0855-Fri., CR2-6
RED SPRITES, BLUE JETS, AND LIGHTNING
Chairperson: L. Hale, CSSL, Pennsylvania State Univ., University Park, PA 16802
Organizers: L. Hale; and Y. Taranenko, Space and Atmospheric Sciences Group, Los Alamos National Laboratory, Los Alamos, NM 87545

G/H5-1
0900

SOME RECENT RESULTS IN SPRITES AND JETS RESEARCH

D. D. Sentman* E. M. Wescott
Geophysical Institute, University of Alaska, Fairbanks
903 Koyukuk Drive, Fairbanks, AK 99775-7320 USA

Red sprites and blue jets are brief optical transients in the middle-and upper-atmosphere excited by lightning. Their existence points to a more direct form of electrical coupling between tropospheric thunderstorms and the ionosphere than has been appreciated in the past. During the spring and summer of 1995 the University of Alaska performed new types of measurements that concentrated on obtaining a more detailed description of these events in several ways. (1) Optical spectra of sprites were obtained for the first time. Analysis of the spectra reveal that the red color of sprites is caused by emission from the first positive band of neutral molecular nitrogen (N2 1P). This emission is substantially the same as that of the lower red border of some auroral curtains, and suggests that electron impact excitation plays a role in sprite production. Current observations do not permit ascertaining the source of exciting electrons, but theoretical considerations indicate that it may be the electrified volume immediately above charged thunderstorms. (2) High spatial resolution imagery of massive sprites has revealed instances of branching structure in sprite tendrils. This branching structure has not been observed in all sprites that have been recorded, and its temporal development is not resolved in our video recordings. However, in the several examples in which such structure has been observed, it emerges from an altitude of approximately 55-65 km, near the base of the bright head of the sprite, and gives the visual appearance of spreading downward and outward along one or more central channels in a manner resembling tropospheric lightning step leaders. (3) Aircraft campaigns were conducted to study sprites and jets associated with tropical thunderstorms sytems in Central and South America. Preliminary results indicate that tropical storm systems may be weak producers of sprites and jets compared to Midwestern mesoscale thunderstorm systems, even in cases where the lightning flash rates are comparable.

In this talk we review these results within the context of new results obtained by other groups.

G/H5-2
0920

COORDINATED RF AND OPTICAL MEASUREMENTS OF SPRITES, JETS AND ELVES IN THE COLORADO SPRITES'95 CAMPAIGN

Walter A. Lyons
ASTeR, Inc.
46050 Weld County Road 13
Ft. Collins, CO 80524

The SPRITES'95 Campaign was conducted from the Yucca Ridge Field Station located 20 km northeast of Ft. Collins, CO during June and July. Two dozen nights provided storms and viewing conditions allowing observations with low-light video systems, spectrometers, photometers and a suite of concurrently recorded ELF and VLF signals. Sprites and related phenomena were associated with large (>20,000 km^2) mesoscale convective systems which also contained significant numbers of positive cloud-to-ground (CG) lightning flashes. By using a common precision timing source (GPS) a variety of remote sensing measurements were synchronized both at Yucca Ridge and at remote sites. Over the course of the summer, sixteen different science teams coordinated observations, many times for the same event. The project management team (ASTeR) provided logistical, forecasting and meteorological data acquisition support, as well as low-light video ground truth for confirming the existence and approximate location of luminous stratospheric/mesospheric phenomena. The first apparent jets imaged from ground-based sensors were obtained on the night of 15 July. Coordinated low-light video, high speed photometer (Tohoku University) and VLF measurements (U.S. Inan, STAR Lab, Stanford University) demonstrated that highly transient (≈ 1 ms) brightenings of the airglow layer (tentatively called elves) are distinct from sprites, and occur at a higher altitude (≈ 100 km) either independent of or before the appearance of sprites. They may be a response to the EMP of large CG events. Audio from several VLF receivers (1-10, 1-50, 1-100 kHz) were simultaneously recorded along with the low-light camera output on SHVS video tapes. Distinct audio signatures appear to accompany many sprites and elves. Video data are being utilized in interpretation of perturbations in phase and amplitude of Navy VLF transmissions recorded at several sites by the University of Otago (R. Dowden). Remote measurements of Q-bursts in the ELF band made by the MIT group at their Schumann resonance station in Rhode Island repeatedly confirmed the previous summer's report of coincidence between sprites, large +CGs and Q-bursts (Boccippio et al., Science, 269, 1088-1091, 1995). The low-light video is also being used to evaluate the ELF and VLF data collected by the Pennsylvania State group (L. Hale, L. Marshall). A number of investigators will report on distinct signatures in the VLF related to sprites and elves. Other components of the experiment included obtaining optical sprite spectra (Lockheed), narrow band photometer readings by Mission Research Corp. and Utah State University (tentatively identifying the 4278 band suggestive of considerable ionization) and high speed (2 ms) optical and infrared images of sprites (Lawrence Livermore National Lab). Results are still pending from bi-static VHF transmission experiments (Djuth, GeoSpace) and active probing of the sprite region by radar at 28 mHz (Tsunoda, SRI International). These experiments will be summarized as results become available and will be placed in the context of the overall SPRITES'95 program.

G/H5-3
0940

POLARITY ASYMMETRY IN GROUND FLASHES ASSOCIATED WITH SPRITES

Earle Williams
Parsons Laboratory
MIT
Cambridge, MA 02139
Dennis Boccippio and Charles Wong
Department of Earth, Atmospheric and Planetary Science
MIT
Cambridge, MA 02139
Walt Lyons
ASTeR, Inc
Ft Collins, CO 80522

Considerable evidence has accumulated that sprites in the mesosphere are associated with positive flashes to ground in the troposphere, as identified by the National Lightning Detection Network. This paper explores reasons for this pronounced asymmetry in polarity. The working hypothesis (Boccippio et al, Science, 1995) is that sprites are created by field enhancements associated with rapid charge rearrangement of electric charge in the cloud below by the ground flash. Observations have shown that special mesoscale meteorological conditions must be met, with stratiform precipitation and laterally extensive radar 'bright-band' in which 'spider' lightning develops. According to this picture, the asymmetry in polarity is attributable to differences in the behavior of positive and negative grouind flashes, the latter polarity dictated by the basic charging process of clouds at different stages of development. As far as ground flashes are concerned, the asymmetry in stroke multiplicity and current between positve and negative events is already well established. Negative flashes are characterized by stroke multiplicity but by a majority of strokes without continuing current, whereas positive flashes most often show one stroke only with a large long continuing current. Consistent with this behavior, negative return stroke velocities fall of rapidly with height above ground, whereas positive return stroke velocities remain high well in to the cloud.

In addition to sprites, ELF transients called Q-bursts accompany the positive ground flashes. Q-bursts can be located by single station Schumann resonance methods on a global basis following impedance methods developed by other investigators. Our comparisons of ELF source spectra for positive and negative flashes tend to show flat (ie.,'white') spectra for negatives (consistent with impulsive discrete stroke current sources), but declining energy with frequency ('red' spectra) for positive flashes. The latter observation is consistent with long continuing current which pervades the stratiform region over distances of tens to hundreds of kilometers on short time scales (<10 msec)and thereby stress the mesosphere to dielectric breakdown to make the sprites.

G/H5-4
1000

DETECTION AND LOCATION OF SPRITES BY VLF PHASE AND GROUP MULTISTATIC RADAR

R. L. Dowden* J. B. Brundell
Physics Department
University of Otago
Dunedin
New Zealand

The luminous columns which appear as a "red sprite" seem to be ionised columns which scatter VLF waves in the earth-ionosphere waveguide. The direct and sprite-scattered waves from three VLF transmitters, NLK, NAA and NSS, are monitored at two sites: on the JILA Tower on CU Campus, Boulder, and at Yucca Ridge, near Fort Collins. At these two sites, 75 km apart (approximately six wavelengths), the phase and amplitude of the two MSK frequencies of the three transmitters have been logged at 0.5 s intervals during all nights since mid-June, 1995.

Since there is a sharp transition from the unperturbed (direct only) signal to that perturbed by the sprite-scattered signal, the phase and amplitude of the scattered signal, relative to the direct signal, can be found by phasor subtraction. In principle, the difference between the phases of the scattered wave measured at two sites, essentially the relative phase delay, can be used to get the direction of arrival (DoA) though the cycle ambiguity has prevented absolute measurements.

For sprites within about 300 km of the VLF receivers, scattered signals are observed even when this requires scattering back towards the transmitter to reach the receiver. In such cases (300 km range) the backscattered wave, which travels 600 km further, arrives 2 ms later than the direct signal. This group delay can be measured to within about 0.1 ms, depending on S/N ratio, by measuring the change in phase over the 100 Hz span of the MSK. The locus of possible sprite positions is on an ellipse having foci at the VLF transmitter and receiver. The locus is very nearly parabolic for sprites close to the receiver and approaches an arc of a circle for back scattered signals. Although, in principle, reception of sprite-scattered signals from three transmitters at a single site provides the sprite position at the intersection of the three ellipses, the S/N ratio is rarely adequate. On the other hand, this method allows a good estimate of sprite *range* if the scattering is "back" (near 180°).

Even with only two VLF receivers the spatial variation of scatter amplitude implies a sprite structure (multiple columns of plasma) consistent with that seen. Use of four VLF receivers in a linear array being set up to provide spacings from 0.3 to 6 wavelengths will provide accurate DoA without cycle ambiguity, increase the range accuracy by data averaging, enable location by a combination of the phase and group delay methods and provide more structural details of sprites by VLF holography.

G/H5-5
1040

RF MEASUREMENTS OF LIGHTNING-INDUCED IONOSPHERIC EFFECTS

K. M. Groves* J. V. Rodriguez J. M. Quinn
Phillips Laboratory/GPIA
29 Randolph Road
Hanscom AFB, MA 01731
P. J. Erickson M. Cox
MIT Haystack Observatory
Route 40
Westford, MA 01886
T. Arce
Engineering and Theory Center, 304
Cornell University
Ithaca, NY 14853

Numerous recent optical measurements of enhanced predominantly red and blue emissions extending from the tops of active thunderstorms to the lower ionosphere have generated keen interest in understanding the interaction of tropospheric electrification processes with the upper atmosphere. Studies have shown that these transient emissions, dubbed "red sprites" and"blue jets", are highly correlated with the occurrence of large positive cloud-to-ground (CG) lightning events and so-called Q-bursts, broadband enhancements of the Schumann Resonance. While various theoretical models have been constructed to explain the occurrence location, duration and optical intensity of sprites and jets, very little quantitative data on the atmospheric heating and ionization associated with these events exists. During July-August 1995 we collected radio frequency (RF) measurements of lightning- induced ionospheric effects in the northeastern United States at multiple frequencies. The primary diagnostic for the investigation was the Millstone Hill UHF incoherent scatter radar located in Westford, Massachusetts. The radar provides quantitative data on ionization levels and electron temperature. A narrowband VLF receiver sited nearby was employed to detect conductivity changes in the D region by monitoring signals from several powerful VLF navigation and communication transmitters. Additionally, a VHF coherent backscatter radar was deployed at Hanscom AFB, Massachusetts for the purpose of diagnosing enhanced ionization in the lower ionosphere. The combined data sets were compared with CG lightning events as recorded by the National Lightning Detection Network to correlate RF signatures with individual lightning strikes. Preliminary results of the measurements campaign will be presented.

G/H5-6
1100

PULSED RADAR INVESTIGATIONS OF RED SPRITES

Roland T. Tsunoda
Geoscience and Engineering Center
SRI International
Menlo Park, California 94025

There is mounting evidence that anomalous ionization is produced during events known as red sprites and blue jets, e.g., in propagation effects on VLF radio waves. Local measurements of the ionization produced is, however, difficult because the levels appear to be extremely low (i.e., less than 104 el/cm^3). Given that these kinds of events are impulsive, likely to be structured, and involve electron acceleration and heating, there is good reason to believe that there would be associated refractive index fluctuations. If so, radar backscatter from these fluctuations may be detectable. Measurements of radar backscatter characteristics are potentially capable of providing information about plasma and other characteristics associated with these events, for example, electron temperature. Using the experimental results reported by Rumi [1957] (G. C. Rumi, "VHF radar echoes associated with atmospheric phenomena," J. Geophys. Res., 62, 547, 1957) as a basis, we fielded a pulsed radar system with parameters similar to his to search for radar signatures that may be associated with red sprites or blue jets. He reported distinct radar signatures, which were characterized by echoes that were discrete in range and with onset and decay times that were extremely rapid. Our radar, which operated at 24.515 MHz with 60-microsecond pulses transmitted at 30-kW peak power through four-element Yagi antennas, was set up next to the Yucca Ridge field site in Colorado and operated during the last week of July 1995. Radar measurements were made on several nights in conjunction with optical sensors located at the Yucca Ridge field site. In this paper, we will briefly review the results obtained by Rumi [1957], and compare them with our first preliminary results obtained from this field experiment. We will present several examples of radar backscatter, show that they resemble those obtained by Rumi, and discuss and interpret some of their characteristics. We hope to have progressed far enough with data analysis by this meeting to present the first Doppler signatures and comparisons with optically detected red sprites; the latter were collected during this campaign.

G/H5-7
1120

MEASUREMENTS OF LIGHTNING-GENERATED ELECTRIC FIELDS IN THE NIGHTTIME D-REGION

Carl L. Siefring*
Plasma Physics Division, Code 6755
Naval Research Laboratory
Washington, DC 20375
siefring@nrlfs1.nrl.navy.mil

There have been very few measurements of lightning-induced electric fields in the nighttime D-region (70-90 km). Some of the only published examples are from the 1981 Thunderstorm sounding rocket experiment led by Cornell University. In this experiment three rockets and a balloon made simultaneous measurements of lightning-generated electric fields in the stratosphere, mesosphere and the ionosphere. Several papers (Siefring and Kelley, 7th Int. Conf. on Atmospheric Electricity, Paper 3.6, 1984; Kelley et al., J. Geophys. Res., 90, 9815, 1985; Holzworth et al., J. Geophys. Res., 90, 9824, 1985) and a Ph.D. thesis (Siefring, Upward Propagating Electric Fields from Thunderstorms and VLF Transmitters, Cornell University, 1987) describe the results of this experiment. The measured lightning-induced electric fields are transient in nature with a time signature similar to the optical brightness of Sprites. The transient electric fields typically had amplitudes near 100 mV/m in the D-region and a time duration of 10 to 20 ms. The source for the measured electric fields is the electrostatic field change that occurs when the thunderstorm charge is neutralized by a lightning return stroke. The frequency response ($\approx$20 kHz) of the airborne instruments were not high enough to measure the characteristics of short duration ElectroMagnetic Pulse (EMP) that occurs when the lightning stroke is initiated, although an initial high-amplitude spike was also a common feature in the data. There were no unusual characteristics of thunderstorm and therefore the measured amplitudes of the fields could be consider as typical or average. Models of D-region breakdown have typically required fields of 10 to 100 V/m to cause ionization in the 70-90 km range. This implies that the amount of charge neutralize by a lightning stroke which generates a Sprite would need to be >100 time larger than average (consistent with the largest 5% of positive strokes). We will discuss these and other measurements and implications for Sprites and future rocket experiments in this region.

G/H5-8
1140

ROCKET BASED STUDIES OF LIGHTNING IN THE IONOSPHERE

R. H. Holzworth*
Univ. of Washington
Geophysics 351650
Seattle, WA 98195-1650
M. C. Kelley
318 E and TC
Cornell University
Ithaca, NY 14853

While no in-situ measurements have been made in the Sprite luminous regions, there have been many in-situ measurements of lightning generated perturbations in the upper atmosphere and ionosphere. The first in-situ rocket observation of lightning related electric pulses at high altitudes in the ionosphere were made in 1981. This pair of rocket flights (Thunder-Hi and Thunder-Lo) obtained an impressive list of first observations including the detection of lightning pulses that are 1 or 2 orders of magnitude above any predicted lightning pulse in the ionosphere. These pulses were found to have an amplitude typically between 5 and 50 mV/m above 100 km, a duration of several ms (thousands of electron Langmuir wave periods), and roughly equal components both parallel and perpendicular to the magnetic field. Subsequently several rocket flights have been conducted over active thunderstorms with plasma and wave instruments. Newly determined characteristics include: the occurrence of a precursor pulse in the electric and magnetic field with duration about 1 ms which precedes the dispersed whistler wave at the corresponding frequency by several ms, evidence for 3-wave processes in the decay of a whistler into another whistler and a low frequency wave, and coupling to enduring lower hybrid waves. During these rocket flights cloud-to-ground lightning wave forms from over 2000 km horizontally distant events have been recorded regularly. Source to reception studies indicate the waves propagated in the waveguide to the ionosphere below the rocket and then upward vertically (in agreement with simple theory). The wave paths with access to the rocket include an aperture-like area at the bottom side ionosphere, and thus form an interference pattern in the wave packet amplitude at the rocket. ¿From the optical instruments on these flights an anomalous optical emission has been detected which is localized, apparently from high altitude, has a weak electrical signature, has a duration of about 1 sec and is associated with fast/early trimpis. Most recently the Thunderstorm-III rocket was launched in September 1995 over an active thunderstorm near Wallops Island, Virginia. This paper will review the earlier rocket results and include the latest results from this rocket.

G/H6-1
0900

ELECTRON PRECIPITATION CAUSED BY CHAOTIC ELECTRON MOTION IN THE MAGNETOSPHERE DUE TO LARGE AMPLITUDE WHISTLER WAVES*

James Faith, S. P. Kuo, and J. Huang
Weber Research Institute
Polytechnic University
Route 110
Farmingdale, NY 11735

Originally due to experimental observations of the perturbation of VLF signals propagating in the Earth ionosphere waveguide called "Trimpi events", and later by direct experimental verification, it has for some time been known that energetic electrons trapped by Earth's magnetic field can under some circumstances precipitate into the polar regions. The correspondence of these precipitation events with the presence of natural or man-made signals propagating between the hemispheres has led to the development of Doppler shifted gyroresonant wave-particle interaction models.

Due to the directional nature of gyroresonant interactions, these theories are unable to explain the simultaneous observation of precipitation events in geomagnetically conjugate regions in both hemispheres (*Geophys. Res. Lett.*, **17**, 259-262, 1990). We show that the interaction of a non resonant whistler wave with a trapped bouncing electron can lead to chaos in the electron trajectory. We find that chaos in the trajectory of a test electron is due to the bouncing motion of the particle between magnetic mirror points. In addition, the onset of chaos is strongly dependent on the wave magnetic field relative to the background magnetic field, where a large wave field will facilitate chaos.

The result of the chaos is to enhance the electron's axial kinetic energy, and allow it to be scattered into the mirror field loss cone. As our model is not based on a resonance condition between the wave and the electron cyclotron frequency, there is no directional dependence in our model, and an electron may be scattered in either direction. Thus our model can explain the simultaneous precipitation events, and augment the previous theories.

*Work supported by AFOSR.

G/H6-2
0920

THE AURORAL PLASMA CAVITIES AS COLLISIONLESS RAREFACTION SHOCK WAVES

Sergey V. Fridman
University of Illinois at Urbana-Champaign, Space Science and Remote Sensing Laboratory, 322-North CSRL, 1308 West Main St., Urbana, IL 61801-2307 (E-mail: sfridman@uiwpls.ece.uiuc.edu)

The auroral plasma cavity was identified by W. Calvert (*Geophys. Res. Lett., 8,* 919, 1981) as a latitudinally bounded region in the magnetosphere where the density of plasma is orders of magnitude lower than density on the surrounding latitudes. The nature of the cavity is still a controversial issue.

A phenomenon very similar to the auroral cavity has emerged from our numerical simulations of the evolution of parallel electric fields and plasma particles in a closed geomagnetic flux tube. A flux tube that belongs to the region of upflowing parallel currents was considered. Macroscopic neutrality of the tube was ensured by a drift current that was carried by energetic electrons. The calculations took into account cold ionospheric particles and energetic magnetospheric protons and electrons. An equilibrium state of cold plasma in the gravity field was accepted as the initial condition. It has been found that under certain conditions an intense parallel electric field is produced. The field appears in the form of two collisionless rarefaction shock waves that have separated from the equatorial plane in the north- and southward directions. Below the front of each shock wave there is mainly ionospheric plasma, while above the front there are upward accelerated ionospheric ions and hot magnetospheric plasma. Thus a macroscopic rarefaction region is formed. The region occupies the fraction of the flux tube which is above the shock fronts. Plasma density in the rarefaction region is of the same order as density of energetic magnetospheric particles (i. e. of the order of or less than 1 cm^{-3}). The region may exist from about 10 minutes up to several hours.

We have compared observed characteristics of plasma inside auroral cavities with our theoretical estimations of plasma parameters upstream of the shock wave. For this purpose we used analytical estimations as well as numerical calculations. The estimations include a general case of oblique (with respect to the geomagnetic field) shocks. Estimated densities agree with the observed values. We show that an upward accelerated ion flow is formed upstream of the rarefaction shock wave. Pitch-angle distribution of accelerated ions may be beam-like or conical depending primarily on the altitude of the shock, so that at higher altitudes there are favorable conditions for formation of the conical distributions. These results agree with observed regularities.

Thus, the rarefaction shock wave suggests a reasonable explanation of the auroral plasma cavity and accompanying phenomena.

G/H6-3
0940

HF RADAR SCATTERING FROM CORONAL MASS EJECTIONS**

P. Rodriguez*
Plasma Physics Division, Code 6755
Naval Research Laboratory
Washington, DC 20375

Coronal mass ejections (CMEs) from the sun are thought to be a primary cause of large geomagnetic storms at earth. Such storms have led to effects such as collapse of electric power grids and spacecraft upsets. With the new cycle of solar activity beginning it is possible that such deleterious effects will increase. Powerful HF radars could help provide a warning of earthward-directed CMEs by backscattering a signal from density enhancements in the leading edge of the CME. Some mass ejections appear to be associated with outward propagating shock waves which should impose a substantial Doppler shift on HF waves launched from the earth. Measuring the frequency shift on the return signal will provide an indication of the earthward-directed velocity of the coronal mass ejection. A combination with the transverse velocity measurement from coronagraph optical images will give the total velocity and direction of the CME, allowing an assessment of the likelihood of geomagnetic storms at earth a few days later. We discuss requirements and plans for experiments in CME detection with HF radars.

** Work supported by ONR.

G/H6-4
1000

INCOHERENT SCATTER OBSERVATIONS OF HELIUM IONS AT SOLAR MAXIMUM AND SOLAR MINIMUM

P. J. Erickson*
Atmospheric Sciences Group
Millstone Hill Observatory
Westford, MA 01886

W. E. Swartz D. T. Farley
School of Electrical Engineering
Cornell University
Ithaca, NY 14853

Recently, there has been a great revival of interest in helium ions in the topside plasmasphere, and several observational campaigns using the incoherent scatter radar facilities at Arecibo, Puerto Rico, Millstone Hill, Massachusetts, and Jicamarca, Peru have sought to investigate the morphology of these ions.

We present incoherent scatter observations of helium ion behavior at mid-latitudes and at the equator for several periods during the current solar cycle. Our analysis uses a constrained nonlinear least-squares technique (Erickson and Swartz, *Geophys. Res. Lett.*, **21**, 2745-2748, 1994). Wintertime solar maximum data from January, 1991 show a downward flow of helium ions over Arecibo during a 6 hour period centered on 2300 LT. In particular, we have made the first direct measurements of helium fluxes at several heights, and have found they can exceed 10^7 $cm^{-2}s^{-1}$ through the 800 km level, a value significantly larger than model predictions. The observed helium peak height agrees with predictions based on the transition from chemical equilibrium to diffusive flow, and peak densities reach 2×10^4 cm^{-3}. Helium remains a minor ion at all altitudes and times.

Arecibo solar minimum equinox observations in September, 1994 reveal a much weaker mid-latitude He^+ layer which remains stable for much of the night at a peak density of approximately 10^3 cm^{-3} and a slightly lower peak height of 700 km. Simultaneous Jicamarca topside equatorial measurements show an 800 km peak in helium with ion concentrations above 10^4 cm^{-3} at local noon, levels which we believe are made possible by vertical drifts driven by an eastward electric field.

G/H6-5
1040

INCOHERENT SCATTER RADAR DETECTION OF ION-ACOUSTIC WAVES OR DUSTY PLASMAS IN THE SPACE SHUTTLE EXHAUST

P. A. Bernhardt* G. Ganguli
Beam Physics Branch
Plasma Physics Division
Naval Research Laboratory
Washington, DC 20375
M.C. Kelley W.E. Swartz
School of Electrical Engineering
Cornell University
Ithaca, NY 14853

Enhancements in the backscatter from the 430 MHz radar at Arecibo were recorded during the Spacelab 2 Mission when the Space Shuttle Orbital Maneuver Subsystem (OMS) engines were fired in the ionosphere. The radar backscatter was increased by almost a factor of two in two 20-km-wide regions above and below the Shuttle orbit. The modifications in the backscatter could have been the result of (1) compression of the electrons to produce higher densities, (2) generation of ion-acoustic waves, (3) variations in the electron to ion temperature ratio, (4) enhanced scatter cross-section by charging of ice particles in the exhaust or (5) excitation of dust-acoustic waves. Modeling of the ionosphere and exhaust plume has been used to evaluate the applicability of these processes. Rapid cooling and condensation of the exhaust are important in determining the scattering properties of the modified ionosphere. A fluid model of the plume was used to calculate the temperature variations and ice particle growth along the plume axis. A dusty plasma is formed when electrons are attached to ice particles in the exhaust plume. The amount of charging is a function of particle size and electron flux onto the particle surface. The calculated neutral temperature inside the exhaust plume is 120 K. This temperature is much less than the ambient plasma temperature. Charge exchange between ambient O^+ and the cold exhaust molecules yields low temperature ion beams that excite weakly-damped, ion-acoustic waves. The enhanced radar echoes are probably the result of scatter from these waves, but the effects of the dusty plasma may be important. During future experiments in a program called SIMPLEX (Shuttle Ionospheric Modification using Pulsed Localized Exhuast), the Space Shuttle will fire the OMS engines over radars located at Arecibo, Puerto Rico; Jicarmarca, Peru; or Kwajalein, Marshall Islands. Measurements of the spectra from these radars will provide the means to distinguish between the various backscatter processes.

G/H6-6 1100 ON NON-LINEAR INTERACTION OF THE SCHUMANN RESONANCE FIELDS AND ROUND-THE-WORLD HF SIGNALS IN THE IONOSPHERE

Yu.M. Yampolski, P.V. Bliokh, V.S. Beley, V.G. Galushko, and S.B. Kascheev,
Institute of Radio Astronomy,
National Academy of Sciences of Ukraine
4, Chervonopraporna Street
310002 Kharkov, Ukraine

The effect of cross-modulation between the Schumann resonance (SR) and HF round-the-world signals (RWS) has been discovered. The eigenfrequencies of the Earth-ionosphere cavity are known to lie near 8; 14; 20; 26... Hz, while the quality factor may change from 5 to 7. This means that about 20% of the total energy per period is dissipated in the ionospheric D layer. Such losses must lead to Joule heating of the electrons $\delta T_e(t)$ and modulation of the collision frequency $\delta\nu$. Since the level of SR field E_{SR} is much lower then the "plasma field" E_P, the electron temperature perturbation is very small: $\delta T_e/T_e \approx E_{SR}^2/E_P^2 \approx 10^{-6}$. On the other hand, since the electron temperature perturbation depends on the square of the Schumann resonance field, only higher order harmonics of the SR apparently should be present in the spectrum of $\delta\nu$. Meanwhile, the experimental data show that there is a linear dependence between the spectra of $\delta\nu$ and E_{SR}. The measurements were carried out as follows. The CW radiation of a ground based HF transmitter was chosen as the probe signal. Doppler spectra of the RWS were analyzed. The receiving site was located at the RINAN Radio Astronomy Observatory near Kharkov. The world largest HF research antenna of the UTR-2 radio telescope was used to receive the probe signals. It has a T-shaped configuration of 1 by 2 km in size. A multichannel receiving complex having high sensitivity and frequency stability was used. The round-the-world HF signals were chosen as they can accumulate the effect of ELF-HF cross-modulation. Spatial filtering of the RWS was realized with the aid of the highly directional antenna. Either presence or absence of the RWS was tested using pulsed mode of the transmitter. The experiments were carried out in September, 1994. Most sure the cross-modulation effect was observed near sunset, when the Solar terminator crossed the radio path (both the transmitter and receiver had almost the same longitude). As a rule, the peaks in the RWS spectra were better pronounced about two first SR maxima, at frequencies about 8 and 14 Hz. The modulation index was estimated as $\mu = 10^{-3} \div 10^{-4}$, which implies a greater heating effect than originally assumed, and a linear dependence between $\delta T_e(t)$ and $E_{SR}(t)$. To explain the experimental facts the following model is suggested. Along with the ELF field of SR, the clear weather field E_0 is always present at the D-layer heights, whose level is evaluated by different authors as 100 V/m at the ground or 0.1 to 1 V/m at $50 \div 60$ km. Hence the heating is caused by the sum of E_0 and E_{SR}:

$$\frac{\delta T_e}{T_e} \sim \frac{(E_0 + E_{SR}(t))^2}{E_P^2} \sim \frac{E_0^2 + 2 \cdot E_0 \cdot E_{SR}(t)}{E_P^2}$$

and the modulation effect is due to the $E_0^2 + 2 \cdot E_0 \cdot E_{SR}(t)$ term. Obviously, in this case

$$\frac{\delta T_e^*}{T_e} \sim \frac{E_0^2 + 2 \cdot E_0 \cdot E_{SR}(t)}{E_P^2} \gg \frac{E_{SR}^2(t)}{E_P^2}$$

and the modulation index is $\mu \simeq 10^{-2} \div 10^{-3}$.

Therefore, the ELF-HF cross-modulation effect revealed is adequately described.

G/H6-7
1120

A THREE DIMENSIONAL IMPEDANCE METHOD TO MODEL GROUND CURRENTS INDUCED BY ELF SOURCES

Daniel A. James Jun Wei Lu David V. Thiel*
Radio Science Laboratory, School of Microelectronic Engineering
Griffith University, (Brisbane)
Qld, Australia 4111.

The three dimensional impedance method has been used to model eddy currents induced in heterogeneous human models by a time varying magnetic field (Orcutt and Gandhi, *IEEE Trans. Biomed. Eng.*,**35 (8)**, 577-583, 1988; Xi and Stuchly, *IEEE Trans. Biomed. Eng.*,**41 (11)**, 1018-1023). In this method, the object is modelled by a cubic 3D mesh of resistive cells with the current solved for each face of every cell. The values of the resistance are determined from the size of the element and the conductivity of the material being modelled.

In this paper, this numerical technique has been applied to non-uniform earth half-spaces immersed in ELF radiation. In particular the potential difference between two conductive stakes located in a uniform magnetic field is calculated in cases where there is a substantial change in conductivity in the vicinity of the two stakes. Two dimensional models have been used both numerically and experimentally, to verify the method. The numerical results compare favourably with experimental results in which the potential was measured along the edge of copper sheeting cut into various shapes located in a uniform, quasi-static magnetic field.

In this paper, the method will be briefly explained, a comparison between theory and measurement based on copper foil experiments will be outlined, and finally, potential difference calculations for spaced stakes in the vicinity of earth inhomogeneities will be presented. The method has great potential for modelling anisotropic earth planes, arbitrarily shaped buried objects, and both finite and infinitely long faults, dykes, pipes and cylinders.

G/H6-8
1140

ELF SURFACE IMPEDANCE MEASUREMENTS FOR SUBSURFACE EARTH MAPPING USING DISCRETE SPHERICS FROM DISTANT LIGHTNING AS A RADIATION SOURCE

Stephen J. Garner Steven O'Keefe David V. Thiel*
Radio Science Laboratory, School of Microelectronic Engineering
Griffith University, (Brisbane)
Qld, Australia 4111.

Electromagnetic surface impedance measurements have been used in subsurface mapping since the 1950's. Initially, the radiation source used was the naturally occurring EM background in the earth-ionosphere waveguide covering the frequency range 1mHz to 10Hz (the MagnetoTelluric method, MT). This was extended to higher frequencies in the audio range (the Audio-MagnetoTelluric method, AMT). In the mid 1960's, geoscientists started using the vertically polarised VLF navigation transmitters spaced around the world, and later still, a local generator operating in the audio frequency range was used (Controlled Source Audio-MagnetoTelluric method, CSAMT). With the advent of the GPS navigation system, it is likely that the VLF and Omega navigation systems will be terminated. In this investigation, the possibility of using distant lightning strikes as a source of vertically polarised, ELF-VLF radiation for surface impedance measurements is explored.

EM lightning spherics observed at distances greater than 500kms have spectral components in the range of 100Hz to 10kHz, with a significant intensity null at approximately 2kHz corresponding to a cutoff frequency in the earth-ionosphere waveguide. Strikes to the ground from cloud generate a predominantly vertically polarised, multi-frequency radio signal. The horizontal electric and orthogonal magnetic field components were recorded for each spheric on the surface of the earth. The srecording system was triggered by a level detection circuit in the magnetic field channel. Both transient records were digitised and transformed into the frequency domain. The surface impedance was determined at each frequency by averaging a number of records, and the apparent resistivity interpreted using a horizontally layered earth structure. If the upper layer resistivity is sufficiently high, then transforming the surface impedance data back into the time domain allows one to determine the time of flight to the first major subsurface boundary. This is equivalent to time domain reflectometry (TDR) commonly used in transmission line assessment.

In this paper, the basic approach to the method will be outlined, the automated data selection procedure will be given, the use of TDR techniques in the interpretation of the surface impedance data explained, and example results will be presented.

Session B-5, 1335-Fri., CR1-9
NUMERICAL METHODS
Chairperson: D.R. Wilton, Dept. of Electrical and Computer Engineering, Univ. of Houston, Houston, TX 77204

B5-1
1340

NUMERICAL MODELING OF MULTI-CHIP MODULES

M. Piket-May J. Dunn E. T. Thiele P. Vichot*
Z. Schoenborn*
Department of Electrical and Computer Engineering
Campus Box 425
University of Colorado
Boulder, CO 80309

In this study, we are considering various design aspects of an MCM which will serve as a 1024 x 1024 switching network to facilitate rapid communication between parallel processors and shared memory chips. Key desired features of this design include low power requirements, low latency, and a high data rate (2.5 Gbits/sec/channel) built into a modular design featuring asynchronous timing and conflict resolution. To achieve these objectives, a novel MCM design has been created which incorporates both conventional technologies and superconducting technologies.

Our research has specifically focused on the design of a clock distribution network whose signal serves as the logic-latching mechanism at the input to the shared memory chips. This clock network is located in a nonsuperconducting layer of the MCM, with its outputs distributed to circuitry in the superconducting strata of the MCM. Since the clock is being used for high speed digital applications, it is critical to maintain a certain degree of signal integrity at the outputs of this clock network. The clock signal must be fed along a single 32 ohm line to some network which will distribute this signal to eight 6 ohm lines. Therefore, the clock must provide a transition from this single, high impedance input to multiple, low impedance outputs, with the realization that the lower impedance requires wider lines. Due to the limited amount of "real estate" within the MCM for each clock and its distribution network, this requires that the impedance transition from the input to the wide, low impedance outputs be done as compactly as possible.

A circuit simulator is being used for the initial designs. Field simulations are then conducted using a combination of frequency and time-domain techniques. The frequency-domain analysis is implemented through the use of a packaged moment method code, while the time-domain analysis employs the FD-TD method.

This talk will highlight the evolution of different designs for the clock distribution network which attempt to meet the specifications given above. Field simulation results for these different designs will be shown to give reasonable agreement between FD-TD and moment method techniques.

B5-2
1400

FINITE-DIFFERENCE ANALYSIS OF GUIDED-WAVES ON PERIODIC DIELECTRIC RODS.

Hung-Yu David Yang,
Department of Electrical Engineering and
Computer Science, University of Illinois,
Chicago, IL 60607-7053

Due to the recent technology advancement on the material processing, there is significant renewed interest on the artificial media for microwave, millimeter and optical applications. In this paper, a finite-difference method is applied to the analysis of wave propagation in an artificial medium composed of planar arrays of dielectric rods. The rods are uniform and infinitely long. However, unlike the cases for dielectric waveguides, wave propagation in any possible direction is of particular interest in this investigation. A five-point finite-difference scheme is applied to the inhomogeneous cross section of the structure. The eigenvalue problem is formulated in terms of the transverse magnetic field components to avoid spurious modes (Bierwirth et al., IEEE MTT-34, pp.1104-1114, Nov. 1986). The periodic nature of the geometry is included in the analysis through the conditions on the boundary lattices. Within a Floquet cell, due to the periodic property, the finite-difference nodes at the boundary are placed only at two of the four sides, and the boundary nodes at one side are related to the nodes next to the opposite side through the finite difference equations. The resulting characteristic equation is the determinant of a large but sparse matrix. A numerical scheme avoiding the direct Gaussian elimination procedure is developed to minimize the required computer storage and time based on the matrix sparsity property. The validity of the analysis is checked against the case of periodic rectangular dielectric waveguides by an integral equation approach (Yang et al., IEEE MTT-38, pp. 873-880, July 1990). Interesting results on the guided wave characteristics will be presented. Guided-wave pass and stop bands varying with the periodicity and the rod parameters will also be discussed.

B5-3
1420

HIGHER ORDER MODELING USING CURVILINEAR ELEMENTS AND SINGULAR BASES

D. R. Wilton W. J. Brown*
Department of Electrical and Computer Engineering
University of Houston
Houston, TX 77204-4793

A standard approach in integral equation modeling is the use of planar triangles to model the material boundaries of three-dimensional objects. So-called divergence-conforming basis functions, having continuous normal components across element boundaries, are usually used to model the surface equivalent currents. It is observed that for object boundaries having significant curvature, planar triangular facet models are slow to converge, and it is the geometry, rather than the variation of the current, which limits the convergence rate. Consequently, for the electric field integral equation (EFIE), several authors have extended the planar triangular element bases to the curvilinear element case (W. L. Wilkes and C.-C. Cha, IEEE AP-S Symposium, 1991) and have observed markedly improved convergence rates.

In this paper, we examine a quadratic curvilinear triangular patch model in detail. The extension of the usual triangular surface patch bases is reviewed and a geometrical interpretation is given. Since accurate integration is necessary to treat curvilinear triangles, a detailed treatment of kernel singularity integration is examined for the EFIE. The approach is then extended to the magnetic field integral equation (MFIE), which case has apparently not been previously considered. In this case, the self term integral no longer involves only the singular part contribution, but also includes a contribution from the curved surface involving the local curvature. Furthermore, the treatment of the kernel singularity is complicated by the fact that terms up through second order must be removed from the integrand and their integrals evaluated analytically.

It is expected that much of the advantage of modeling curvature may be lost if an improved treatment of edges is not available for curved objects with edges. This will be particularly true when higher order bases—which we are also investigating—are used. Consequently, we will report on our recent use of singular basis functions with the EFIE for modeling singular fields near boundary edges. A derivation of divergence-conforming elements having an arbitrary order of singularity will be presented. Computations are currently in progress using the singular elements for structures having knife-edges, and the results of these computations will be reported.

B5-4
1440

A FILTER-LIKE ABSORBING BOUNDARY CONDITION FOR THE FINITE-DIFFERENCE TIME-DOMAIN METHOD

Chien-Nan Kuo* Tatsuo Itoh
Electrical Engineering Department
University of California, Los Angeles
Los Angeles, CA 90095

This paper presents the synthesis of an absorbing boundary condition (ABC) for the Finite-Difference Time-Domain (FDTD) method in the frequency domain based on the digital filter design technique. Because of the central difference scheme employed in the FDTD method, the value of the field components on the ABC plane is determined by the fields inside the computation domain. Many boundary conditions have been developed to annihilate the wave reflection from this artificial interface, such as different approaches to approximate the wave equation, mathematical operators applied to minimize the artificial reflection, and absorbers placed to reduce the reflected wave.

Essentially, the relationship between the boundary field and the interior field can be treated as a digital filter. The system function of the digital filter equal to the exponential function of the propagating constant in the guiding structure in ideal cases, but, otherwise, a difference between these two quantities results in the reflection from the ABC plane. In order to minimize the reflection coefficient, the filter is chosen such that the difference is minimized over the interested frequency range.

In this presentation, this filter-like ABC is applied to several waveguiding structures, such as the microstrip line and the rectangular waveguide. The value of the field next to the ABC plane is taken as the input of the filter, which employs the infinite-impulse response (IIR) filter for this application. The system function of the IIR filter is optimized in the frequency domain to match the exponential function of the propagating constant over the wideband frequency range. The stability of the ABC is investigated by the poles of the digital filter. On the implementation, the high-order filter is decomposed into several second-order filters to minimize the round-off error in computation. It is observed from numerical results that the reflection coefficient of the simulation agrees with theoretical data.

B5-5
1500

THE MOMENT METHODS WITH ORTHOGONAL WAVELET BASIS FUNCTIONS ON THE INTERVAL

Gaofeng Wang and Deguang Feng
Tanner Research Inc., 180 N. Vinedo Ave., Pasadena, CA 91107

Recently, it has been found that using orthogonal wavelets as basis functions can speed up numerical solutions of the integral equations arising in electromagnetics. The wavelet expansion can adaptively fit itself to various length scales by distributing the localized basis functions near the discontinuities and the more spatially diffused ones over the smooth regions. Moreover, the cancellation property of the wavelets can eliminate, to a great extent, the coupling between the distant parts of the physical configuration under study. The moment-method matrix obtained by using an orthogonal wavelet expansion is rendered sparsely populated.

Originally, orthogonal wavelets are bases on the whole real line. Some difficulties arise when applying such wavelets on the real line to problems in bounded domains. To express the unknown functions in finite intervals, the wavelet on the real line must be truncated at boundary points, which leads to artificial jumps or unexpected oscillations near the boundaries (B. Z. Steinberg & Y. Leviatan, IEEE Trans., AP-41(5), 610-619). To overcome these difficulties, the periodic orthogonal wavelets were used (G. Wang, IEEE Trans., AP-43(2), 170-178). However, the periodic wavelets are only good for the unknown functions that possess of periodic nature. Semi-orthogonal spline wavelets on [0, 1] were introduced to solve first-kind integral equations (J. C. Goswami, A. K. Chan, & C. K. Chui, IEEE Trans., AP-43(6), 614-622). The semi-orthogonal spline wavelets on [0, 1] are applicable to non-periodic unknown functions on finite bounded domains, but no longer lead to zero residual methods since the basis functions are not completely orthogonal. Recently, the intervallic orthogonal wavelets, constructed from Coiflets, were applied to solve surface integral equations (G. Pan & J. Y. Du, PIERS'95, 132, Seattle, July 1995). But only the scaling functions were used, which results in an analysis at only the finest level instead of a multiresolution analysis and doesn't take advantages of the wavelet functions.

Here, the orthogonal wavelets on the interval, constructed from Daubechies compactly supported wavelets (A. Cohen, I. Daubechies, & P. Vial, Appl. Comput. Harmonic Analy., 1, 54-81, 1993), are employed in the moment method to solve integral equations on bounded domains. This approach eliminates the artificial jumps near the boundaries and imposes no restriction to the unknown functions. Both the scaling functions and the wavelet functions on [0, 1] are employed to form multi-level wavelet expansions. Thus a multiresolution analysis on the finite bounded domain is generated from this approach. Numerical examples are provided to illustrate validity and merits of this technique.

F6-1
1340

PRECIPITATION SHAFT INTERCEPTS WITH A MOBILE 2D VIDEO DISDROMETER: COORDINATED MEASUREMENTS WITH THE CSU–CHILL RADAR

V. N. Bringi* M. Schoenhuber† V. Chandrasekar J. Hubbert
H. E. Urban† R. S. Vanderlinde and W. L. Randeu†
Colorado State University, Fort Collins, CO
†Joanneum Research Institute, Graz, Austria

The 2D video disdrometer, developed by the Joanneum Research Institute, is a new instrument for accurately measuring the sizes and shapes of hydrometeors within a precipitation shaft. Two video cameras record the front and sideviews of each hydrometeor and their fall velocity. The resolution of the digitizing grid is 0.25 mm. In the summer of '95, the disdrometer was brought to Colorado State University and, for the first time, installed in a "hail" chase van for storm core intercepts together with coordinated radar data collection with the CSU–CHILL system.

Examples of particle size distribution and hydrometeor shapes will be given from a variety of intense convective precipitation events, together with radar signatures of reflectivity, differential reflectivity, linear depolarization, specific differential phase and copolar correlation coefficient. Implication for the radar modelling of mixed phase precipitation events will be discussed.

Several case studies will be analyzed from data collected on 17 June, 22 June and 8 August 1995. Time series of radar data collected in ppi/rhi format for each convective precipitation event is compared with corresponding time series from the disdrometer. The variables compared are Z_H, Z_{DR}, rainfall rate, and rain accumulation over the event. Typical storm cell intercepts lasted around 5-10 minutes. The interest here is to see how accurately the radar measurements track the drop size distribution, in particular to see if radar derived rainfall accumulation based on Z_h, Z_{DR} and specific differential phase agree with disdrometer rainfall amounts to within the accuracy limits placed by natural drop size distribution fluctuations.

F6-2
1400

DIFFERENTIAL PHASE MEASUREMENTS OF RAIN

A. Ryzhkov and D. Zrnic
National Severe Storms Laboratory
Norman, Oklahoma

Polarimetric estimates of rainfall based on specific differential phase K_{DP} have several advantages compared to the traditional technique that uses radar reflectivity factor Z. K_{DP} is immune to radar calibration errors, attenuation in precipitation, beam blockage, and is less sensitive to the presence of hail and variability of drop size distribution.

Specific differential phase, however, is very low and noisy at low rain rates R, especially at S band. Therefore, originally this method was suggested and used for heavy rainfall estimation. Here we show how K_{DP} can be applied for all rain rates.

We capitalize on the fact that despite its noisiness in light rain K_{DP} estimate is unbiased. Therefore we can reduce the standard error of the estimate after spatial and temporal averaging, provided that rain field is sufficiently uniform which is usually the case for stratiform widespread precipitation.
Although pointwise R estimate is poor, the areal rain accumulations over typical watersheds areas can be accurately determined.

Two types of spatial filtering of the raw differential phase data are proposed: light filtering with low averaging scale for high reflectivity areas and heavy filtering with large averaging scale for low reflectivity regions. The standard deviation of K_{DP} as a function of the averaging scale is examined both theoretically and experimentally.

To assess the performance of the new version of the $R(K_{DP})$ algorithm we have analyzed rain totals for 15 Oklahoma storms over a micronetwork of 42 densely located rain gauges. One- to four- hour areal rain depths T have been examined using $R(K_{DP})$ and the standard R(Z) Marshall-Palmer algorithms. With one case excluded the fractional standard error of T estimate is about 15% if $R(K_{DP})$ algorithm is applied. The R(Z) estimator exhibits much worse performance. Further improvement of the polarimetric method might be possible if differential reflectivity data are included.

F6-3
1420

STUDIES OF HIGH CLOUDS WITH 8-MM RADAR AND IR RADIOMETER

S.Y. Matrosov[1], R.A. Kropfli[2], J.B. Snider[1]
[1]CIRES, University of Colorado, Boulder CO 80309
[2]NOAA Environmental Technology Laboratory
325 Broadway, Boulder, CO 80303

Millimeter wavelength radar is an efficient tool for studies of nonprecipitating clouds. It can provide fine spatial resolution and low clutter which is important for observing relatively thin clouds at close range. The Ka-band cloud Doppler radar operated by the NOAA Environmental Technology Laboratory (ETL) has a 0.5^{o} degree beam width and provides a 37 m radial resolution. Doppler velocities can be measured by this radar with an accuracy of about 5 cm/sec. The radar sensitivity of about -30 dBZ at 10 km range allows radar observations of tenuous cirrus clouds.

This radar has participated in a number of experimental programs, e.g., FIRE-II, ASTEX, ARIZONA-95 where nonprecipitating clouds were the main interest. Methods to analyze cloud radar data and to retrieve microphysical parameters of ice clouds using these data were developed in ETL. It was shown that radar data alone are generally insufficient to get estimates of cloud microphysical parameters. Such estimates in this case can be made using different empirical relationships between radar measurables and cloud parameters of interest. The potential accuracy of these estimates is rather poor because different combinations of cloud microphysical parameters can result in the same value of radar reflectivity. A more robust way, however, to resolve this potential ambiguity and get better estimates of cloud parameters is to use complementary IR measurements with a collocated radiometer.

The combined radar and radiometer data collected during different ice cloud events from experiment programs mentioned above were used to retrieve and analyze such microphysical parameters as cloud particle characteristic size, ice mass content, particle concentration, and gravitational ice mass flux. These cloud properties are important for parameterizing clouds in general circulation models and also for better understanding of cloud development and evolution. The potential accuracy of the retrievals was estimated both theoretically and by comparing remotely sensed cloud parameters with those measured using traditional particle sampling techniques from research aircraft flying in the vicinity of radar resolution volume.

F6-4
1440

MEASUREMENTS AND MODELLING OF X-BAND REFLECTIVITY AND ATTENUATION IN MELTING SNOW

Dr. F. Fabry
Atmospheric Technology Division
National Center for Atmospheric Research
Boulder, CO 80307-3000

Measurements in the vertical of X-band and UHF (915 MHz) radar reflectivity were made over a season in Montreal (Canada) to determine the attenuation at X-band frequencies in melting snow as a function of precipitation intensity. Statistics of signal loss across the radar bright band were computed.

These data and earlier measurements of bright band parameters (intensity, thickness; F. Fabry and I. Zawadzki, J. Atmos. Sci., 52, 838-851, 1995) were then used as benchmarks to test various scattering models of the melting layer and determine the best simple approximation for the scattering and attenuation properties of melting snowflakes at microwave frequencies. Models using a concentric sphere approach (water around snow) and matrix-inclusion models with water as the matrix both overestimate significantly the bright band intensity and attenuation when reasonable snow density and melting hydrometeor fall speeds are used.

New mixture models using ice-water mix as inclusions and air as the matrix fare considerably better, particularly if the center of the snowflake is modelled to be denser than its periphery. One of these models simulate with reasonable accuracy all of our bright band measurements. Based on this model, predictions of melting layer scattering and attenuation at other wavelengths are made. At X-band and nearby frequencies, the specific attenuation of melting snow is of the order of three times the one of rain. Since melting layers are generally 500 meters thick, it can be deduced that in stratiform rain, total melting snow attenuation is comparable to half of the total rainfall attenuation expected on an earth-to-space link.

F6-5
1500

DISTINGUISHING FROZEN AND LIQUID PRECIPITATION USING A DUAL POLARIZATION WEATHER RADAR SYSTEM

P. C. Kennedy, D. A. Brunkow, and S. A. Rutledge
Colorado State University, Ft. Collins Colorado

The intensity of the copolar echo back scattered from precipitation particles has always been one of the most fundamental quantities sensed by meteorological radars. Diagnoses of storm reflectivity structures has been of fundamental utility in the real time identification of severe thunderstorms (D. W. Burgess and L. R. Lemon, Radar in Meteorology, 619-647, 1990). However, these single polarization observations generally provide limited insights into the thermodynamic phase of the precipitation particles (e.g. rain vs. hail, etc.) Improved characterizations of precipitation particle regimes are possible through the use of dual polarization radars. In this paper, we present two storms whose reflectivity patterns were similar, but whose precipitation characteristics, as revealed by dual polarization observations, were different.

The dual polarization measurements were taken by the 11 cm wavelength CSU-CHILL radar located near Greeley, CO. The transmit polarization of this system alternates between horizontal (H) and vertical (V) on a pulse to pulse basis. The co- and cross-polarized return signals are processed in separate receivers. The dual polarization measurements considered here are: (1) differential reflectivity (Zdr), (2) specific differential propagation phase (Kdp), and (3) linear depolarization ratio (Ldr). Differential reflectivity is given by the ratio of the H co-polar return to the V co-polar return. It provides a reflectivity weighted measure of the mean particle shape (A. Jameson, J. Atmos. Sci., 1792-1802, 1983). Specific differential propagation phase is due to the different propagation constants experienced by the H and V pulses when the beam path contains asymmetrical, preferentially oriented particles (T. A. Seliga, and V. N. Bringi, Radio Sci., 217-275 1978). Kdp is increased when oblate scatterers, which retard the H pulse's propagation more than that of the V pulse, are present in the beam path. Linear depolarization ratio (cross-polar return / co-polar return) is a measure of the scatterer's ability to induce a cross polarized component into the backscattered signal. In general, asymmetrical particles whose orientation is canted with respect to the polarization plane of the incident pulse (including orientation changes associated with tumbling fall modes) increase Ldr (A. Jameson, Bull. Amer. Metero. Soc., 1365-1373, 1992). It should be noted that due the larger refractive index of water as compared to ice, the Zdr, Kdp, and Ldr returns for a given set of scatterers are all affected by the wetness of the particles.

Presented below are tabulations of the above quantities for the near-surface echo core regions (reflectivities > 50 dBZ) of two convective storms. Surface observations coincident with these radar data confirm that the 28 April storm's precipitation was primarily frozen, while that of the 8 August case was almost entirely liquid.

Date/Time (MDT)	#Gates	Ref (dBZ)	Zdr (dB)	Kdp ($^{o}km^{-1}$)	Ldr (dB)
4/28/95 1907 (ice)	161	54.3	0.4	0.3	-23.5
8/8/95 1937 (rain)	101	52.3	4.2	2.1	-29.9

In the 28 April case, the preponderance of ice in the form of graupel and small hail produced low Zdr and Kdp values. Presumably, the combined effects of particle shape asymmetries and gyrating fall motions lead to a slight Ldr enhancement from these primarily unwetted ice particles. In the 8 August case, the predominance of oblate water drops is evidenced by the large Zdr and Kdp values. It is speculated that these large drops underwent lesser tumbling motions than did the graupel particles, slightly reducing the rain case Ldr from that observed in the graupel shower.

F6-6
1540

SNOWFALL RATE MEASUREMENT USING RADAR AND OPTICAL TECHNIQUES

Roy M. Rasmussen J. Vivekanandan*
National Center for Atmospheric Research
P.O. Box 3000
Boulder, CO 80307

Snowfall rate can be monitored by snow gages (measurement of snow mass), microwave radar (measurement of backscattered power), and optical (change in visibility) techniques. The direct measurement of snow mass by a weighing gage provides a good estimate of point liquid equivalent snowfall rate. A well-calibrated snow gage measurement may also be used as a standard to calibrate snowfall inferred by means of other techniques. In the case of the microwave method, the scattering characteristic of a snow particle depends on its size and bulk density. Since there is a large variationin size and density of snow particles for a given snowfall rate, it is difficult to estimate snowfall rate accurately using reflectivity alone. The primary advantage of radar is its extensive spatial coverage. Optical techniques make use of the attenuation of a light beam or change in visibility for estimating snowfall. It offers some distinct advantages over the snow gage and microwave methods in terms of temporal resolution. The measurement principle is immune to environmental and physical parameters such as wind speed, temperature and instrumentation setup.

During the winter season, NCAR conducted a field program to collect radar reflectivity, visibility and other environmental observables such as temperature and wind speed. Simultaneous observations by a number of instruments and manual measurements of snowfall resulted in a unique data set. We analyzed these data sets to improve the measurement accuracy of snowfall rate. Also, model computations of visibility and radar reflectivity are studied to quantify the ambiguity in snowfall rate estimation due to variation in bulk density and median snowflake size.

F6-7
1600

POLARIMETRIC MEASUREMENTS IN A SEVERE HAILSTORM

J. Hubbert* V.N. Bringi V. Chandrasakar A. Abou-El-Magd
Department of Electrical Engineering
Colorado State University
Fort Collins, CO, 80523
S. Bolen
Rome Laboratory/OCSA
26 Electronics PKY
Griffiss AFB
Rome, NY, 13441-4514

On 7 June 1995 a severe hailstorm with golf ball size hailstones caused nearly $28 million in damages in Weld county, Colorado. This event was captured by the CSU-CHILL fully polarimetric S-band radar over a period of one hour. The CSU-CHILL radar has recently been upgraded with a new reflector dish giving an a two-way integrated cross-polar ratio (ICPR) around -35 dB, an additional receiver and an additional transmitter. The improvements make possible simultaneous copolar and crosspolar channel measurements so that the complete scattering covariance matrix can now be constructed. In addition, a mobile chase van equipped with a NCAR hail catcher and a capacitive rain gauge intercepted the storm core providing direct measurements of in-situ data on hail shapes and sizes as well as rainfall accumulations. These data are compared to the radar measurements of reflectivity (which reached 70 dBZ), differential reflectivity (Z_{DR}), linear depolarization ratio (LDR), specific differential phase (K_{DP}) and copolar correlation coefficient (ρ_{HV}). LDR measurements down to -32 to -35 dB have been experimentally verified in light rain. Radar signatures within the main updraft region show positive Z_{DR} columns where supercooled raindrops are ascending, and an enhanced LDR "cap" on the Z_{DR} column is interpreted as the freezing of these drops which then become the hail embryos.

F6-8
1620

MULTIPARAMETER RADAR AND AIRCRAFT OBSERVATIONS OF A HAILSTORM

V. Chandrasekar V. N. Bringi A. Abou-El-Magd*
Colorado State University
Ft Collins, CO 80523
J. W. Strapp
Atmospheric Environment Service
Canada

During the summer of 1995 the CSU-CHILL multiparameter radar and an instrumented aircraft (T-28 operated by the South Dakota School of Mines and Technology) were used to collect coordinated measurements over hailstorms in Northern Colorado .

This paper presents a preliminary comparison of the radar and aircraft data collected on a hailstorm which occurred on 22 June 1995 . The multiparameter radar data consists of the following parameters : a) Reflectivity , b) Differential reflectivity , c) Specific differential propagation phase , d) Copolar correlation between two polarizations , and e) Linear depolarization ratio . The T-28 aircraft was equipped with a High Volume Particle Spectrometer capable of collecting two dimensional images of hydrometeors encountered in the flight path .

On 22 June the T-28 made four penetrations through a storm cell located 35 km north east of the radar . The storm had echoes in excess of 60 dBZ associated with marble size hail . The hail shaft extended all the way to the ground . Penetrations were at altitudes between 4.0 and 4.5 km to collect data in the hail region . Simultaneously the radar was collecting data in a PPI sector scan mode covering the elevations of the aircraft locations . A comparative study of the multiparameter radar data and the insitu aircraft observations for this storm are presented with the objective of interpreting multiparameter radar signatures .

F6-9
1640

DUAL-FREQUENCY FULLY POLARIMETRIC MILLIMETER-WAVE RADAR MEASUREMENTS

John M. Firda* Robert E. McIntosh
Microwave Remote Sensing Laboratory
Rm. 101 Knowles Engineering Building
University of Massachusetts
Amherst, MA 01003

Improved understanding of the role of clouds on the atmosphere has increased scientists' need for radar measurements of cloud reflectivity, mean velocity, and Doppler spectral width. Such cloud microphysics studies shed light on how clouds modulate the atmosphere's radiation budget. Derived information from experiments is useful for estimating particle size and ice water content. Likewise, polarimetric measurements aid in identifying cloud particle phase in precipitation.

The University of Massachusetts' Cloud Profiling Radar System (CPRS) was developed to facilitate these measurements (S.M. Sekelsky, Meteorology and Atmospheric Physics, In Press). CPRS is a dual-frequency, fully polarimetric, millimeter-wave scanning Doppler radar capable of making high resolution measurements of cloud particles. CPRS is a ground based system that transmits and receives vertical and horizontal polarizations at 33.12 and 94.92 GHz through a single 1-meter dielectric lens antenna. The CPRS antenna produces colocated beams at the two transmit frequencies to ensure the radars are sampling the same cloud volume.

During the spring of 1995, CPRS obtained fully polarimetric measurements of precipitating stratus clouds during the Ground Based Remote Sensing IOP (GBRS-IOP) in Lamont, Oklahoma. Measurements of copolar cross correlation magnitude ($|\rho_{hv}(0)|$) and specific differential phase (K_{DP}) are presented at vertical incidence and with RHI scans. A decrease of $|\rho_{hv}(0)|$ is seen in the presence of ice aggregates which is consistant with the linear depolarization ratio. Small changes in K_{DP} are also observed and are compared to differential reflectivity (Z_{DR}) measurements.

The colocated millimeter-wave measurements of $|\rho_{hv}(0)|$ and K_{DP} are the first of their kind. These measurements provide a unique opportunity to compare polarimetric measurements with respect to frequency and elevation angle and demonstrates the utility of such measurements.

F6-10
1700

THE EFFECTS OF MODELING THE RADAR IN SCATTERING MATRIX TRANSFORMATION THEORY: THE INCOHERENT CASE

J. Hubbert* V.N. Bringi
Department of Electrical Engineering
Colorado State University
Fort Collins, CO 80523

The foundations of radar polarimetry are based on the well known radar voltage equation (Kennaugh, *Tech. Reps. 381-1 to 394-24 Ohio St. Un. Ant. Lab.*, 1949-1952)

$$\mathcal{V} = \mathbf{h}_r^T \mathbf{S} \mathbf{h}_t \tag{1}$$

It is important to observe that modeling of the radar transmit/receive network is included along with modeling of the scatterer in (??). ¿From the radar voltage equation the standard change of basis formulation is derived as

$$\mathbf{S}' = \mathbf{U}^{\mathbf{T}} \mathbf{S} \mathbf{U} \tag{2}$$

Based on this equation optimum polarizations are derived and polarization response plots are made (Agrawal and Boerner, *TGARS*, **27**, 1989)(Ulaby and van Zyl, *Radar Pol. for Geosc. Appl.*, 1990). Since modeling of the radar is included in (??) it follows immediately that modeling of the radar is also included in (??) and thus, it is of interest to identify how this radar modeling effects optimum polarizations and polarization response plots. In optic polarimetry the change of basis transformation is (Azzam and Bashara, *Ellip. and Polar. Light*, 1989)

$$\dot{\mathbf{S}}' = \mathbf{U}^{-1} \dot{\mathbf{S}} \mathbf{U} \tag{3}$$

Hubbert (*TGARS*,**32**, 1994) has compared (??) and (??) and shows that the copolar reception polarization state is defined differently in each discipline. Hubbert also shows how the copolar reception state might be defined so that the above mentioned radar modeling effects can be separated from those effects directly attributed to the scatterer(s). The resulting analysis is termed specular null polarization theory (SNPT). In this paper SNPT is extended to incoherent scattering where a covariance matrix is needed to fully characterize the scatterers instead of the 2×2 Sinclar scattering matrix or the 2×2 Jones scattering matrix which are used for coherent scattering. Optimum polarizations and polarization response plots are calculated for ensemble of precipitation particles using the transition matrix approach (Vivekanandan, et al. *TGARS* **31**, 1993) and are compared to optimum polarizations and polarization response plots that result when traditional radar polarimetry theory (Tragl,*TGARS*, **8**, 1990) (Tragl et al., *Preprints Intern. Conf. Ant. and Prop.*, **IEE Publ. 33**, 1991) is applied.

Session G-5, 1335-Fri., CR2-26
EQUATORIAL IRREGULARITIES
Chairperson and Organizer: B.G. Fejer, Center for Atmospheric and Space Sciences, Utah State Univ., Logan, UT 84322

G5-1
1340

EAST-WEST AND UP-DOWN SPECTRAL ASYMMETRIES IN ECHOES FROM THE EQUATORIAL ELECTROJET ABOVE ALCÂNTARA, BRAZIL

Wesley E. Swartz*
School of Electrical Engineering
316 Rhodes Hall
Cornell University
Ithaca, NY 14853

Doppler spectral measurements of echoes from the equatorial electrojet above Alcântara, Brazil (44.4°W, 2.3°S) were made almost every day from mid-August through the third week in October, 1994 using the Cornell University Portable Radar Interferometer (CUPRI). Although asymmetries in electrojet spectra are nothing new, some of the details which we observed do not seem to completely fit current theories. The east-west asymmetry was unexpectedly the same as reported by Balsley (*Radio Sci*, **70**, 3175-3182, 1965) and Ierkic et al. (*Geophys. Res. Lett.*, **7**, 497, 1980) at Jicamarca, Peru, yet the up-down asymmetry changed sign in the upper altitudes of a strongly driven daytime electrojet, a feature that has not been seen at Jicamarca.

The site at Alcântara was certainly an ideal one for radar observations of the electrojet. The dip equator at 100 km was directly overhead as predicted by the IGRF model and verified to within a degree by moving the CUPRI radar beam north and south of vertical. Yet the strong altitude dependence of the position of the dip equator, the large declination, and its nearness to the geographic equator provided a configuration quite different from Jicamarca. The unprecedented concentrated length of the high resolution spectral data set should provide a nice complement to the scattered days of similar observations made at Jicamarca.

G5-2
1400

THE TEMPORAL BEHAVIOR OF LOW LATITUDE ELECTRON AND ION TEMPERATURES

Nestor Aponte* Wesley E. Swartz Donald T. Farley
School of Electrical Engineering
316 Rhodes Hall
Cornell University
Ithaca, NY 14853

Measurements of incoherent scatter correlation functions and Faraday rotation have been made at Jicamarca during the last decade or so and are producing F-region electron and ion temperatures and densities. Until recently, though, there were a number of problems with the temperature estimates which we did not understand and which required tedious "by hand" rejection of contaminated data. Now we believe we understand the problems (mainly satellite contamination and three ion mixtures) and we have begun to take a detailed look at the thermal morphology of the region over the full solar cycle for which we have data.

At the equator the magnetic field prevents vertical heat conduction in the electron and ion gases. There is no downward conduction to maintain a positive gradient at high altitudes, and so the profiles become isothermal above the F2 peak. Below the peak, the electron temperature exceeds the ion temperature during the day just as at mid-latitudes. At night the electron and ion temperatures become equal to the neutral temperature, even to very high altitudes. However, at night the analysis becomes more complicated because of the greater percentages of the light ions of helium and hydrogen. Because of the isothermal profiles in the upper altitudes, we have a direct measure of the neutral temperatures which can be unambiguously compared with exospheric temperatures from neutral models such as MSIS (no thermal balance calculation depending on the neutral density is required).

G5-3
1420

RADAR IMAGING OF IRREGULARITIES IN THE EQUATORIAL IONOSPHERE

D. L. Hysell* J. D. Burcham
Department of Physics and Astronomy
Clemson University
Clemson, SC 29643

Multiple-baseline interferometry data taken at Jicamarca have been used to construct images of intermediate-scale waves in spread F and the electrojet. Interferometric imaging offers a way to resolve structures smaller than the radar scattering volume that are not resolved with standard RTI or single-baseline techniques. Imaging furthermore provides a means of distinguishing spatial from temporal variations in the scattering medium and can be use to diagnose the flow around plasma instabilities.

We turn to maximum-entropy imaging techniques, well known to radio astronomers, in an attempt to process the interferometry data in an optimal way. These techniques determine the "most likely" image possible consistent with whatever data are known (and to a specified accuracy). The formulation of the maximum-entropy problem will be discussed, and example data will be shown. With maximum-entropy techniques, we are able to resolve scattering structures only a few tenths of a degree wide. Animated series of radar images show intermediate-scale waves forming, propagating, and dissipating in a bottomside spread F layer. These data clearly illustrate the roles played by vertical elongation and shear in the evolution of bottomside spread F.

Computer simulations can be used to predict the morphology of intermediate-scale waves in spread F and the electrojet. A new diagnostic method has been developed which extracts from these simulations quantities that are equivalent to radar interferometry measurements. Direct comparisons between simulation runs and imaging data are then possible.

G5-4
1440

INVESTIGATING CHARACTERISTICS OF THE EQUATORIAL IONOSPHERE USING DIGISONDE DRIFT MEASUREMENTS AT JICAMARCA

Z. Kecic[1], B.W. Reinisch[1], J.L. Scali[1], and C. Calderon[2]
1 Center for Atmospheric Research, University of Massachusetts, Lowell.
2 Jicamarca Radio Observatory, Instituto Geofisico del Peru.

Half-hour Digisonde drift measurements made from November 1994 to June 1995 are used to construct the monthly average velocity variations observed at Jicamarca. The results are interpreted in terms of the well known dynamics of the equatorial region as described from previous ISR measurements of the plasma motion. The analysis shows that the Digisonde averaged zonal velocity component is in good agreement with established velocity patterns. The monthly average meridional velocity is also given and the results are interpreted in terms of the diurnal variations of the neutral winds . The apparent vertical velocity derived from the Digisonde measurements is discussed in terms of the effects of chemistry and plasma motion.

The analysis further discusses the characteristics of the velocities during spread-F conditions when ISR measurements are usually not available. Average velocities for days when spread-F is observed are compared with those velocities obtained during days when no spread-F is detected, in order to determine whether velocity differences are statistically significant. The continuous Digisonde drift database is used to show the daily variability of the velocity components and how consistently events from day to day can be tracked by the Digisonde drift method.

G5-5
1500

RELATIONSHIPS BETWEEN INCOMPRESSIBLE FLOW AND TWO-DIMENSIONAL SHAPE OF EQUATORIAL PLASMA BUBBLES

Roland T. Tsunoda
Geoscience and Engineering Center, SRI International
Menlo Park, California 94025

Equatorial plasma bubbles are localized plasma-depleted regions that develop in the nighttime equatorial ionosphere. These regions have been shown to be vertically extended in altitude, relatively narrow in longitude, and to involve entire geomagnetic flux tubes. While there is near consensus agreement within the geophysical community that the primary source mechanism is the collisional Rayleigh-Taylor instability, several of the observed bubble properties have puzzled researchers. These include observtions of (1) bubbles that appeared to be collapsing, possibly suggesting the subsequent formation of closed "cylinder-like" depleted regions; (2) bubbles that appeared to have associated upward plasma velocities that were supersonic; and (3) bubbles that ppeared to bifurcate spontaneously, producing branchlike patterns. In this paper, we present examples of these types of observations, using spatial maps of radar backscatter plumes obtained with the ALTAIR radar, which is located in the central Pacific sector. We show that these features can be interpreted in terms of the shapes and distortions produced by patterns of two-dimensional, incompressible plasma flow in the plane transverse to the geomagnetic field. As an example, we show that the appearance of a collapsing bubble can be produced by the upward, buoyant force at high altitudes and the downward force that is produced at low altitudes by a westward electric field. We point out that the nature of plasma bubbles at late times, that is, at times after their growth phase is completed, has not yet been investigated in any detail, especially by numerical simulations on the nonlinear Rayleigh-Taylor instabiity.

G5-6 1540 THE MISETA SPACED ANTENNA SCINTILLATION SYSTEM: CLIMATOLOGY OF ZONAL DRIFTS.

C. E. Valladares
Institute for Scientific Research
Boston College
Newton, MA 02159

The Spaced-receiver scintillation system located at Ancon, Peru has been used to establish the climatology of the zonal drift of km-scale irregularities. Comparison of this drift climatology to the climatology of the plasma drift measured at Jicamarca using the Incoherent Scatter (IS) technique has revealed a seasonally dependent relation. For the solstices both drift data sets are in good agreement. For the equinoxes the drift curves differ. This discrepancy is evident near the local midnight hours, more specifically between 22 and 04 LT. The scintillation drifts obtained during quiet magnetic conditions were ~ 50 m/s larger than the IS counterparts. It is suggested that this discrepancy may be due to the intrinsic conditions prevailing when the measurements are conducted. Scintillation drifts pertain to Equatorial Spread-F (ESF) events, Jicamarca drifts pertain to times of no ESF. Two plausible mechanisms have been considered for an essential qualitative explanation of this finding. Firstly, it is known that during ESF the post-sunset enhancement produces an uplift of the F-region and a consequent reduction of the ion drag. The smaller ion drag will facilitate a larger zonal wind, in this way resulting a larger zonal plasma drift. Alternatively, during nighttime hours the equatorial disturbance dynamo seems to produce anomalous westward reversals of the normally eastward zonal drifts. It is proposed that if the magnetic conditions remain active when the disturbance dynamo effect reaches equatorial latitudes then ESF will develop, but if the conditions are quiet then ESF will be inhibited. Data collected by scintillation receivers, the Jicamarca IS radar, digisondes, and the Fabry-Perot interferometer during the MISETA/Chile campaign of the September 1994 equinox have been used to test these two hypotheses. The results of this study will be summarized here.

G5-7 1600 SPREAD-F AND THE STRUCTURE OF EQUATORIAL AIRGLOW DEPLETION BANDS OBSERVED NEAR THE SOUTHERN ANOMALY REGION.

G.S. Sales, B.W. Reinisch, J. Scali
Center for Atmospheric Research
University of Massachusetts Lowell
Lowell, MA 01854

E. Weber, T. Bullett
Geophysics Directorate
Phillips Laboratory
Hanscom AFB, MA 01731

Using the Phillips Laboratory Digisonde sounding system and the all-sky imaging photometer measuring airglow emission at the 630.0 nm, it is possible to investigate the internal structure of the evolving equatorial bubbles from a site in Chile (22° S, 70° W), located midway between the magnetic equator and the southern anomaly region. During the nighttime periods on 1 and 3 October, 1994 bubble formation was observed by the photometer, extensive spread-F was seen on the local vertical ionograms. There was no apparent connection between the location of the emission depletion bands and the character of the spread-F. However, at these times, the Digisonde, operating in the "drift" mode, was able to detect and locate medium scale irregular structures and a comparison between these source location data and the all-sky images indicates that these irregularities, essentially, lie within the bubble and clearly track along with the general west to east drift of the airglow depletion bands.

From a single sounding site the Digisonde is able to measure the group delay and the radial component of the velocity of these irregularities as a function of sounding frequency. These data, combined with the general west-east drift determined using the allsky images, can be used to investigate the structure of the irregularities and their motions. Along with the anlaysis of these experimental data, a simple model of the depletion bands has been constructed and used with a 3-D ray tracing program to simulate the interaction of the radio waves with these F-region structures. The insite gained by this approach has led to a better understanding of the sounder data as it relates to the internal band structure.

The results of this analysis indicates that these irregularities affecting the radio signals are concentrated within the transition region at the boundaries of the depletion bands as well as at the top of the depletion which is only at an altitude of 400 to 500 km at Agua Verde, Chile.

G5-8
1620

SATELLITE SIGNATURES OF THE LONGITUDINAL, SEASONAL AND NIGHT-TO-NIGHT OCCURRENCE MORPHOLOGY OF EQUATORIAL SPREAD *F*

P. J. Sultan
Phillips Laboratory/GPIA
29 Randolph Road
Hanscom AFB, MA 01731

The occurrence of plasma irregularities related to equatorial spread *F* (ESF) at a given geographic longitude is controlled in part by the local ionospheric eastward electric field near sunset (which should be strong) and the meridional neutral winds at that longitude (which should be small). Both of these parameters can be shown to have a dependence on both longitude sector and the time of the year - resulting in the occurrence of so-called "spread *F* seasons" at particular geomagnetic longitudes. The strength of the eastward electric field can be related to the longitudinal gradient in integrated Pedersen conductivity, which in turn partly is dependent on the difference in *E* region sunset times at magnetically conjugate points (R. T. Tsunoda, *J. Geophys. Res.*, **90**, 447, 1985). Meridional neutral winds can be inferred from latitudinal ion density profiles measured daily by Defense Meteorological Satellite Program (DMSP) polar orbiting satellites near 18 LT (around 1.5 hours before the typical onset time of ESF irregularities) every 30° of longitude. By combining these two geophysical parameters, it should be possible to generate reliable predictors ESF occurrence at all longitudes on a night-to-night basis.

The present study focusses on three longitude sectors: mid-Atlantic, western Pacific, and Indian. DMSP-inferred *F* region neutral winds in each sector are combined with a parameter corresponding to the difference in *E* region sunset times creating a new parameter that measures the nightly likelihood of ESF at each sector. Preliminary results show that this predictor well duplicates the seasonal patterns of ESF ocurrence in each sector. Future work will directly compare predicted ESF occurrence with ground-based scintillation observations from these and other longitude sectors.

G5-9
1640

LONGITUDINAL DEPENDENCE OF EQUATORIAL F-REGION PLASMA DRIFTS

B. G. Fejer, E. R. de Paula, and L. Scherliess
Center for Atmospheric and Space Sciences
Utah State University
Logan, Utah 84322-4405

We use Ion Drift Meter (IDM) observations from the AE-E and DE-2 satellites, incoherent scatter radar measurements from the Jicamarca Radio Observatory, and ionosonde measurements from the South American, Indian, and African equatorial regions to examine the longitudinal dependence of equatorial F-region plasma drifts in the evening sector. The vertical plasma drifts (zonal electric fields) show largest longitudinal effects during June solstice when prereversal velocity enhancements are only observed in the central Pacific region. In this case, the earliest reversal time from upward to downward drifts occurs in the western American sector and the latest occurs in the Brazilian-African sector. We show that the solar cycle dependence of the average prereversal velocity drifts observed with the Jicamarca radar and with the IDM are in good agreement. On the other hand, comparisons of simultaneous evening velocity peaks measured with the Jicamarca radar with those inferred from Huancayo ionosonde data indicate the latter technique significantly underestimates the prereversal velocity enhancements near the F-region peak during periods of high solar activity. The zonal plasma drifts exhibit largest longitudinal effects in the late afternoon and early morning hours. We will also discuss the relationship between the F-region zonal and the vertical plasma drifts in the evening sector.

G5-10
1720

THEORETICAL MODELING OF THE 1994 CHILE/MISETA CAMPAIGN

Dwight T. Decker*
Institute for Space Research, Boston College
Chestnut Hill, MA 02167
David N. Anderson
Phillips Laboratory, GPIM
Hanscom AFB, MA 01731-3010

During the Chile/MISETA campaign, 27 Sept. to 3 Oct. 1994, a number of ground-based and satellite-borne instruments obtained data on electron density profiles, neutral wind velocities, vertical and horizontal ExB drift speeds, optical and radar signatures of equatorial bubbles and spread F/scintillation occurrences. In this paper we use the Phillips Laboratory Global Theoretical Ionospheric Model (GTIM) to calculate electron and ion densities as a function of altitude (90 to 1600 km), latitude (±30° dip latitude) and local time (24 hours) and compare these calculated ambient ionospheric profiles with specific observations on specific campaign days. Included as inputs to the time-dependent, theoretical model are 1.) the observed vertical ExB drifts from the Jicamarca incoherent scatter radar facility and 2.) observed nighttime meridional neutral winds measured by a Fabry-Perot interferometer at Arequipa, Peru (3° S dip latitude). Supplementing these inputs are neutral temperatures and densities from the MSIS86 model and neutral winds from the HWM87 model. A primary objective of the study is to calculate flux-tube integrated plasma instability growth rates and loss rates to try to better understand the physical mechanisms which are responsible for initiating or suppressing the growth of low latitude plasma instabilities which are observed on some nights but not on others.

Session G/H-7, 1335-Fri., CR2-6
RED SPRITES, BLUE JETS, AND LIGHTNING
Chairperson: Y. Taranenko, Space and Atmospheric Sciences Group, Los Alamos National Laboratory, Los Alamos, NM 87545
Organizers: L. Hale, CSSL/Pennsylvania State University, University Park, Pa 16802; and Y. Taranenko

G/H7-1
1340

IONOSPHERIC DISTURBANCES PRODUCED BY QUASI-ELECTROSTATIC THUNDERCLOUD FIELDS AND LIGHTNING EMP

Umran S. Inan
Space, Telecommunications and Radioscience Laboratory
Stanford University, Stanford, CA 94305

Sprites and blue jets provide spectacular evidence of the electrical coupling between thunderclouds and the overlying mesosphere and the lower ionosphere. On the other hand, earlier evidence of such coupling was in the form of early/fast perturbations of subionospheric VLF signals. These perturbations occur in response to sudden changes in the electrical conductivity of the lower ionosphere, either due to the heating of the ambient electrons by lightning fields, and/or ionization changes. Experimental evidence indicates that the size of the disturbed ionospheric regions maybe 100-200 km in extent, considerably larger than the apparent physical dimensions of Red Sprites. Heating by quasi-electrostatic thundercloud fields can lead to ionization at mesospheric and lower ionospheric altitudes. However, the transverse extent of ionization regions are typically <50 km. One process which can lead to disturbances with large transverse extent is heating of ambient electrons and resulting ionization changes by lightning EMP. However, ionospheric disturbances produced by EMP-induced heating typically occur at relatively high altitudes (>80 km). Results from a new two-dimensional model of the EMP-ionosphere interaction [Inan, U. S., W. A. Sampson, and Y. N. Taranenko, Space-Time Structure of Optical Flashes and Ionization Changes Produced by Lightning EMP, submitted to Geophys. Res. Lett., 1995a] and new observations of VLF perturbations associated with sprites [Inan, U. S. ,T. F. Bell, V. P. Pasko, D. D. Sentman, E. Wescott, and W. A. Lyons, VLF Signatures of Ionospheric Disturbances Associated with Sprites, submitted to Geophys. Res. Lett., 1995b] will be presented.

G/H7-2 1400 **RED SPRITES PRODUCED BY QUASI-ELECTROSTATIC THUNDERCLOUD FIELDS**

Victor P. Pasko, Umran S. Inan, and Timothy F. Bell
Space, Telecommunications and Radioscience Laboratory
Stanford University, Stanford, CA 94305

A two-dimensional quasi-electrostatic (QE) model is used to study ambient electron heating, ionization of neutrals and excitation of optical emissions in the mesosphere/lower ionosphere by QE fields that temporarily exist at high altitudes following the sudden removal (e.g., by a lightning discharge) of thundercloud charge at low altitudes [Pasko, V. P., U. S. Inan, T. F. Bell, and Y. N. Taranenko, Red Sprites Produced by Quasi-Electrostatic Heating and Ionization in the Lower Ionosphere, submitted to J. Geophys. Res., 1995]. The model predicts significant (several orders of magnitude) modification of the lower ionospheric conductivity in a region with 50-60 km transverse extent in the form of depletions of electron density due to dissociative attachment to O_2 molecules or in the form of enhancements of electron density due to breakdown ionization. Results of calculations of the optical emission intensity of the 1st positive band of N_2 are in good agreement with observations of the upper part (`head' and `hair' [Sentman et al., Geophys. Res. Lett., 20, 2857, 1995]) of the Red Sprites. Most recent results from the QE model will be discussed, including mechanisms of formation of carrot-like structures, and the relationship between the onset of luminosity in sprites versus the time of causative CG discharges.

G/H7-3
1420

NUMERICAL SIMULATIONS OF LOWER IONOSPHERIC BREAKDOWN CAUSED BY LIGHTING-GENERATED ELECTRIC FIELDS

Harvey Rowland* Richard F. Fernsler Carl L. Siefring
Paul A. Bernhardt
Plasma Physics Division
Naval Research Laboratory
Washington, DC 20009

Lightning-generated electric fields can be responsible for atmospheric breakdown and optical emissions from the mesosphere. Recently, H. Rowland, et al. [*Geophysics Research Letters*, **22**, 361, 1995a and *Journal of Geophysical Research*, submitted, 1995b] have used a simulation model to study the ionospheric breakdown caused by lightning driven electromagnetic pulses (EMP). Pasko et al. [*Geophysics Research Letters*, **22**, 365, 1995] study breakdown due to the quasi-static fields. We have continued our simulations using a more realistic lightning current profile, including the continuing current, with current amplitudes approximating the largest 5% of positive strokes. In this case, we model both the EMP and quasi-static electric fields and their effect on the lower ionosphere. In our simulations, the EMP generated ionization appears first and is confined in a narrow altitude range (70-90 km) with a large horizontal extent (100s of km). This is similar to the characteristics of the airglow observed from the shuttle by Boeck et al. [*Geophysics Research Letters*, **19**, 99, 1992]. The quasi-static fields cause a different pattern of ionization with characteristics similar to Sprites. In this case, a 'narrow' column (~10s of km) ionization forms above the lightning current channel. This column begins to form near 90 km and grows downward in altitude as time progresses. In simulations, using larger lightning currents, we have been able to observe columns of ionization extending as low as 50 km in altitude. Breakdown acts to limit the coupling to higher altitudes in the ionosphere of both the EMP and the quasi-static fields.

G/H7-4
1440

MESOSPHERIC ELECTRICAL TRANSIENTS

Les Hale
CSSL/Penn State,
University Park, PA 16802

The phenomenon of "red sprites" has stimulated interest in the coupling of lightning-related electromagnetic energy to the mesosphere. "Radiation" and "induction" fields couple energy on a time scale too short to sustain the observed visible sprites, which requires a "quasi-static" mechanism. "Relaxation time" solutions are not relevant to this problem. C. and P. Greifinger [JGR 81, 2237, 1976] suggested a "variable capacitor" model which works well at ULF, but is only relevant to "red sprites" if their discharge occurs virtually simultaneously at all altitudes (velocity $>10^7$ m/sec). A strong "millisecond" ELF pulse, necessary to satisfy post-stroke boundary conditions, was predicted by a numerical model [Hale and Baginski, Nature 329, 814, 1987], and subsequent analysis by Z. Ma [Ph.D. Thesis, 1995] shows lengthening of this pulse by the magnetic field. This appears to explain rocket data [Kelley, et al., JGR 90, 9815, 1985] and to be adequate to power "red sprites."

Any calculation depends on the electrical conductivity profile. Typical profiles (below, right) show that ELF energy can penetrate the mesosphere at night but further structuring may occur during sprite-producing conditions, and more data, which will require a rocket program, are urgently needed.

Observations by Lee Marshall, et al., [1995 Fall AGU] of distant E and H waveforms related to sprites identified by Walt Lyons show an easily identifiable characteristic waveform (below, left), with the visible sprite (observed by Fukunishi, et al.) closely related to structure in the waveform.

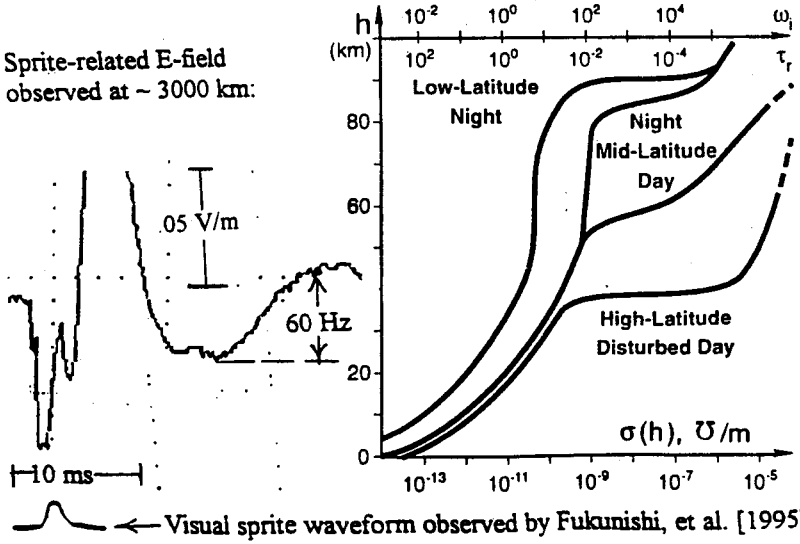

← Visual sprite waveform observed by Fukunishi, et al. [1995].

G/H7-5
1500

Simulations of Energy Coupled to the Mesosphere by Lightning

Michael E. Baginski, A. S. Hodel
Dept. of Elect. Eng.
Auburn Univ., AL 36849
Keith Thomas WL/MNMF Eglin AFB
Edward C. Shaffer, LTC, Dept. EE, U.S. Military Academy, West Point NY.

The quasi-static coupling of electromagnetic energy into the mesosphere by large positive cloud-to-ground lightning is characterized using a finite element routine that assumes the earth's magnetic field to be vertically oriented. Observations of red sprites in this region are the primary motivation for undertaking this study. The change in the electron density (and therefore the conductivity) in the in the region of the sprite is incorporated in the study, which solves Maxwell's equations and the applicable ionization equations in the time domain. Due to the complexity of the problem, only a measured night time conductivity profile will be considered and appropriately modified by the temporal evolution of the strongly coupled set of equations. The effects that radiation associated with horizontal lightning may have on the Sprite phenomenon are also considered.

A major assumption used for the research is that there are slight variations in the spatial structure of the conductivity. These spatial variations are considered the plausible reasons that sprites tend to develop at a number of singular points in the ionosphere before spreading.

Major observations obtained from the simulations are that the primary mode of energy coupling to the ionosphere responsible for sprites is likely to be quasi-static. This result is also strongly implied by previously measured data [Kelley, et al., JGR 90, 9815, 1985] and by optical observations.

G/H7-6
1540

ON THE IONIZATION AND OPTICAL AND INFRARED EMISSIONS OF RED SPRITES

L.S. Jeong, W.A.M. Blumberg, R.H. Picard, and J.R. Winick
Phillips Laboratory
Hanscom AFB, MA 01731-3010
R.A. Armstrong and J. Shorter
Mission Research Corporation
Nashua, NH 03062
J.T. Kroll
Air Force Office of Scientific Research
Bolling AFB, DC 20332-0001

The optical and infrared emission characteristics of red sprites depend strongly on the energy distribution of electrons produced by the dielectric breakdown in the mesosphere and stratosphere associated with these transient events. The level of ionization in sprites has been a point of speculation since the first broad-band visible imagery data were collected from the ground, aircraft, and space shuttle. To characterize the ionization in sprites, a photometer filtered at 427.8 nm was used in the Summer '95 measurement campaign conducted from the Yucca Ridge Field Station in Colorado to make measurements of the N_2^+ first negative band emission in sprites. The results of these measurements will be presented and their implications for the production of high energy electrons will be discussed.

Spectrally-resolved visible emission measurements made independently by two research groups during the Summer '95 campaign have identified the red emission in sprites as N_2 first positive band emission. The source of this emission has been attributed to electron impact excitation of nitrogen by low energy (10 eV) electrons. These observations combined with the apparent absence of emission from the $N_2^+(3,0)$ Meinel band have been used to infer that the sprite electron energy spectrum is characterized by electron energies below the ionization threshold of nitrogen. We will present the results of a kinetic analysis of these visible spectral data and examine the implications for the interpretation of our 427.8 nm photometer measurements and the ionization associated with sprites. These results will also be compared with more direct measurements of ionization levels made by other investigators using radar, ELF, and other techniques as well as with the results of theoretical modeling studies.

The assessment of altitude profiles of low and high energy electrons will be used to perform model calculations of the transient emission predicted for the 4.3 micron band of CO_2. The paper will conclude with a discussion of plans for a Summer '96 measurement campaign to validate the data on the ionization and emissions of red sprites.

G/H7-7 1600

RUNAWAY MODEL OF VHF EMISSIONS FROM UPWARD DISCHARGES

Robert Roussel-Dupré, and Yuri Taranenko (Space and Atmospheric Sciences Group, MS D466, Los Alamos National Laboratory, Los Alamos, NM 87545; 505-667-9228; e-mail: rroussel-dupre@lanl.gov)

The VHF radio emissions expected from upward discharges driven by runaway air-breakdown are computed with a detailed two dimensional fluid model coupled to Maxwell's equations. The effect of the geomagnetic field is omitted. The same model has been used for computing optical and gamma-ray emissions (Taranenko and Roussel-Dupré, accepted to GRL, 1995) and showed good agreement with optical (e.g., Sentman et al., GRL, **22**, 1209,1995; Wescott et al., GRL, **22**, 1213,1995) and gamma-ray (Fishman et al., Science, **264**, 1313, 1994) observations. The relativistic electron beam produced in a runaway discharge contributes an intense forward directed component with a peak amplitude at approximately 13^{o} to the beam motion. The peak intensity is calculated to be 1000 times greater than obtained for an angle of 90^{o}. The contribution due to the low-energy secondary electron population dominates at angles greater than approximately 25^{o}. The nature of the electric field configuration produced in an upward discharge is such that an initial radio pulse is produced at low altitudes (~25-40 km) followed by a secondary pulse at high-altitudes (50-75 km). The duration of each pulse is calculated to be several microseconds while the separation between pulses is tens of microseconds depending on the angle of the observer relative to the beam direction of motion. A detailed comparison of our model with recent BLACKBEARD measurements of Transionospheric Pulse Pairs (TIPPs) is provided. Agreement is obtained between theory and experiment for the intensity, pulse duration, and pulse separation. The fact that TIPPs are more readily observed from space is attributed to the forward directed nature of the radio emissions. The agreement with observations suggests that TIPPs may well be associated with recent optical measurements of 'sprites' and that the source is an upward discharge driven by runaway air breakdown.

G/H7-8
1620

PHENOMENOLOGY OF TRANS-IONOSPHERIC PULSE PAIRS

R. S. Massey, D. N. Holden, R. Franz R. S. Massey*
Space and Atmospheric Sciences Group
MS-D466
Los Alamos National Laboratory
Los Alamos, NM 87545

The source of trans-ionospheric pulse pairs, the intense radio bursts observed by the Blackbeard wide-band transient digitizer on the ALEXIS LEO satellite, remains enigmatic. Since our initial report of this phenomenon at the 1995 URSI meeting, hundreds more TIPP events have been recorded, for a total of nearly 700. In this paper we update our original analysis of 84 TIPP events (R. S. Massey and D. N. Holden, *Phenomenology of trans-ionospheric pulse pairs*, *Radio Science*, **30**, 1645-1659, 1995). In that paper we presented the distributions of a number of interesting parameters, including the pulse energies, pulse separations, pulse durations, ionospheric dispersion, and subsatellite point. Those estimates of the distributions were limited by the small number of samples. In this paper we present statistical results from the much larger database.

Some of the new data were obtained with the satellite positioned over the United States. Differences between this data set and the "equatorial" data set will be described. These data were obtained by operating the Blackbeard instrument in a different frequency band (115-145 MHz) where interference is substantially lower than for the original 29-95 MHz band. The pulse spectrum remains approximately flat across this higher frequency band, further limiting the duration of the micropulses within the pulse envelope.

We have also attempted to find matches between TIPP occurrences over the United States, and lightning events recorded by US National Lightning Detection Network. To date, no coincidences have been found.

G/H7-9
1640

TIPPs: COMPARISON OF RUNAWAY MODEL PREDICTIONS AND EXPERIMENT

R. A. Roussel-Dupré* R. S. Massey, Y. Taranenko
Space and Atmospheric Sciences Group
MS-D466
Los Alamos National Laboratory
Los Alamos, NM 87545

The VHF radio emissions expected from upward discharges driven by runaway air-breakdown were computed with a two dimensional fluid model coupled to Maxwell's equations. The relativistic electron beam produced in a runaway discharge contributes an intense forward directed component with a peak amplitude at approximately 130 to the beam motion. The peak intensity is calculated to be 1000 times greater than obtained for an angle of 900. The contribution due to the low-energy secondary electron population dominates at angles greater than approximately 250. The nature of the electric field configuration produced in an upward discharge is such that an initial radio pulse is produced at low altitudes (25-40 km) followed by a secondary pulse at high-altitudes (50-75 km). The duration of each pulse is calculated to be several microseconds while the separation between pulses is tens of microseconds depending on the angle of the observer relative to the beam direction of motion. A detailed comparison of our results with recent BLACKBEARD measurements of Transionospheric Pulse Pairs (TIPPs) is provided. Excellent agreement is obtained between theory and experiment for the intensity, pulse duration, and pulse separation in specific cases. The atmospheric conditions necessary to reproduce the large variety of TIPP events is reviewed. Correlations between various characteristic parameters such as total electron content (TEC) along the ray path vs. pulse separation, brightness of the second pulse relative to the first pulse, pulse separation vs. energy in the first pulse, pulse duration vs. pulse separation, and total pulse energy vs.TEC are examined in the context of theoretical predictions. An analysis of the spectral profile of TIPPs is also presented. Suggestions for future experiments are proffered.

J2-1
1340

SCIENTIFIC GOALS FOR VSOP AND RADIOASTRON

J. Anton Zensus*
National Radio Astronomy Observatory
Charlottesville, VA 22903

The VSOP mission and the Radioastron project constitute the second generation of spaced-based VLBI experiments, following the demonstration of space VLBI (e.g. Linfield et al., 1989, ApJ 336, 1105), which revealed extreme brightness temperatures in a number of compact sources.

VSOP (scheduled launch in September 1996) will allow high resolution imaging of selected objects (primarily compact radio sources associated with active galactic nuclei), reflected in the chosen apogee height of 22,000 km, and the extensive use of imaging ground VLBI arrays. The scientific program will be anchored in Key Science Programs chosen from a general call for proposals and designed to ensure optimal scientific pay-off. A focus will be on imaging of AGN with unprecedented resolution on sub-parsec scales. A subset of sources with known apparent superluminal motion will be monitored to investigate the evolution in the vicinity of the core. Aiming at cosmological questions, the dependence of proper motion on redshift will be investigated. Other goals include the measurement of spot sizes in OH and water maser sources, direct distance measurements (using water masers), and high-resolution imaging of radio stars.

While VSOP will perform a limited search for high-brightness temperature sources, this will be the main goal of the Radioastron mission, with its apogee altitude of 77,000 km. In addition there will be a focus on measuring the distribution of radio source size for AGN, interstellar scattering, and proper motion-redshift dependence. The actual scope of the Radioastron science program will be affected by the results from the VSOP experiments.

J2-2
1400

VLBI OBSERVING SYSTEM FOR VSOP

J. S. Ulvestad* D. W. Murphy
Jet Propulsion Laboratory
California Institute of Technology
Pasadena, CA 91109

The VLBI Space Observatory Programme (VSOP) satellite is scheduled for launch in September 1996. It will orbit with a perigee height of 1000 km, an apogee height of 22,000 km, and an inclination of 31°. This paper describes the VLBI observing system for VSOP and its differences from ground radio telescope VLBI systems.

The radio telescope aboard VSOP will have a polyhedral structure with an area equivalent to that of an 8-meter circular antenna. Six extensible trusses will provide the antenna deployment and backup structure. The overall shape of the mesh surface will be maintained by a wire-tension-truss design, which includes several thousand cables anchored to the trusses and to the spacecraft body. Feeds and receivers for observing at 1.6, 4.8, and 22.2 GHz are located at the Cassegrain focus. Aperture efficiencies are expected to be between 40% and 50%, while system temperatures will range from 100 K to 200 K. The on-board science subsystem contains the local-oscillator chain as well as the sampling and digitizing hardware necessary for VLBI observations. For most observations, the two independent intermediate-frequency channels will have bandwidths of 16 MHz each, with 2-bit sampling employed. This 128-Megabit/s observing mode is compatible with VLBA data-acquisition systems.

VSOP carries no VLBI data recorder or high-stability frequency reference, so these must be located on the ground, thousands of kilometers from the rest of the VLBI observing system. A reference tone derived from a hydrogen maser must be uplinked and used to drive all oscillators on the spacecraft. Digitized data must be downlinked and recorded on the ground. Therefore, VLBI observing can take place only when the spacecraft can communicate with a tracking station. A set of five tracking stations will be used for VSOP, providing coverage over 50% to 90% of each orbit.

In addition to the tracking station coverage, there are other significant constraints on VLBI observing with VSOP. First, power considerations prevent observations from being made within 70° of the Sun. Second, the spacecraft orbit precesses rapidly; apogee moves from south to north and back again in about 1.2 years, while the VSOP orbital plane precesses through an entire cycle in about 1.8 years. Third, observations are not possible when the Earth eclipses the Sun. Hence, the possible (u,v)-plane coverage changes substantially over the course of a few months. When a radio source lies in the orbital plane, nearly 1-dimensional (u,v) coverage is obtained. A few months later, the same radio source may lie in a direction perpendicular to the orbital plane, thus permitting improved 2-dimensional (u,v) coverage.

J2-3
1420

US Participation in Current Space VLBI Missions

J. D. Romney*
National Radio Astronomy Observatory
Socorro, NM 87801

US scientists and institutions are participating in numerous aspects of the two Space VLBI missions currently under development, VSOP (a project of Japan's Institute of Space and Astronautical Science) and Radioastron (a project of Russia's Astro Space Center). These US activities, funded by NASA, are centered at two institutions, the Jet Propulsion Laboratory (JPL) and the National Radio Astronomy Observatory (NRAO).

Both organizations are developing a network of earth stations to support the missions' phase-transfer links and 128-Mbit/sec data downlinks. A 13.7-m station was completed in 1994 at Green Bank, developed by upgrading the antenna which once formed the 35-km baselines of the NRAO Interferometer, and three new 11-m stations are nearing completion, one at each of the principal DSN sites. These four stations, plus the domestic earth stations in the missions' home countries, will provide nearly continuous tracking coverage, far more than could be achieved by the domestic stations alone.

JPL personnel have provided major assistance to the two missions in areas including design of the spacecraft and orbit, planning for mission operations and science scheduling, and development of the VSOP Announcement of Opportunity, and to US astronomers in preparation of VSOP proposals. After launch, JPL will provide orbit determination and oversee US data flow.

The VLBA, NRAO's dedicated VLBI instrument, will commit up to 30% of its scheduled observing time to joint observations with the current Space VLBI missions. The VLBA correlator will process Space VLBI observations which use the VLBA or other NRAO telescopes. Although not designed specifically to support Space VLBI observations, this possibility was anticipated in the correlator's design. Thus, only relatively minor modifications, currently partially complete, are necessary: incorporate software predicting the spacecraft position and velocity; read and apply timing corrections derived from the ground-to-space phase transfer process; extend the rate range of the correlator's delay tracking subsystem; and accommodate the large residual fringe rate window required by the limited accuracy of orbit reconstruction.

NRAO's imaging software, AIPS, is being modified to accommodate the unique requirements of imaging Space VLBI observations. Among the new features already incorporated or under development are: baseline-oriented fringe fitting tasks, with flexible and adaptive residual rate and delay windows; an interactive source model fitting program; and a fringe-rate mapping routine. NRAO will provide post-launch user support for analysis of Space VLBI observations at a level commensurate with that available currently to users performing ground-based observations.

J2-4
1440

IMAGING CONSIDERATIONS FOR VSOP

Chris Flatters
National Radio Astronomy Observatory
P. 0. Box 0
Socorro, NM 87801-0387

The VLBI Space Observatory Program (VSOP) will place an a radio telescope with a diameter of 8 meters into orbit. This telescope will be used in conjunction with ground-based VLBI arrays to provide data for high-resolution imaging of radio sources. The planned orbit is specifically designed to provide good u-v coverage but the characteristics of the orbiting antenna mean that special care must be taken when mapping sources using data from it. The two main concerns are the low sensitivity of the orbiting antenna relative to ground-based telescopes and the rapid motion of the spacecraft.

The low sensitivity of baselines to the orbiter means that points in the outer part of the u-v plane, which come exclusively from orbiter baselines, will have smaller statistical weights than those in the inner part of the plane. This will tend to degrade resolution if natural weighting in used because the points in the outer part of the plane will contribute relatively little to the image. This effect will be reinforced by the fact that density of u-v samples in the outer part of the plane is much less than that in the inner part of the plane due to the motion of the spacecraft. Uniform weighting will increase the resolution at the cost of reducing dynamic range. The careful use of weighting schemes that can vary parametrically between the extremes of natural and uniform weighting should be able to produce maps with resolutions close to that given by uniform weighting with only a small penalty in dynamic range.

The rapid motion of the spacecraft, particularly near perigee, also constrains the length of time over which data may be averaged. The motion of the spacecraft within a long averaging period will produce azimuthal "smearing" which limits the field of view. This is an important constraint on self-calibration since long averaging times may be necessary to reduce the SNR on the orbiter baselines sufficiently for self-calibration to be effective.

J2-5
1500

A PROPOSED SECOND-GENERATION SPACE VLBI MISSION

R. P. Linfield* J. S. Ulvestad J. G. Smith
Jet Propulsion Laboratory
California Institute of Technology
Pasadena, CA 91109

We have proposed a highly sensitive, second-generation space VLBI mission called ARISE (Advanced Radio Interferometry between Space and Earth). Recently, a mission concept study for ARISE was successfully proposed to NASA in response to a NASA Research Announcement for "New Mission Concepts in Astrophysics."

The two key attributes of ARISE, when compared to the first-generation space VLBI missions (VSOP and RadioAstron), are its much greater sensitivity and its coverage of higher observing frequencies. Through a large radio telescope (25–30 m diameter), low system temperatures (10–40 K) and a high data rate (8 Gbit/s), the interferometer sensitivity of ARISE would be a factor of about 50 better than for VSOP or RadioAstron. Detection thresholds would be well below 10 mJy at 5 GHz and 22 GHz. ARISE would also push into new (for space VLBI) frequency bands: 43 GHz and (with somewhat less sensitivity) 86 GHz.

The ARISE spacecraft would achieve a large collecting area at low cost by employing an inflatable antenna. A 14-m inflatable antenna developed by the L'Garde Corporation is scheduled to be deployed and have its surface figure tested in a Space Shuttle experiment planned for early 1996.

In addition to high-dynamic range imaging and monitoring of classic VLBI sources, ARISE would explore areas of astrophysics that are not accessible to VSOP or RadioAstron. The exploration of active galactic nuclei (AGN) would be expanded to include much weaker objects such as Seyfert galaxies, normal galaxies, and lobe-dominated radio galaxies. The high sensitivity also would enable imaging of a number of radio stars in their quiescent states. The high-frequency capability would permit very high resolution 86-GHz observations of AGN at the base of their relativistic jets, in a frequency regime where the jets are optically thin. Finally, this high-frequency capability would permit single-dish mapping of a number of star formation regions in the molecular oxygen complex near 60 GHz, which cannot be observed from inside the Earth's atmosphere.

J2-6
1520

GLOBAL GROUND VLBI NETWORK AS A TIED ARRAY FOR SPACE VLBI.

L. Kogan
National Radio Astronomy Observatory,
PO Box 0, Socorro, NM 87801

The both now planned space VLBI (SVLBI) missions RADIOASTRON and VSOP have a small space antenna and as a result a comparatively poor sensitivity. Baselines between a ground based and the space antenna is not known in advance with an accuracy typical for ground based VLBI. Many sources can be partially resolved on the baselines SPACE-EARTH. Therefore the typical correlated flux density for interferometer SPACE-EARTH is less than for a ground based interferometer. In this situation the problem of minimization of a detectable flux density is rather actual. Phasing of group of ground based antennas can decrease the minimum detectable flux density on the interferometer between the combined Earth radio telescope and the space one. It is known that global fringe fitting procedure provides decrease in detection threshold for the case of 'n' identical antennas in $\sim \sqrt{n/2}$ times. (W.D. Cotton and F.R. Schwab, VLBA Scientific memo # 2, 1993; A.E.E. Rogers, VLBA Scientific memo # 4, 1993). The estimation of the detection threshold decrease provided by global fringe fitting procedure in the case of unidentical antennas has been performed. It has been shown that phasing of group of ground based antennas and global fringe fitting procedure provide identical decrease in detection threshold for interferometer Earth-Space in the case of small space antenna comparatively with a ground based one.
Therefore it is not necessary to invent something special to achieve the minimum detectable flux density for interferometer Earth-Space. The standard global fringe fitting procedure (FRING in AIPS for example) realizes it.
The minimum detectable flux density has been calculated for interferometer RADIOASTRON/VSOP and Earth represented by group of phased antennas in USA, Europe, and Australia.

J2-7
1600

LOW FREQUENCY RADIO ASTRONOMY IN EARTH ORBIT AND ON THE MOON

Kurt W. Weiler*
Code 7214
Naval Research Laboratory
Washington, DC 20375-5300

Exploring the astrophysics of the Universe at very low radio frequencies requires going to space. At frequencies between $\sim$ 1 and $\sim$ 30 MHz, a frequency range over which the Earth's ionosphere transmits poorly or not at all, high resolution and sensitivity surveying and mapping will open a new window in the electromagnetic spectrum for astronomical investigations. Also, extending observations down to such low frequencies will bring astronomy to the fundamental physical limit below which the Milky Way becomes optically thick over relatively short path lengths due to diffuse free-free absorption in the ISM. There are many scientific areas to be explored in this new observing window

Mapping of the Galactic background emission is of prime importance for determining the distribution of relativistic cosmic ray electrons and their low frequency injection and acceleration. The diffuse free-free absorption of low frequency radiation and its scattering and refraction by the density fluctuations is an important probe of the ISM.

The low frequency radio spectra of extragalactic sources will allow the separation of a number of different emission and absorption processes and determine what types of relativistic electron energy loss processes dominate. Measuring the brightness of large scale, low energy electron distributions will limit theories of the evolution and lifetime of radio galaxies since at these frequencies the radiative lifetimes of synchrotron electrons approach the age of the universe.

Supernova remnants will be prominent sources at low radio frequencies and millisecond pulsars, while no longer pulsing due to interstellar scattering and dispersion, should appear as very prominent point sources due to their steep spectra.

Coherent emission, which is prominent in the solar system, is relatively unimportant in most cosmological radio sources. However, at these low frequencies it will likely become a common process, possibly revealing a new class of emitters.

Arrays to carry out these objectives in high earth orbit and on the near or far side of the moon will be discussed. There are a number of technical problems to be solved, such as full sky mapping, and there are environmental limitations, such as magnetospheric refraction and natural and man-made interference. Possible solutions will be discussed.

J2-8
1620

A LUNAR ORBITING LOW FREQUENCY RADIO ASTRONOMY OBSERVATORY CONCEPT

R. G. Stone* M. D. Desch
Laboratory for Extraterrestrial Physics
Goddard Space Flight Center
Greenbelt, MD 20771

The Lunar Orbiting Low Frequency Radio Astronomy Observatory (LOREX) concept is to make radio observations from lunar orbit to study emissions from galactic and extra galactic radio sources. Designed to operate at frequencies from 1 to 10 MHz, a range which could be extended, the LOREX will open up a new spectral band for astrophysical studies, a band not accessible to ground based radio observatories owing to the opacity of the Earth's ionosphere. The spacecraft would be capable of studying astrophysical phenomena at a spatial resolution determined by the Fresnel fringes produced by sources occulted by the lunar limb. The science to be produced by LOREX includes: extending the spectra of known radio sources beyond their present limits, observing new, possibly coherent, steep spectra emitters, and studying the distribution of low energy cosmic ray particles. LOREX would act as a pathfinder mission for a lunar based observatory in the next century. The electromagnetic environment as determined by space borne radio observations will also be discussed as they may impact proposed space astronomical observations. Specifically, a major concern for observations in this frequency band is the expected high level of electromagnetic interference from Earth-based transmitters. Power levels at lunar orbit have been observed in the past to exceed 10's of dB above the galactic background level, which would effectively prevent observations of astrophysical interest. Recent high-resolution data from the WAVES radio astronomy instrument onboard the WIND spacecraft have confirmed the existence of high levels of electromagnetic noise, primarily from commercial broadcast stations operating just above the ionosphere critical frequency. However, we have identified a fair number of relatively broad bands in the 2 – 15 MHz spectral region in which the electromagnetic interference is greatly reduced. We will present observations of these bands and show statistical analyses of the electromagnetic noise at various amplitude levels. Finally, we will discuss the efficacy of making observations in these bands from lunar orbit in the context of LOREX.

J2-10
1640

THE ASTRONOMICAL LOW-FREQUENCY ARRAY

D. L. Jones* and the ALFA Midex Proposal Team†
Jet Propulsion Laboratory
Mail Code 238-332
4800 Oak Grove Drive
Pasadena, CA 91109

The low frequency end of the electromagnetic spectrum, from a few tens of MHz down to $\sim$ 100 kHz, is largely inaccessible from the Earth due to the ionosphere and RFI. From space, however, a cluster of very small, inexpensive satellites operating as an interferometer array could provide radio images of the entire sky with angular resolution limited only by scattering in the interplanetary and interstellar media. Data from such an array could answer a wide range of astrophysical questions about the solar system, the galaxy, and the distant universe.

We present an innovative concept for the deployment and operation of a low-frequency array in space. A solar orbit is used to get far from the Earth to reduce radio interference and to minimize the cost of precise trajectory determination and control. The array consists of 16 identical spin-stabilized microsats, which are deployed into a volume 100-200 km in diameter by a single bus. Precise control of the microsat positions is not required because of the very long wavelengths being observed. Each microsat includes a pair of orthogonal dipole antennas in the spin plan, and autonomously keeps its spin axis pointed at the Sun. The deployment bus is 3-axis stabilized and is used to monitor the three-dimensional geometry of the array and to relay data from each microsat to Earth. Cross-correlation of the data and the production and deconvolution of full-sky images can be done on existing parallel computers. A detailed study of imaging algorithms for this mission is currently underway.

By basing the design of the flight hardware on previously flown commercial satellites and minimizing the complexity of ground operations, we believe that ALFA can be developed and flown as a medium-class Explorer mission.

Part of this work was carried out at the Jet Propulsion Laboratory, California Institute of Technology, under contract with the National Aeronautics and Space Administration.

† The ALFA proposal team consists of R.J. Allen (STScI), W.H. Blume (JPL), M.M. Desch (GSFC), W.C. Erickson (U. Tasmania and U. Maryland), M.L. Kaiser (GSFC), N.E. Kassim (NRL), T.B.H. Kuiper, R.P. Linfield, M.J. Mahoney, K.A. Marsh (JPL), R. Michalski (CTA Space Systems), R.E. Oberto (JPL), R.A. Perley (NRAO), R.A. Preston (JPL), R.G. Stone (GSFC), and K.W. Weiler (NRL).

J2-11
1700

"FIRST", A SUBMILLIMETER SPACE MISSION

T. G. Phillips*
California Institute of Technology
Pasadena, CA 91125

FIRST (Far-Infrared and Submillimeter Space Telescope), an ESA mission, is a high sensitivity submillimeter spectroscopy and continuum satellite, approved as a "Horizon 2000" Cornerstone mission for launch in 2005/6. It has an ESA assigned budget of 400 MAU (1984 European accounting units; 1 MAU is slightly more than $1M.) The primary goals of the mission are the detection and study of distant and possibly primordial galaxies ($1 < z < 5$), and the detection and study of stars forming in the local interstellar medium.

The NASA goal is to contribute to the technical and scientific aspects of the program, to provide a significantly enhanced international mission, through the use of advanced US technology, and also results in core program and open time science opportunities to US astronomers. NASA would be a partner in FIRST with ESA, at a level still to be determined. Our own project in this field, SMIM, is similar to FIRST, and although planned some time ago, could not be constructed on a competitive timescale, so the US submillimeter community has decided to try to join the European project.

The FIRST mission, as approved, is a 3-m diameter, radiatively cooled (165 K) telescope for high-throughput spectroscopy and photometry in the submillimeter and far-infrared range (85 – 900 μm, 3.5 – 0.33 THz). Best angular resolution is about 7". The payload consists of a cryogenic focal plane system with: superconducting tunnel junction (SIS) heterodyne detectors providing near quantum-noise performance for high spectral resolution ($R \geq 10^6$) in the 500 – 1200 GHz range; imaging photoconductor arrays for photometry ($R \sim 3$) or medium resolution spectroscopy ($R \sim 10^4$) in the 85 – 210 μm band; and bolometer arrays for spectroscopy in the 200 – 300 μm band and photometry in the 200 – 900 μm band. The nominal mission lifetime is 2 years, but could be extended to six years depending on the final cryogenic technology employed.

Saturday, 13 January, 0855-1300

Commision G Special Session, 0900-Sat., CR2-26
RADAR TECHNIQUES WORKSHOP

JSS-1
0900

THE COSMIC MICROWAVE BACKGROUND RADIATION IN THEORY AND EXPERIMENT

Dale Fixsen*
Goddard Space Flight Center
Code 685.0
Greenbelt Rd.
Greenbelt, MD 20771

The FIRAS (Far InfraRed Absolute Spectraphotometer) instrument aboard COBE, the COsmic Background Explorer, collected 10 months of data covering most of the sky from .105 mm to 5 mm. These data offer the best opportunity to date to test the black body spectrum predicted by the big bang theory. The data are of sufficient quality to look for perturbations introduced by galaxy formation and other possible occurrences in the young universe. To account for the data the big bang model must include more than uniform temperature and density. These perturbations, first found by COBE DMR, as well are coming into view with a new generation of instruments such as MSAM (Medium Scale Anisotropy Measurement). With three balloon flights and 15 hours of observation this instrument is able to detect the fluctuations in temperature on angular scales of one half degree.

JSS-2
0930

REDSHIFT DISTORTIONS AND OMEGA

Andrew Hamilton*
University of Colorado
JILA
Box 440
Boulder, CO 80309

Peculiar velocities of galaxies induce line of sight distortions in the pattern of clustering of galaxies observed in redshift space. On small scales, the large orbital velocities of galaxies in collapsed clusters produce the well known 'fingers-of-god'. On large scales, peculiar infall towards overdense regions causes the opposite effect, an apparent squashing of clusters in redshift space. The amplitude of the squashing depends on the cosmological density Omega. I review recent theoretical and observational work on the large scale squashing effect, and the values of the cosmological density Omega which have been inferred.

JSS-3
1000

RADIO SOURCES AS COSMOLOGICAL PROBES

Ed Fomalont*
NRAO
Edgemont Rd.
Charlottesville, VA 22903

The energy in the microwave radiation emitted by quasars and galaxies can approach 10^{26} watt/Hz/ster. This energy is easily detected by radio telescopes at a typical flux density of 10^{-26} watt/Hz/m^2. These objects are then at a distance of $10^{26}m$, or 10 billion light years. Since we believe the age of the universe is approximately 10 billion years (determined from the observed rate of expansion of the nearby galaxies), we are observing emission from these radio sources at an early stage in the universe development. We believe that the sources are affected by the two major "cosmological" properties: evolution—the change of the intrinsic properties of the radio sources in the early universe environment; and geometry—the effect of the overall mass distribution of the universe on the space propagation of the radio source. Clearly, radio sources can be used as an effective probe of the cosmological evolution and geometry.

Three of the most important parameters which describe the cosmological geometry are: H_o, the Hubbel constant; q_o, the deceleration parameter; omega, the density parameter. If there were little cosmological evolution of the radio emission from quasars and galaxies, the above three parameters could be measured relatively easily from the collective properties of radio sources. Some of those discussed in this talk are: (1) The number of radio sources in the sky as a function of flux density; (2) the angular size of radio sources versus their redshift (speed of recession); (3) The spatial clustering of radio sources; (4) The rotational properties of large galaxies; (5) The relativistically expansion of some sources.

The cosmological evolution of radio sources, however, has a stronger influence in the appearance of distant radio sources, than that of cosmological geometry—as interpretation of the above properties of the sources will attest. However, with the wealth of recent observations of medium and high redshift objects, astronomers are beginning to unravel the cosmological and geometric properties of the universe. Recent results and anticipated experiments in the near future will be described.

JSS-4
1100

A RADIO SEARCH FOR PRIMORDIAL PROTOCLUSTERS

I. M. Avruch
Department of Physics
Research Laboratory of Electronics
Room 26-348
Massachusetts Institute of Technology
Cambridge, MA 02139
J. Weintroub*
Lyman Laboratory of Physics
Harvard University
Cambridge, MA 02138

There are no astronomical observations between recombination (red-shift $z \approx 1100$) and the epoch of the most distant quasars ($z \approx 5$). Very little is known definitively about the manner in which the very smoothly distributed matter at recombination (as inferred from measurements of the cosmic microwave background) condensed to form the stars, galaxies, and galaxy clusters which we see today. Theories of structure formation would benefit from observational constraint. It is likely that massive self-gravitating clouds of neutral hydrogen are formed at some high red-shift. We are trying to observe these in the hyperfine line ($\lambda = 21$ cm), at red-shifts $4.7 \leq z \leq 5.5$ (a 32 MHz band centered at 235 MHz).

The expected signal is very weak. In order to make a detection in a reasonable time we require the large collecting area of the Arecibo Observatory. Our experiment, installed in the summer of 1994, runs continuously and in the main independently of scheduled observations and the observatory upgrade. Dual broadband point feeds are mounted on the telescope catwalk where it intersects the focal surface, allowing continuous transit observations. The dedicated receiver includes low-noise preamplifiers, RF and IF filters and mixers, and a custom power-accumulating FFT spectrometer with 10-kHz resolution and 32-MHz instantaneous bandwidth (4k channels per feed). The spectrometer output is time tagged and logged to disk on a control PC, and digital audio data tapes are shipped biweekly to Cambridge.

Strong RFI virtually blankets our system except for a few early morning hours, and spillover losses are unexpectedly high. We are redesigning our feed to lower horizon sensitivity and maximize overall SNR. Design requirements are derived by modeling the effects of spherical aberration and squint on system gain and noise temperature.

JSS-5
1130

COSMOLOGICAL IMPLICATIONS OF GRAVITATIONAL LENSES

Jacqueline N. Hewitt*
MIT
Bldg 26-331
77 Mass Ave
Cambridge, MA 02139

Gravitational lensing occurs when radiation from a distant object passes through a foreground gravitational field. Astrophysical phenomena that are recognized as gravitational lensing include "strong lensing", in which multiple images of the background source are formed; "weak lensing", in which just distortions are produced; microlensing; and some statistical properties of samples of high redshift objects. Gravitational lenses are beginning to be applied to some long-standing problems in cosmology, such as the nature and distribution of dark matter in the universe and the values of cosmological parameters, including the age and scale of the universe.

JSS-6 1200 DISCUSSION: PRESENT ISSUES, FUTURE INSTRUMENTS: B.F. Burke, MIT, Cambridge, MA 02138

INDEX

Thursday, 11 January (cont.)

0855-1000

G-4	TOMOGRAPHIC STUDIES OF IONOSPERIC PLASMAS-II	CR2-26

1015-1200

G/H-2	IONOSPHERIC MODIFICATION WITH HIGH POWER RADIO WAVES	CR2-26

1335-1700

B-4	THEORETICAL ELECTROMAGNETICS	CR1-9
D-3	MICROMACHINING FOR MICROWAVES	CR2-28
F-4	ACTIVE REMOTE SENSING OF THE OCEAN	CR1-42
G/H-3	IONOSPHERIC MODIFICATION WITH HIGH POWER RADIO WAVES	CR2-26
J/F-2	RADIO FREQUENCY PHASE SHIFTS CAUSED BY THE TROPOSPHERE	CR0-30

1355-1700

G/H-4	MID-LATITUDE IONOSPHERIC INEQUALITIES	CR2-6

1700-1800

Commission B Business Meeting	CR2-28
Commission C Business Meeting	CR0-36
Commission G Business Meeting	CR2-26
Commission J Business Meeting	CR0-30
Commission K Business Meeting	CR1-40

1900-2200

DON SPAULDING MEMORIAL SESSION	CR2-28

Friday, 12 January

0835-1200

E-1	HIGH POWER ELECTROMAGNETICS	CR1-46
F-5	PASSIVE REMOTE SENSING OF THE ENVIRONMENT	CR1-42

0855-1200

B/C/J-1	PHASED ARRAY FEEDS IN RADIO ASTRONOMY	CR0-30
D/A-1	HIGH FREQUENCY PACKAGES	CR2-28
G/H-5	RED SPRITES, BLUE JETS, AND LIGHTNING	CR2-6
G/H-6	SPACE PLASMA WAVES AND RADAR/RADIO REMOTE SENSING	CR2-26

1335-1700

B-5	NUMERICAL METHODS	CR1-9
F-6	RADAR REMOTE SENSING OF THE TROPOSPHERE	CR1-42
G-5	EQUATORIAL IRREGULARITIES	CR2-26
G/H-7	RED SPRITES, BLUE JETS, AND LIGHTNING	CR2-6
J-2	RADIO ASTRONOMY FROM SPACE	CR0-30

Saturday, 13 January

0855-1300

COSMOLOGY AND RADIO ASTRONOMY (Commision J Special Session)	CR2-28

0855-1700

RADAR TECHNIQUES WORKSHOP (Commision G Special Session)	CR2-26